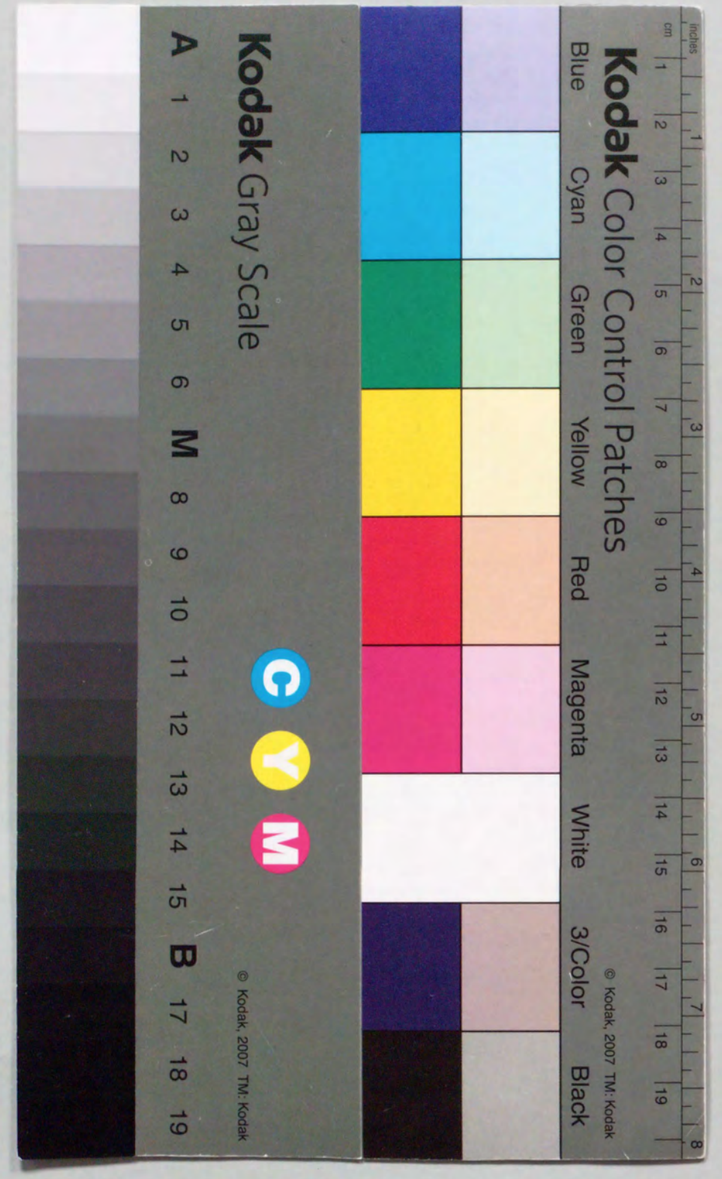

Proton and Neutron Halos of β-Emitting Nuclei Detected by Nuclear Quadrupole Moments

Takashi Ohtsubo

DISSERTATION IN PHYSICS

THE OSAKA UNIVERSITY

GRADUATE SCHOOL OF SCIENCE

TOYONAKA, OSAKA

Proton and Neutron Halos of β-Emitting Nuclei Detected by Nuclear Quadrupole Moments

Takashi Ohtsubo

ABSTRACT

The nuclear quadrupole moments of light short-lived nuclei in a region far from stability lines have been determined in order to study their nuclear structures and to identify the neutron and proton halos in nuclei. For this purpose, the nuclear quadrupole moments of short-lived β emitters (^{8}Li($I^{\pi} = 2^{+}$, $T_{1/2} = 0.84$ s), ^{8}B($I^{\pi} = 2^{+}$, $T_{1/2} = 0.769$ s), ^{12}B($I^{\pi} = 1^{+}$, $T_{1/2} =$ 20.2 msec), and ^{12}N($I^{\pi} = 1^{+}$, $T_{1/2} = 11.0$ msec)) were precisely measured. For the present purpose, the electric quadrupole interactions of each nucleus implanted in several selected single crystals were studied by detecting the β-NMR of the β emitters. The crystals in which well-defined electric field gradients were obtained were $LiIO_3$, $LiNbO_3$, highly oriented BN, and GaN. In these crystals the implanted β emitters were located at substitutional sites of their stable isotopes. ^{8}B and ^{12}B nuclei were also implanted in a Mg crystal in order to utilize any internal field gradients obtained at its interstitial site. The field gradients in insulator crystals were measured by detecting the Fourier-Transformed NMR (FT-NMR) of stable isotopes of ^{7}Li, ^{11}B and ^{14}N in $LiIO_3$, $LiNbO_3$, BN and GaN, respectively. Also, the field gradient in a Mg crystal was measured by detecting the β-NMR of ^{12}B in a crystal.

In order to observe very small electric quadrupole effects in the β-NMR spectra of β emitters, the conventional β-NMR was very much improved as a New Nuclear Quadrupole Resonance Technique (NNQR). This technique is especially efficient and was designed to study the quadrupole interactions of high-spin states.

The quadrupole coupling constants were determined to be $|eQ/h|$(^{8}Li in $LiIO_3$)| = 29.6 ± 1.1 kHz, $|eQ/h|$(^{8}Li in $LiNbO_3$)| = 44.68 ± 0.88 kHz, $|eQ/h|$(^{8}B in Mg)| = 243.6± 6.0 kHz, $|eQ/h|$(^{12}B in BN)| = 944 ± 17 kHz, $|eQ/h|$(^{12}B in Mg)| = 47.0 ± 0.1 kHz, $|eQ/h|$(^{12}N in BN)| = 56.8 ± 3.2kHz

and $|eqQ/h(^{12}\text{N in GaN})| = 27.5 \pm 2.0$ kHz. For stable isotopes, the coupling constants were determined to be $|eqQ/h(^{7}\text{Li in } LiIO_3)| = 36.4 \pm 0.5$ kHz, $|eqQ/h(^{7}\text{Li in } LiNbO_3)| = 53.3 \pm 0.5$ kHz, $|eqQ/h(^{11}\text{B in BN})| = 2902 \pm 12$ kHz, $|eqQ/h(^{14}\text{N in BN})| = 110.7 \pm 4.1$ kHz and $|eqQ/h(^{14}\text{N in GaN})| = 49 \pm 15$ kHz. Since the quadrupole moments of the stable isotopes are known to be $Q(^{7}\text{Li}) = +40.0 \pm 0.6$ mb $Q(^{11}\text{B}) = +40.59 \pm 0.10$ mb [Su91] and $Q(^{14}\text{N}) = +20.0 \pm 0.2$ mb [Sc92], the electric field gradients were obtained to be $|q(\text{Li site of } LiIO_3)| = 3.8 \pm 0.1 \times 10^{19}$ V/m^2, $|q(\text{Li site of } LiNbO_3)| = 5.5 \pm 0.1 \times 10^{19}$ V/m^2, $|q(\text{B site of BN})| = 2.96 \pm 0.02 \times 10^{21}$ V/m^2, $|q(\text{N site of BN})| = 2.29 \pm 0.24 \times 10^{20}$ V/m^2 and . $|q(\text{N site of GaN})| = 1.0 \pm 0.3 \times 10^{20}$ V/m^2. Finally, the quadrupole moments of β-emitting nuclei were determined to be $|Q(^{8}\text{Li})| = 32.7 \pm 0.6$ mb, $|Q(^{8}\text{B})| = 68.3 \pm 2.1$ mb, $|Q(^{12}\text{B})| = 13.20 \pm 0.25$ mb and $|Q(^{12}\text{N})| = 10.3 \pm 0.7$mb.

The value of $Q(^{8}\text{B})$ is twice as large as that predicted by the Cohen-Kurath wave functions in the harmonic-oscillator potential. It was found by subtracting the contribution of deeply bound neutrons that the last valence proton in ^{8}B carry more than 90% of the observed moment. This value is accounted for by the Cohen-Kurath wave functions in a Woods Saxon potential in which the depth of the potential was adjusted so as to reproduce the empirical nucleon separation energies. This anomalous value is accounted for by the proton halo due to the loosely bound valence configuration. This is the first experimental evidence of a proton halo covering a neutron core. Similarly, the neutron contribution in $Q(^{8}\text{Li})$ suggests a neutron skin covering a proton core.

The value of $Q(^{12}\text{B})$ is in good agreement with that predicted by the Cohen-Kurath wave functions in the Woods Saxon potential. A thin, but definite, neutron skin is clearly shown, which results from a rather shallowly bound neutron configuration.

In spite of the rather shallow configuration of the valence proton in ^{12}N (the one proton separation energy is 0.6 MeV), the experimental value, $|Q(^{12}\text{N})|$, is well reproduced by the Cohen Kurath wave functions in the harmonic-oscillator potential, $Q(^{12}\text{N, HO}) = 11$ mb, rather than in the Woods Saxon potential, $Q(^{12}\text{N,.WS}) = 5$ mb. Additional theoretical studies concerning its structure are needed.

CONTENTS

Page

ABSTRACT i

LIST OF TABLES ix

LIST OF FIGURES xi

ACKNOWLEDGMENTS xv

1. INTRODUCTION 1

2. THEORETICAL BACKGROUND CONCERNING THE ELECTRIC QUADRUPOLE MOMENTS 8

2-1 Quadrupole moments of A=8 and 12 systems given by the *jj* model 8

2-2 Advanced shell-model description 10

2-3 Known quadrupole moment values of ^{8}Li and ^{12}N 12

3. EXPERIMENTAL METHOD 13

3-1 NMR 13

1) Nuclear magnetic resonance 13

2) Electric quadrupole interaction in high field 16

3-2 β-NMR 22

1) Production of spin polarized β-emitters through nuclear reactions 22

2) Preservation of the spin polarization in crystals 25

3) Detection of polarization 28

4) Resonant destruction of polarization by rf magnetic fields (NMR) 30

5) Adiabatic fast-passage (AFP) method 33

6) Modified β-NMR for measuring the electric quadrupole coupling frequency (ν_Q) — NNQR method 36

3-3 Causes of line broadening of the NMR spectra 42

1) Dipole-dipole interaction 42

2) Spread in the electric field gradients 46

3) Intensity of the rf field 46

4) Chemical shifts 47

3-4 Implantation media 50

1) h-BN (hexagonal Boron Nitride) 51

2) GaN (Gallium Nitride) 55

3) AlN (Aluminum Nitride) 55

4) $LiIO_3$ (Lithium Iodate) 57

5) $LiNbO_3$ (Lithium Niobate) 57

6) Mg (Magnesium) 57

3-5 Fourier-Transformed NMR (FT-NMR) 61

1) Principle of the FT-NMR method 61

2) Typical NMR spectra of highly oriented BN 61

4. EXPERIMENTAL APPARATUS 66

4-1 Target system 66

4-2 β-ray counter system 70

4-3 Electronic circuit systems for the β-ray detection and spin control 74

1) β-ray detection system 74

2) Rf system for the β-NMR 79

3) System control by micro computers 85

4-4 Preparation and treatment of the implantation media 94
1) BN 94
2) GaN 94
3) AlN 96
4) $LiIO_3$ 96
5) $LiNbO_3$ 96
6) Mg 96

5. EXPERIMENTAL RESULTS 99

5-1 Quadrupole moment of ^{12}B 99

1) β-NMR detection of ^{12}B in BN 99

2) Measurement of the electric field gradient by detecting FT-NMR for ^{11}B in BN 105

3) Temperature dependence of the quadrupole interaction of ^{11}B in BN 108

4) Electric quadrupole moment of ^{12}B 108

5-2 Quadrupole moment of ^{12}N 110

1) β-ray detection of ^{12}N in BN, GaN, and AlN 110
(i) Polarization maintained in crystals 110
(ii) Temperature dependence of the β-NMR 113
(iii) Double quantum transition 116
(iv) β-NMR detection of ^{12}N 121
a. BN 122

b. GaN 122
c. AlN 127

2) Measurement of the electric field gradients by detecting the FT-NMR of ^{14}N in BN and GaN 127

3) Electric quadrupole moment of ^{12}N 130

5-3 Quadrupole moment of ^{8}Li 131

1) β-NMR detection of ^{8}Li 131

2) Measurement of the electric field gradients by detecting the FT-NMR of ^{7}Li in $LiIO_3$ and $LiNbO_3$ 137

3) Electric quadrupole moment of ^{8}Li 137

5-4 Quadrupole moment of ^{8}B 141

1) Measurement of the Larmor frequency and electric field gradient by detecting the β-NMR of ^{12}B in Mg 141

2) β-NMR detection of ^{8}B 147

3) Electric quadrupole moment of ^{8}B 147

6. DISCUSSION 150

6-1 Hyperfine interactions of ^{8}Li in $LiIO_3$ and $LiNbO_3$ and quadrupole moment of ^{8}Li 150

6-2 Quadrupole moment of ^{12}N and its hyperfine interactions 150

6-3 Proton halo in ^{8}B discovered by its quadrupole moment 152

6-4 Neutron skins in ^{8}Li and ^{12}B detected by their quadrupole moments 158

6-5 Quadrupole moment of ^{12}N 160

6-6 Other interpretations of the quadrupole moments and radii for ^{8}Li and ^{8}B 161

7. CONCLUSION 164

REFERENCES 165

Appendix A. Field gradients in Mg detected by ^{12}B and ^{12}N 170

Appendix B. Theoretical calculation of the field gradient at the trigonal site of Mg and the nuclear quadrupole moment of ^{12}N 170

Appendix C. A computer program list for NNQR: spin control and data-acquisition systems. 175

TABLES

Page

1-1 Separation energy of the last nucleon in p-shell nuclei 4

2-1 Quadrupole moments given by the single-particle model 10

3-1 Experimental conditions for the production of polarized nuclei 27

3-2 Dipolar broadenings of the samples. 46

4-1 General parameters of rf coil. 85

5-1 Fitting result of the double quantum transition of ^{12}B in BN at H_0 = 5kOe and T = 300K. 102

5-2 Electric quadrupole moment of ^{12}B 109

5-3 Experimental results of the double quantum transition of ^{12}N in BN, GaN and AlN 121

5-4 Experimental results of the quadrupole coupling frequency ν_Q of ^{12}N in BN and GaN 126

5-5 Results of the FT-NMR spectra on ^{14}N in BN and GaN 130

5-6 Experimental results of β-NMR at magic angle for ^{8}Li in $LiIO_3$ and $LiNbO_3$. 131

5-7 Experimental results of the quadrupole coupling frequency ν_Q of ^{8}Li in $LiIO_3$ and $LiNbO_3$. 134

5-8 Observed electric field gradients at Li site in $LiIO_3$ and $LiNbO_3$ and the present quadrupole moment values. 141

5-9 Fitting results of the double quantum transition of ^{12}B in Mg and the single quantum transition of 12B in Pt at T ~ 100K and T ~ 300K. 143

5-10 Knight shifts of ^{12}B in metals. 145

6-1 Parameters used for the measurements of quadrupole moments 151

6-2 Theoretical and experimental quadrupole moments of the nucleus in A = 8, 11, 12 systems. 153

6-3 Root mean square (rms) radii of the proton and neutron distributions in nuclei of A = 8, 11,12 systems. 157

6-4 Calculation of rms radii of the proton and neutron distributions in the nuclei of A = 8. 157

A-1 List of the computer programs. 175

FIGURES

Page

3-1 Energy levels in the Zeeman Hamiltonian for I = 1. 14

3-2 Classical view of NMR: the spin movement in a magnetic field and resonance phenomena. 15

3-3 Quantum mechanical explanation of the NMR for polarized nuclear ensemble. 17

3-4 Definition of Euler angles. 18

3-5 Energy levels and transition frequencies for spin I = 1 nuclei perturbed by an electric quadrupole interaction. 21

3-6 Angle dependence of the resonance frequencies perturbed by an electric quadrupole interaction for spin I = 1. 23

3-7 Angle dependence of the resonance frequencies perturbed by an electric quadrupole interaction for spin I = 2. 24

3-8 Definition of the polarity of polarization through nuclear reactions. 26

3-9 Energy-level schemes of the A = 12 system. 29

3-10 Energy-level schemes of the A = 8 system. 31

3-11 Time sequence program for the β-NMR detection. 32

3-12 Adiabatic fast-passage (AFP) method. 34

3-13 Optimum rf amplitude modulation (AM) for the AFP method. 37

3-14 Difference between partial and complete depolarization. 38

3-15 Principle of the newly developed multiple rf operation (NNQR method). The case of the spin is I = 2 (a) and I = 1 (b). 39

3-16 Dipole-dipole interaction. 43

3-17 Effect of strong rf field on the resonance shape. 48

3-18 Effect of multiple rf field on the resonance shape. 49

3-19 Crystal structure of hexagonal boron nitride (h-BN). 52

3-20 Distribution of the *c*-axes of a highly oriented BN sample. 53
3-21 X-ray reflection method used to measure the distribution of the *c*-axes in a highly oriented BN sample. 54
3-22 Crystal structure of GaN and AlN (Wurtzite structure). 56
3-23 Crystal structure of $LiIO_3$. 58
3-24 Crystal structure of $LiNbO_3$ (Ilmenite structure). 59
3-25 Crystal structure of Mg (hexagonal). 60
3-26 Principle of pulsed NMR. 62
3-27 FID (free induction decay) signal of the spin rotating with ω_L perturbed by the pulsed rf with frequency ω. 63
3-28 Theoretical FT-NMR spectrum for ^{11}B in highly oriented BN. 65

4-1 Beam-transport system. 67
4-2 Overview of the reaction and NMR chamber. 68
4-3 Target dimensions. 69
4-4 Distributed energy of the recoil nuclei into the recoil catcher. 71
4-5 Detailed geometry around the recoil catcher. 72
4-6 Magnetic shield for the β-ray detection system. 73
4-7 Typical time spectra of the β counting for (a) ^{8}Li and ^{8}B, (b) ^{12}B and ^{12}N. 75
4-8 Block diagram of the computer control. 77
4-9 Block diagram of the β-ray detection system. 78
4-10 Block diagram of the rf control system (2AP mode). 80
4-11 Block diagram of rf control system (2AP, 2rf mode 1). 81
4-12 Block diagram of rf control system (2AP, 2rf mode 2). 82
4-13 Timing chart of the rf control. 83
4-14 Rf resonator system. 84
4-15 Q-curve of the parallel resonator system. 86

4-16 Overview of the rf coil. 87
4-17 Time sequence program of the experiment (2AP mode). 89
4-18 Time sequence program of the experiment (8AP mode). 91
4-19 Time sequence program of the experiment (2rf (NNQR) mode). 93
4-20 The BN sample and its cleavage. 95
4-21 Photograph of the surface of the GaN crystal. 97

5-1 Detection of double quantum transition (DQ) of ^{12}B in BN. 100
5-2 Detection of DQ transition of ^{12}B in BN with a monochromatic rf. 101
5-3 Two single quantum (SQ) frequencies and the Larmor frequency ν_L as a function of the coupling constant (eqQ/h). 103
5-4 Typical NNQR spectrum for ^{12}B in BN. 104
5-5 Stacking of BN samples for a pulsed NMR study. 106
5-6 FT-NMR spectra of ^{11}B in BN at (a) $\alpha = 80°$, (b) $\alpha = 60°$ and (c) $\alpha = 0°$. 107
5-7 H_1 dependence of the NMR effect for ^{12}N in (a) BN and (b) GaN. 111
5-8 H_0 dependence of the asymmetry of the β-ray counting for ^{12}N. 112
5-9 Comparison with the maintained polarization of ^{12}N in GaN deduced from the H_0 dependence and the NMR. 114
5-10 Temperature dependence of the NMR effect for ^{12}N in BN. 115
5-11 H_1 dependence of the double quantum (DQ) transition for ^{12}N in (a) BN, (b) GaN and (c) AlN. 117
5-12 Detection of DQ transition of ^{12}N in BN. 118
5-13 Detection of DQ transition of ^{12}N in GaN. 119
5-14 Detection of DQ transition of ^{12}N in AlN. 120

5-15 Typical NNQR spectrum of ^{12}N in BN. 123
5-16 Typical NNQR spectrum of ^{12}N in GaN. 124
5-17 Typical NNQR spectrum of ^{12}N in AlN. 125
5-18 Typical FT-NMR spectra of ^{14}N in BN. 128
5-19 Typical FT-NMR spectrum of ^{14}N in GaN. 129
5-20 Typical β-NMR spectrum of ^{8}Li in $LiIO_3$. 132
5-21 Typical β-NMR spectrum of ^{8}Li in $LiNbO_3$. 133
5-22 Typical NNQR spectrum of ^{8}Li in $LiIO_3$. 135
5-23 Typical NNQR spectrum of ^{8}Li in $LiNbO_3$. 136
5-24 Typical FT-NMR spectrum of ^{7}Li in $LiIO_3$. 138
5-25 Typical FT-NMR spectrum of ^{7}Li in $LiNbO_3$. 139
5-26 FT-NMR signal of ^{7}Li in $LiIO_3$ and $LiNbO_3$ as a function of the orientation angle of the crystal *c*-axis relative to H_0. 140
5-27 Detection of DQ transition of ^{12}B in Mg with a monochromatic rf. 142
5-28 Typical β-NMR spectrum of ^{12}B in Pt with a monochromatic rf. 144
5-29 Typical NNQR spectrum of ^{12}B in Mg. 146
5-30 Typical NNQR spectrum of ^{8}B in Mg. 148

6-1 Density distribution of protons and neutrons in ^{8}B nuclei. 155
6-2 Density distribution of protons and neutrons in ^{8}Li nuclei. 156

A-1 Four different types of the unit-cell used in the calculations. 172
A-2 Energy scheme indicating the relative energies per unit cell (in eV) for various site occupations of N impurities in Mg. 173

ACKNOWLEDGMENTS

The author wishes to extend his thanks to all of those who have helped to make this work successful:

Professor T. Minamisono for his proposing the present experiment, providing earnest guidance during the work, and discussing the thesis.

Associated Professor Y. Nojiri for his constant collaboration, discussions, and encouragement.
Research Associate K. Matsuta for his constant collaboration, discussions, and encouragement.
Research Associate M. Fukuda for his constant collaboration, discussions, and encouragement.

Professor H. Sagawa for this study, which include the theoretical calculation, and for discussing.
Dr. H. Kitagawa for this study, which include the theoretical calculation, and for discussing.

Associated Professor N. Nakamura for discussing the FT-NMR spectrum
Research Associate S. Takeda for this studies, which including the FT-NMR and for discussing the FT-NMR spectrum.
Professor H. Akai for discussing and calculating the Hyperfine interactions of light impurities in metals.

Mr. Y. Takahashi for this technical supports during the present experiment and for the Van de Graaff Accelerator.

Mr. M. Sakamoto for this technical supports during the present experiment and for developing the experimental setup.
Mr. H. Iwata and T. Mizuta for this technical supports in the electronics during the present experiment.
Mr. K. Onishi for this computing supports during this experiment.

Dr. A. Kitagawa for this for his constant discussing and encouragement.
Y. Matsuo, I. Minami, Y. Someda, Y. Nakayama and T. Araki, all students, for their collaboration over a period of many years.
S. Fukuda, T. Izumikawa, M. Tanigaki, T. Miyake, T. Yamaguchi and K. Sato for their supports in the experiment.

Mr. Myers read this thesis and pointed out a lot of incorrect expressions.

Dr. H. Tanji and Dr. S. Suzuki who belong to Denki Kagaku Kogyo for offering and analyzing highly oriented BN crystals.
Mr. Toyoda and Mr. Anbe who belong to NGK for offering $LiIO_3$ single crystals.

Professor K. Asayama for discussing and operating the NMR of ^{14}N.
Mr. Ohmori, Mr. Sekine who belong to Mitsui-Toatsu Chemistry co. and Mr. Deguchi who belongs to Nihon Denshi co. for discussing and operating the NMR of ^{14}N.
Dr. H. Nakada for calculating the quadrupole moment of ^{12}N.

The present study was partly supported by the Fellowships of the Japan Society for the Promotion of Science for Japanese Junior Scientists.

Chapter 1

INTRODUCTION

The electric quadrupole moment of a nucleus is one of the best probes for studying the nuclear structure and nucleon-nucleon interactions. It gives the deviation of the electric charge distribution, i.e., the angular and radial nucleon distributions, in a nucleus from its spherically symmetric distribution [Mi92, Ki93]. It therefore directly gives the angular and radial distributions of valence nucleons in the nucleus, especially when its core is spherical.

Among others, the electromagnetic moments of nuclei in a 1p shell ($4 < Z, N < 16$) have been well studied both experimentally and theoretically. The nuclear properties, level energies, nuclear magnetic moments and nuclear quadrupole moments have been well reproduced by systematic shell model studies. The first such inclusive study concerning this 1p shell was carried out by Cohen and Kurath (CK) in 1965 [Co65]. In their framework they derived the effective nuclear interaction working in the 1p shell by fitting the known energy levels. Their success was because of only small configuration mixing effects in the wave functions of 1p-orbitals with those of 1d-orbitals. This suppression is due to the rather large energy difference between the 1p-orbitals and upper 1d-orbitals. Following their successes, the technique has been improved and expanded by many nuclear physicists to meet the present dramatically increasing precise nuclear data. Regarding the nuclear quadrupole moments of the nuclear ground states, the known values that are experimentally unambiguous are well reproduced by the CK wave functions in the harmonic-oscillator potential. For example, the quadrupole moments of ^{11}B, and ^{11}C are well reproduced theoretically by Sagawa and Kitagawa [Sa93]. Unfortunately,

although the quadrupole moments of ^{8}Li and ^{12}N are known, the values are not decisive, because of various experimental difficulties. It has also been understood that the values of ^{8}B and ^{12}N, even though we need them for the present aim of the study, may not be measured without developing some ingenious experimental techniques.

Owing to the recent experimental progress in producing unstable nuclear beams, new studies concerning unstable nuclei far from the stable line have become possible, and completely new nuclear phenomena have been disclosed. Among such studies, measurements of interaction cross sections of unstable nuclei at a high energy of 800A MeV with stable nuclei was started by Sugimoto and Tanihata at Lawrence Berkeley Laboratory [Ta85]. Based on this systematic study, a peculiar phenomenon, a huge neutron halo in the neutron-rich nucleus ^{11}Li, was discovered. An increase in the root mean square radius (rms radius) $\delta\langle r^2\rangle^{1/2}(^{11}\mathrm{Li}) = \langle r^2\rangle^{1/2}(^{11}\mathrm{Li}) - \overline{\langle r^2\rangle^{1/2}(^{11}\mathrm{Li})}$ reached as large as ~0.8 fm. Here, $\overline{\langle r^2\rangle^{1/2}(^{11}\mathrm{Li})}$ is the rms radius of ^{11}Li estimated from the known rms radii of the lighter Li isotopes [Ta85]. Several theoretical calculations with a Hartree-Fock model have been reported [Ta89], but they fail to reproduce the experimentally determined radii of neutron rich nuclei. Bertch et al. [Be89] pointed out the importance of the separation energies of valence nucleons; the density distribution of very shallowly bound nucleons in the nucleus is greatly extended outside the core formed by the rest nucleons. Their calculation was able to reproduce the interaction radii quite well in neutron rich nuclei.

Such halos, however, have been discovered only in neutron-rich nuclei, and not in proton-rich nuclei, by the interaction cross section measurements. Theoretically, it is understood that a prominent proton halo in proton rich nucleus is difficult to be formed since such a similar halo effect for protons is suppressed by the existence of repulsive Coulomb

force and/or centrifugal force in the nucleus [Ta89]. But, because of the charge symmetry of the nuclear force, a proton skin, no matter how thin it is, can be expected especially in the light proton rich nuclides. Therefore, not depending on whether a radial matter swelling exists or not, a very thin halo or skin must be experimentally confirmed.

To detect any effects, such a thin skin, by measuring the interaction cross sections is not very clever way, since it is mainly designed to detect total matter distributions, but not such thin-skin effects. In this cross section, the effects due to the skin is only a small fluctuation in the total cross section. On the other hand, an ingenious technique to measure the nuclear quadrupole moment of a proton-rich nucleus is especially suitable and sensitive for and to the skin effect, since the value is solely dependent on the radial and angular distributions of the last valence nucleons at the nuclear surface for a spherical nucleus.

Of specific interest is the mirror pairs of mass A = 8 and 12 systems: ^{8}Li, ^{8}B, ^{12}B and ^{12}N. The ^{8}B nucleus, whose quadrupole moment has not yet been studied, is one of the best candidates for a proton halo or skin, since the separation energy of the last proton is only 137keV, which is an extremely small value compared with a normal one which has ~8MeV for stable nuclei. The one-nucleon separation energies of the rest nuclides are also relatively small, as shown in Table 1-1. Regarding the nuclear quadrupole moments of the four nuclides, only the experimental value of ^{12}B, $Q(^{12}\mathrm{B})$, is reliably known [Mi78]. Since huge discrepancies are known among the reported values for each ^{12}N or ^{8}Li nuclides, $Q(^{12}\mathrm{N})$ [Ra80, Mi70] and $Q(^{8}\mathrm{Li})$ [Ac74, Mi75], the values of which are not precise enough for the present aim of studies must be experimentally remeasured to have conclusive values.

Regarding the experimental technique to measure the quadrupole moments, because all those interesting nuclides are β-emitting and short-

Table 1-1 Separation energy of the last nucleon in p-shell nuclei. $E_{sp}(N)$ is the one nucleon separation energy. Nuclei given by Bold characters nuclei are studied in the present experiment. Nuclei given by Italic characters nuclei are candidates that may have halos. Nuclei given by Bold italic characters are observed halo or skin structure that may have [Br86].

Nucleus	Z	N	I^π	E_{sp}(p) (MeV)	E_{sp}(n) (MeV)
^{6}He	2	4	0^+	—	*1.450 (2n)*
^{6}Li	3	3	1^+	—	—
^{7}Li	3	4	$3/2^-$	9.975	7.251
^{7}Be	4	3	$3/2^-$	5.607	—
^{8}He	2	6	0^+	—	*2.136 (2n)*
^{8}Li	3	5	2^+	12.454	**2.032**
^{8}B	5	3	2^+	**0.137**	13.021
^{9}Li	3	6	$3/2^-$	13.933	4.062
^{9}Be	4	5	$3/2^-$	16.886	—
^{9}C	6	3	$(3/2^-)$	*1.296*	—
^{10}Be	4	6	0^+	19.636	6.812
^{10}B	5	5	3^+	6.587	—
^{10}C	6	4	0^+	—	21.283
^{11}Li	3	8	$3/2^{(-)}$	—	*0.197 (2n)*
^{11}Be	4	7	$1/2^+$	—	*0.504*
^{11}B	5	6	$3/2^-$	11.228	11.453
^{11}C	6	5	$3/2^-$	8.689	13.122
^{12}Be	4	8	0^+	23.112	3.168
^{12}B	5	7	1^+	14.094	**3.370**
^{12}C	6	6	0^+	15.957	18.721
^{12}N	7	5	1^+	**0.601**	—
^{13}B	5	8	$3/2^-$	—	4.878
^{13}C	6	7	$1/2^-$	17.533	4.946
^{13}N	7	6	$1/2^-$	1.943	20.063
^{13}O	8	5	$(3/2^-)$	*1.516*	—
^{14}Be	4	10	0^+	—	*1.479 (2n)*
^{14}B	5	9	2^-	—	*0.969*
^{14}C	6	8	0^+	20.831	8.176
^{14}N	7	7	1^+	7.551	10.554
^{14}O	8	6	0^+	4.628	23.175
^{15}B	5	10	$3/2^-$	18.059	2.765
^{15}C	6	9	$1/2^+$	21.080	1.218
^{15}N	7	8	$1/2^-$	10.208	10.832
^{15}O	8	7	$1/2^-$	7.296	13.222

lived, the best way is to observe the quadrupole effects in the β-NMR spectra. The conventional β-NMR technique developed by K. Sugimoto et al.[Su66], and very much improved by T. Minamisono et al [Mi73], is well known to be very efficient for studying the magnetic interaction of nuclei with an external strong magnetic field. However, the method was not efficient for detecting quadrupole effects in β-NMR spectra due to the wide spread of NMR spectra caused by the quadrupole interaction. To improve the conventional β-NMR towards an efficient measurement of the quadrupole effects, some ingenious experimental techniques must be added to the NMR method, which is essentially based on the following four steps: 1) the production of polarized β-emitting nuclei through a nuclear reaction, 2) the preservation of its polarization by using a static strong magnetic field and implantation of polarized nuclei in a suitable media, 3) the observation of nuclear polarization based on the asymmetric β-ray distribution from the polarized nuclei, and 4) the resonant destruction of nuclear polarization by a radio-frequency (rf) magnetic fields. Furthermore for the success of the present quadrupole interaction studies, in addition to the above four steps, we must obtain well defined electric field gradients with which the nuclides interact. Such suitable fields must be looked for experimentally, for example, in various metal and /or insulator crystals.

The quadrupole spectrum of a nuclide with nuclear spin I interacting with a unique electric field gradient at high field splits into $2I$ NMR-lines. This means that the detection of the one line among the $2I$ lines by an rf magnetic field gives only a partial destruction of the whole polarization. For example, such an partial NMR for $I = 1$ case is only one fourth of the case when a perfect destruction of polarization is obtained for the spin I. For the nuclides with higher spin I, the NMR effect is less detectable.

In order to solve this experimental difficulty in the present study, an ingenious new technique, the New Nuclear Quadrupole Resonance

technique (NNQR), was developed [So90, Mi93]. In this technique, all of the transition frequencies that correspond to a quadrupole coupling frequency, that is $2I$ rf's for spin I, are applied simultaneously during an rf application time in order to destroy the entire polarization. The NMR spectrum is detected as a function of coupling frequency. Here a set of $2I$ rf's is theoretically given for an electric quadrupole coupling frequency, if the Larmor frequency, the crystal orientation and the symmetry of the field gradients are known based on other experiments. The change in the polarization under the right quadrupole coupling frequency is maximum, and the original polarization is completely destroyed. With this new method, the efficiency of the NMR detection has been greatly improved; an one-day NNQR detection for the spin $I = 1$ case is equivalent to an entire month of measurement using the conventional technique. For the nuclides with higher spin I, therefore, the present NNQR is more efficient than the conventional β-NMR.

In addition to the measured coupling constant, we need to measure the electric field gradient at the probe nucleus experimentally, in order to extract the nuclear quadrupole moment from the coupling constant. This measurement is necessary because it is very difficult to estimate the electric field gradient theoretically in solid at the present stage where the environment surrounding the implanted nuclide is not known well. In the present study, we used proper crystals as implantation media containing stable isotopes of the implanted nuclei [Mi74]. Since the majority of the implanted nuclei that can be handled by the present NMR method sit in the substitutional sites of their isotopes in insulator crystals that contains the isotopes of the implanted nuclides, they are naturally exposed to the same electric field gradient that the stable isotopes are exposed to. Therefore the electric field gradient is measured by detecting the Fourier-Transformed NMR technique (FT-NMR) [Fu81] of each stable isotope in each crystals.

In this paper we report on studies concerning the quadrupole effects of ^{8}Li in $LiIO_3$ and $LiNbO_3$, the effects of ^{12}B and ^{8}B in highly oriented BN and single crystal Mg and, finally, the effects of ^{12}N in BN, GaN and AlN. We also report on the FT-NMR detection of ^{7}Li in $LiIO_3$ and $LiNbO_3$, ^{11}B in BN , and ^{14}N in BN and GaN crystals. Based on these results, the quadrupole moments of ^{8}Li, ^{8}B, ^{12}B and ^{12}N are deduced. Also, the NNQR technique and the first fruits produced by the newly developed method are given. In the following chapter (chapter 2), given are the definition of the quadrupole moment and a recent investigation of the quadrupole moment in the p-shell nuclei. The principle of the β-NMR detection is presented in chapter 3. The experimental set up is summarized in chapter 4. The experimental results are summarized in chapter 5. The results of the present experiment are discussed in chapter 6 in connection with the hyperfine interactions and the nucleon distribution in nucleus.

Chapter 2

THEORETICAL BACKGROUND CONCERNING THE ELECTRIC QUADRUPOLE MOMENTS

2-1 Quadrupole moments of A = 8 and 12 systems given by the jj model

The electric quadrupole moment is a measure of the extent to which the nuclear charge distribution deviates from spherical symmetry. The moment is defined by [Bo69]

$$Q = \left\langle I, M = I \middle| Q_{op} \middle| I, M = I \right\rangle , \tag{2-1}$$

where the quadrupole operator is given by

$$eQ_{op} = \int \rho_e(\vec{r}) r^2 \left(3\cos^2\theta - 1\right) dv , \tag{2-2}$$

in terms of the charge density ($\rho_e(\vec{r})$) in the nucleus.

In the shell-model description, for a single proton in an orbit (nlj), one obtains

$$\begin{aligned} Q_{sp} &= \left\langle j, m = j \middle| r^2 \left(3\cos^2\theta - 1\right) \middle| j, m = j \right\rangle \\ &= 2\langle jj20|jj\rangle \langle j\tfrac{1}{2}20|j\tfrac{1}{2}\rangle \left\langle j \middle| r^2 \middle| j \right\rangle \\ &= -\frac{2j-1}{2j+2} \left\langle j \middle| r^2 \middle| j \right\rangle , \end{aligned} \tag{2-3}$$

where the radial average is given by

$$\left\langle j \middle| r^2 \middle| j \right\rangle = \int r^4 R_{nl}^2 dr . \tag{2-4}$$

Here, R_{nl} is the radial wave function.

Since neutrons carry no electric charge in this model, the quadrupole moment vanishes for a single-neutron configuration. However, in fact, the nuclei that have a single-neutron configuration have finite values of the quadrupole moment. One good example is the ground state of ^{17}O(I^π = 5/2$^+$). ($Q_{exp}(^{17}\mathrm{O})$ = –26mb, $Q_{sp}(\mathrm{d}_{5/2})$ = –66mb [Bo69]) This is because the nucleus cannot be described by such a simple configuration. The

configuration mixing of the nucleons must be considered in nuclei. The effective charge of a nucleon in a nucleus is introduced in order to include this effect. This effective charge has been investigated in every nuclear shell region to account for the quadrupole moment and the E2 electric properties, e.g., the transition probability of γ-ray E2 transition.

Since ^{8}Li, ^{8}B, ^{12}B and ^{12}N are odd-odd nuclei, it is thus necessary to consider an additivity rule by using simple angular momentum recoupling techniques [de63, He90]. If the proton and the neutron states are defined by $|j_p\rangle$ and $|j_n\rangle$ and their corresponding electric quadrupole moments are described by $Q(j_p)$ and $Q(j_n)$, respectively, the quadrupole moment of an odd-odd nucleus is obtained as follows using the assumption of weak coupling in obtaining the eigenstate $|j\rangle = |j_p \otimes j_n; j\rangle$:

$$\begin{aligned} Q(J) = &\begin{pmatrix} J & 2 & J \\ -J & 0 & J \end{pmatrix} (-)^{J_p + J_n + J} (2J+1) \\ &\times \left[\begin{Bmatrix} J_p & J & J_n \\ J & J_p & 2 \end{Bmatrix} \frac{Q(J_p)}{\begin{pmatrix} J_p & 2 & J_p \\ -J_p & 0 & J_p \end{pmatrix}} + \begin{Bmatrix} J_n & J & J_p \\ J & J_n & 2 \end{Bmatrix} \frac{Q(J_p)}{\begin{pmatrix} J_n & 2 & J_n \\ -J_n & 0 & J_n \end{pmatrix}} \right] . \end{aligned} \tag{2-5}$$

For an A = 8 isospin pair, the last two nucleons are in $p_{3/2}$ orbitals for both a proton and a neutron. For an A = 12 isospin pair, last nucleons are in $p_{3/2}$ and $p_{1/2}$ orbitals for a proton and a neutron, respectively, for ^{12}B and, vice versa, for ^{12}N. The electric quadrupole moments with a single particle description are thus calculated, and are shown in Table 2-1 along with the experimental values.

This table shows that the single-particle description is not suitable for the electric quadrupole moment in this region at all. In this framework, the theoretical values for the present A = 8 system are all zero in spite of the large experimental values.

Table 2-1 Quadrupole moments given by the single-particle model. Here, $\langle r^2\rangle_p^{1/2} = 2.5$ fm is assumed to calculate Q_{sp}. The sign of Q_{sp} for ^{11}B and ^{12}B are suggested to the hole states $(\pi p_{3/2})^{-1}$.

A	nucleus	$I\pi$	Q_{sp} (mb)	Q_{exp} (mb)	reference
8	^{8}Li	2^+	0	(+) 32.7 ± 0.6	present
	^{8}B	2^+	0	(+) 68.7 ± 2.1	present
11	^{11}B	$3/2^-$	+25	+40.59 ± 0.10	[Su91]
	^{11}C	$3/2^-$	0	+33.27 ± 0.24	[Su92]
12	^{12}B	1^+	+10	(+) 13.20 ± 0.25	present
	^{12}N	1^+	0	(+) 10.3 ± 0.7	present

2-2 Advanced shell-model description

Kitagawa and Sagawa performed a shell-model calculation for the nuclides in the 1p-shell region using the Cohen-Kurath and Millener-Kurath model with effective interactions CKPOT and CKI [Ki93a]. They employed the proton-neutron formalism in order to take into account the difference between protons and neutrons in the shell-model wave functions. The quadrupole moment is defined as a diagonal matrix element of the E2 operator:

$$M(E2) = \sum_{\pi} e_p^{eff}\left(\tfrac{1}{2} - t_{z,i}\right) r_i^2 Y_{2,\mu}(\hat{r}_i) + \sum_{\nu} e_n^{eff}\left(\tfrac{1}{2} + t_{z,i}\right) r_i^2 Y_{2,\mu}(\hat{r}_i) \quad . \tag{2-6}$$

Here t_z is the isospin operator. The values of $e_p{}^{eff}$ and $e_n{}^{eff}$ are the effective charges of protons and neutrons in the nucleus, respectively. The quadrupole moment can be expressed by the one-particle spectroscopic factors as,

$$\begin{aligned} eQ = & \sum_{j_1, j_2, \alpha_C, J_C, T_C, t_{z1}, t_{z2}} \sqrt{\tfrac{16}{5}\pi}\left\langle j_1 \middle\| r^2 Y_2 \middle\| j_2 \right\rangle \frac{1}{\sqrt{2J+1}(2T+1)} (-)^{T_C + \frac{1}{2} - T + 2J} \\ & \times \delta_{t_{z1}, t_{z2}} \left\langle t_{z1} \middle| \begin{Bmatrix} e^{IS} \\ e^{IV}\tau_3 \end{Bmatrix} \middle| t_{z2} \right\rangle \left\langle T_C M_{TC} \tfrac{1}{2} t_{z1} \middle| T M_T \right\rangle^2 \\ & \times \langle JJ20|JJ\rangle \begin{Bmatrix} J & j_2 & J_C \\ j_1 & J & 2 \end{Bmatrix} \\ & \times \left\langle JT \middle\| a_{j_1}^{\dagger} \middle\| a_C J_C T_C \right\rangle \left\langle a_C J_C T_C \middle\| \tilde{a}_{j_2} \middle\| JT \right\rangle \end{aligned} \quad , \tag{2-7}$$

where the isoscalar and isovector effective charges are defined as

$$e^{IS} = \tfrac{1}{2}\left(e_\pi^{eff} + e_\nu^{eff}\right) \text{ and}$$
$$e^{IV} = \tfrac{1}{2}\left(e_\pi^{eff} - e_\nu^{eff}\right) \quad . \tag{2-8}$$

They used two kinds of single-particle wave functions, i.e., those in harmonic oscillator (HO) and in Woods-Saxon (WS) potentials. They considered the separation energy of the valence nucleon to account for the experimental values. The single-particle wave function for a valence nucleon was determined by adjusting the depth of the WS potential so as to reproduce the separation energy for each configuration. The effective charges were taken from empirical values, $e_p{}^{eff} = 1.3e$ and $e_n{}^{eff} = 0.5e$, given by the E2 giant quadrupole resonance in these region [Sa84]. The calculation are discussed along with the experimental value in Chapter 6.

Another investigation concerning the 1p-shell nuclei with the shell-model description was carried out by Nakada et al. [Na93]. Their study was a development of the large-scale shell model by Wolters et al. [Wo90]. It involved a shell model calculation in $(0+2)\hbar\omega$ model space. They determined the wave functions in order to fit the experimental energy levels, including the binding energies, of the A = 4-16 nuclei. The advantage of their method is that since their description includes the configuration mixings up to $2\hbar\omega$, it is not necessary to introduce any effective charges. However, it must be noted that in their view a core

excitation (deformation) occurs considerably, even in the spherical region. This means that the wave functions that they used are not sufficiently suitable. Moreover, this model fails to reproduce the experimental nucleon radius determined by the interaction cross section [Sa94]. Further improvement on their model may be needed.

2-3 Known quadrupole moment values of ^{8}Li and ^{12}N

The discrepancy between the two data concerning the quadrupole moment $Q(^{8}\mathrm{Li})$, i.e., one reported by Ackermann [Ac74] using the hyperfine interaction of ^{8}Li in $LiNbO_3$ and the other by Minamisono et al. [Mi75] using the hyperfine interaction in $LiIO_3$, has been an open problem. It therefore prevents us from studying the nuclear structure of the nucleus. In order to solve this problem, we studied the hyperfine interactions of ^{8}Li in both $LiIO_3$ and $LiNbO_3$ using a newly developed β-NMR method, New Nuclear Quadrupole Resonance technique (NNQR). Additionally, the electric field gradients for both the cases were measured by using the FT-NMR method for calibration.

Radutsukiĭ et al. [Ra80] obtained the quadrupole moment of ^{12}N from the analyses of the energy dependence of the cross section of the pion photoproduction near the threshold during studies of the $^{12}\mathrm{C}(\gamma, \pi^{+})^{12}\mathrm{B}$ and $^{12}\mathrm{C}(\gamma, \pi^{-})^{12}\mathrm{N}$ reactions. Using current algebra, the energy dependence of the cross section of these reactions can be also strongly connected with the electromagnetic properties of these nuclei. They deduced the quadruple moment of ^{12}N as being $Q(^{12}\mathrm{N}) = +49\mathrm{mb}$. However, since this result is far from any predictions obtained from the hyperfine studies [Mi72, Mi94], it has become necessary to measure the quadrupole moment by a more direct method. In this experiment, the quadrupole moment of ^{12}N was measured spectroscopically for the first time. A comparison with these measured value will be made in chapter 6.

Chapter 3

EXPERIMENTAL METHOD

3-1 NMR

1) Nuclear magnetic resonance

In a static magnetic field (H_0), the Hamiltonian of a nuclear spin I with a magnetic moment of $\bar{\mu} = \gamma_N h\bar{I} = g\mu_N\bar{I}$ can be written as

$$H_M = -\bar{\mu}\cdot\bar{H}_0 = -g\mu_N\bar{H}_0\cdot\bar{I} \ . \qquad (3\text{-}1)$$

The eigenstates of this Zeeman Hamiltonian are split into $2I$ states characterized by the magnetic quantum numbers $m = I, I-1, \ldots, -I$, i.e., $|-I\rangle$, $|-I+1\rangle, \ldots, |I-1\rangle, |I\rangle$. The energies of these states are

$$E_M(m) = -\mu H_0 m \ . \qquad (3\text{-}2)$$

When a photon corresponding to the energy difference between the $|m\rangle$ and $|m-1\rangle$ substates are applied, a transition between these states occurs with the resonant absorption of a photon. For a pure Zeeman split, all of the resonance energies between neighboring states ($\Delta m = 1$) are equal. This resonance frequency is called the "Larmor frequency" ν_L. Fig. 3-1 shows the energy levels as well as a resonance peak for a typical pure Zeeman Hamiltonian.

This phenomenon can be described by classical dynamics. A nuclear spin precesses around the direction of the external magnetic field with an angular frequency of ω_L (Fig. 3-2),

$$\omega_L = \gamma_N H_0 \ . \qquad (3\text{-}3)$$

For the NMR, a rotating magnetic field (H_1) perpendicular to an external field with an angular frequency of ω is applied to this system. In a rotating frame fixed to the H_1 field, the spin must rotate around the effective magnetic field (H_{eff}), as shown in Fig. 3-2. Here, H_{eff} is composed of H_1 and the reduced z component, $(\bar{H}_0 - \bar{\omega}/\gamma_N)$. If ω coincides with ω_L (the on

Energy levels in the Zeeman Hamiltonian for I=1.

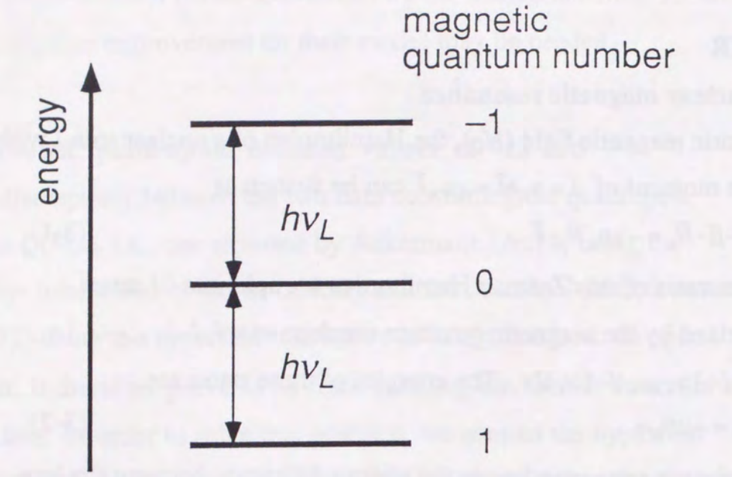

Resonance frequency of the transition $\Delta m = 1$

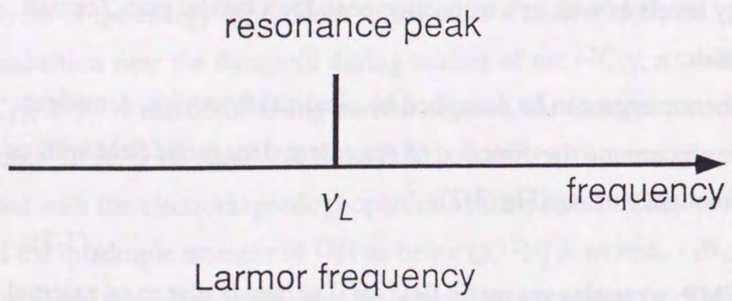

Figure 3-1 Energy levels in Zeeman Hamiltonian for I=1.

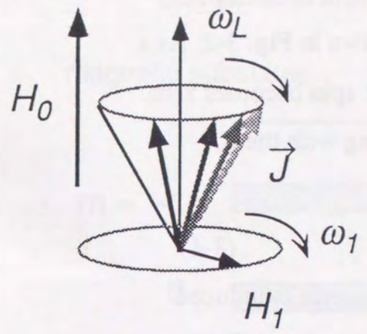

A spin is precessing around the external field H_0 by angular velocity ω_L

Rotating field H_1 (ω_1) is applied perpendicular to H_0 ($\omega_1 \sim \omega_L$)

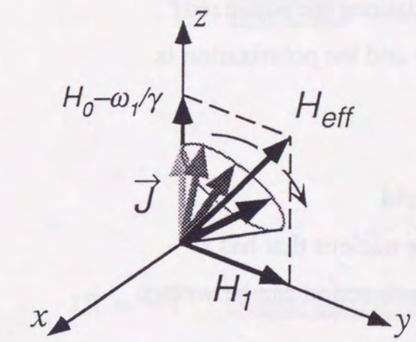

In the rotating frame fixed to H_1 The spin is precessing around H_{eff}

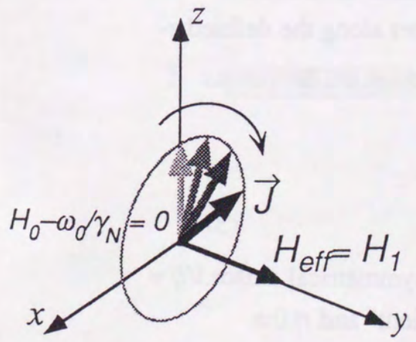

When $\omega_1=\omega_L$, the spin is precessing around H_1: hence, $\langle J_z \rangle = 0$

Figure 3-2 Classical view of NMR:
the spin movement in a magnetic field and resonance phenomena.

resonance condition), the reduced z component of the spin becomes zero and, therefore, the spin should rotate around H_1 as shown in Fig. 3-2. As a result, the expectation value of the z-component of the spin becomes zero. The polarization (P) of a spin ensemble is defined along with the populations (a_m) of the magnetic substates (m) as

$$P = \frac{\langle I_z \rangle}{I} = \frac{1}{I}\sum_m m \cdot a_m \quad , \tag{3-4}$$

where the a_m are normalized as $\sum a_m = 1$. When a resonance is induced between two levels, the populations of both levels are equalized. For a pure magnetic interaction case, all of the substate populations are equalized simultaneously by applying the Larmor frequency and the polarization is destroyed completely as seen in Fig. 3-3.

2) Electric quadrupole interaction in high field

If an electric field gradient (q) interacts with the nucleus that has a quadrupole moment (Q), the Hamiltonian of this interaction can be written as follows

$$H_Q = \frac{eqQ}{4I(2I-1)}\left\{3I_z^2 - I(I+1) + \frac{\eta}{2}\left(I_+^2 + I_-^2\right)\right\} . \tag{3-5}$$

Here, $I_\pm$ are the ascending and descending operators along the defined z-axis. Also, the parameters of the electric field gradient are defined as

$$q = V_{zz} \quad ,$$
$$\eta = \frac{V_{xx} - V_{yy}}{V_{zz}} \quad ,$$
$$|V_{zz}| \geq |V_{yy}| \geq |V_{xx}| \quad , . \tag{3-6}$$

The X, Y and Z axes are the principal axes of the symmetrical tensor $Vij = \frac{\partial^2 E}{\partial i \partial j}$. In this paper we call q the "electric field gradient" and η the "asymmetry factor". In general, the principal axes of the electric field gradient are not necessarily identical to the external magnetic field. To transform the axes, the Euler angle is adopted, as shown in Fig. 3-4. With this transformation, the total Hamiltonian is described as follows:

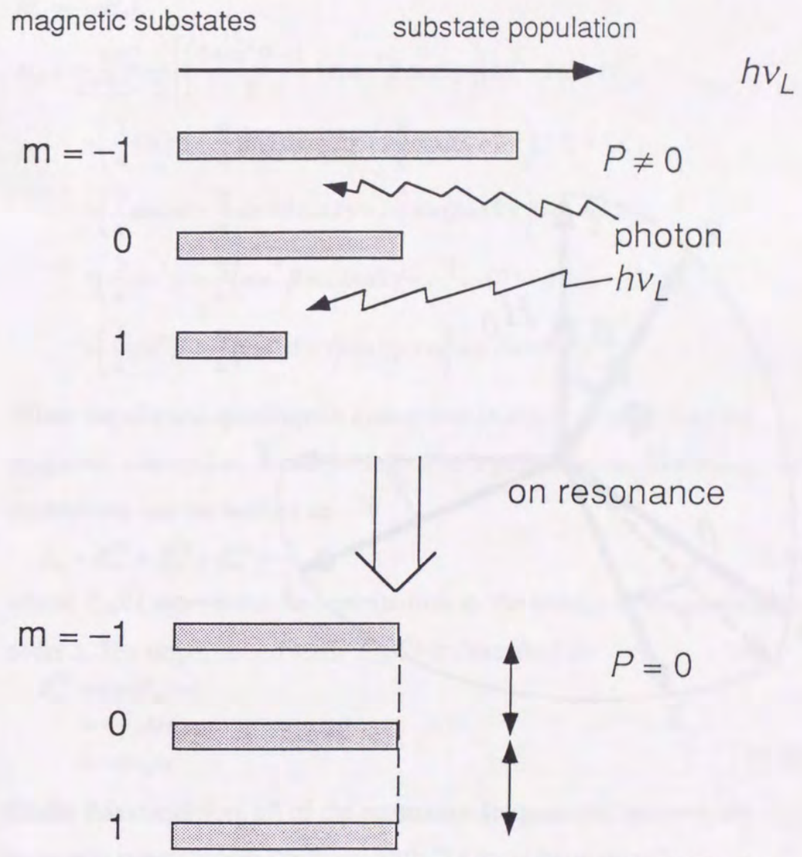

Figure 3-3 Quantum mechanical explanation of the NMR for polarized nuclear spin ensemble.

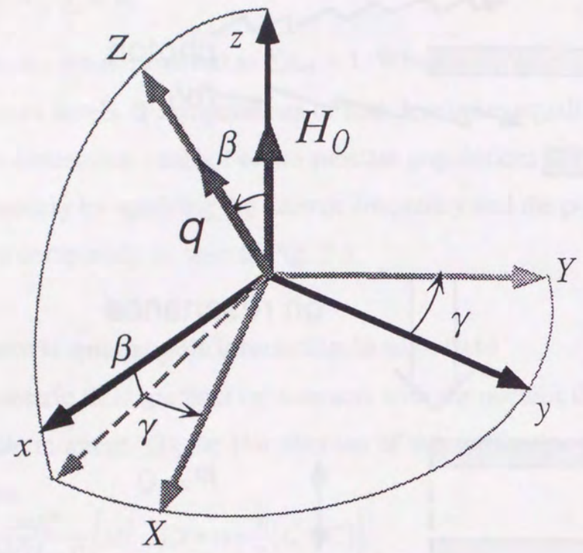

Figure 3-4 Definition of Euler angles.

X,Y, Z are the principal axes of the electric field gradient.

$q = V_{zz}$ is the largest component of the electric field gradient.

$$H = H_M + H_Q$$

$$H_M = -\mu H_0 I_z$$

$$\begin{aligned} H_Q = \frac{eqQ}{4I(2I-1)}\Bigg[& \left(\frac{3\cos^2\beta-1}{2}+\eta\sin^2\beta\cos 2\gamma\right)\left\{3I_z^2 - I(I+1)\right\} \\ & +\left(\frac{3}{4}\sin 2\beta - \frac{\eta}{4}\sin 2\beta\cos 2\gamma + i\frac{\eta}{2}\sin\beta\sin 2\gamma\right)(I_+I_z + I_zI_+) \\ & +\left(\frac{3}{4}\sin 2\beta - \frac{\eta}{4}\sin 2\beta\cos 2\gamma - i\frac{\eta}{2}\sin\beta\sin 2\gamma\right)(I_-I_z + I_zI_-) \\ & +\left(\frac{3}{4}\sin^2\beta + \frac{\eta}{4}\left(\cos^2\beta+1\right)\cos 2\gamma - i\frac{\eta}{2}\cos\beta\sin 2\gamma\right)I_+^2 \\ & +\left(\frac{3}{4}\sin^2\beta + \frac{\eta}{4}\left(\cos^2\beta+1\right)\cos 2\gamma + i\frac{\eta}{2}\cos\beta\sin 2\gamma\right)I_-^2\Bigg] \end{aligned} \quad (3\text{-}7)$$

When the electric quadrupole interaction is much smaller than the magnetic interaction, it can be treated as a perturbation. The energy of eigenstates can be written as

$$E_m = E_m^{(0)} + E_m^{(1)} + E_m^{(2)} + \cdots , \quad (3\text{-}8)$$

where $E_m^{(i)}$ represents the contribution to the energy of the perturbation of order i. The unperturbed term $E_m^{(0)}$ is described as

$$\begin{aligned} E_m^{(0)} &= \langle m|H_M|m\rangle \\ &= -\gamma_N \hbar H_0 m \\ &= -h\nu_L m \end{aligned} . \quad (3\text{-}9)$$

Under this condition, all of the resonance frequencies between the magnetic substates are the same with "Larmor frequency ",

$$\nu_L = \frac{g\mu_N}{h}H_0 . \quad (3\text{-}10)$$

According to first-order perturbation calculation, the contribution to the energy of the magnetic substates m is given as

$$\begin{aligned} E_m^{(1)} &= \langle m|H_Q|m\rangle \\ &= \frac{\nu_Q}{6}\left(\frac{3\cos^2\beta-1}{2}+\eta\sin^2\beta\cos 2\gamma\right)\left\{3m^2 - I(I+1)\right\} , \end{aligned} \quad (3\text{-}11)$$

where $\nu_Q = \dfrac{3eqQ}{2I(2I-1)h}$ is the coupling frequency of the quadrupole interaction.

According to second-order perturbation calculation, the second order energy shift is given as,

$$E_m^{(2)} = \sum_m{}' \frac{\langle m|H_Q|n\rangle\langle n|H_Q|m\rangle}{E_n - E_m} \quad , \tag{3-12}$$

where $\sum_m{}'$ means summation over n, except for m ($n \neq m$). For nuclear spin $I = 1$, the second-order contribution for each magnetic substate (m) can be derived as

$$E_1^{(2)} = -E_{-1}^{(2)} = -\frac{1}{18}\frac{h\nu_Q^2}{\nu_L}(B+C)$$
$$E_0^{(2)} = 0 \quad . \tag{3-13}$$

Here,

$$B = \left(\tfrac{3}{4}\sin^2\beta + \tfrac{\eta}{4}(\cos^2\beta + 1)\cos 2\gamma\right)^2 + \left(\tfrac{\eta}{2}\cos\beta\sin 2\gamma\right)^2$$
$$C = \left(\tfrac{3}{4}\sin 2\beta - \tfrac{\eta}{4}\sin 2\beta\cos 2\gamma\right)^2 + \left(\tfrac{\eta}{2}\sin\beta\sin 2\gamma\right)^2 \quad . \tag{3-14}$$

On the other hand, for a nuclear spin $I = 2$, the second-order contribution for each magnetic substate (m) can be derived as

$$E_2^{(2)} = -E_{-2}^{(2)} = -\frac{h\nu_Q^2}{\nu_L}(B+3C)$$
$$E_1^{(2)} = -E_{-1}^{(2)} = -\frac{h\nu_Q^2}{\nu_L}\left(\frac{B}{2} + \frac{5}{6}C\right)$$
$$E_2^{(2)} = 0 \quad . \tag{3-15}$$

The changes in the energies for these first- and second-order perturbation calculations are schematically shown in Fig. 3-5. Finally, the transition frequency between m and m–1 substates is given as follows. Instead of a single Larmor line, $2I$ NMR lines (ν_m) are observed,

$$\nu_m = \frac{E_{m-1} - E_m}{h}$$
$$= \nu_L + \nu_m^{(1)} + \nu_m^{(2)} \quad . \tag{3-16}$$

The first-order contribution in the frequency ($\nu_m{}^{(1)}$) is given by

$$\nu_m^{(1)} = \frac{E_{m-1}^{(1)} - E_m^{(1)}}{h}$$
$$= -\nu_Q\left(m - \frac{1}{2}\right)\left(\frac{3\cos^2\beta - 1}{2} + \eta\sin^2\beta\cos 2\gamma\right) \quad . \tag{3-17}$$

They are distributed at constant intervals, and symmetrical around ν_L as shown in Fig. 3-5.

The second-order contribution is also added as

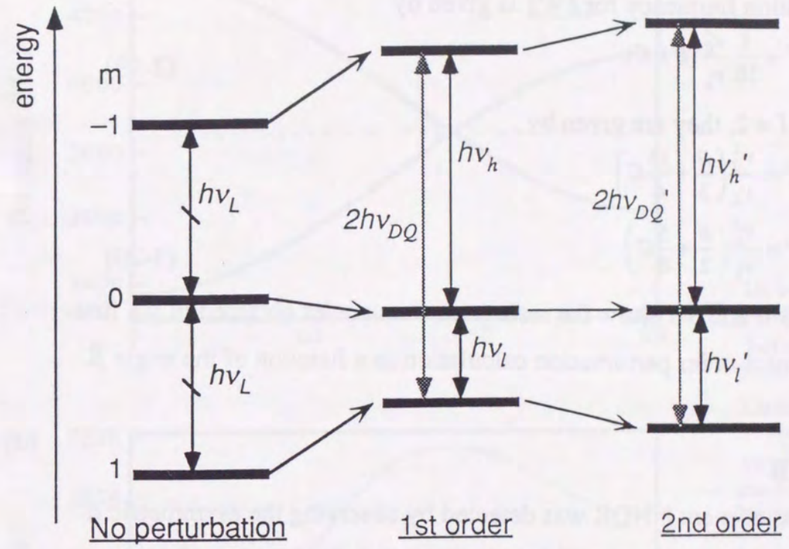

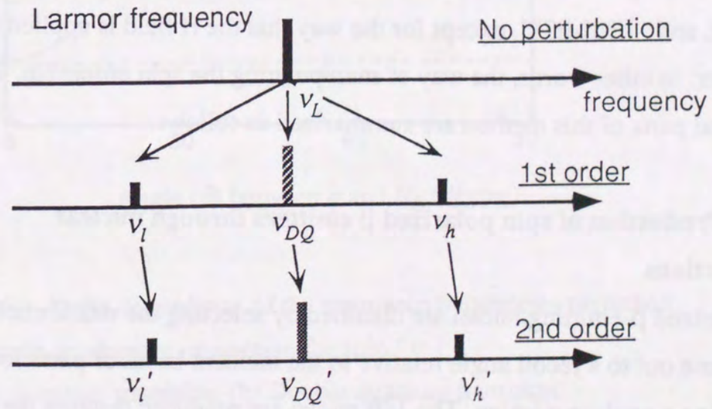

Figure 3-5 Energy levels and transition frequencies for spin $I = 1$ nuclei perturbed by an electric quadrupole interaction.

$$\nu_m^{(2)} = \frac{E_{m-1}^{(2)} - E_m^{(2)}}{h} \quad . \tag{3-18}$$

Each transition frequency for $I = 1$ is given by

$$\nu_1^{(2)} = \nu_0^{(2)} = \frac{1}{18}\frac{\nu_Q^2}{\nu_L}(B+C) \quad . \tag{3-19}$$

Regarding $I = 2$, they are given by

$$\nu_2^{(2)} = \nu_{-1}^{(2)} = \frac{\nu_Q^2}{\nu_L}\left(\frac{B}{2}+\frac{13}{6}C\right)$$

$$\nu_1^{(2)} = \nu_0^{(2)} = \frac{\nu_Q^2}{\nu_L}\left(\frac{B}{2}+\frac{5}{6}C\right) \quad . \tag{3-20}$$

Figures 3-6 and 3-7 show the resonance frequencies obtained in the first- and the second-order perturbation calculation as a function of the angle β.

3-2 β-NMR

In this experiment NNQR was detected by observing the asymmetric β decay of the polarized nuclei (β-NMR method) as the function of the quadrupole coupling frequency. It is essentially the same as the conventional β-NMR method used in previous studies concerning ^{17}F [Mi74], and ^{12}B [Mi78], except for the way that the rf field is applied for NMR or, in other words, the way of manipulating the spin ensemble. The essential parts of this method are summarized as follows:

1) Production of spin polarized β emitters through nuclear reactions

Polarized β-emitting nuclei are obtained by selecting the recoil nuclei that come out to a recoil angle relative to the incident beam of particle following a nuclear reaction. The ^{12}B nuclei are produced through the ^{11}B (d, p) ^{12}B reaction with a 1.5 MeV deuteron beam. The polarization reaches 12% at a recoil angle of 40 ± 5 degrees relative to the direction of the incident beam [Ta76]. The ^{12}N nuclei are produced through the ^{10}B

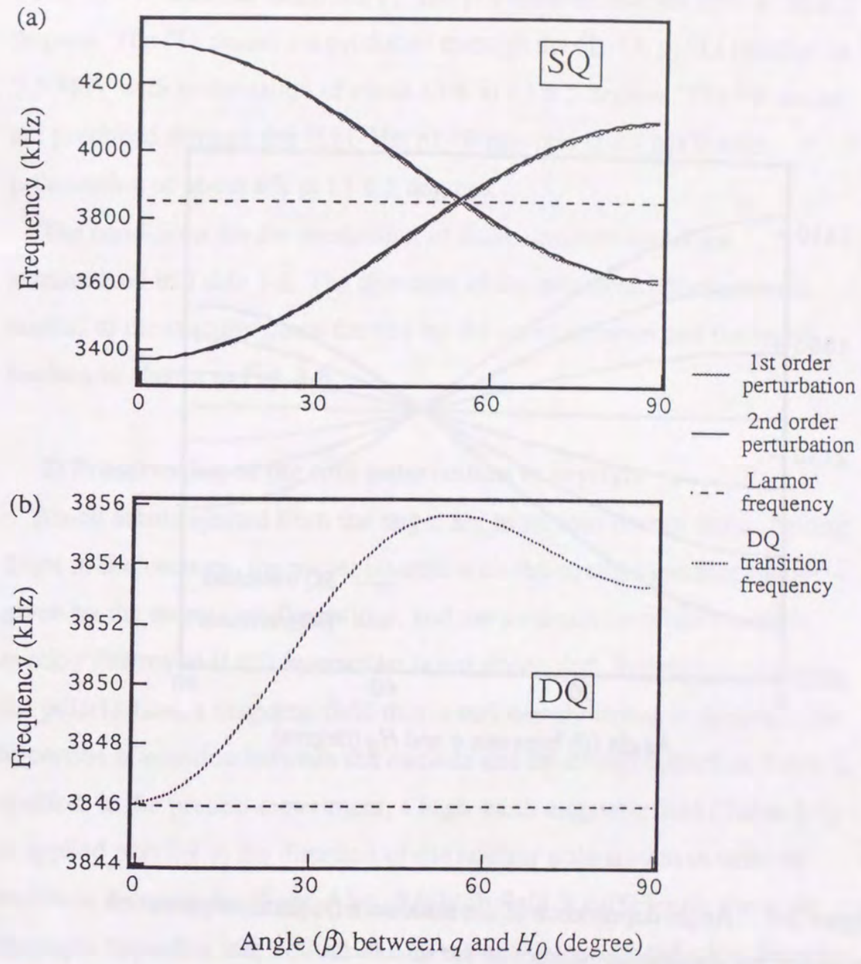

Figure 3-6 Angle dependence of the resonance frequencies perturbed by an electric quadrupole interaction for spin $I = 1$.
(a) Single quantum transition. (b) Double quantum transition.

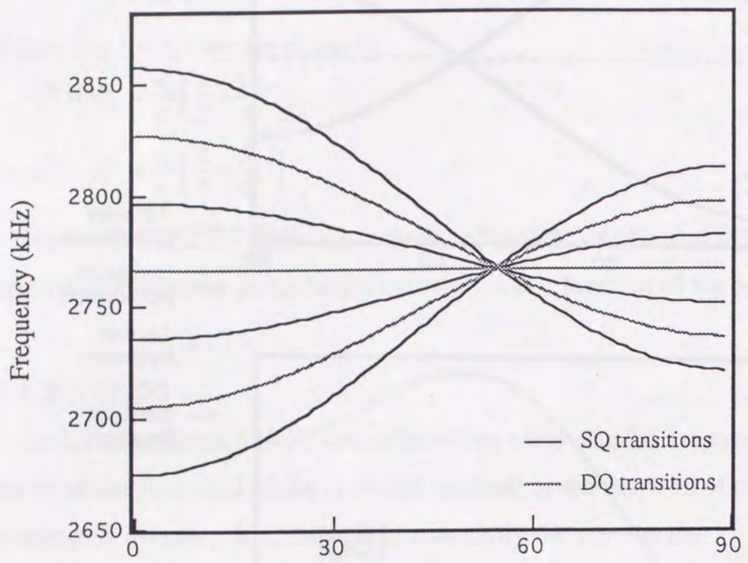

Figure 3-7 Angle dependence of the resonance frequencies perturbed by an electric quadrupole interaction for spin $I = 2$.

(^{3}He, n) ^{12}N reaction at 3.0 MeV. The polarization reaches 20% at 20 ± 5 degrees. The ^{8}Li nuclei are produced through the ^{7}Li (d, p) ^{8}Li reaction at 3.5 MeV with polarization of about 12% at 13 ± 5 degrees. The ^{8}B nuclei are produced through the ^{6}Li (^{3}He, n) ^{8}B reaction at 4.7 MeV with polarization of about 6% at 13 ± 5 degrees.

The conditions for the production of these unstable nuclei are summarized in Table 3-1. The direction of the produced polarization is normal to the reaction plane formed by the incident beam and the recoil nucleus as shown in Fig. 3-8.

2) Preservation of the spin polarization in crystals

Recoil atoms ejected from the target are in various charge states. During flight in the vacuum, the nuclei interact with the strong hyperfine fields given by the atomic configurations, and the polarization of the nuclei is quickly destroyed if this interaction is not decoupled. In order to maintain the polarization, a magnetic field that is sufficiently strong to decouple the hyperfine interaction between the nucleus and its atomic hyperfine fields is applied. In the present experiment, a high static magnetic field (Table 3-1) is applied parallel to the direction of the nuclear polarization in order to maintain it during the flight. Also, this high field is sufficiently strong to decouple hyperfine interactions due to various defects or radiation damages created in the crystal at room temperature during the last stage of implantation.

In order to achieve NMR detection, the recoil nuclei are implanted into a catcher crystal to stop them in it and to expose them in a well defined electric field gradient. Implanted nuclei are mainly located in a substitutional site of the stable isotopes in the insulator crystal. The ^{8}Li nuclei was located in a Li site, the ^{12}B nuclei in a B site and the ^{12}N nuclei in a N site. The polarization of the implanted nuclei located in the

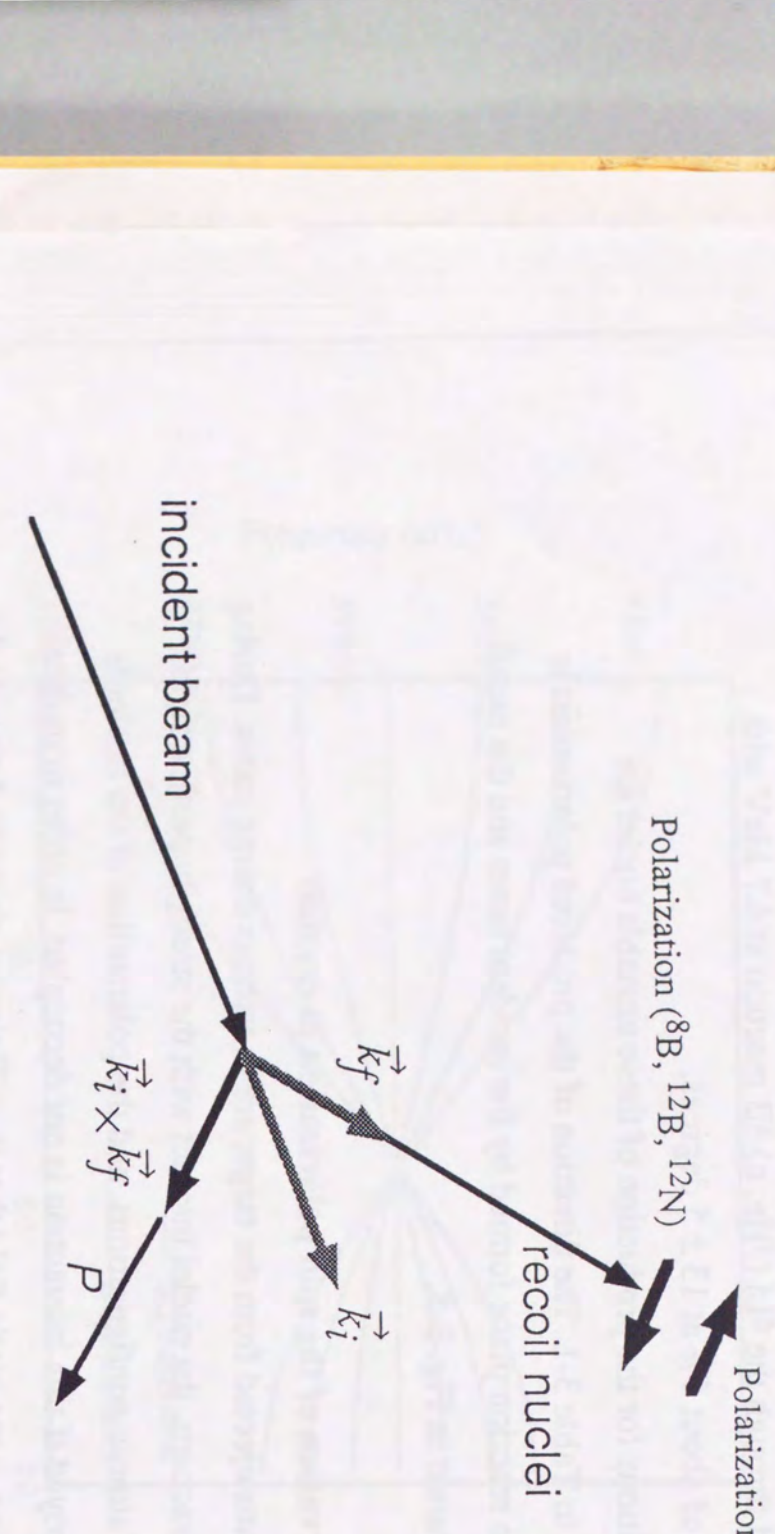

Figure 3-8 Definition of the polarity of polarization through nuclear reactions.

Table 3-1

Experimental conditions for the production of polarized nuclei

	^{8}Li	^{8}B	^{12}B	^{12}N
Half life ($T_{1/2}$)	838 (6) msec	770 (3) msec	20.20 (2) msec	11.000 (16) msec
Reaction	^{7}Li (d, p) ^{8}Li	^{6}Li (^{3}He, n) ^{8}B	^{11}B (d, p) ^{12}B	^{10}B (^{3}He, n) ^{12}N
Q-value	–0.189 MeV	-1.974 MeV	1.149 MeV	1.572 MeV
Beam Energy	3.5 MeV	4.7 MeV	1.5 MeV	3.0 MeV
Recoil angle	13 ± 8 °	13 ± 8 °	40 ± 8 °	20 ± 8 °
Mean Recoil Energy	0.7 MeV	1.0 MeV	0.2 MeV	0.7 MeV
Stopper	Pt, $LiIO_3$, $LiNbO_3$	Pt, Mg	Pt, Mg, BN, Mylar	Pt, BN, GaN, AlN, Mylar
Max Range	1.6 μm	3.4 μm	0.9 μm	2.7 μm
Magnetic field	4000.0 Oe	7000.0 Oe	5000.0 Oe	5000.0 Oe
Polarization	12%	6%	12%	17%

interstitial site or substitutional site of other elements are found destroyed due to mainly by the paramagnetic interactions with unpaired electrons.

3) Detection of polarization

Nuclear polarization is observed by detecting the asymmetric distribution of β rays emitted from polarized nuclei. The angular distribution of β rays is asymmetric if the nuclei are polarized, due to parity non conservation in the weak interaction. It is given as [Mo73]

$$W(\theta) = 1 + (\tfrac{v}{c}) AP\cos\theta \quad , \tag{3-21}$$

where θ is the angle between the direction of the emitted β ray and the polarization axis. A is the asymmetry parameter that is determined from the β-decay theory, v/c is the ratio of the velocity of the β particle to the light velocity, and P is the nuclear polarization. Since the mean energy of the β ray from the $A = 8$ and 12 systems are high, about 5 and 8 MeV, respectively, the ratio v/c is about 1.

The asymmetry parameter is given as [Mo73]

$$A = \pm\lambda_{ii'} \frac{|C_A|^2 \left|\int \sigma\right|^2}{|C_V|^2 \left|\int 1\right|^2 + |C_A|^2 \left|\int \sigma\right|^2} - 2\delta_{ii'} \sqrt{\frac{i}{i+1}} \frac{C_A C_V \int \sigma \int 1}{|C_V|^2 \left|\int 1\right|^2 + |C_A|^2 \left|\int \sigma\right|^2} \quad , \tag{3-22}$$

where the upper sign refers to β^+ decay and the lower sign to β^- decay, respectively. The coefficient $\lambda_{ii'}$ is

$$\lambda_{ii'} = 1 \quad \text{for} i \to i' = i-1$$

$$\frac{1}{i+1} \text{ for } i \to i' = i$$

$$\frac{-i}{i+1} \text{ for } i \to i' = i+1 \quad , \tag{3-23}$$

where <1> is the Fermi matrix element, C_V the Fermi coupling constant, <σ> the Gamow-Teller matrix element, and C_A the Gamow-Teller coupling constant. The β decay of ^{12}B and ^{12}N are pure Gamow-Teller transitions (Fig. 3-9) [Az90]. Their asymmetry parameters are $A = \pm 1$, where the + sign denotes ^{12}N and the – sign ^{12}B. On the other hand, the β decays of ^{8}Li and ^{8}B are mixed with a Gamow-Teller transition and a

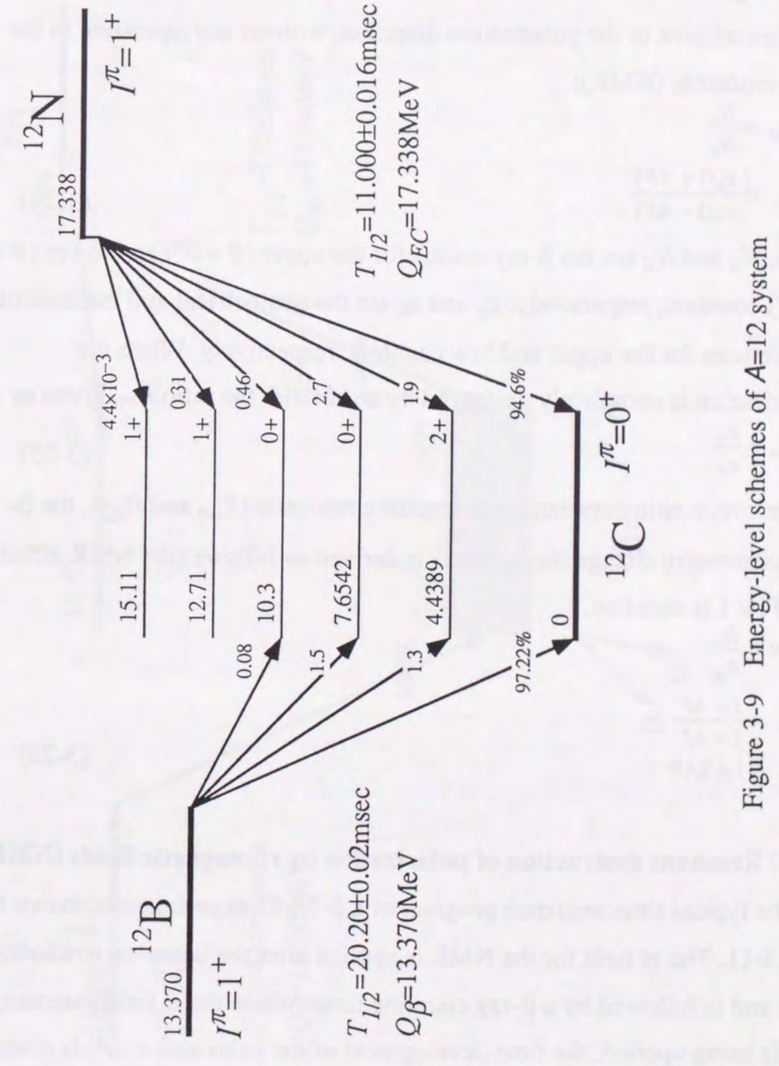

Figure 3-9 Energy-level schemes of A=12 system

Fermi transition (Fig. 3–10) [Aj88]. However, the mixing of a Fermi transition is negligibly small [Tr75]. Their asymmetry parameters are $A = \pm 1/3$, where the + sign denotes ^{8}B and the – sign ^{8}Li.

In an actual measurement, it has been observed the ratio R_{off} of the β-ray counting rates from the counters that are located above and below the catcher relative to the polarization direction, without any operation to the spin ensemble (NMR):

$$R_{off} = \frac{N_u}{N_d} = \frac{\varepsilon_u(1+AP)}{\varepsilon_d(1-AP)} \cdot \quad (3\text{-}24)$$

Here, N_u and N_d are the β-ray counts for the upper ($\theta = 0°$) and lower ($\theta = 180°$) counters, respectively. ε_u and ε_d are the geometrical and instrumental efficiencies for the upper and low counters, respectively. When the polarization is completely destroyed by an rf field, the ratio R_{on} given as

$$R_{on} = \frac{\varepsilon_u}{\varepsilon_d} \cdot \quad (3\text{-}25)$$

Therefore, a ratio between these counting rate ratio (R_{on} and R_{off}), the β-ray asymmetry change due to the rf is derived as follows (the NMR effect), if $|AP| \ll 1$ is satisfied,

$$\Delta R = \frac{R_{on}}{R_{off}} = \frac{1+AP}{1-AP} \equiv 1+2AP \cdot \quad (3\text{-}26)$$

4) Resonant destruction of polarization by rf magnetic fields (NMR)

The typical time sequence program of a β-NMR experiment is shown in Fig. 3-11. The rf field for the NMR is applied after the beam-on irradiation time and is followed by a β-ray counting time. While the rf field (intensity: H_1) is being applied, the time development of the polarization (P) is given by the following differential equation:

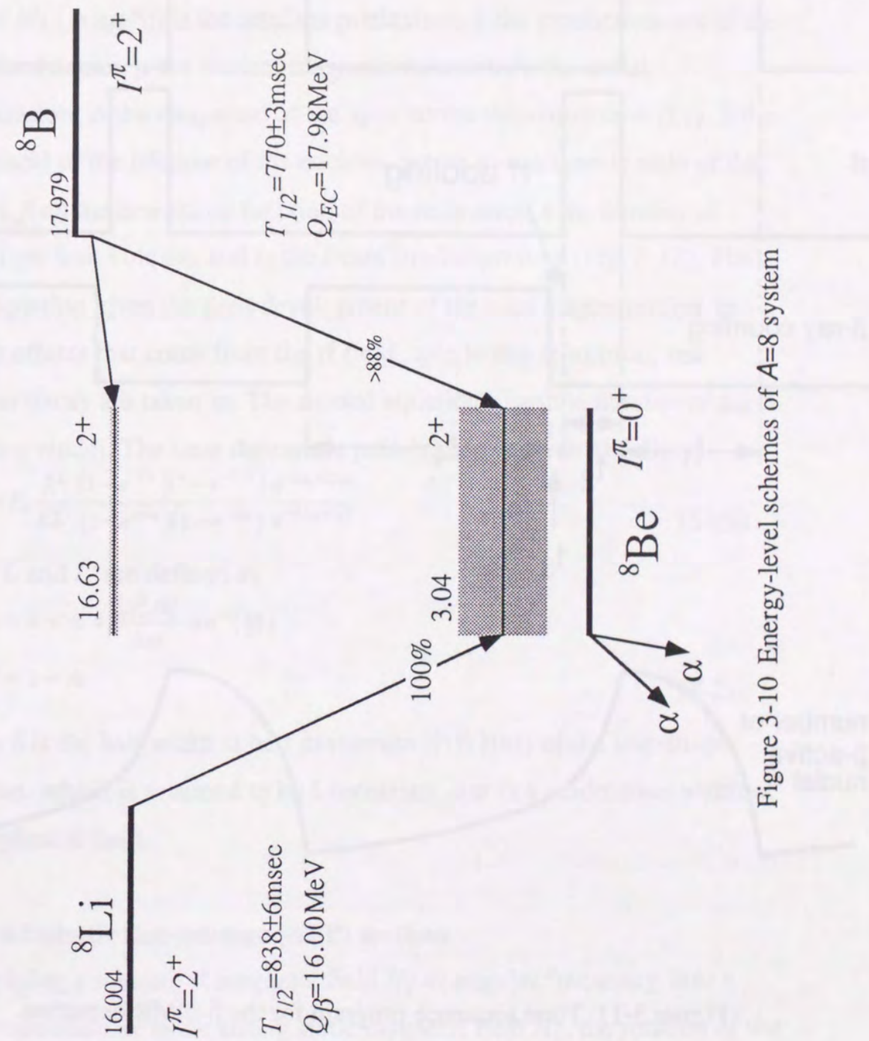

Figure 3-10 Energy-level schemes of A=8 system

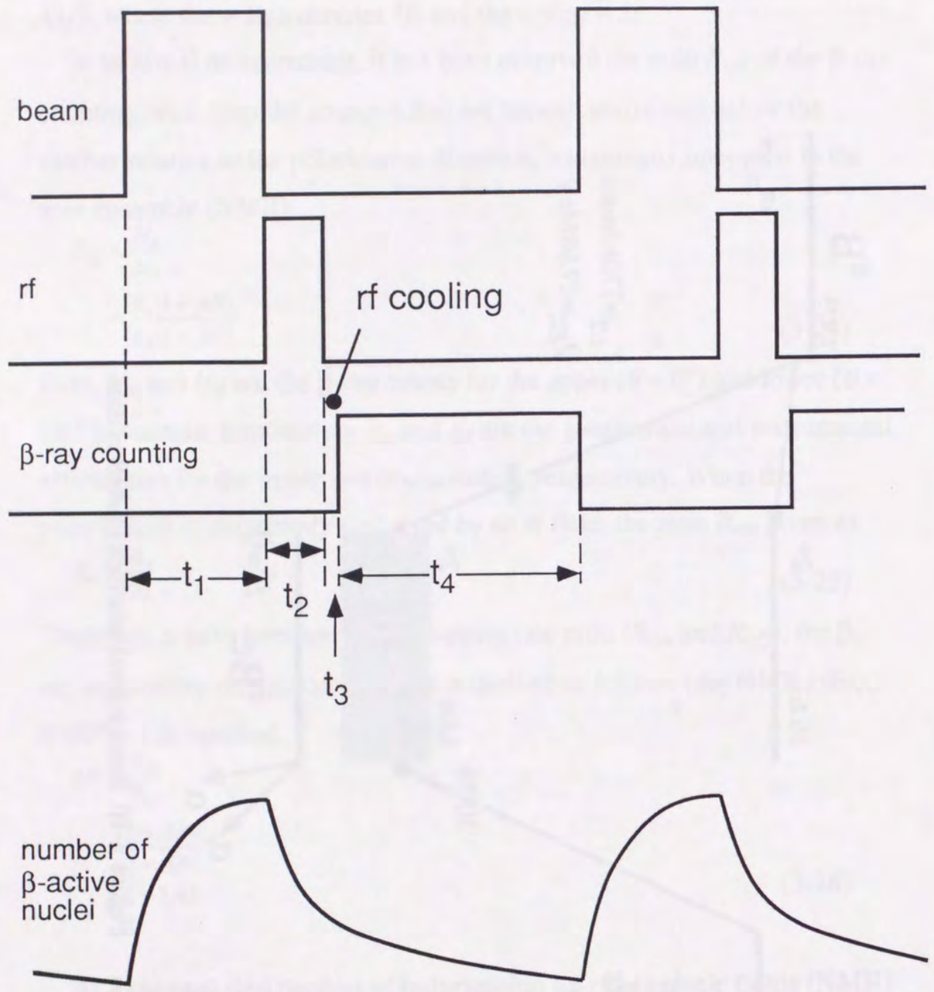

Figure 3-11 Time sequence program for the β-NMR detection.

$$\frac{dM_z}{dt} = \tilde{q}\mu P_0 - \left(\Lambda + \lambda + \pi\gamma_N^2 H_1^2 f(\omega)\right) M_z$$

$$\frac{dn}{dt} = \begin{cases} \tilde{q} - \lambda n & (0 \le t \le t_1) \\ -\lambda n & (t \ge t_1) \end{cases} , \qquad (3\text{-}27)$$

where M_z ($= n\mu P_0$) is the total magnetization, $\tilde{q}$ the production rate of the polarized nuclei, μ the nuclear magnetic moment, P_0 the initial polarization, Λ the reciprocal of the spin-lattice relaxation time (T_1), λ the reciprocal of the lifetime of the nucleus, γ_N the gyromagnetic ratio of the nuclei, $f(\omega)$ the line-shape function of the resonance, n the number of nuclei per unit volume, and t_1 the beam irradiation time (Fig. 3-11). The first equation gives the time development of the total magnetization, in which effects that come from the rf field, spin lattice relaxation, and nuclear decay are taken in. The second equation gives the number of the β-emitting nuclei. The time dependent polarization is given as follows:

$$P = P_0 \frac{\lambda^2}{LL'} \frac{\left(1 - e^{-Lt_1}\right)\left(1 - e^{-L't_4}\right)}{\left(1 - e^{-\lambda t_1}\right)\left(1 - e^{-\lambda t_4}\right)} \frac{e^{-Lt_4 - L't_3}}{e^{-\lambda(t_2 + t_3)}} . \qquad (3\text{-}28)$$

Here, L and L' are defined as

$$\begin{cases} L = \lambda + \Lambda + \dfrac{2\gamma_N^2 H_1^2}{\Delta\omega} \tan^{-1}\left(\dfrac{\Delta\omega}{2\delta}\right) \\ L' = \lambda + \Lambda \end{cases} , \qquad (3\text{-}29)$$

where δ is the half width at half maximum (HWHM) of the line-shape function, which is assumed to be Lorentzian, $\Delta\omega$ is a modulation width of the applied rf field.

5) Adiabatic fast-passage (AFP) method

Applying a rotating rf magnetic field H_1 of angular frequency ω to a spin perpendicular to the strong static magnetic field H_0, the rotation of the spin can be described by use of the rotating frame that rotates with the same angular velocity of rf field. In the rotating frame, the effective magnetic field is given by $\vec{H}_{eff} = \vec{H}_0 + \frac{\vec{\omega}}{\gamma_0}$ as shown in Fig. 3-12. The spin is

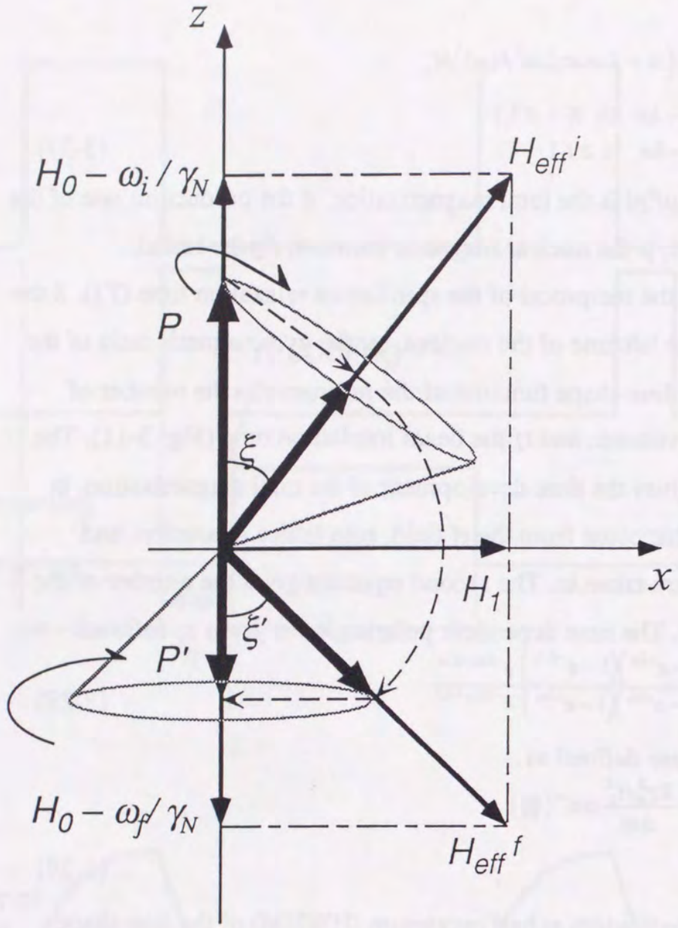

Figure 3-12 Adiabatic fast-passage (AFP) method.
The axes are fixed to the rf (H_1) rotating flame. It supposes the shape of rf rectangle. The appreciable reduction of the polarization is occurred through the spin inversion.
$P' = P \cos \xi \cdot \cos \xi'$.

trapped in and precesses around this effective field H_{eff}. First, put the ω far away of ω_L and drug it slowly toward ω_L and the spin direction follows H_{eff}. Therefore, if ω is swept across ω_L, the direction of the spin is inverted (Fig. 3-12). This method is called the "Adiabatic Fast Passage" method [Ab61]. The method was introduced to the conventional β-NMR method by Minamisono [Mi73]. To perform this operation, the intensity of H_1 and the sweep rate of the frequency must satisfy the following condition,

$$\left|\frac{d\omega}{dt}\right| \ll (\gamma_N H_1)^2 . \qquad (3\text{-}30)$$

Furthermore, in a crystal there exists the dynamic (time dependent) fluctuation of magnetic field due to the surrounding nuclear magnetic moment (D). In order to decouple this interaction, the following condition must be satisfied,

$$\gamma_N H_1 > 2\pi D . \qquad (3\text{-}31)$$

The former relation is derived based on the condition that the effective field changes far slowly compared with the spin rotation. The latter relation means that the applied oscillating field is sufficiently larger than the dynamic dipole magnetic field.

The achievement of spin inversion by the AFP method depends on the rf intensity as a function of time. If a constant H_1 is used, the achievement of inversion is deduced showing in Fig. 3-9. Up on applying on rf field, the spin precesses around $H_{eff}{}^i$ and the expectation value is equal to the projected value to $H_{eff}{}^i$. The expectation value of the spin along H_{eff} is maintained during a frequency sweep if the equations given above are satisfied. Up on stopping rf field, the spin is projected back to the direction of the external field. Then, the achievement ε of the inversion is given by

$$\varepsilon = \frac{H_0 - \frac{\omega_1}{\gamma_N}}{\sqrt{\left(H_0 - \frac{\omega_1}{\gamma_N}\right)^2 + H_1^2}} \frac{H_0 - \frac{\omega_2}{\gamma_N}}{\sqrt{\left(H_0 - \frac{\omega_2}{\gamma_N}\right)^2 + H_1^2}} . \qquad (3\text{-}32)$$

It is evident that a constant H_1 with narrow range of frequency modulation (FM) can not invert spin perfectly. In order to achieve

complete inversion, an amplitude modulated (AM) rf is employed so as to minimize any reduction of the projection at both the beginning and end of the rf application as shown in Fig. 3-13. It is known that the influence of AM and the frequency can be neglected under the conditions of this experiment.

6) Modified β-NMR for measuring the electric quadrupole coupling frequency (ν_Q) — NNQR method

If one limit interest to only β-NMR, detection of the quadrupole interactions of short-lived β-emitting nuclei is usually more difficult and time consuming than the conventional β-NMR detection of a pure magnetic interaction. In order to cope with these difficulties, the method must be improved so as to enable the detection of the coupling constant both easily and efficiently.

It is very difficult to observe a split spectrum due to the electric quadrupole interaction by detecting the β-NMR, as shown in the following. Consider the case when a split line is saturated by an rf, the polarization change is very small (Fig. 3-14). It is only $3/2\times\{I(I+1)(2I+1)\}^{-1}$ of the total polarization for the nuclide with spin I when the population differences of the neighboring magnetic substates are equal as shown in Fig. 3-14. For the case of $I = 1$ and $I = 2$, it is 1/4 and 1/20 of total polarization, respectively. To overcome this difficulty we decided to saturate all lines simultaneously applying all transition rf fields given by a quadrupole coupling constant in order to perfectly destroy the polarization. An outline of this method is given in Figs. 3-15a and 15b.

If the Larmor frequency and the field gradient as well as its orientation relative to H_0 are known, all of the $2I$-transition frequencies for a given electric quadrupole coupling constant can be calculated for a nucleus at a high field. Any change in the nuclear polarization is detected as a function

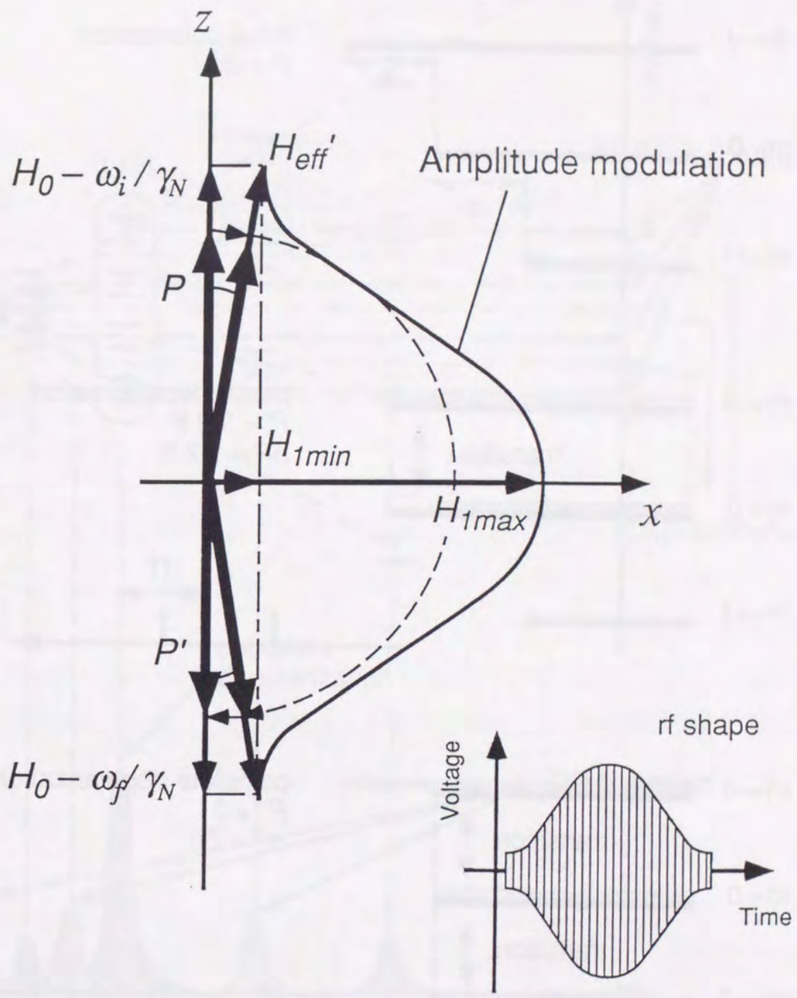

Figure 3-13 Optimum rf amplitude modulation (AM) for the AFP technique.
The axes are fixed to the rf (H_1) rotating flame. It shows that the reduction of the polarization due to the spin inversion is small. $P' \equiv P$

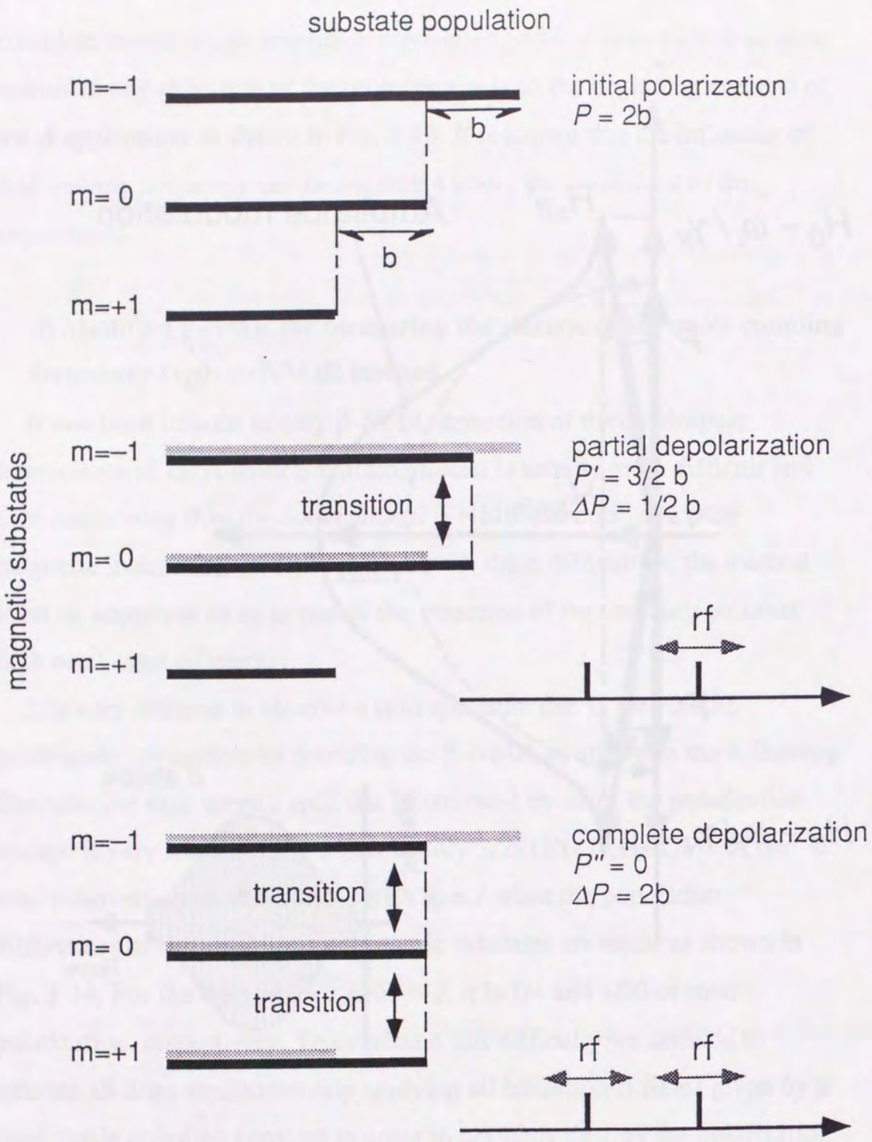

Figure 3-14 Difference between partial and complete depolarization. Single rf can induce just one of two transitions. The polarization change due to partial depolarization is only 1/4 of complete depolarization.

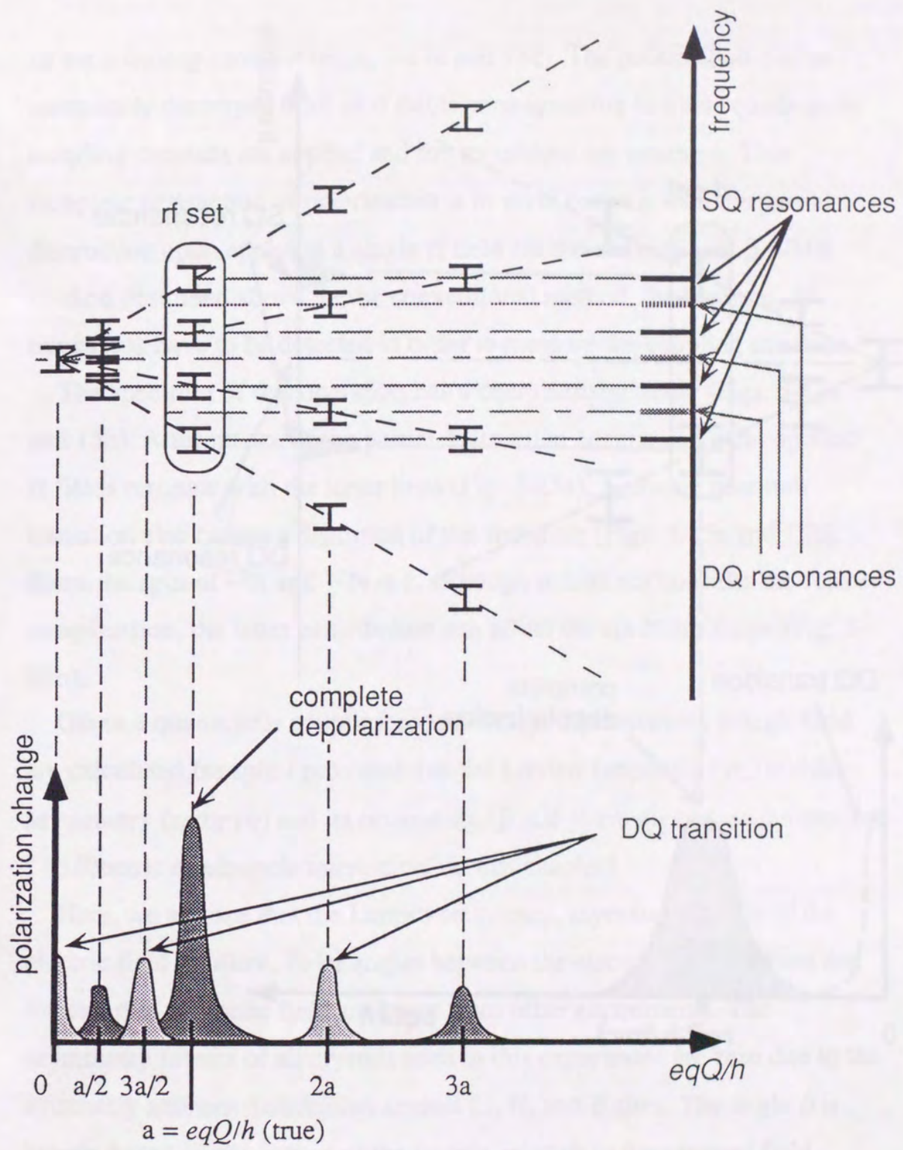

Figure 3-15a Principle of the newly developed multiple rf operation (NNQR method). The case of the spin $I = 2$
If the intensity of rf (H_1) is enough high, the double quantum transitions are occurred.

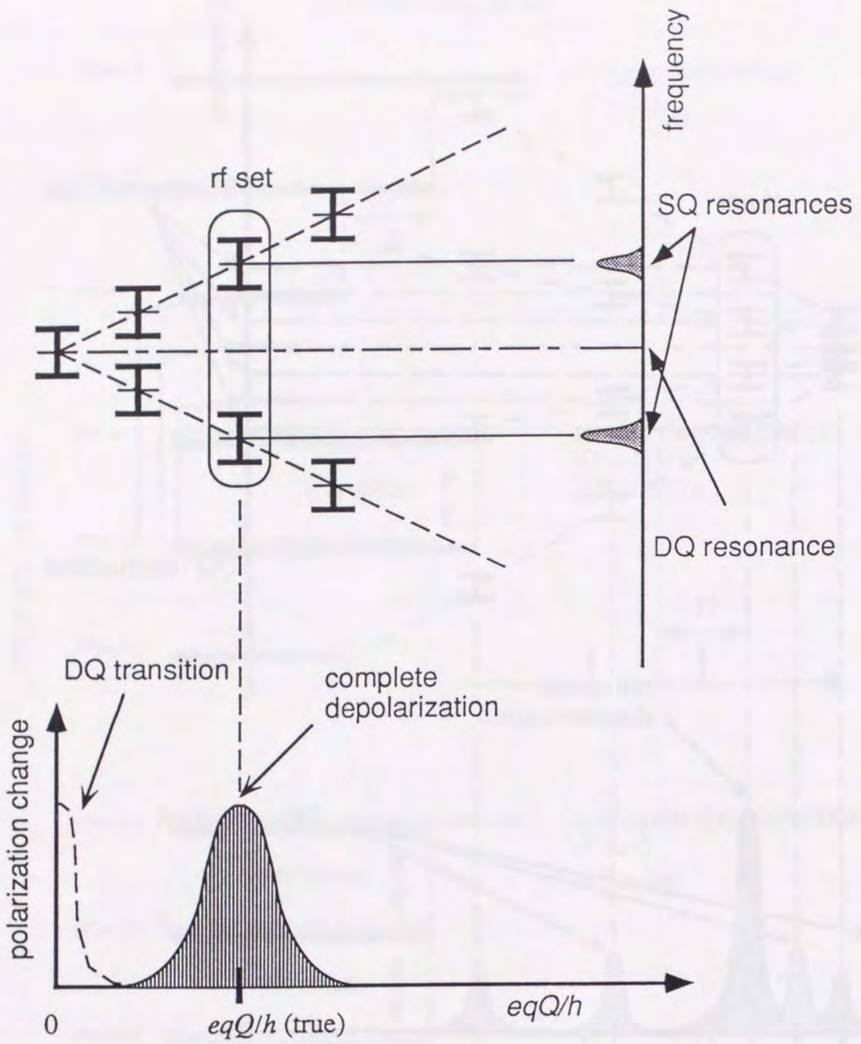

Figure 3-15b Principle of the newly developed multiple rf operation (NNQR method). The case of the spin $I = 1$.
If the intensity of rf (H_1) is enough high, the double quantum transition is occurred at $eqQ/h = 0$.

of the coupling constant (Figs. 3-15a and 15b). The polarization can be completely destroyed if all of rf fields corresponding to a true quadrupole coupling constant are applied and the transitions are saturated. This complete destruction of polarization is in vivid contrast with the partial destruction upon applying a single rf field for the conventional β-NMR method described above. In the conventional method, furthermore, $2I$ transitions have to be detected in order to measure the coupling constant.

The spectrum of this operation has a characteristic shape (Figs. 3-15a and 15b). A resonance of the partial destruction occurs, i.e., outer applied rf fields resonate with the inner lines (Fig. 3-15a). A double quantum transition also causes a distortion of the spectrum (Figs. 3-15a and 15b). Since the spin of ^{12}B and ^{12}N is 1, although it does not consider the former complication, the latter contribution can affect the spectrum shape (Fig. 3-15b).

Given a quadrupole coupling constant (ν_Q), $2I$ transitions at high field are calculated for spin I provided that the Larmor frequency (ν_L) and the asymmetry factor (η) and its orientation (β and γ) are given (see the section " 2) Electric quadrupole interaction" in this chapter).

Here, we assume that the Larmor frequency, asymmetry factor of the electric field gradient, Euler angles between the electric field gradient and the external magnetic field are know from other experiments. The asymmetry factors of all crystals used in this experiment are zero due to the symmetry ambient distribution around Li, N, and B sites. The angle β is known based on the setting of the sample relative to the external field.

Larmor frequency (ν_L) was derived based on the double quantum transition (DQ) between $m = 1$ and -1 for ^{12}B and ^{12}N. The frequency of DQ (ν_{DQ}) is not equal to ν_L if the quadrupole interaction is not sufficiently smaller than the magnetic interaction (Fig. 3-5). Given the quadrupole coupling frequency, ν_L can be calculated from ν_{DQ}.

As for ^{8}Li and ^{8}B, since the polarization change by the double quantum transition ($m = 1 \leftrightarrow -1$) is small, Larmor frequency (ν_L) of these nuclei were derived from the transition frequency at magic angle $\beta_M = \mathrm{Cos}^{-1}\sqrt{\frac{1}{3}}$. In this condition, all of the transition frequencies coincide if the second-order perturbation is negligible (Fig. 3-7). Given the quadrupole coupling frequency, ν_L can be calculated from ν_{DQ}.

3-3 Causes of the line broadening of the NMR spectra

There are many interactions which can affect the NMR spectrum, and are important for analyzing it. In this section we summarize these interactions:

1) Dipole-dipole interaction

The nucleus in the solid is surrounded by host nuclei. If these nuclei have magnetic-dipole moments, they cause a dynamic magnetic field at the nucleus. The Hamiltonian of this dipole-dipole interaction between two nuclei (Fig. 3-16) is given as [Ab61]:

$$W_{12} = \frac{\gamma_1\gamma_2\hbar^2}{r_{12}^3}\left\{\vec{I}_1\cdot\vec{I}_2 - 3\frac{(\vec{I}_1\cdot\vec{r}_{12})(\vec{I}_2\cdot\vec{r}_{12})}{r_{12}^3}\right\}, \qquad (3\text{-}33)$$

where r_{12} is the distance between two nuclei; γ_1 and γ_2 are the gyromagnetic rations of the probe and host nuclei. It can be seen that the host nuclei produce a local field (H_{12}) at the site of any implanted nuclei,

$$W_{12} = -\vec{\mu}_2\vec{H}_{12} = -\gamma_2\hbar\vec{I}_2\cdot\vec{H}_{12}\ . \qquad (3\text{-}34)$$

Because host nuclei have thermal vibration, this interaction causes a dynamic magnetic field at a nucleus site. The resonance line is thus broadened due to this contribution.

The Hamiltonian of the dipole-dipole interaction between like spins can be decomposed as follows [Ab61]:

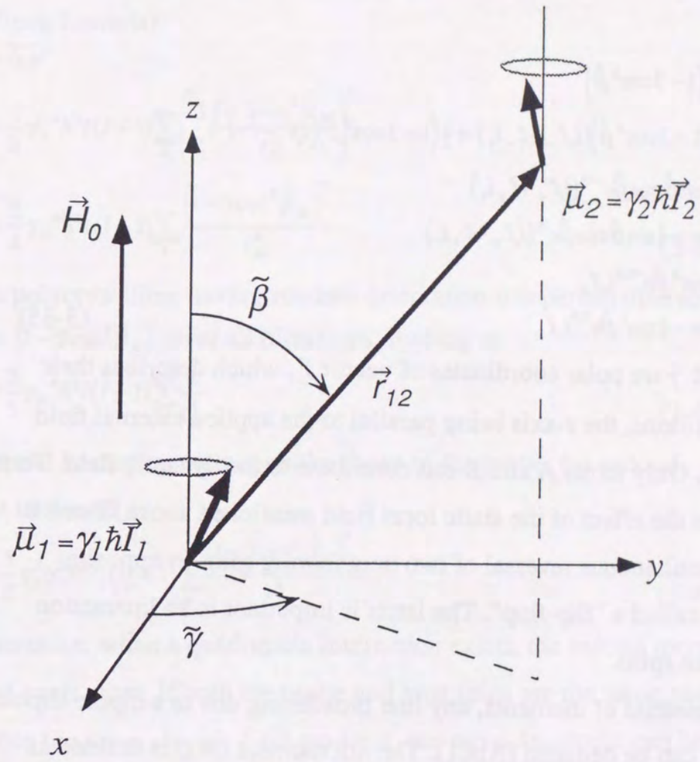

Figure 3-16 Dipole-dipole interaction.

$$W_{ii'} = \frac{\gamma_N{}^2\hbar^2}{r^3}\left\{\vec{i}\cdot\vec{i}\,' - 3\left[i_z\cos\tilde{\beta} + \sin\tilde{\beta}\left(i_x\cos\tilde{\gamma} + i_y\sin\tilde{\gamma}\right)\right]\left[i'_z\cos\tilde{\beta} + \sin\tilde{\beta}\left(i'_x\cos\tilde{\gamma} + i'_y\sin\tilde{\gamma}\right)\right]\right\}$$
$$= \frac{\gamma_N{}^2\hbar^2}{r^3}(A+B+C+D+E+F)$$

where

$$\begin{cases} A = i_z i'_z\left(1-3\cos^2\tilde{\beta}\right) \\ B = -\frac{1}{4}\left(1-3\cos^2\tilde{\beta}\right)\left(i_+ i'_- + i'_- i_+\right) = \frac{1}{2}\left(1-3\cos^2\tilde{\beta}\right)\left(i_z i'_z - \vec{i}\cdot\vec{i}\,'\right) \\ C = -\frac{3}{2}\sin\tilde{\beta}\cos\tilde{\beta}e^{-i\tilde{\gamma}}\left(i_z i'_+ + i'_z i_+\right) \\ D = C^* = -\frac{3}{2}\sin\tilde{\beta}\cos\tilde{\beta}e^{i\tilde{\gamma}}\left(i_z i'_- + i'_z i_-\right) \\ E = -\frac{3}{4}\sin^2\tilde{\beta}e^{-2i\tilde{\gamma}} i_+ i'_+ \\ F = E^* = -\frac{3}{4}\sin^2\tilde{\beta}e^{2i\tilde{\gamma}} i_- i'_- \end{cases} \quad . \qquad (3\text{-}35)$$

Here, $\tilde{\beta}$ and $\tilde{\gamma}$ are polar coordinates of vector $\vec{r}$, which describes their relative positions, the z-axis being parallel to the applied external field (Fig. 3-16). Only terms A and B can contribute to the dynamic field. Term A describes the effect of the static local field mentioned above. Term B shows a simultaneous reversal of two neighboring spins in opposite directions, called a "flip-flop". The latter is important in an interaction between like spins.

Using the method of moments, any line broadening due to a dipole-dipole interaction can be deduced [Ab61]. The nth moment (M_n) is defined as

$$M_n = \int(\omega-\omega_0)^n f(\omega)d\omega \quad , \qquad (3\text{-}36)$$

where $f(\omega)$ is a normalized shaped function with a maximum at a frequency ω_0. A Gaussian curve is described by a normalized function,

$$f(\omega) = \frac{1}{\Delta\sqrt{2\pi}}e^{\left(\frac{-(\omega-\omega_0)^2}{2\Delta^2}\right)} \quad , \qquad (3\text{-}37)$$

from which a relation between the nth moments and the line width can be derived as

$M_2 = \Delta^2$, $M_4 = 3\Delta^4$, ..., $M_{2n} = 1\cdot3\cdot5\cdots(2n\text{-}1)\Delta^{2n}$,

in which the odd moments vanish. The half width at half-maximum intensity (δ) (HWHM) turn out to be

$$\delta = \Delta\sqrt{2\log 2} = 1.18\Delta \quad . \qquad (3\text{-}38)$$

Here, we treat the condition in which the host and probe spins are alike. The second moment with the surrounding dipoles is expressed as follows (Van Vleck formula):

$$M_2 = \overline{\Delta\omega}^2$$
$$= \frac{1}{3}\gamma_N{}^4\hbar^2 I(I+1)\sum_k\left(\frac{3}{2}\frac{1-3\cos^2\tilde{\beta}_{jk}}{r_{jk}^3}\right)^2$$
$$= \frac{3}{4}\gamma_N{}^4\hbar^2 I(I+1)\sum_k\frac{\left(1-3\cos^2\tilde{\beta}_{jk}\right)^2}{r_{jk}^6} \quad . \qquad (3\text{-}39)$$

For a polycrystalline having random orientation it is permissible to average $\left(1-3\cos^2\tilde{\beta}_{jk}\right)^2$ over all directions, leading to

$$M_2 = \frac{3}{5}\gamma_N{}^4\hbar^2 I(I+1)\sum_k\frac{1}{r_{jk}^6} \quad . \qquad (3\text{-}40)$$

When the host spins are not unlike those of the probe, the second moment is altered as

$$M_2 = \frac{1}{3}\gamma_1^2\gamma_2^2\hbar^2 I_2(I_2+1)\sum_k\frac{\left(1-3\cos^2\tilde{\beta}_{jk}\right)^2}{r_{jk}^6} \quad . \qquad (3\text{-}41)$$

Furthermore, when a quadrupole interaction exists, the second moment is altered even more. If both the probe and host spins are the same and experience the same electric field gradient, the second moment can be written as

$$\overline{\Delta\omega}^2 = F_L(I)\gamma_N{}^4\hbar^2\sum_k\left(\frac{3}{2}\frac{1-3\cos^2\tilde{\beta}_{jk}}{r_{jk}^3}\right)^2$$
$$F_L(I) = \tfrac{4}{27}I(I+1) + \frac{2I^2(I+1)^2 + 3I(I+1) + \frac{13}{8}}{18(2I+1)} \quad . \qquad (3\text{-}42)$$

From these relations, the line broadening due to any dipole-dipole interactions from surrounding nuclei can be estimated.

The calculated dipolar broadenings of the samples used in this experiment are listed in Table. 3-2.

Table 3-2
Calculated dipolar broadenings of the samples.

media	crystal structure	site	ΔH (Oe)
$LiIO_3$	hexagonal	Li	2.2
$LiNbO_3$	Ilmenite	Li	0.9
hexagonal BN	hexagonal layer	B	1.7
		N	4.0
GaN	Wurtzite	N	2.7

2) Spread in the electric field gradients

Many defects in the stopper sample are caused during the process of implantation. Even though implanted nuclei cause many defects before stopping, the final sites of the implanted nuclei can be considered to be far from these [Mi74]. If there is a defect near to the final site, any implanted nuclei are perturbed by a strong field gradient, perhaps destroying their polarization. The contributions from defects on the electric field gradient at an implanted nucleus are added to the proper one. The electric field gradients are then distributed around a proper value. This was observed in many cases, for example ^{17}F in MgF_2 [Mi74] or ^{41}Sc in TiO_2 [Mi93]. In these studies, the deviation of the field gradient was $\Delta q/q$ = 5~10% at HWHM.

3) Intensity of the rf field

The finite intensity of rf field causes the resonance spectrum to spread. In order to simplify the situation, a delta function is assumed as the

resonance shape. In the rotating flame fixed to the rotating field (H_1) that is near to the Larmor frequency, $\omega = \omega_L + \Delta\omega$, the spin rotates along the effective field (Fig. 3-2). The expectation value along this field is reduce by factor of ζ,

$$\zeta = \cos\xi = \frac{\Delta\omega/\gamma_N}{\sqrt{\left(\Delta\omega/\gamma_N\right)^2 + H_1^2}} \ . \qquad (3\text{-}43)$$

After applying an rf field, the polarization is reduced by factor of ζ^2. Calculations of the spectrum with any intensity of the rf field for ^{12}N at H_0 = 5kOe are shown in Fig. 3-17. It causes Δ(HWHM) = 1.8 kHz for H_1 = 5 Oe. If the applied rf field consists of many pulses, the destruction is repeated and the width of the obtained spectrum becomes wider. Fig. 3-18 shows two cases (1 pulse and 5 pulses), each condition of the rf field is the same except for the number of rf fields.

4) Chemical shifts

In a magnetic field, atomic electrons cause a static field at the nucleus. The magnetic field felt by the nucleus is different from the external one. This shift of the magnetic field at the nucleus is called a chemical shift. If the electrons constitute closed shells, the orbital motions in the external magnetic field produce a diamagnetic field at the inner nucleus. On the other hand, admixtures with exited orbital states produce a paramagnetic field. The former is called a diamagnetic shift, and the latter is called a paramagnetic shift. The amount of the these shifts is proportional to the external field. They depend on the electric structure of the surroundings of the nucleus. It is therefore very difficult to estimate these chemical shifts in a solid because of the difficulty for estimation of the electronic structure in a solid.

In a metal, free electrons produce a local field at the probe nucleus, i.e., a Fermi contact interaction occurs between these *s*-like free electrons and

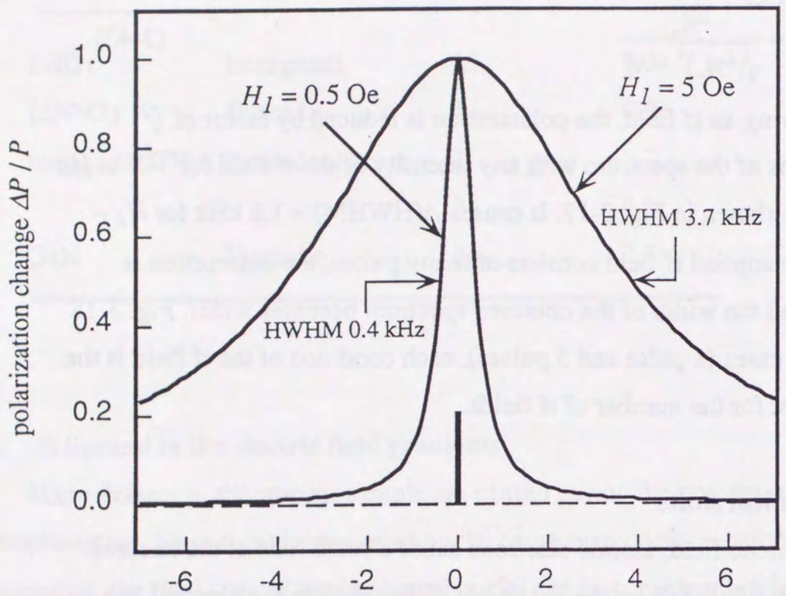

Figure 3-17 Effect of strong rf field on the resonance shape. This is the case of ^{12}N. It is supposed that the inherent resonance peak is the delta function.

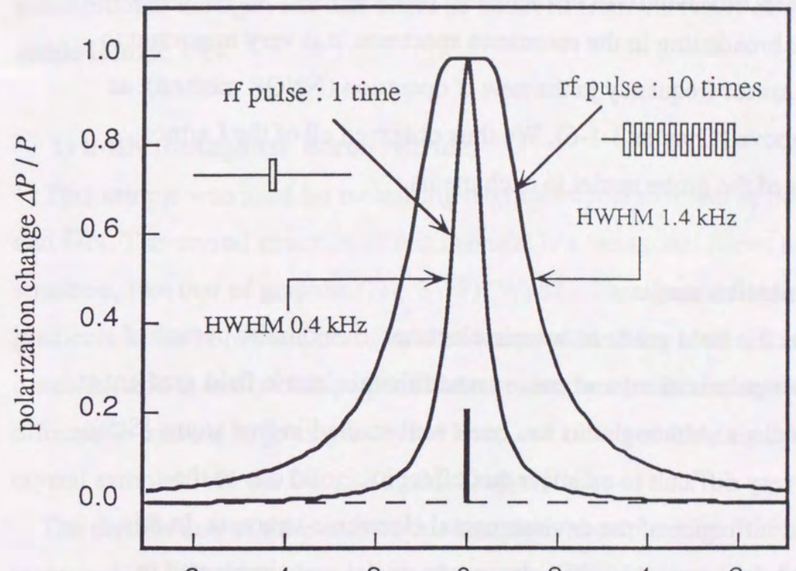

Figure 3-18 Effect of multiple rf field on the resonance shape. This is the case of ^{12}N. It is supposed that the inherent resonance peak is the delta function and H_1 = 0.5 Oe.

the nucleus. This shift of the magnetic field in metals is called a Knight shift. The amount of the shift is proportional to the external field.

In this study, probe nuclei were implanted in a metal, a semiconductor, and an insulator. The shifts of the magnetic field in these materials are expected to be different from one another. Although they do not cause any appreciable broadening in the resonance spectrum, it is very important to know the Larmor frequency in the new rf operation (NNQR method), as described above (Chapter 3-1-6). We thus observed all of the Larmor frequencies of the probe nuclei in each media.

3-4 Implantation media

In the electric field gradient, atomic electrons' motions are perturbed (Sternheimer polarization) and cause an additional electric field gradient at the inner nucleus. Although this has been well studied in free atoms [St50, St85], it is very difficult to estimate this effect in a solid due to the complicated influence of the environmental electronic structure. In this study, in order to avoid this difficulty, probe nuclei were implanted in media which included their stable isotopes. The electric field gradient of the isotope is equal to that at the implanted nucleus, due to the same environmental electronic structure. The electric field gradients can therefore be deduced from the observed electric quadrupole coupling constant of the isotopes with their known quadrupole moments.

In the following we summarize the catcher media used in this experiment. These media have isotope elements of implanted nuclei, except for the case of ^{8}B. The electric field gradient at the implanted nuclei is obtained from NMR studies of its stable isotopes. In the case of ^{8}B, its electric field gradient can be found by studying the hyperfine interactions of its isotope ^{12}B in Mg metal.

In order to obtain the electric quadrupole moment, although we need information concerning the electric field gradient, it is very difficult to estimate it in solids. We therefore utilized the field gradient of a substitutional nitrogen site that could be deduced from the NMR of the stable isotope ^{14}N.

1) h-BN (hexagonal Boron Nitride)

This sample was used for measuring the quadrupole moment of both ^{12}B and ^{12}N. The crystal structure of this material is a hexagonal boron nitride structure, like that of graphite (Fig. 3-19) [Wy82]. The electric field gradients at the boron and nitrogen sites are parallel to the *c*-axis. It is an insulator, and is easily cleft perpendicular to the *c*-axis. Since it is very difficult to make a large single-crystal lump, we obtained a highly oriented crystal sample from the Denki Kagaku Kogyo [De].

The distribution of the *c*-axis of this sample is shown in Fig. 3-20. It was measured by reflecting X-rays at the Bragg angle (26.6 degree) relative to the direction of X-ray incidence (Fig. 3-21) [Su90, Wa86]. The effect on the NMR spectrum due to the distribution is discussed later.

The electric structure of BN has been investigated [Hu85, Ca87, Or90, Ga 93]. The electric quadrupole coupling constant at the boron site was reported by Silver and Conor. Silver reported on the cw-NMR of powder BN at room temperature [Si60] $|eqQ/h\ (^{11}\text{B in BN})| = 2.96 \pm 0.10$ MHz and $\eta = 0$ based on the crystal structure. Conor determined it by using newly developed equipment [Co90]. They measured the NQR spectrum of ^{11}B in BN at 4.2K using a SQUID spectrometer, $|eqQ/h\ (^{11}\text{B in BN; 4.2K})| = 2934 \pm 4$ kHz and $\eta = 0.0$. However, we have not adopted this value, since the measuring temperature was so very far different. As for a nitrogen, there is no information concerning the electric field gradient. We

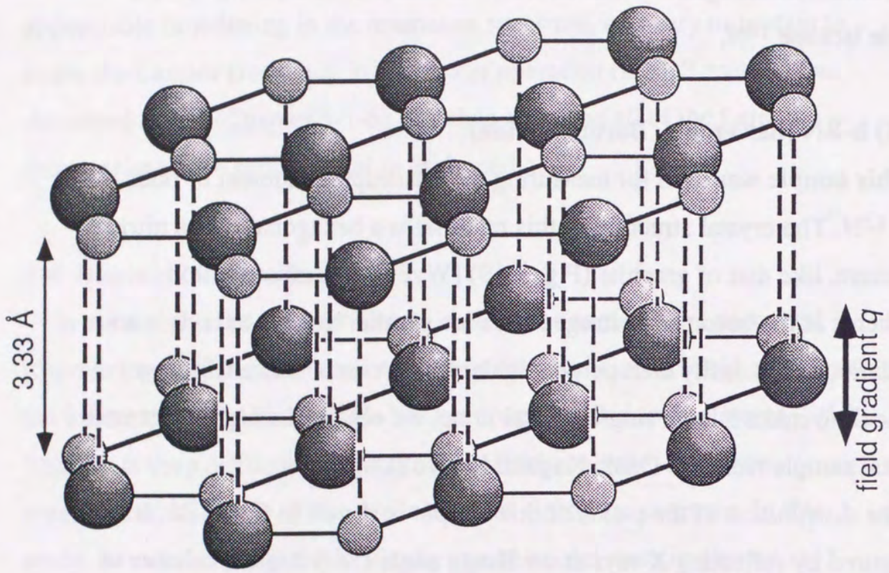

$a_0 = 2.504$ Å B-N (plane) $a_0 / \sqrt{3}$

$c_0 = 6.661$ Å B-N (perpendicular) $c_0 / 2$

Figure 3-19 Crystal structure of hexagonal boron nitride (h-BN)

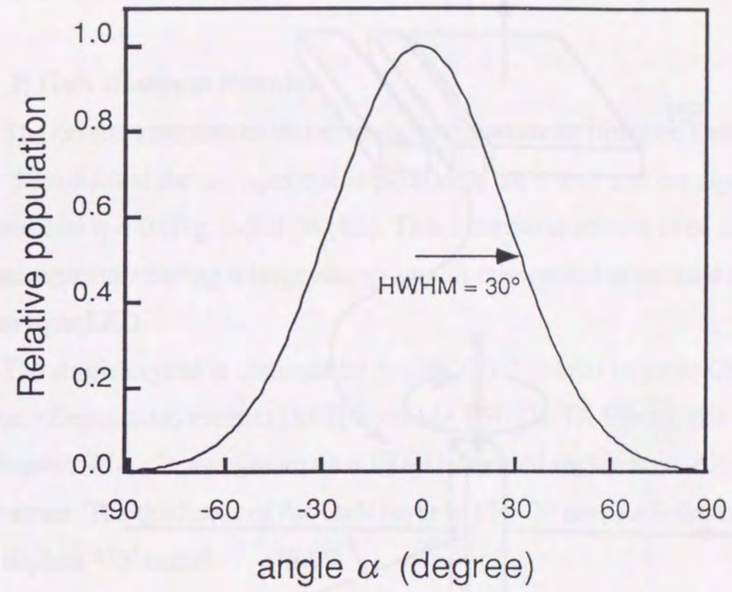

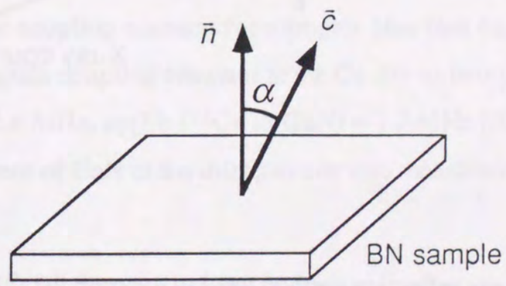

Figure 3-20 Distribution of the *c*-axes of a highly oriented BN sample.

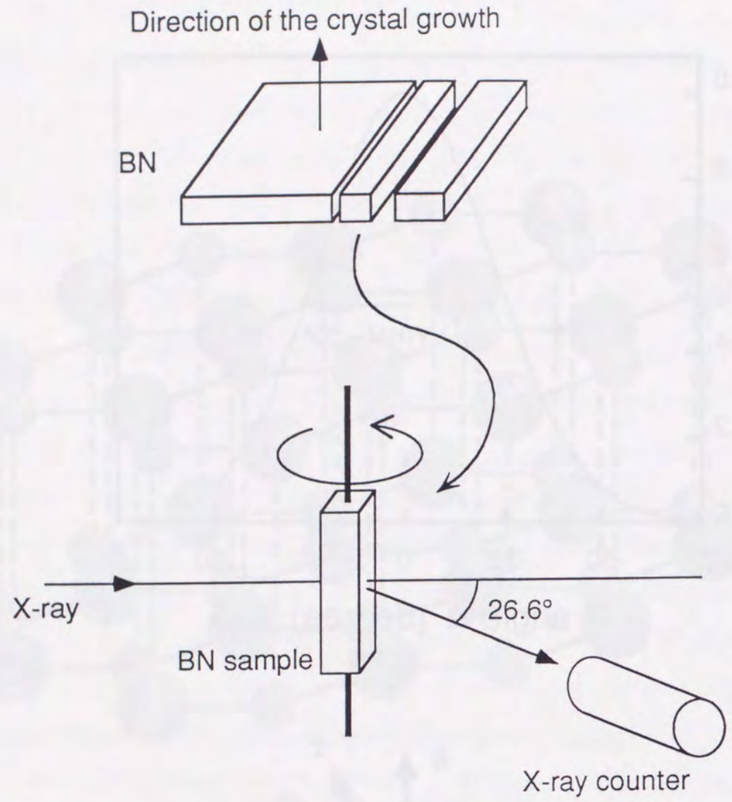

Figure 3-21 X-ray reflection method used to measure the distribution of the *c*-axes in a highly oriented BN sample.
In this condition, when the *c*-axis is parallel to the X-ray direction, the intensity of the reflected X-ray is maximum at the angle 26.6°.

measured electric field gradients at both the boron and nitrogen sites by a pulsed FT-NMR method.

2) GaN (Gallium Nitride)

The crystal structure of this material is the wurtzite structure and the field gradient at the nitrogen site is parallel to the *c*-axis and the asymmetry parameter $\eta = 0$ (Fig. 3-22) [Wy82]. This material is known to be a semiconductor having a large energy gap. It is expected to be used for a blue light LED.

The single crystal is obtained by the MOCVD (Metal Organic Chemical Vapor Deposition) method [It85] from MATSUSHITA Electronics Company[Ma]. It was grown on a (0001)-oriented sapphire (α-Al_2O_3) substrate. The thickness of the GaN layer is 15 ~ 30 μm, sufficiently thick to implant ^{12}N nuclei.

Although the electric structure of GaN has been studied by many authors [Hu85, Go91, Pe92], there is no information concerning the electric quadrupole coupling constant for nitrogen. Hee Han has reported the electric quadrupole coupling constant at the Ga site as being eqQ/h (^{69}Ga in GaN) = 2.8 MHz, eqQ/h (^{71}Ga in GaN) = 1.7 MHz [Ha88]. The electric field gradient of GaN at the nitrogen site was measured by a pulsed FT-NMR method.

3) AlN (Aluminum Nitride)

The crystal structure of this material also is a wurtzite structure [Wy82]. Although we can not obtain a single-crystal sample, we can use a polycrystal sample. This type sample is offered by KAWASAKI SEITETSU [Ka] as a plate.

The electric structure of AlN has also been studied [Hu85, Ch93]. Hee Han reported on the electric quadrupole coupling constant at the Al site as

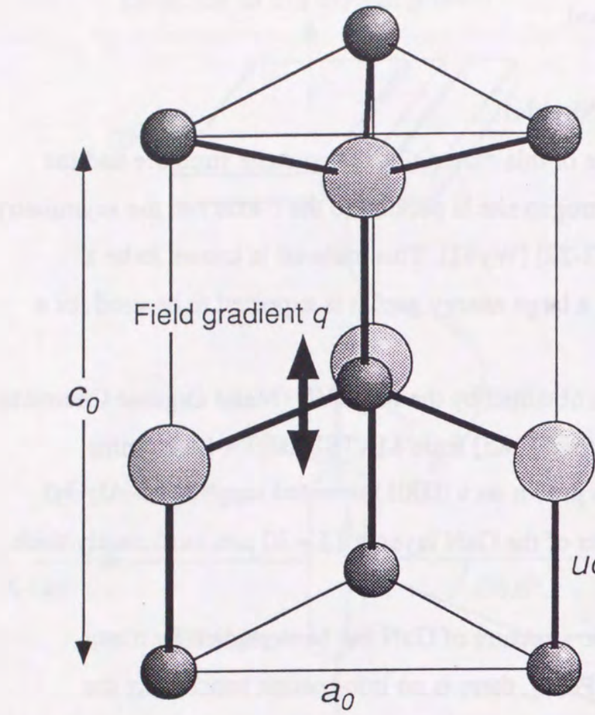

N

Ga or Al

	GaN	AlN
a_0	3.18 Å	3.111Å
c_0	5.166Å	4.978Å
u	—	0.385

Figure 3-22 Crystal structure of GaN and AlN (Wurtzite structure). Crystal parameters are also shown.

being eqQ/h (^{27}Al in AlN) = 2.2 MHz [Ha88]. We did not use this type sample to determined the quadrupole moment, since we could not measure the coupling constant of ^{12}N in AlN precisely enough.

4) $LiIO_3$ (Lithium Iodate)

The crystal structure of $LiIO_3$ is shown in Fig. 3-23. This medium is well known as being piezoelectric. The single-crystal specimen of $LiIO_3$ was provided by Dr. R.S. Feigelson. The electric quadrupole coupling constant at the Li site at room temperature had been determined by Sarnatskii [Sa72] using a cw-NMR, $|eqQ/h$ (^{7}Li in $LiIO_3)| = 44 \pm 3$ kHz. Since the configuration around the Li atom is symmetric in the a-a plane, the asymmetry factor (η) is zero.

5) $LiNbO_3$ (Lithium Niobate)

The crystal structure of $LiNbO_3$ is an Ilmenite structure, as shown in Fig. 3-24. A single-crystal specimen of $LiNbO_3$ was obtained from NGK co. [Ng] as a plate. The electric field gradient at the lithium site at room temperature was studied by Peterson and Halstead [Pe67, Ha70] using cw-NMR, $|eqQ/h$ (^{7}Li in $LiNbO_3)| = 54.7 \pm 0.3$ kHz. The asymmetry factor (η) is zero, due to its symmetric configuration around a Li atom in the a-a plane.

6) Mg (Magnesium)

The crystal structure of magnesium is a hexagonal closest-packed (hcp), as shown in Fig. 3-25. The single-crystal of Mg was purchased from Murakami Engineering [Mu]. The hyperfine interactions of ^{12}B in this metal has been studied using the β-NMR method by many authors [Ta77, Ha73, Ki93c]. A. Kitagawa reported on the electric quadrupole coupling

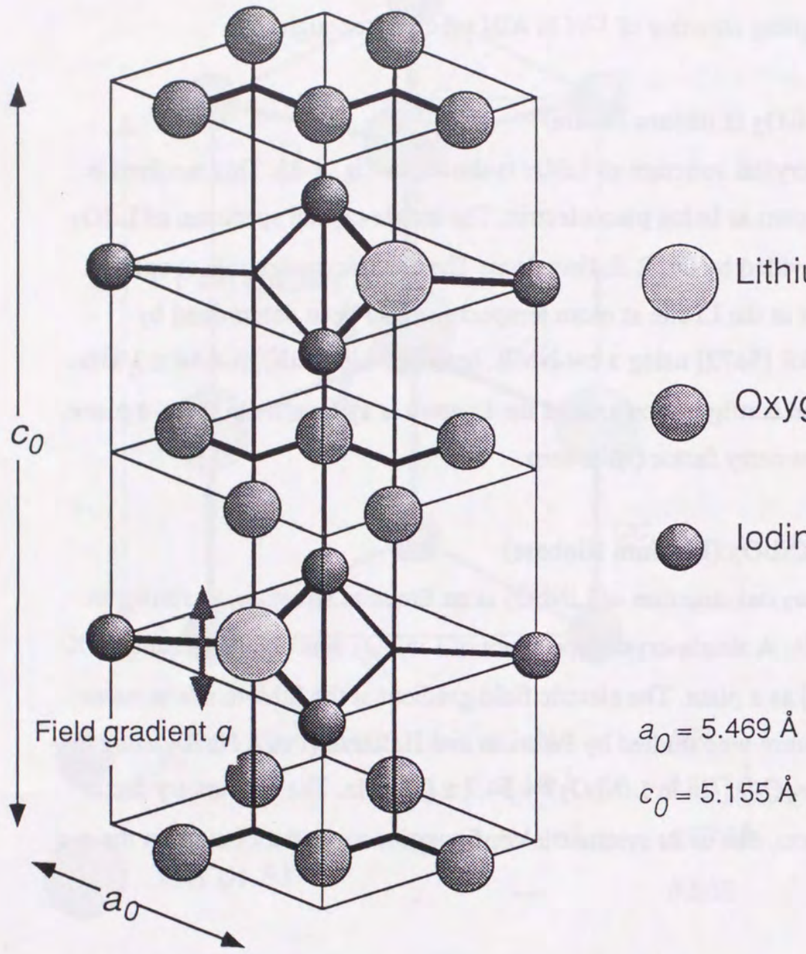

Figure 3-23 Crystal structure of $LiIO_3$.

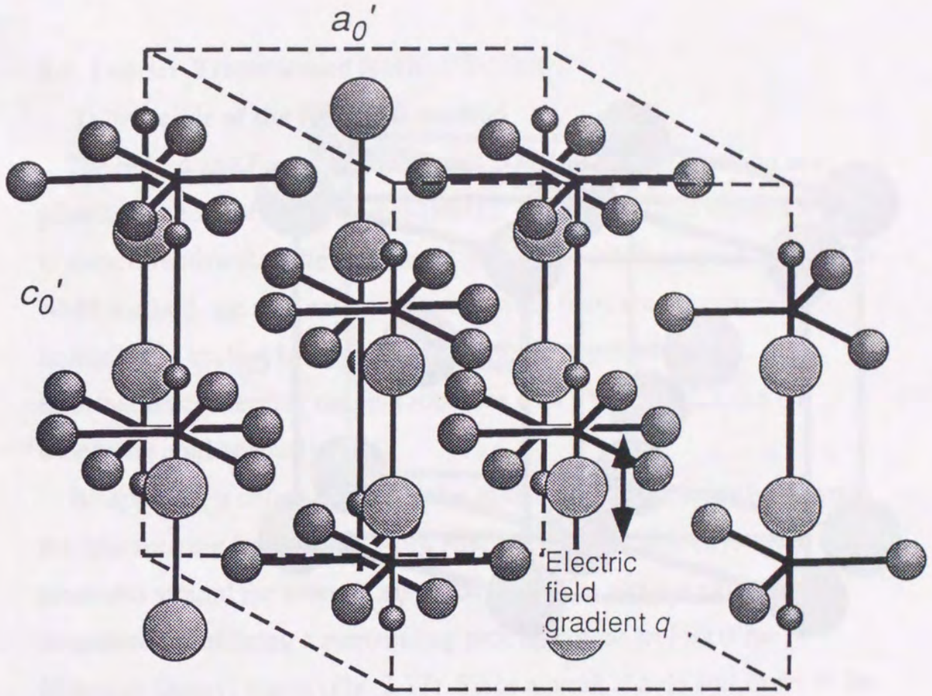

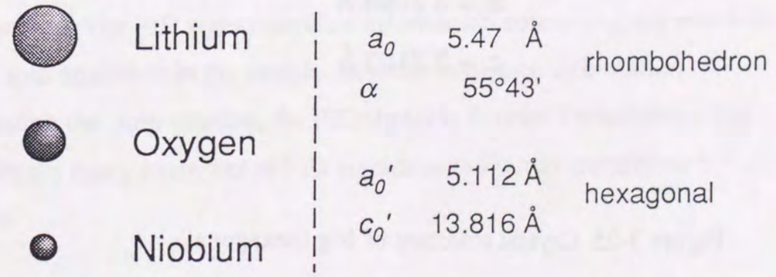

Figure 3-24 Crystal structure of $LiNbO_3$ (Ilmenite structure).

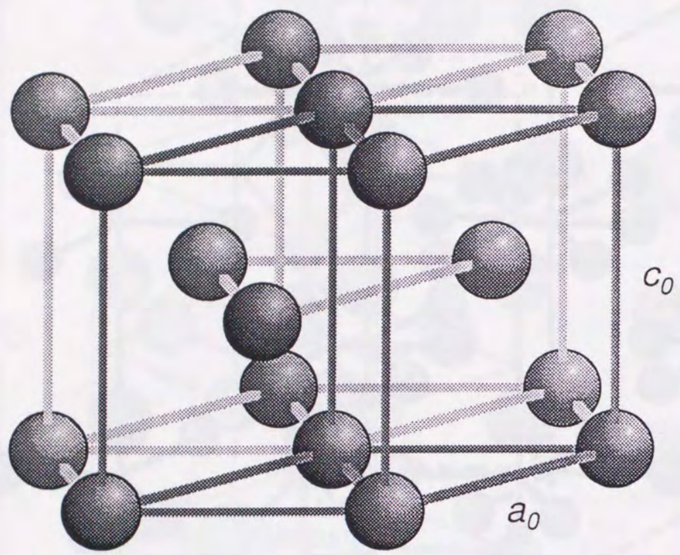

$a_0 = 3.2094$ Å

$c_0 = 5.2103$ Å

Figure 3-25 Crystal structure of Mg (hexagonal).

constant at room temperature as being $eqQ/h(^{12}\text{B in Mg}) = -47.0 \pm 0.1$ kHz [Ki90, Ki93c].

3-5 Fourier-Transformed NMR (FT-NMR)

1) Principle of the FT-NMR method

The pulsed and Fourier-Transformed NMR (FT-NMR) method is a popular method for NMR studies [Fu81]. The merit of this method is that it is more effective than the continuous-wave (cw) NMR method. In the FT-NMR method, the spin ensemble over a wide frequency region can be immediately excited by applying a strong, short-pulsed rf field. Information concerning the spin rotations over a wide region can be observed simultaneously.

By applying a strong, short rf pulse to the sample, the spins lie down in the spin rotating frame (Fig. 3-26). After a pulse, the sideways spins precesses around the external magnetic field. The rotation can be monitored by utilizing a surrounding pick up coil as an FID (Free Induction Decay) signal (Fig. 3-27). Since a weak rf field still flows in the coil after the pulse, the differential frequency relative to the applied rf can be observed. The FID signal contains information concerning the rotations of the spin ensemble in the sample. In order to deduce information concerning the spin rotation, the FID signal is Fourier Transformed. Fig. 3-27 shows many examples of FID signals with Fourier-transformed spectra.

2) Typical NMR spectra of highly oriented BN

The BN crystals used in this study were not perfect single crystal, as described above. The distribution of the *c*-axes that are related to the orientation of the field gradient affects the NMR spectrum. The NMR spectra are calculated based on several angles (α) between the magnetic

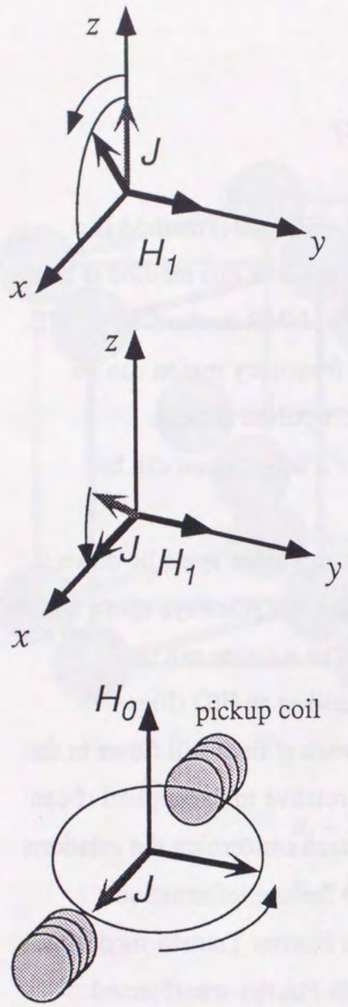

High intensity pulsed rf is applied
A nuclear spin start precessing
effective z axis in the rotating
frame fixed to the H_1 field.

Rf pulse is applied till the spin lay
in the x-y plane. (90° pulse)

After the 90° rf pulse, the spin is
precessing around H_0. This
precessing is detected by a pair of
pick up coils.

Figure 3-26 Principle of pulsed NMR.

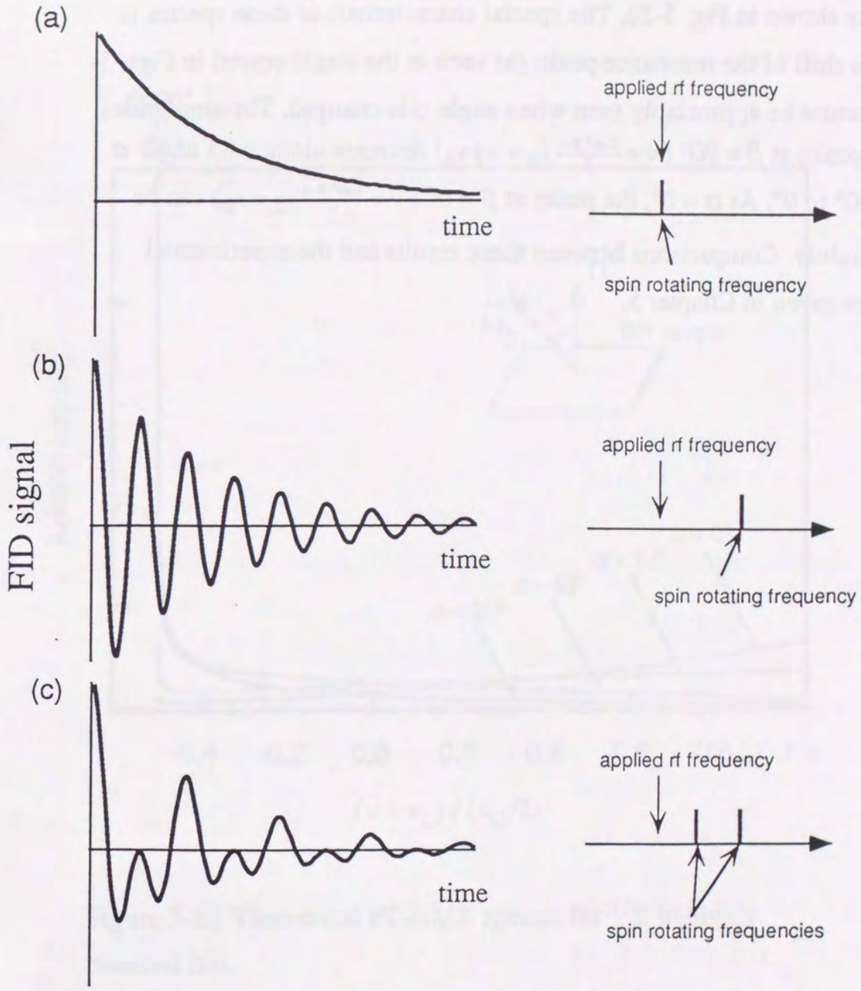

Figure 3-27 FID (free induction decay) signal of the spin rotating with frequency ω_L perturbed by the pulsed with frequency ω.

If the rotation frequency of the spin is same with the applied rf, FID signal is shown as the exponential decay corresponding with the transverse relaxation time (a). FID signals include the frequency differential from applied rf. (b), (c)

field and the crystal direction, in which the *c*-axes are mainly distributed; they are shown in Fig. 3-28. The special characteristic of these spectra is that the shift of the resonance peaks (as seen in the single crystal in Figs. 3-6, 7) cannot be appreciably seen when angle α is changed. The amplitudes of the peaks at $\beta = 90°$ ($\nu = \frac{3\cos^2\beta - 1}{2}\nu_Q = -\frac{1}{2}\nu_Q$) decrease along with angle α from 90° to 0°. At $\alpha = 0°$, the peaks at $\beta = 0°$ ($\nu = \frac{3\cos^2\beta - 1}{2}\nu_Q = \nu_Q$) can be seen slightly. Comparisons between these results and the experimental ones are given in Chapter 5.

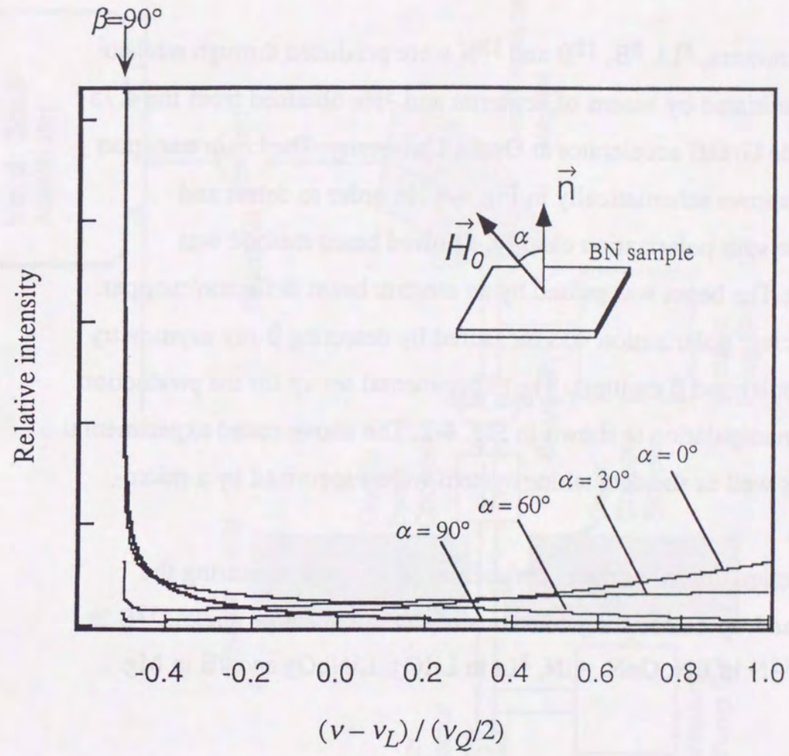

Figure 3-28 Theoretical FT-NMR spectra for ^{11}B in highly oriented BN.
They are resonance spectra between magnetic substates $m = \pm 1/2 \leftrightarrow \pm 3/2$. Note that the frequency of the peak corresponding to β=90° is not changed, but its amplitude is changed.

Chapter 4

EXPERIMENTAL APPARATUS

The β emitters, ^{8}Li, ^{8}B, ^{12}B and ^{12}N were produced through nuclear reactions initiated by beams of deuteron and ^{3}He obtained from the 4.75-MV Van de Graaff accelerator at Osaka University. The beam transport system is shown schematically in Fig. 4-1. In order to detect and manipulate spin polarization cleanly, a pulsed beam method was employed; The beam was pulsed by an electric beam deflector/chopper.

The nuclear polarization was measured by detecting β-ray asymmetry from the polarized β emitters. The experimental set up for the production and spin manipulation is shown in Fig. 4-2. The above stated experimental systems as well as the data taking system were supervised by a micro-computer.

This section describes the experimental setup used measuring the electric quadrupole coupling constants of several unstable nuclei: ^{12}B in BN, Mg, ^{12}N in BN, GaN, AlN, ^{8}Li in $LiIO_3$, $LiNbO_3$ and ^{8}B in Mg.

4-1 Target system

The target for the production of ^{12}B and ^{12}N was natural boron or enriched ^{10}B. The chemical forms used here were Li_2O and ^{6}LiF for ^{8}Li and ^{8}B production, respectively. A boron target was prepared by evaporating metallic boron on a Ta backing plate (0.5mm thick) with an electron bombarder. For the evaporation of lithium compounds on a copper backing (1mm thick), a conventional thermal evaporation technique was used. In order to stand for the intense beams of 20μA, the target was placed on a water-cooled target holder (Fig. 4-2). Fig. 4-3 shows the target's dimensions. To reduce the beam intensity for a unit area of the target, the

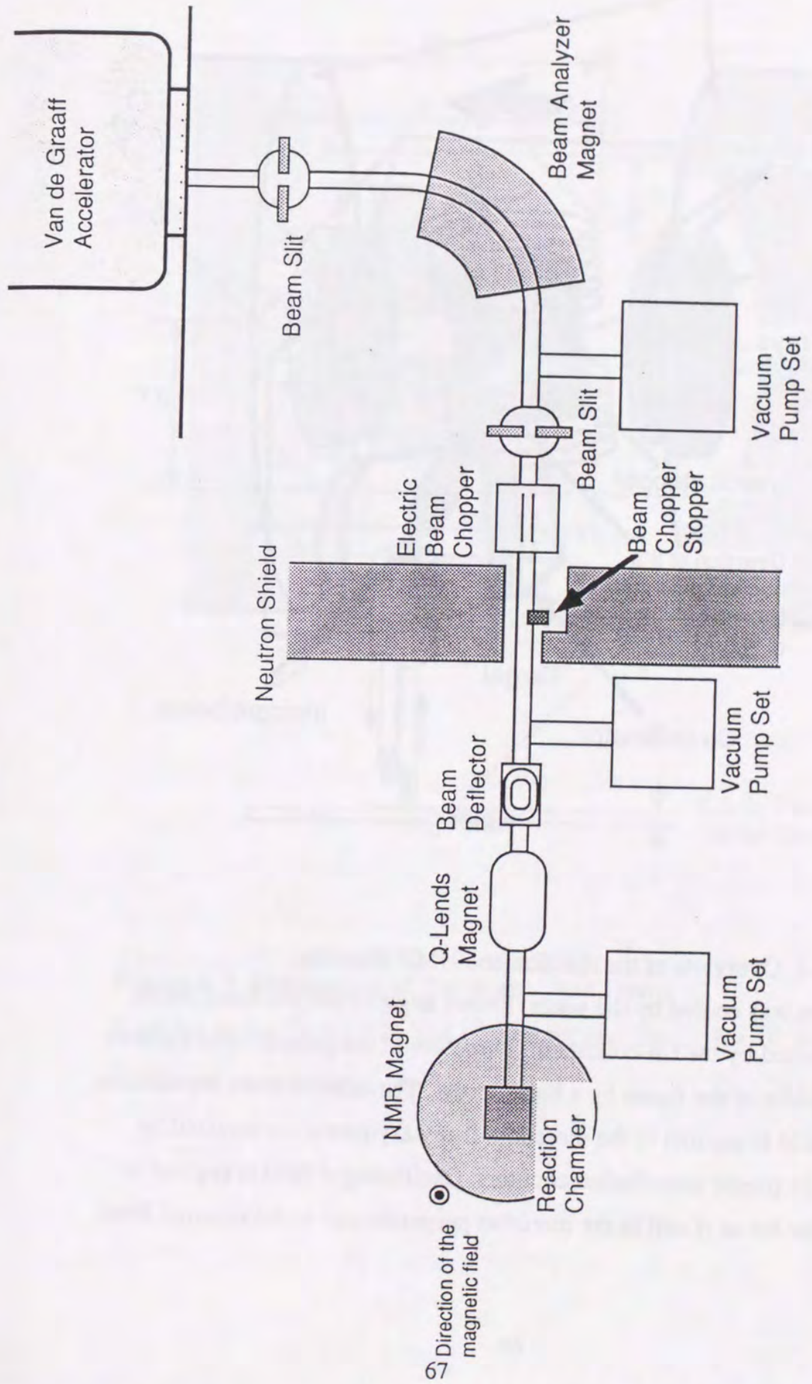

Figure 4-1 Beam transport system.

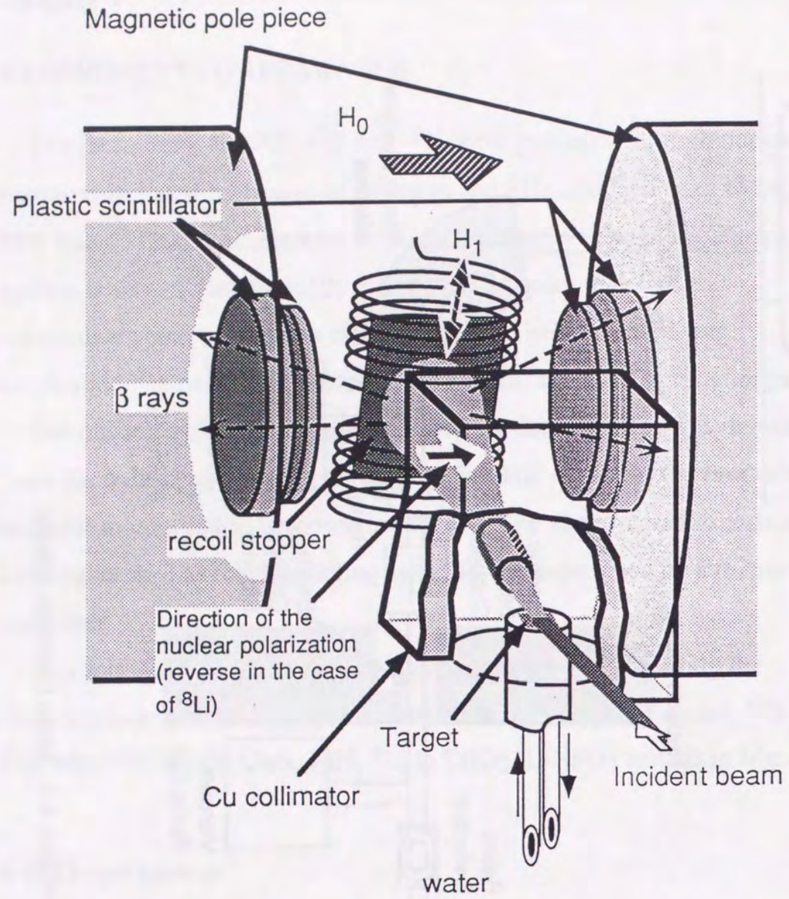

Figure 4-2 Overview of the reaction and NMR chamber.
The target was cooled by the water. Recoil angle of the produced nuclei were selected by the Cu-collimator. Direction of the polarization is shown in the middle of the figure by a black arrow. The external field to maintain polarization is parallel to the direction. β-ray asymmetry is detected by two sets of plastic scintillation counters. Oscillating rf field is applied to the catcher by an rf coil in the direction perpendicular to the external field.

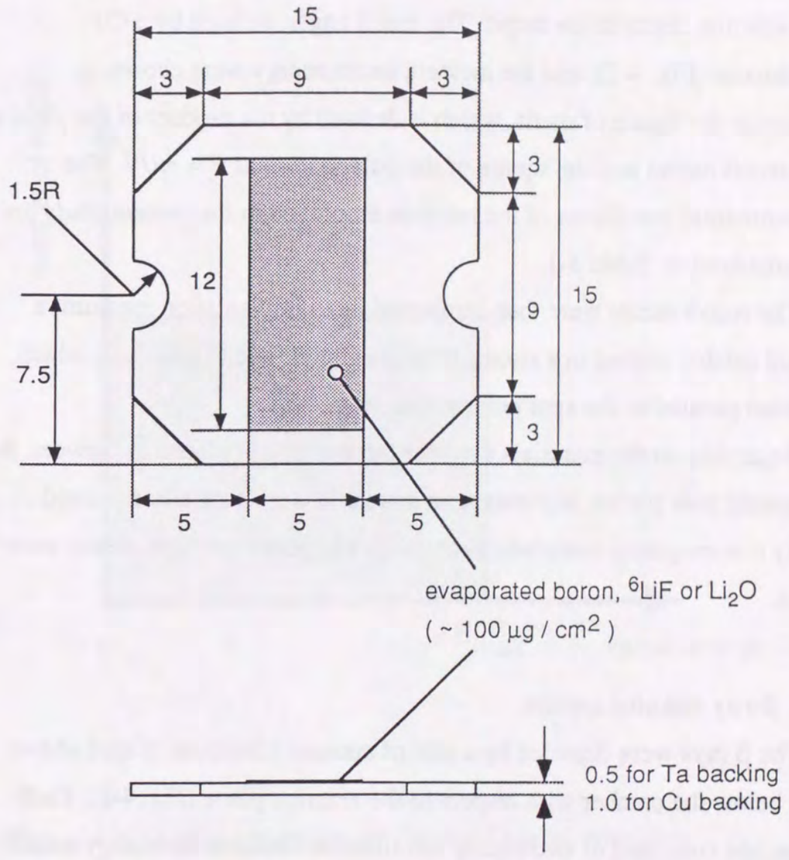

Figure 4-3 Dimensions of the target. (unit : mm)
Backing is the Ta for ^{12}B and ^{12}N target and the Cu for ^{8}B and ^{8}Li target, respectively.

target was tilted with a glancing angle of 5° with respect to the incident beam. The energy of the recoil nuclei ejected from the target was spread homogeneously from zero to the maximum energy (Fig. 4-4) in terms of the reaction depth in the target. The recoil angle, defined by a Cu collimator (Fig. 4-2), and the incident beam energy were chosen to optimize the figure of merit, which is defined by the product of the yield of the recoil nuclei and the square of the polarization as $F = n \times P^2$. The experimental conditions of the reaction employed in the present study are summarized in Table 3-1.

The recoil nuclei were then implanted in an implantation medium; a recoil catcher placed in a strong static magnetic field (Table 3-1), which applied parallel to the spin polarization (Fig. 4-2).

Regarding to the materials used for the equipment placed in between the magnetic pole pieces, any magnetic materials were carefully removed . Only non-magnetic materials, such as Cu block and stainless steels, were used.

4-2 β-ray counter system

The β rays were detected by a pair of counter telescopes placed above and below the catcher with respect to the reaction plane (Fig. 4-2). Each telescope consisted of two plastic scintillation counters: an energy sensitive 10mm thick E counter and a thin 2mm thick ΔE counter. The geometry of the counters is shown in Fig. 4-5. A plastic scintillator and a photo tube were connected by a light guide made of acrylates as shown in Fig. 4-6. For the connection an optical cement (admixture of Epikote 828 and Epomite B002 (Petro Chemicals Inc.), the ratio is 2 : 1) was used. A thin Cu plate (0.5mm) was placed between the two counters in order to stop any low energy β rays that comes from background activities. To avoid any gain shift of the photo tube due to its strong field, the counter system was

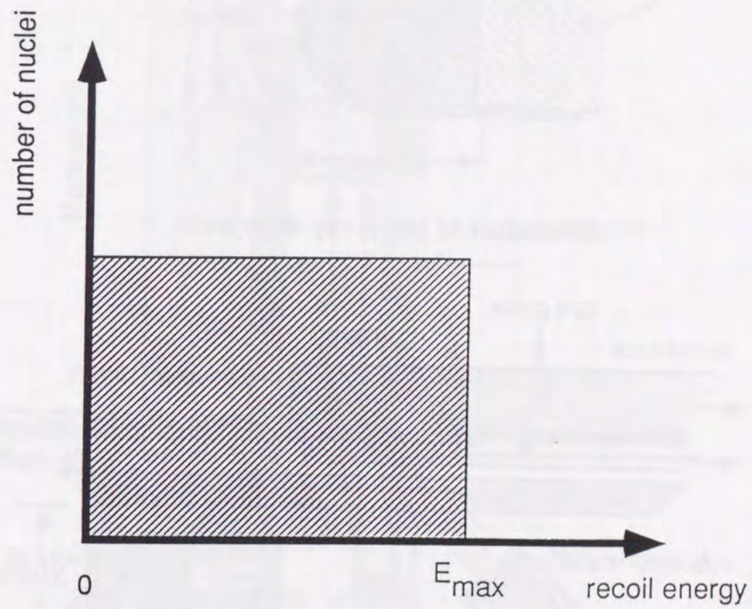

Figure 4-4 Distributed energy of the recoil nuclei emerging from the target.
The continuous distribution was due to the distribution of the reaction depth in the target and the energy loss before emerging out from the target.

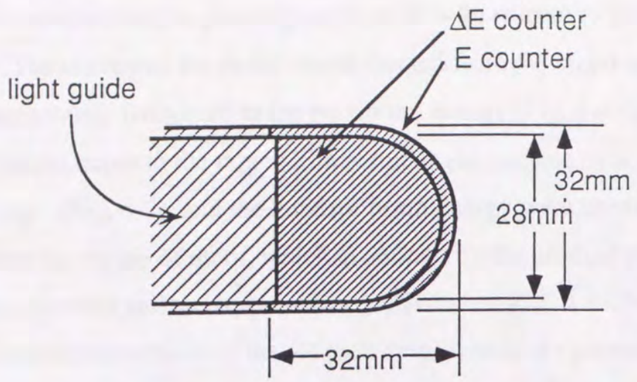

dimension of the β-ray detectors

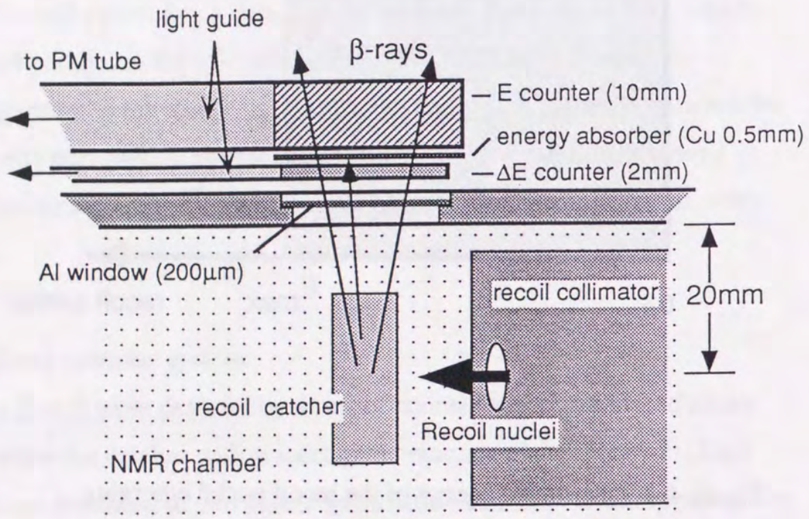

Top view of the NMR chamber and the β-ray detectors

Figure 4-5 Detailed geometry around the recoil catcher

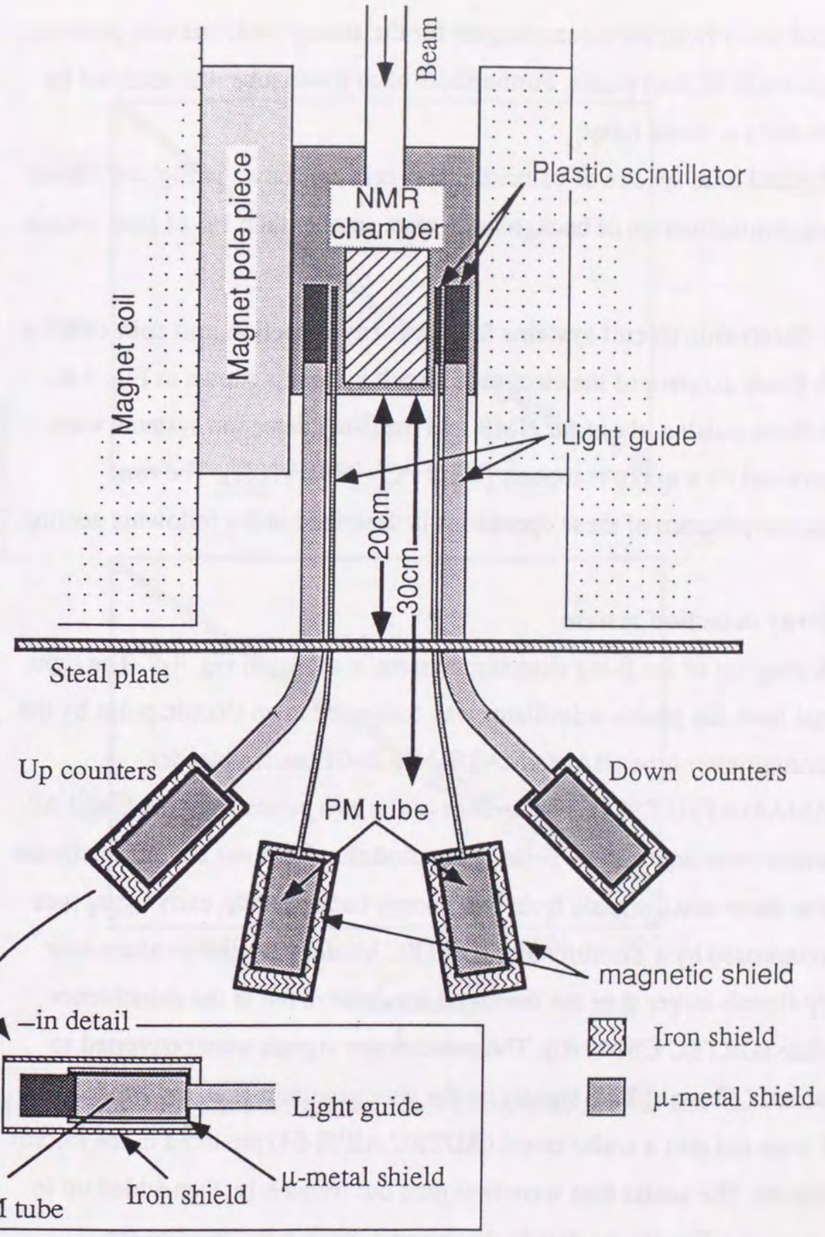

Figure 4-6 Magnetic shield for the β-ray detection system.
Top view of the β-ray detection system.

placed away from the electromagnet for the strong field, and was placed in a box made of steel plates. Furthermore each photo tube was shielded by steel and a μ-metal tubes.

Typical time spectra of coincidental β rays are shown in Fig. 4-7. In all cases, contamination of backgrounds were smaller than 1% of total counts.

4-3 Electronic circuit systems for the β-ray detection and spin control

A block diagram of the electronic circuit system is shown in Fig. 4-8. The beam pulsing, the rf for NMR and the β-ray detection systems were supervised by a micro computer (NEC PC - 9801 VX21). The time sequence program of these operations is described in the following section.

1) β-ray detection system

A diagram of the β-ray detection system is shown in Fig. 4-9. The light signal from the plastic scintillator was converted to an electric pulse by the photomultiplier tube (HAMAMATSU R329-01) with a bleeder (HAMAMATSU E934). The timings of the two pulses from the E and ΔE counters were adjusted by pulse-delay modules. To reject any noise signals and/or these small signals from low energy backgrounds, each signal was discriminated by a discriminator (ORTEC Model 924) and an attenuator. Only signals larger than the threshold levels were fed in the coincidence module (ORTEC C314/NL). The coincidence signals were converted to stretched (~5msec) TTL signals by the gate generator (LeCroy Model 222), and were fed into a scalar board (ADTEC AB98-04) mounted in the micro-computer. The scalar data were first read out frequently, then added up in the memory. Finally the data in the memory were transferred to the magnetic disk periodically.

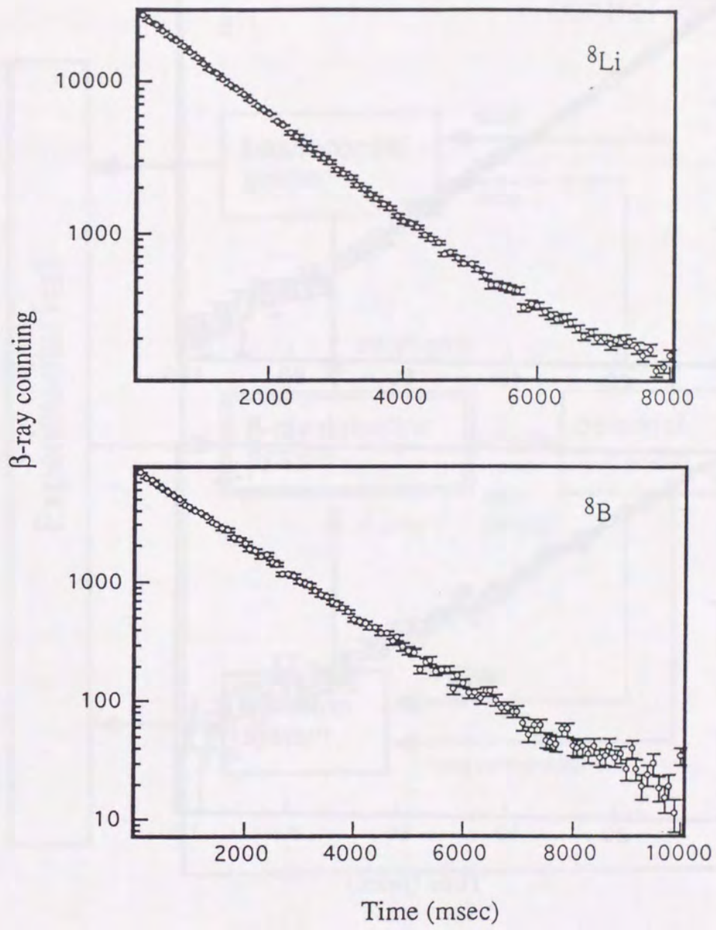

Figure 4-7(a) Typical time spectra of the β counting for ^{8}Li and ^{8}B.

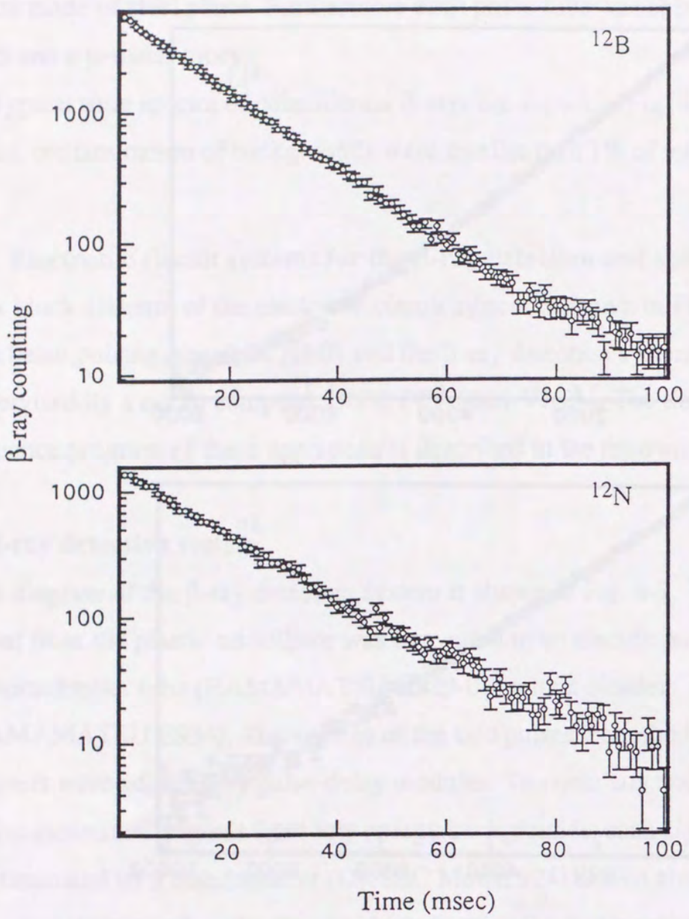

Figure 4-7(b) Typical time spectra of the β counting for ^{12}B and ^{12}N.

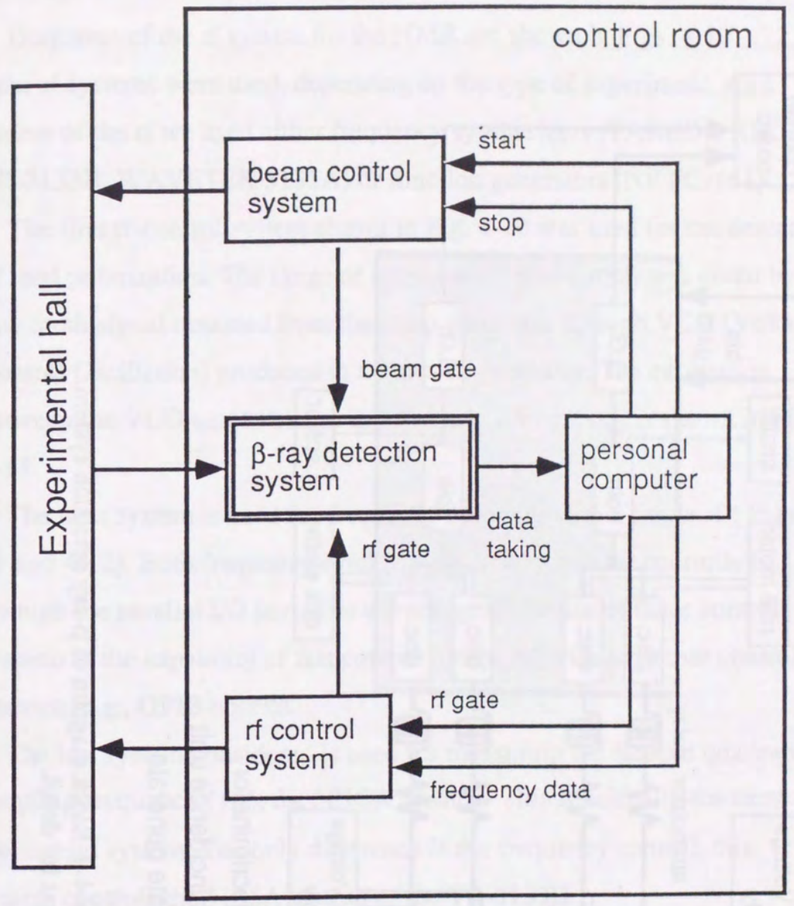

Figure 4-8 Block diagram of the computer control.
Beam, rf and β-ray detection data taking were supervised by a personal computer (NEC PC-9801 VX21).

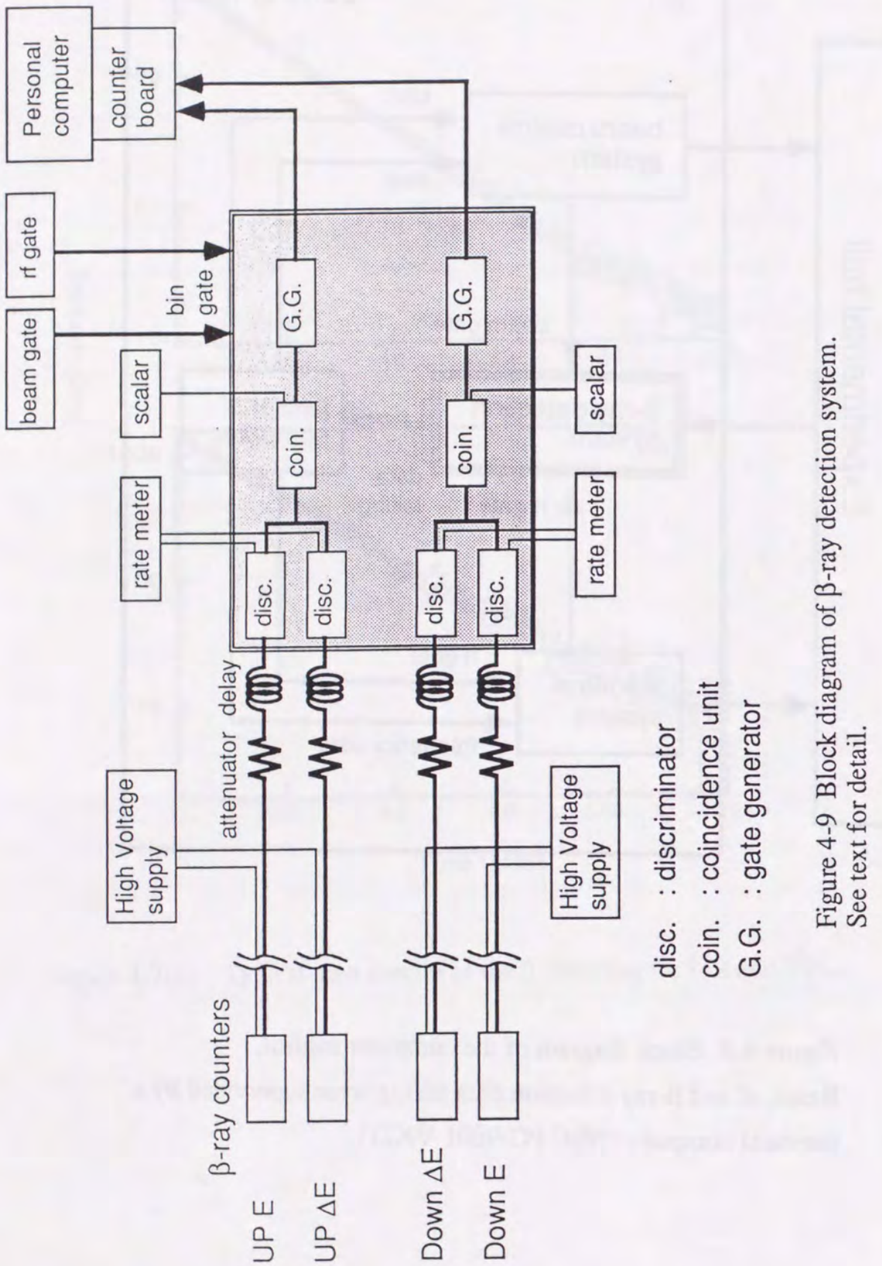

Figure 4-9 Block diagram of β-ray detection system. See text for detail.

2) Rf system for the β-NMR

Diagrams of the rf system for the NMR are shown in Figs. 4-10 ~ 12. Four rf systems were used, depending on the type of experiment. As a source of the rf we used either frequency synthesizers (TAKEDA RIKEN TR-3133B, WAVETEK 5135A) or function generators (NF FG-161).

The first rf-control system shown in Fig. 4-10 was used for the detection of total polarization. The range of a frequency modulation was given by a saw tooth signal obtained from the ramp generator through VCO (Voltage Control Oscillation) produced in a function generator. The calibration between the VCO input voltage and the output frequency is shown in Fig. 4-13.

The next system is used for frequency mapping with a single rf (Figs. 4-11 and 4-12). Both frequency synthesizers were computer controlled through the parallel I/O port. The advantage of the use of these control systems is the capability of fast control compared with any other control systems, e.g., GPIB control.

The last system considered is used for measuring the electric quadrupole coupling frequency (ν_Q), the NNQR method. This is basically the same as the second system. The only difference is the frequency control, this system controls the 5135A instead of the TR-3133B.

We used two kinds of modified drive systems for the NMR rf coil. One was a serial resonance circuit (Fig. 4-14a); the other was a parallel resonance circuit (Fig. 4-14b). The capacity "C" in the figures denotes a variable vacuum capacitor having a wide capacity range of 50 ~ 1500 pF, capable of standing for high voltages of up to 10kV. Since the inductance of the NMR rf coil was about 15μH, the system covered a range of resonance frequencies from 1.1 to 5.8 MHz. The Q values of these circuits were Q_{ser} ~ 80 and Q_{par} ~ 4; hence, the former was suitable for narrow-

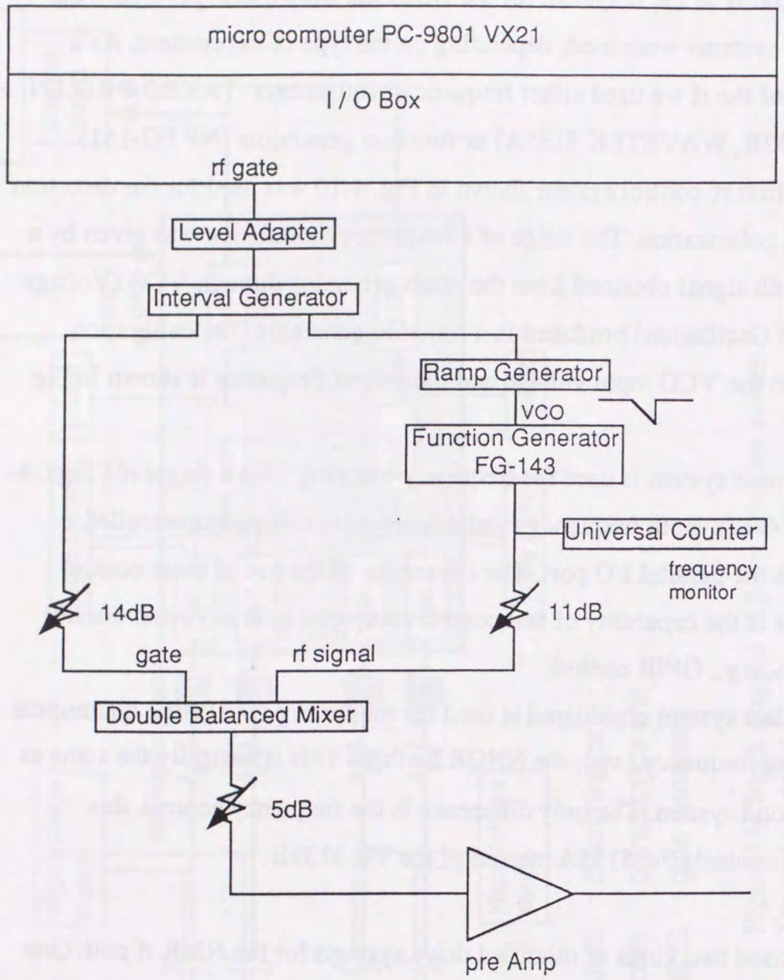

Figure 4-10 Block diagram of the rf control system (2AP mode). Frequency was turned manually.

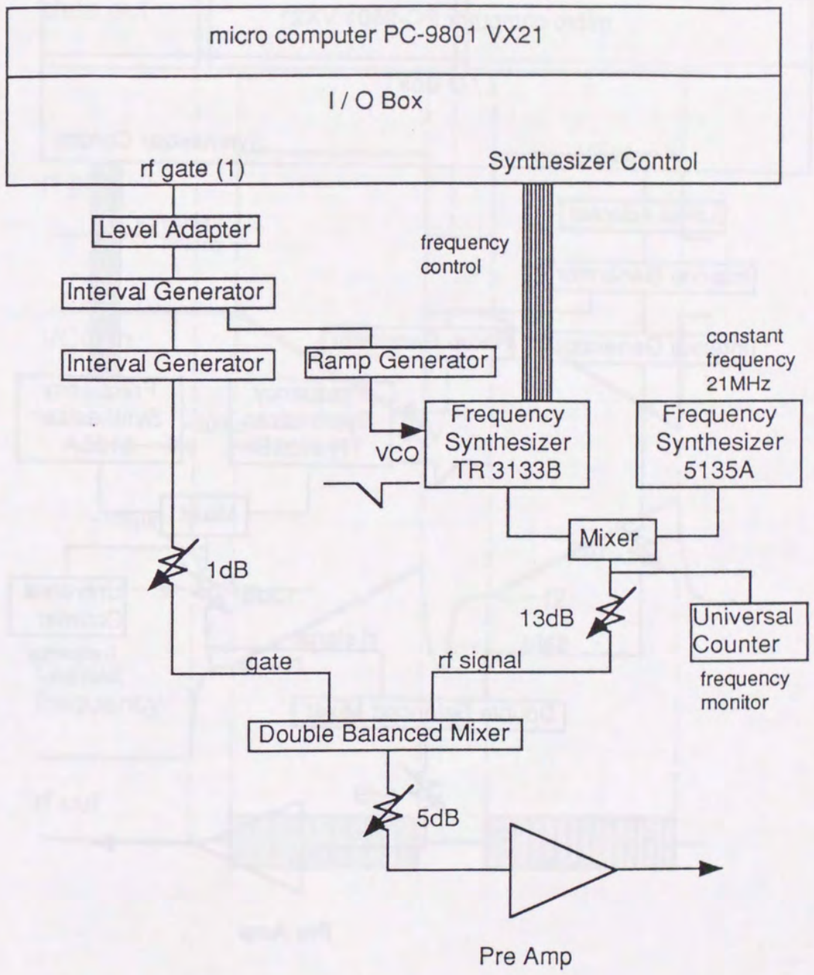

Figure 4-11 Block diagram of the rf control system (2AP, 2rf mode 1). The frequency synthesizer (TAKEDA RIKEN TR3133B) was controlled by the computer.

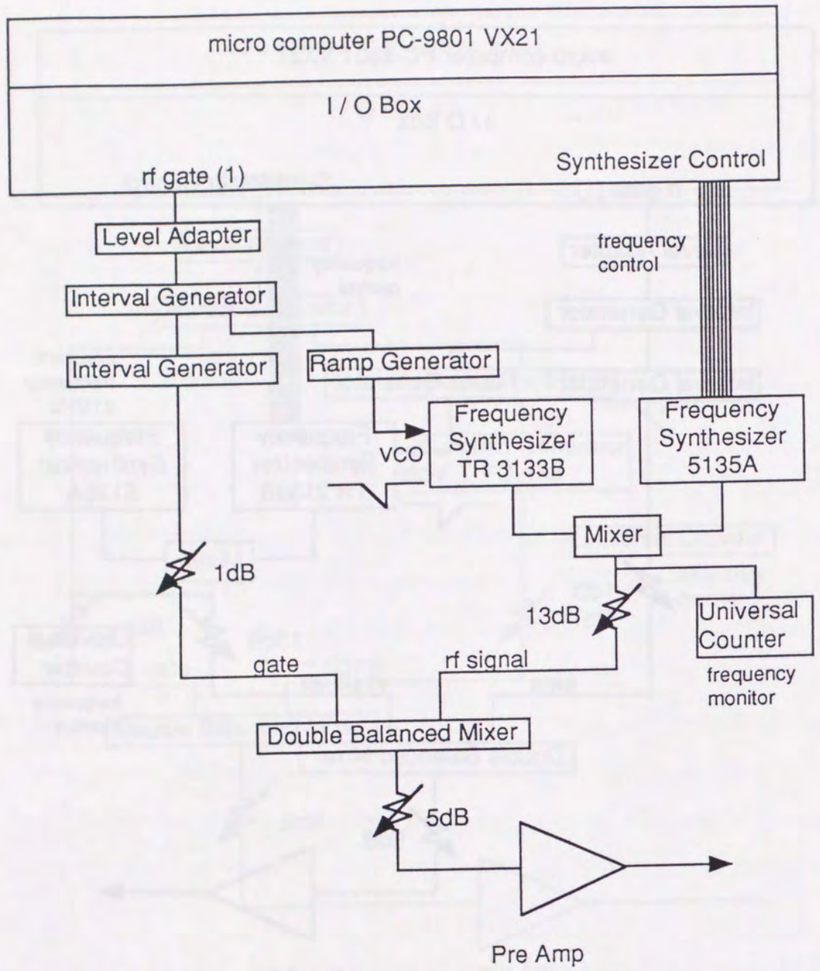

Figure 4-12 Block diagram of the rf control system (2AP, 2rf mode 2). The frequency synthesizer (WAVETEK 5135A) was controlled by the computer.

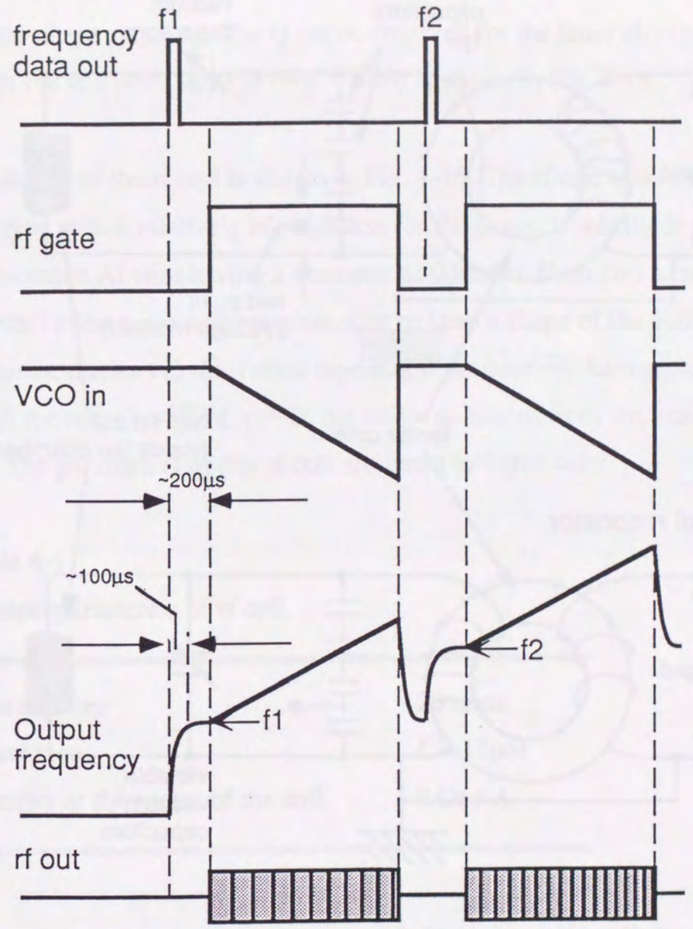

Figure 4-13 Timing chart of the rf control.
Frequency was controlled both digitally and through VCO. It takes about 100µs for the frequency synthesizer to output a stable frequency after the frequency data was set by the computer. The rf gate is applied considering this delay.

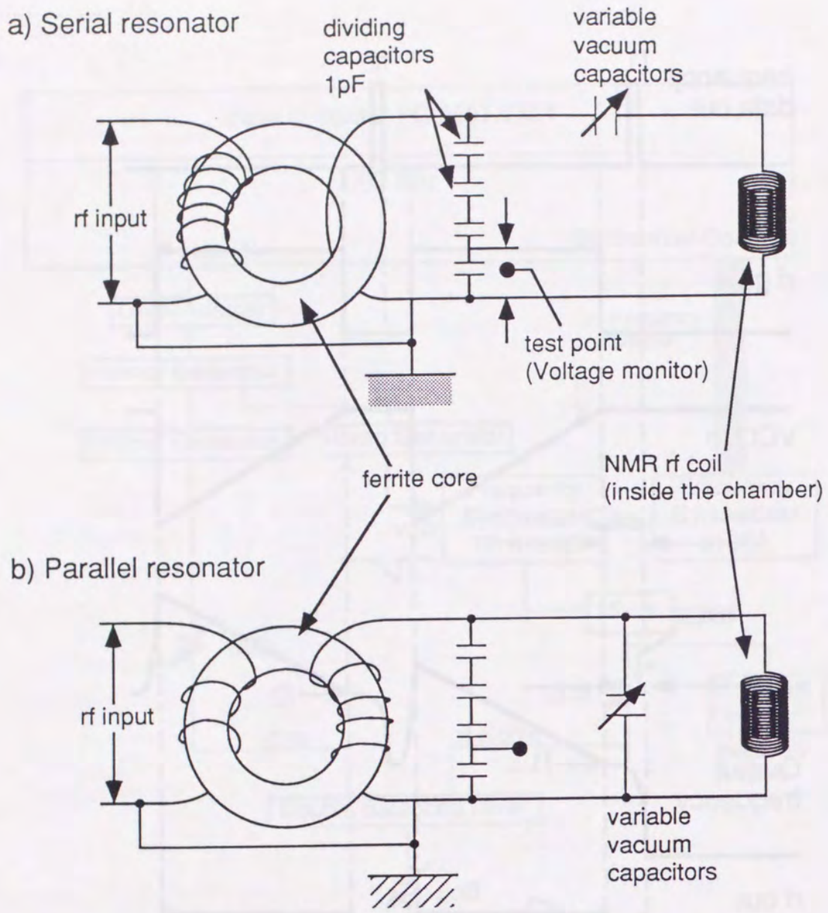

Figure 4-14 Rf resonator system

a) Narrow band rf system.

The ferrite core is for impedance matching.

b) Wide band rf system.

The number of turns for the rf input at ferrite core was determined to achieve the enough power and low Q-value.

range mapping with a high rf field H_1 (DQ), while the latter was suitable for wide-range mapping. The Q curve observed for the latter circuit through the test point voltage (Fig. 4-14b) is shown in Fig. 4-15.

An sketch of the rf coil is shown in Fig. 4-16. The rf coil was of the barrel type with a relatively big aperture for the beam. It was made of formal-coated Al wire having a diameter of 0.95mm. Each coil turn was tied with Teflon tapes to three glass rods to keep a shape of the coil. Since the fluorine nucleus in the Teflon tape might produce ^{20}F background through the reaction $^{19}F(d, p)^{20}F$, the coil was hidden from any scattered beam. The parameters of this rf coil are listed in Table 4-1.

Table 4-1

General parameters of rf coil.

Turn number	20 turns
Inductance	$L = 15\mu H$
Intensity at the center of the coil	8 Oe / A

This system can produce an intense rf field of about $H_1 \sim 40$ Oe at the center of the stopper.

3) System control by micro computers

A block diagram of the control by a computer is shown in Fig. 4-8. It consists of three blocks. Signals used for the control by the micro-computer NEC PC-9801 VX were TTL logic pulses.

The beam-gate-control system utilized three logic signals: "Start", "Stop" and a return signal "Monitor". When the electrostatic beam chopper

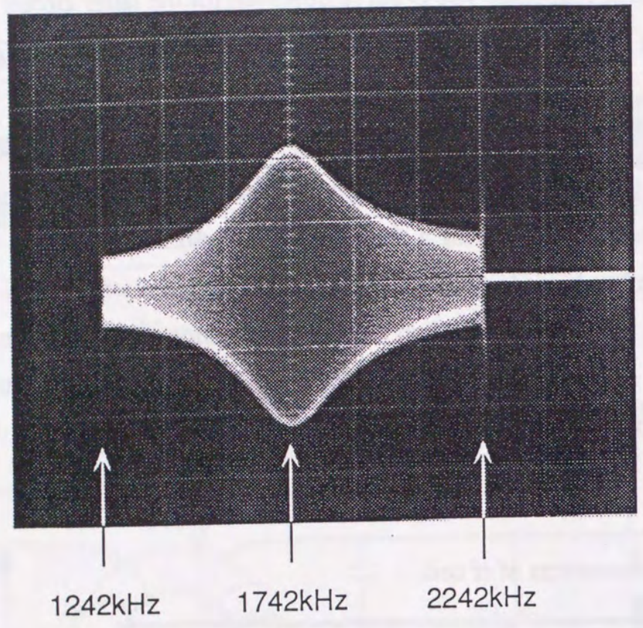

Q = 3.9

Figure 4-15 Q-curve of the parallel resonator system.
The very low Q-value is useful for wide range mapping.

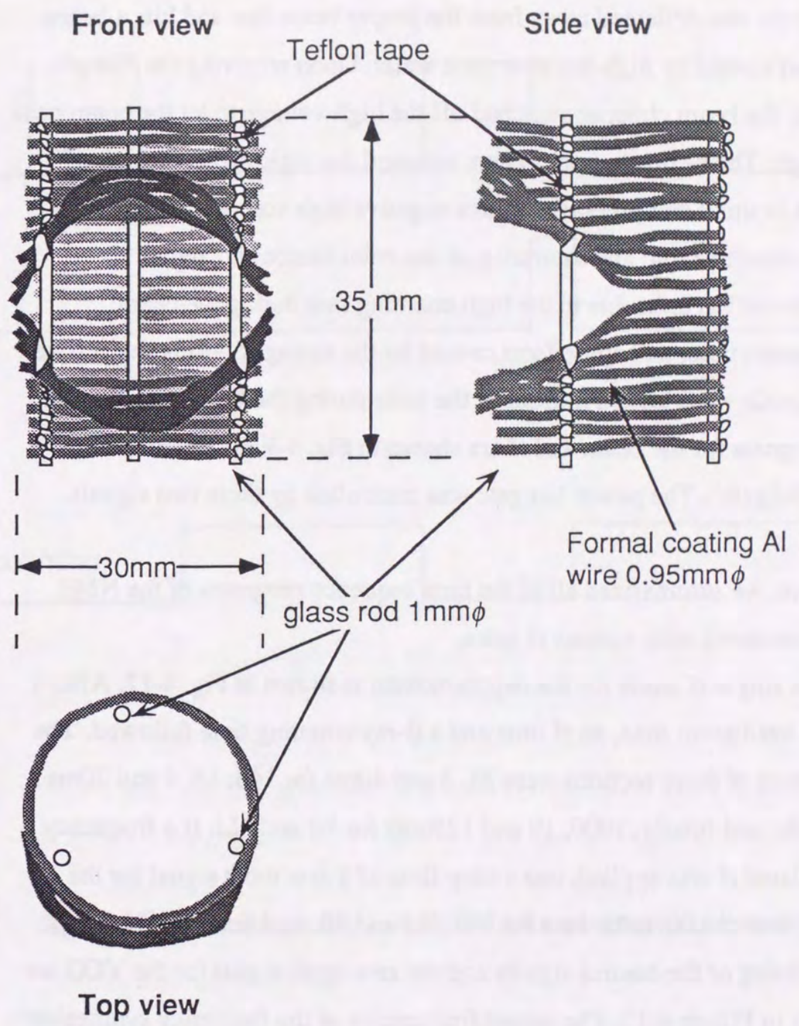

Figure 4-16 Overview of the rf coil.

received a "Start" signal, it applied a high voltage (~2.5kV) to the deflector plate with its response time shorter than 100μsec. Due to this high voltage the beam was deflected away from the proper beam line and hits a beam stopper cooled by high-resistive pure water. Upon receiving the "Stop" signal, the beam chopper switched off the high voltage to let the beam pass through. The beam chopper system returned the logic signal "Monitor" which is small and proportional to a negative high voltage.

In order to avoid any saturation of the coincidence and signal discrimination units due to the high counting rate during the beam irradiation time, and any effects caused by the strong rf during the rf time, the signals were locked in front of the units during the beam and rf times. The signals for the beam and rf are shown in Fig. 4-9 as "Beam monitor" and "Rf gate". The power bin gate was controlled by these two signals.

Here, we summarized all of the time sequence programs of the NMR measurements with various rf gates.

The single rf mode for the depolarization is shown in Fig. 4-17. After a beam irradiation time, an rf time and a β-ray counting time followed. The durations of these sections were 25, 5 and 40ms for ^{12}B; 15, 4 and 20ms for ^{12}N; and finally, 1000, 10 and 1250ms for ^{8}B and ^{8}Li. If a frequency modulated rf was applied, one sweep time of a saw tooth signal for the VCO, was chosen to be 1ms for ^{12}B, ^{8}Li and ^{8}B, and that for ^{12}N 0.8ms. The timing of the control signals and the saw-tooth signal for the VCO are shown in Figure 4-12. The output frequencies of the frequency synthesizer were also controlled by use of the numerical data in the computer. These data were sent to the synthesizer immediately after the beam was initiated in order to produce the frequency as described.

The asymmetry change of the on-resonance cycle from that of the off-resonance cycle is defined as follows:

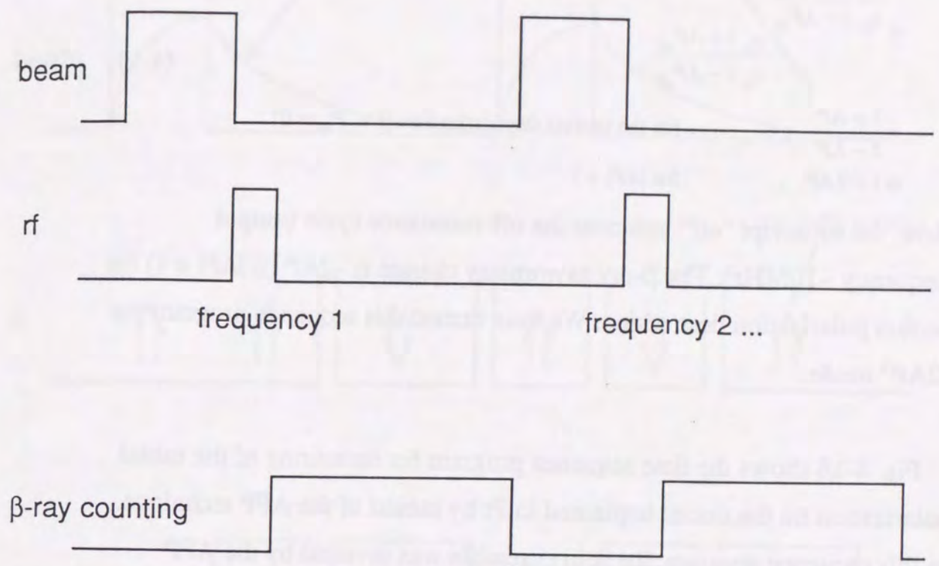

Figure 4-17 Time sequence program of the experiment (2AP mode).

$$\Delta = \frac{R_{on}}{R_{off}}$$

$$= \frac{\dfrac{\varepsilon_u}{\varepsilon_d}\dfrac{1+AP_{on}}{1-AP_{on}}}{\dfrac{\varepsilon_u}{\varepsilon_d}\dfrac{1+AP_{off}}{1-AP_{off}}} \qquad (4\text{-}1)$$

$$= \frac{1+AP}{1-AP}, \qquad \text{for the perfect depolarization (i.e. } P_{on}=0)$$

$$\cong 1+2AP, \qquad \text{for } |AP| \ll 1 .$$

Here, the subscript "off" indicates the off-resonance cycle (output frequency ~10MHz). The β-ray asymmetry change is $-2AP$ (if $|AP| \ll 1$) for perfect polarization destruction. We thus named this sequence program the "2AP" mode.

Fig. 4-18 shows the time sequence program for measuring of the initial polarization on the nuclei implanted in Pt by means of the AFP technique. In this sequence program, the spin ensemble was inverted by the AFP method. For a perfect cancellation of the effect caused by the fluctuation of the beam position on the target, a count time was further divided in two counting sections. In between the two sections one extra rf time was prepared where the same rf for the beam-count cycle was applied. After rf of the right on-resonance frequency, the spin direction was inverted by the rf. Direction of spin ensemble in each β-ray counting sections are shown in the figure by arrows. The advantage of this sequence program is that the influence from any fluctuation of the incident beam position is excluded, and the figure of merit is improved over that of the depolarization mode by a factor of 4. Neglecting the degree of achievement for the spin inversion and relaxation of the polarization, and assuming no background counting, the NMR effect is described as follows:

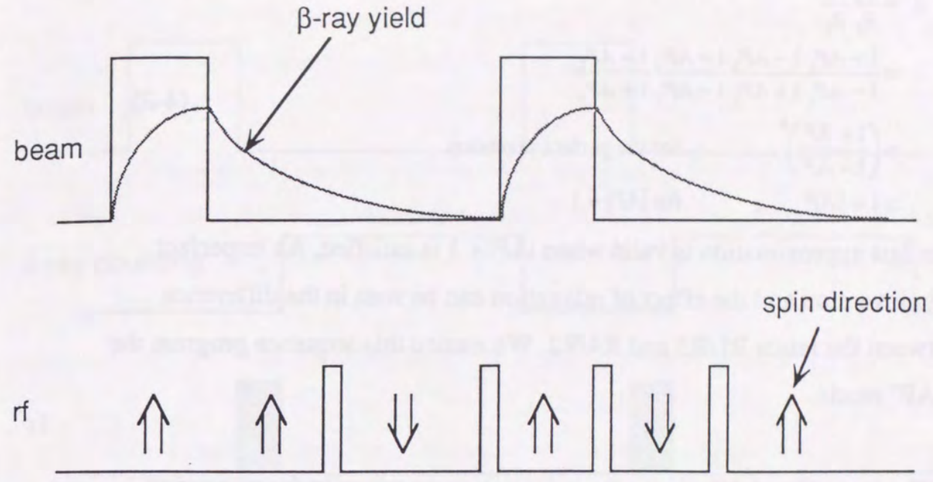

Figure 4-18 Time sequence program of the experiment (8AP mode). Arrows indicate the direction of the spin with perfect inversion by the AFP.

$$\Delta' = \frac{R_1}{R_3}\frac{R_4}{R_2}$$
$$= \frac{1+AP_1}{1-AP_1}\frac{1-AP_3}{1+AP_3}\frac{1+AP_4}{1-AP_4}\frac{1-AP_2}{1+AP_2} \qquad (4\text{-}2)$$
$$= \left(\frac{1+AP}{1-AP}\right)^4, \qquad \text{for the perfect inversion}$$
$$\equiv 1+8AP \quad , \qquad \text{for } |AP| \ll 1 .$$

The last approximation is valid when $|AP| \ll 1$ is satisfied. An imperfect spin inversion and the effect of relaxation can be seen in the difference between the ratios R1/R3 and R4/R2. We named this sequence program the "8AP" mode.

The last (Fig. 4-19) shows the main sequence program for measuring the electric quadrupole coupling frequency (ν_Q). There is only a slight difference between the time sequence program for the spin $I = 1$ and that for $I = 2$, i.e., the number of the rf frequencies to be applied is different. In the following is a description for the case $I = 1$. Since the resonance peak is split by the coupling frequency (ν_Q; Fig. 3-15b), two kinds of rf's were applied alternately, as shown in figure, in order to destroy the polarization. There was a slight difference between the ^{12}B and the ^{12}N cases. For ^{12}B, rf time follows immediately after the beam end, like in all the other sequence programs. For ^{12}N, the rf time begins at the beam time, because the lifetime of ^{12}N is too short relative to the sequence. The frequency data are sent immediately after the rf start signal. There is a certain dead time for the frequency synthesizer to give out the frequency, about 40μs for WAVETEK 5135A, and 100μs for TAKEDA RIKEN TR3133B. Therefore rf gates are delayed by 100~200μs from the rf-data signals as shown in the figure. We named this the "NNQR" mode. It is abbreviated as "New Nuclear Quadrupole Resonance".

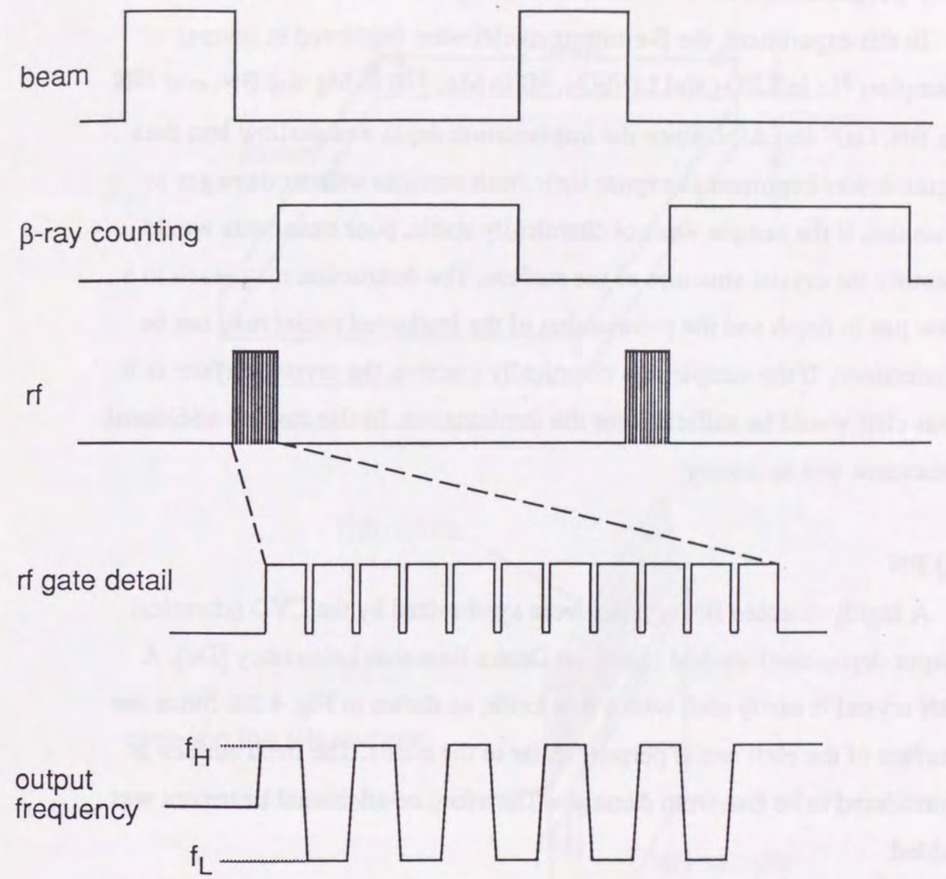

Figure 4-19 Time sequence program of the experiment (2rf (NNQR) mode).

The frequency operation in the rf gate was different from the 2AP mode. This is shown in the case for the spin $I = 1$.

4-4 Preparation and treatment of the implantation media

In this experiment, the β-emitting nuclei were implanted in several samples; ^{8}Li in $LiIO_3$ and $LiNbO_3$, ^{8}B in Mg, ^{12}B in Mg and BN, and ^{12}N in BN, GaN and AlN. Since the implantation depth was shallow less than 1μm, it was important to expose their fresh surfaces without damages to vacuum. If the sample was not chemically stable, poor treatments would destroy the crystal structure of the surface. The destruction may reach to a few μm in depth and the polarization of the implanted nuclei may not be maintained. If the sample was chemically inactive, the crystal surface as it was cleft would be sufficient for the implantation. In this case no additional treatment was necessary.

1) BN

A highly oriented BN crystals were synthesized by the CVD (chemical vapor deposition) method [Su90] at Denka Research Laboratory [De]. A BN crystal is easily cleft with a thin knife, as shown in Fig. 4-20. Since the surface of the cleft one is perpendicular to the *c*-axis. The fresh surface is considered to be free from damages. Therefore no additional treatment was added.

After a few days of implantation using the selected β emitters of 10^2/s, the amount of implanted nuclei reached nearly 10^9, and the sample has a slight brownish color. Colored samples were not used for further implantation experiment.

2) GaN

GaN samples were supplied as single crystals that were grown by the MOCVD (metal organic chemical vapor deposition) method [It85]. It was considered that the surface of the supplied sample was suitable for the

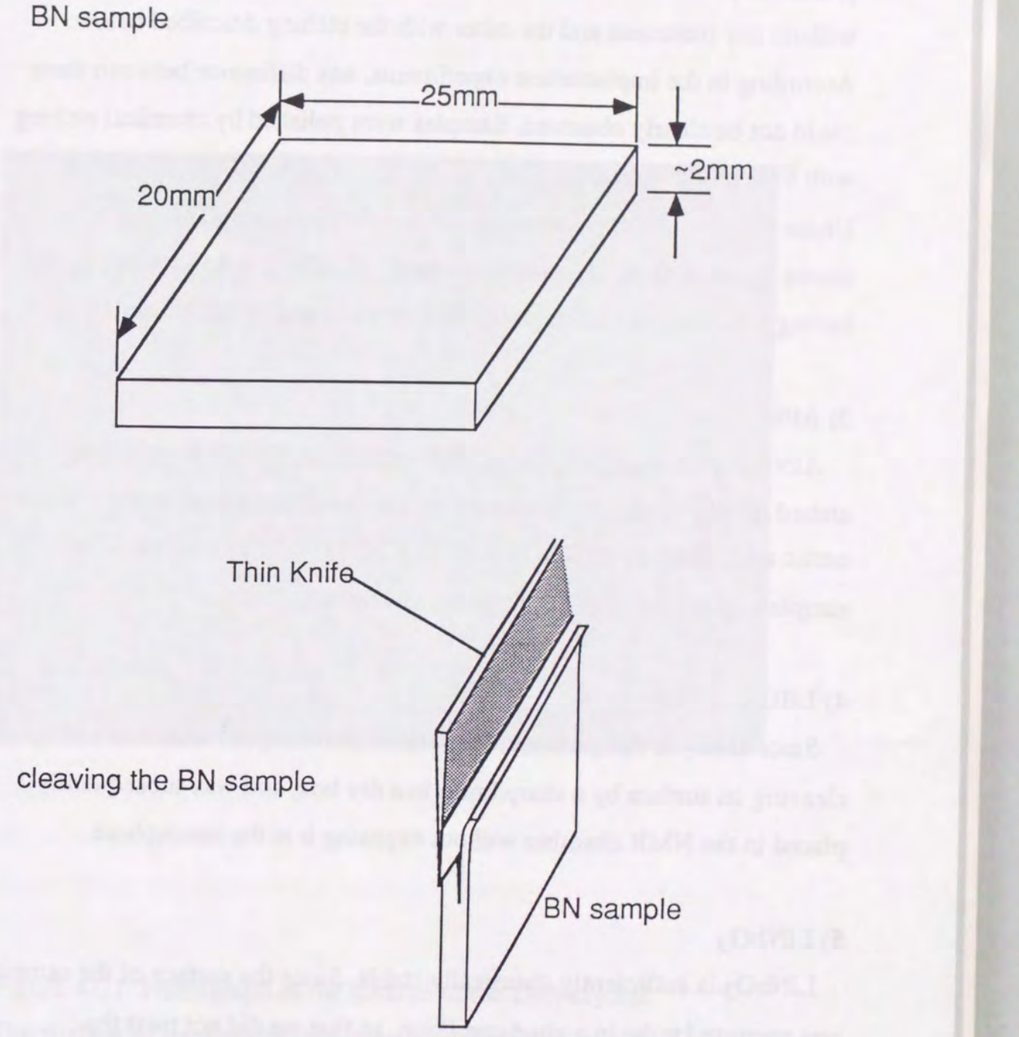

Figure 4-20 The BN sample and its cleavage.
Highly oriented hBN sample is easily cleft perpendicular to the c-axis by a thin knife.

present implantation experiment. We prepared two types of catcher; one without any treatment and the other with the etching described below. According to the implantation experiments, any difference between them could not be clearly observed. Samples were polished by chemical etching with 85% phosphoric acid (H_3PO_4) for 30 minutes at room temperature. Under this condition, the etching rate was 0.1μm/min [Si76]. Fig. 4-21 shows the surface of a GaN crystal observed using a metallic microscope having a the magnification × 600. Hexagonal patterns can be clearly seen.

3) AlN

AlN samples were polycrystal. The surface of the AlN sample was etched [Pe76] by use of the etchant which consisted of pure water: glacial acetic acid: nitric acid (HNO_3: 1.40N) = 10 : 10 : 10 by volume. The sample was etched in this etchant for one minute.

4) $LiIO_3$

Since $LiIO_3$ is deliquescent, the surface of the crystal was obtained by cleaving its surface by a sharp knife in a dry box, and was subsequently placed in the NMR chamber without exposing it to the atmosphere.

5) $LiNbO_3$

$LiNbO_3$ is sufficiently chemically stable. Since the surface of the sample was supposed to be in a good condition, so that we did not treat the $LiNbO_3$ samples.

6) Mg

A Mg metallic single crystal was polished by chemical etching with 10% citric acid ($C_6H_8O_7$) for a few minutes and was rinsed in a 2.8% ammonia

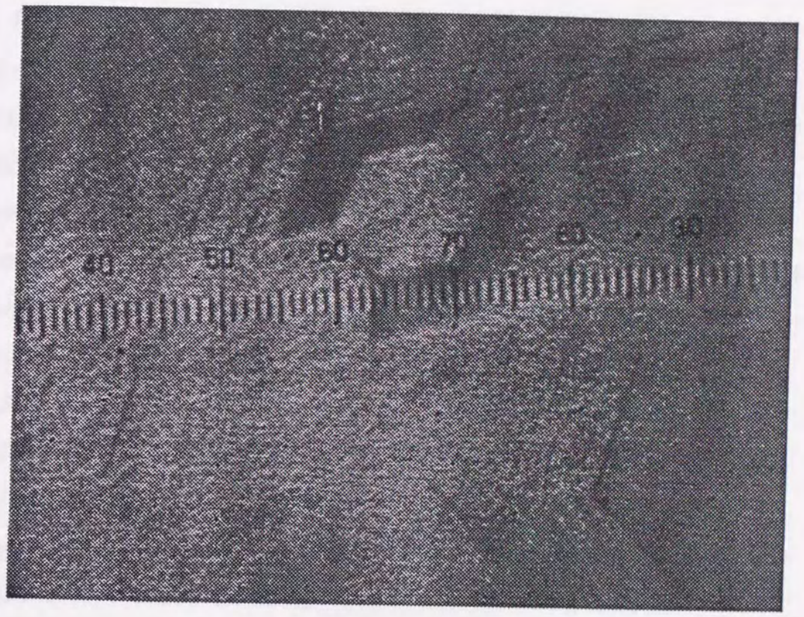

Figure 4-21 Photograph of the surface of the GaN crystal. The surface of the GaN crystal grown by MOCVD on a Al_2O_3 plate. (600 magnifications) : 1 division = 2.5 μm. The hexagonal structure can be seen clearly at the surface.

solution under ultrasonic agitation for a few seconds. The surface was then dried by blowing its surface with a strong flow of dry N_2 gas.

Chapter 5

EXPERIMENTAL RESULTS

5-1 Quadrupole moment of ^{12}B

1) β-NMR detection of ^{12}B in BN

The quadrupole coupling constant (eqQ/h) of stable ^{11}B at the boron site of BN was reported by Connor [Co90] and Silver [Si60], who used the conventional NMR detection of the stable isotopes. The quadrupole moment of ^{12}B had been reported by Minamisono et al. [Mi78]. With these values, the coupling constant (eqQ/h) for ^{12}B was given with the relative error of ~10%.

As a first step, the polarization maintained during the implantation was measured for ^{12}B in a BN crystal. An rf oscillating field (H_1) with a very wide frequency modulation (FM; 1 MHz), which covered all of the resonances of ^{12}B in BN, was applied. The observed polarization (P) was about 2.5%. About 36 Oe of H_1 was sufficiently strong for a perfect destruction of the polarization. Two thirds of the polarization produced in the nuclear reaction was destroyed during the implantation.

In the next step, the resonance frequency of the double quantum transition (ν_{DQ} :$m = 1 \leftrightarrow -1$) was observed. A double quantum transition requires an even stronger field (H_1). H_1 was 46 Oe and FM was ±20 kHz. A rough mapping result is shown in Fig. 5-1. The observed polarization change was consistent with that observed in the previous step (single quantum transition: SQ). Mapping of the frequency was then carried out with a monochromatic (no FM, and H_1 = 28 Oe) rf. A typical observed spectrum obtained at H_0 = 5kOe and T = 300K is shown in Fig. 5-2. The half width at half maximum (HWHM) of the observed spectrum was

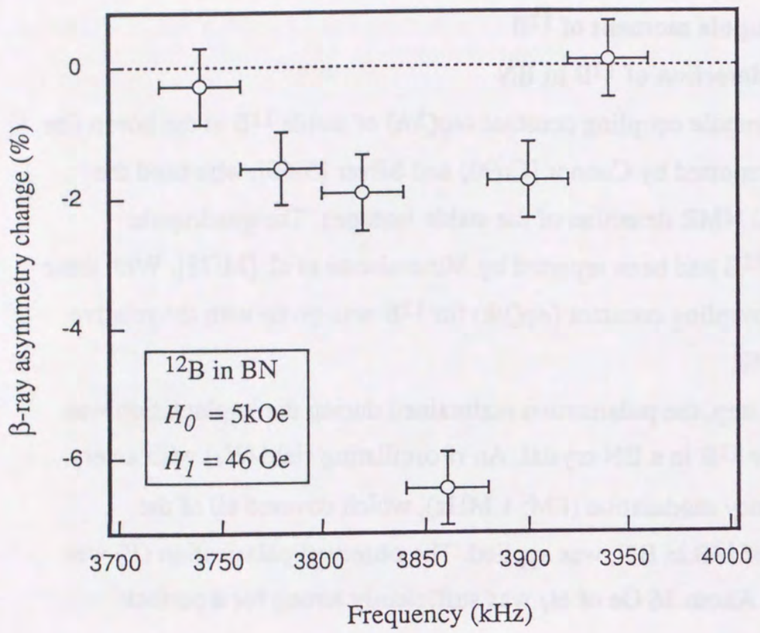

Figure 5-1 Detection of double quantum transition (DQ) of ^{12}B in BN. The double quantum transition frequency was roughly measured by the β-NMR method. The horizontal bar expresses FM. The highly oriented axis of BN was perpendicular to the external field.

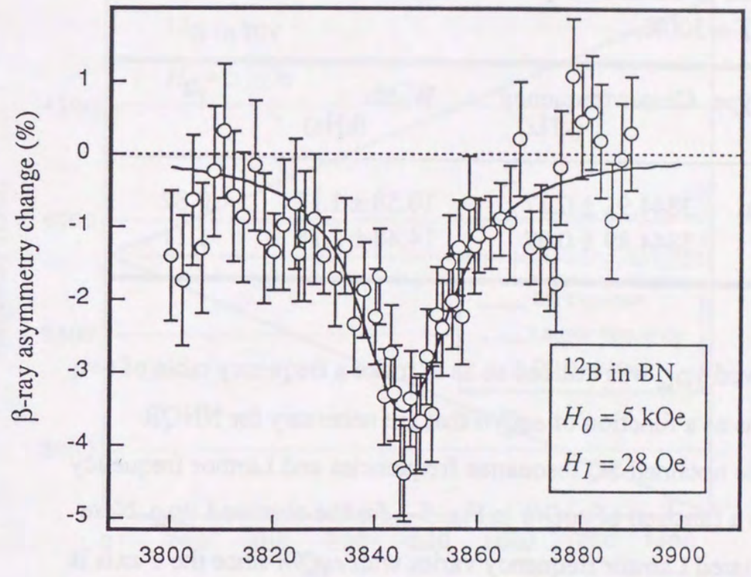

Figure 5-2 Detection of DQ transition of ^{12}B in BN with a monochromatic rf.
The double quantum transition frequency was measured precisely. The highly oriented axis of BN was perpendicular to the external field. The solid curve is the best theoretical fit to the data.

obtained by fitting a theoretical spectral function to the data. The experimental results are shown in Table 5-1.

Table 5-1
Fitting result of the double quantum transition of ^{12}B in BN at H_0 = 5kOe and T = 300K.

Function type	Center frequency (kHz)	Width (kHz)	χ^2
Lorentzian	3844.91 ± 0.77	10.58 ± 1.17	0.82
Gaussian	3844.89 ± 0.97	14.48 ± 1.18	1.11

The observed ν_{DQ} was utilized so as to make a frequency table of two SQ transitions as a function of eqQ/h that are necessary for NNQR detection. The obtained SQ resonance frequencies and Larmor frequency are shown as a function of eqQ/h in Fig. 5-3 for the observed ν_{DQ}. Note that the estimated Larmor frequency varies with eqQ/h since the c-axis is placed vertical to the externally applied strong magnetic field.

Finally, a typical spectrum obtained at H_0 = 5kOe and T = 300K was observed by the NNQR method, as shown in Fig. 5-4. The horizontal axis is the quadrupole coupling frequency (ν_Q; = 3/4 eqQ/h for $\beta = 90°$) and the vertical axis the β-ray asymmetry change. The angle between the external field and the main c-axis of BN was $\beta = 90°$. At higher frequencies, the resonance curve is consistent with the predicted shape for the substitutional boron site. The asymmetry parameter of the electric field gradient was expected to be $\eta = 0$ based on the symmetry of the BN crystal structure in the a-a plane. The intensity of the applied rf field was 3 Oe. FM was ±40 kHz. At lower frequencies, a small lump can be seen, which is considered to come from the substitutional nitrogen site. The spin of the nucleus

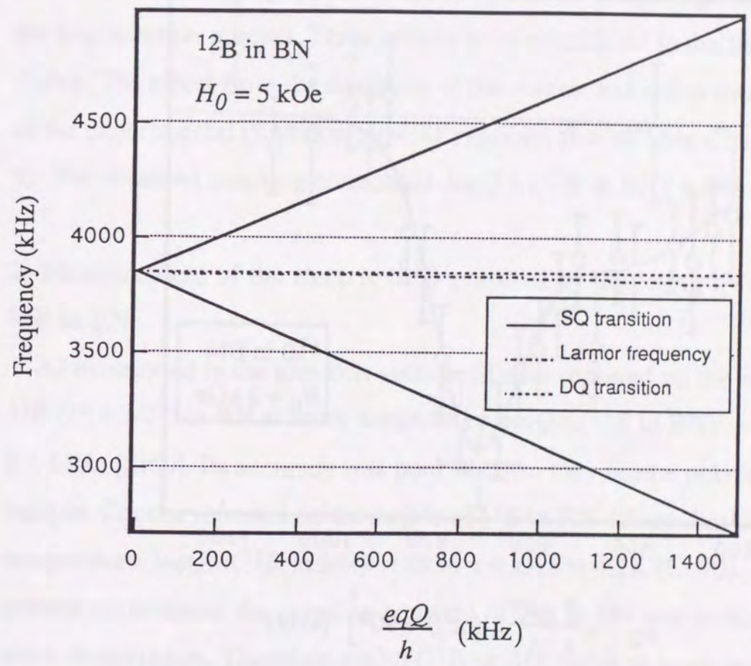

Figure 5-3 Two single quantum (SQ) frequencies and the Larmor frequency ν_L as a function of the coupling constant (eqQ/h). The rf frequency table for the control of the frequency synthesizer was made from this data.

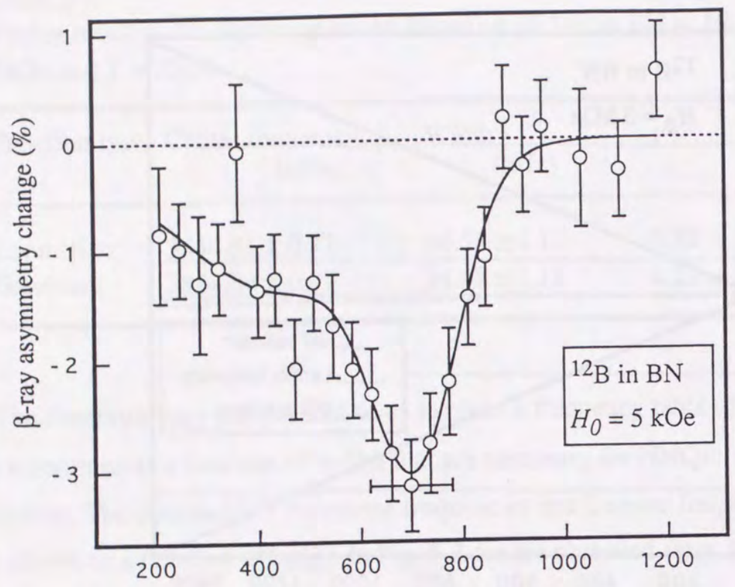

$$\nu_Q \left[= \frac{3}{4}\frac{eqQ}{h} : \text{for } \beta = 90° \right] \text{ (kHz)}$$

Figure 5-4 Typical NNQR spectrum for ^{12}B in BN.
The quadrupole coupling constant of ^{12}B in BN was detected by use of the NNQR method. The holding external magnetic field was H_0 = 5 kOe. The highly oriented axis was perpendicular to the H_0. The solid curve is the best theoretical fit to the data.

settled in an interstitial site is rapidly depolarized through the paramagnetic relaxation mechanism before the β-ray counting time is started. The width of the spectrum mainly results from the FM. Other causes are the dipolar broadening, rf intensity, and fluctuation of the electric field gradient due to the implantation process. These effects were considered in the line-shape fitting. The effect from the deviation of the *c*-axes was rather small because of the experimental condition ($\alpha = 90°$; mainly, $\beta = 90°$; see Chapter 3-5-2). The obtained coupling constant is $|eqQ/h$ (^{12}B in BN)| = 944 ± 17 kHz.

2) Measurement of the electric field gradient by detecting FT-NMR for ^{11}B in BN

As mentioned in the previous section, Silever reported on the eqQ/h of ^{11}B ($I\pi = 3/2-$) in BN at room temperature, $|eqQ/h(^{11}$B in BN)| = 2.96 ± 0.1 MHz [Si60]. Its accuracy was poor because they used a polycrystal sample. Connor reported on the eqQ/h of ^{11}B in BN detected at liquid-He temperature, $|eqQ/h(^{11}$B in BN)| = 2934 ± 4 kHz at 4.2K [Co90]. In the present experiment, the coupling constant of ^{12}B in BN was measured at room temperature. Therefore eqQ/h (^{11}B in BN) value at room temperature must be measured in order to avoid any uncertainty that may come from the temperature dependence of eqQ value. We measured the coupling frequency by means of the pulsed Fourier-transformed NMR method (FT-NMR).

The samples were cut and stacked for the FT-NMR method as shown in Fig. 5-5. The NMR spectra were observed at several angles (α) between the main *c*-axis of the BN sample and the external field. As mentioned in the preceding section (Chapter 3-4-1), the *c*-axes of the present BN crystal were distributed around the main direction. The NMR spectrum thus showed a characteristic dependence of the angle relative on the external magnetic field. Figs. 5-6(a)~(c) show the NMR spectra for several angles

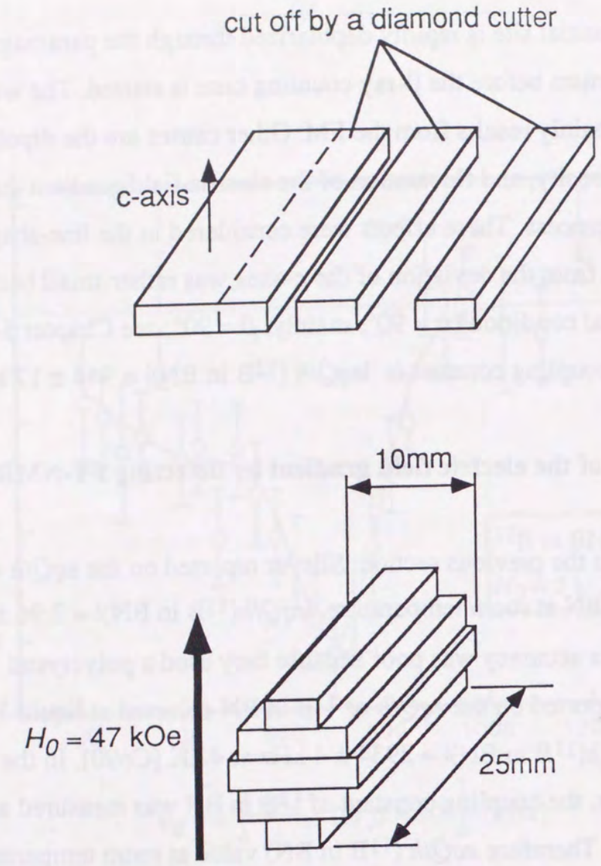

Figure 5-5 Stacking of BN samples for a pulsed NMR study.

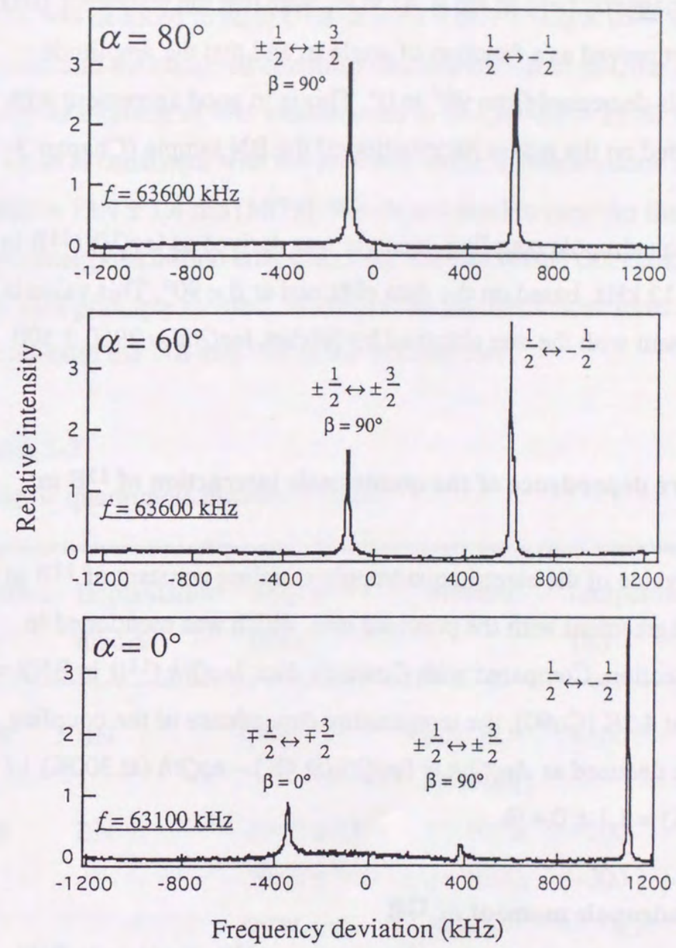

Figure 5-6 FT-NMR spectra of ^{11}B in BN at (a) α =80°, (b) α =60° and (c) α = 0°. The external field was H_0 = 47 kOe. Horizontal axis shows the frequency deviation from the applied rf frequency f. Two resonance peaks are shown. The right peak is for the transition between 1/2 ↔ −1/2. The left one is for ±1/2 ↔ ±3/2. The frequencies of the peaks show the main component of the spectrum is correspond β = 90° at α =80°. The frequency of the peak is not change but the amplitude decreased when the angle α is decreased. At α = 0° (c), a peak for β = 0° can be seen but the amplitude is small. It is because of the distribution of the c-axes in the BN sample.

at an external magnetic field of H_0 = 47 kOe. Note that the resonance peak at $\beta = 90°$ is not moved as a function of angle α, and that the amplitude decreases as α is decreased from 90° to 0°. This is in good agreement with a prediction based on the c-axes distribution of the BN sample (Chapter 3-5-2).

The electric quadrupole coupling constant was derived as $|eqQ/h|$ (^{11}B in BN)| = 2902 ± 12 kHz based on the data obtained at $\beta = 90°$. This value is in good agreement with the one obtained by Nesbet, $|eqQ/h|$ = 2960 ± 100 kHz.

3) Temperature dependence of the quadrupole interaction of ^{11}B in BN

The present value of the electric quadrupole coupling constant of ^{11}B in BN is in good agreement with the previous one, which was mentioned in the preceding section. Compared with Connor's data, $|eqQ/h|$ (^{11}B in BN)| = 2934 ± 4 kHz at 4.2K [Co90], the temperature dependence of the coupling constant can be deduced as $\Delta eqQ/h$ = {eqQ/h(at 4K) – eqQ/h (at 300K) } / eqQ/h (at 300K) = 1.1 ± 0.4 %.

4) Electric quadrupole moment of ^{12}B

Using the known electric quadrupole moment of ^{11}B, the electric field gradient at the substitutional B site for the ^{12}B nucleus can be derived as given in Table 5-2. The quadrupole moment $Q(^{11}B)$ = +40.65 ± 0.26 mb, as reported by Nesbet [Ne70] is in good agreement with the improved value $Q(^{11}B)$ = +40.59 ± 0.10 mb for which Sundholm et al. [Su91] calculated the field gradient by use of the improved electronic structure. Since these values agree with each other, we adopted the latter value for the present standard. Considering this value $Q(^{11}B)$ and the obtained coupling constant eqQ of ^{11}B in BN, the electric field gradient at ^{11}B

nucleus was deduced to be $|q$ (^{11}B in BN)| = (4.7 ± 0.2) × 10^{20} V/m^2. From this value and the observed coupling constant of ^{12}B in BN, the electric quadrupole moment of ^{12}B was deduced to be $|Q(^{12}B)|$ = 13.20 ± 0.25 mb. This value is consistent with the previous value by Minamisono et al., $|Q(^{12}B)|$ = 13.4 ± 1.4 mb [Mi78]. We do not need to consider the Sternheimer polarization effect, because the theoretical calculation is based on the first principle method. Moreover the electronic structures are the same for both the ^{11}B and ^{12}B in the BN samples.

Table 5-2
Electric quadrupole moment of ^{12}B.

Nucleus	Implantation media	$\|eqQ/h\|$ (kHz)	Method	Temperature (K)	Ref.
^{12}B	BN	944 ± 17	NNQR (β-NMR)	~300	present
^{11}B	BN	2902 ± 12	FT-NMR	~300	present
		2960 ± 100	cw-NMR	~300	[Si60]
		2934 ± 4	NQR	4.2	[Co90]
			$Q(^{11}B)$ = +40.59 ± 0.10 mb		
			$\|Q(^{12}B)\|$ = 13.20 ± 0.25 mb		
^{12}B	ZrB_2	38.7 ± 1.1	β-NMR	~300	[Mi78]
^{11}B	ZrB_2	118 ± 10	cw-NMR	~300	[Si60]
			$\|Q(^{12}B)\|$ = 13.4 ± 1.4 mb		

5-2 Quadrupole moment of ^{12}N

There was no helpful information available concerning the quadrupole moment of ^{12}N and the electric field gradient of the samples. The experiment therefore rather complicated compared with the ^{12}B case.

1) β-ray detection of ^{12}N in BN, GaN, and AlN

(i) Polarization maintained in crystals

As the first step, the maintained polarization of ^{12}N in several materials was studied using a widely frequency-modulated oscillating field. Fig. 5-7 shows the field (H_1) strength dependence of the β-ray asymmetry change in BN and GaN, respectively. It is very interesting that the maintained polarizations in these media were almost equal. The initial polarization of ^{12}N was measured by implanting ^{12}N in Pt metal, which is a good medium for preservation. Since $AP_0 = 17\%$, about 2/5 of the initial polarization was maintained in these nitride samples.

To account for these results, the external magnetic field dependence of the β-ray asymmetry measured for BN and GaN. Mylar and Pt were also used to measure the asymmetry for normalization. In the Mylar, polarization was completely destroyed. The results are shown in Fig. 5-8(a) (for BN) and (b) (for GaN). Since the efficiency of the β-ray counters, unfortunately, depends on the external field slightly, normalization of the dependence was as follows: (1) In each magnetic field, the Mylar result was considered as normalization. (2) At zero magnetic field, the polarization was expected to be perfectly destroyed in all samples. The differences among the results of the up-down ratio (U/D) at zero field for different media were due to the different settings and the thicknesses of the samples. To reduce this geometrical asymmetry, the ratios at the zero field of each medium were normalized using one of the Mylar data. (3) The maintained polarization was measured by detecting the β-NMR of each

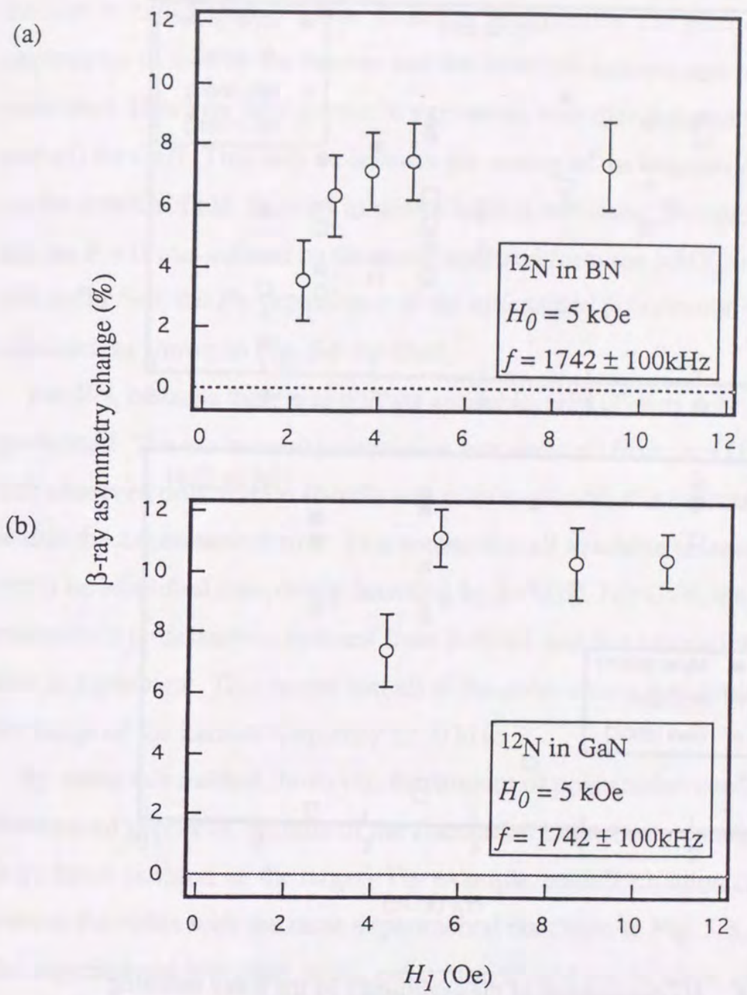

Figure 5-7 H_1 dependence of the NMR effect for ^{12}N in (a) BN and (b) GaN.
The crystal c-axis is perpendicular to the external field.

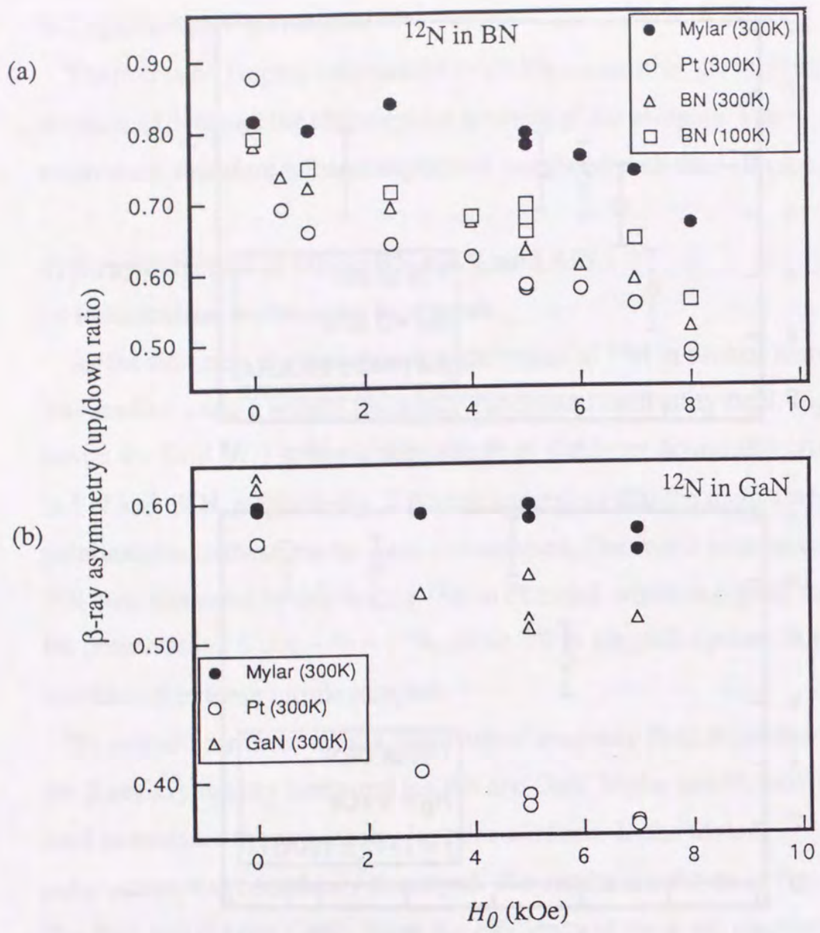

Figure 5-8 H_0 dependence of the asymmetry of the β-ray counting for ^{12}N.

Including the data at liquid N_2 temperature for BN. The effect on the β-ray counter system by the external field can be seen from the up/down ratio for Mylar and Pt metal.

nuclide in Pt at 5 kOe or 7 kOe. Based on these results, the geometrical asymmetry caused by the catcher and the detection systems can be estimated. However they are not in agreement with that deduced from (1) and (2) for GaN. This may be because the setting of the samples depends on the external field. In order to normalize this influence, the up/down ratio for the $P = 0$ was defined by the result obtained from the NMR in Pt. With this definition, the H_0 dependence of the maintained polarization was obtained, as shown in Fig. 5-9 for GaN.

For BN, because there was no data available, step (3) was not performed. The maintained polarization was deduced from step (1) and (2). The observed polarization (NMR) was consistent with this estimation within the experimental error. This means that all available resonance could be identified completely detecting by β-NMR. For GaN, the maintained polarizations deduced from β-NMR and this estimation were also in agreement. This means that all of the polarization was spread within the range of the Larmor frequency ±100 kHz.

By using this method, however, the amount of polarization could not be determined precisely, because of the fluctuation in the beam condition (e.g., beam position on the target). For example, such fluctuation can be seen in the ratios with the same experimental condition in Fig. 5-8. Thus, the experimental precision of this estimation should not be taken too seriously.

(ii) Temperature dependence of the β-NMR

Fig. 5-10 shows the temperature dependence of the maintained polarization by use of the NMR detection of ^{12}N in BN. The observed polarization decreased as the temperature decrease. At the same time, although the external field dependence of the β-ray asymmetry was measured, no significant dependence was observed within the present error

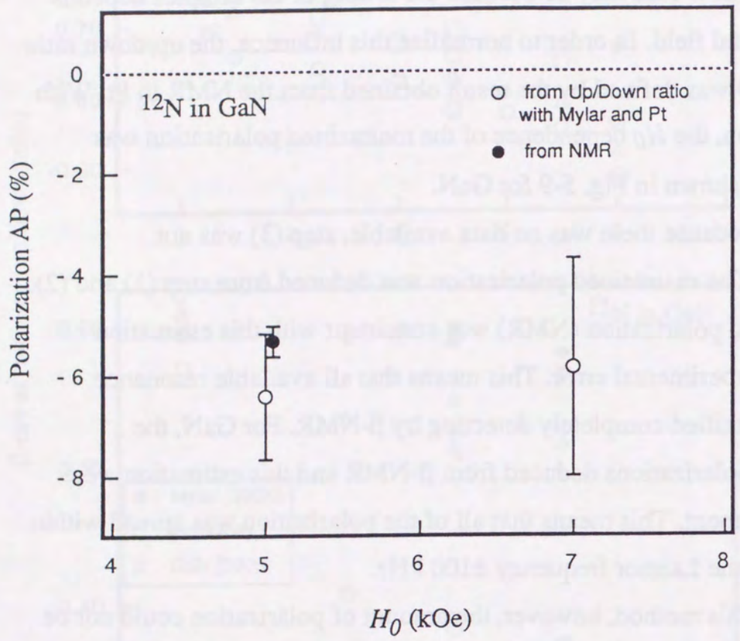

Figure 5-9 Comparison with the maintained polarization of ^{12}N in GaN deduced from the H_0 dependence and the NMR. They are in good agreement with each other.

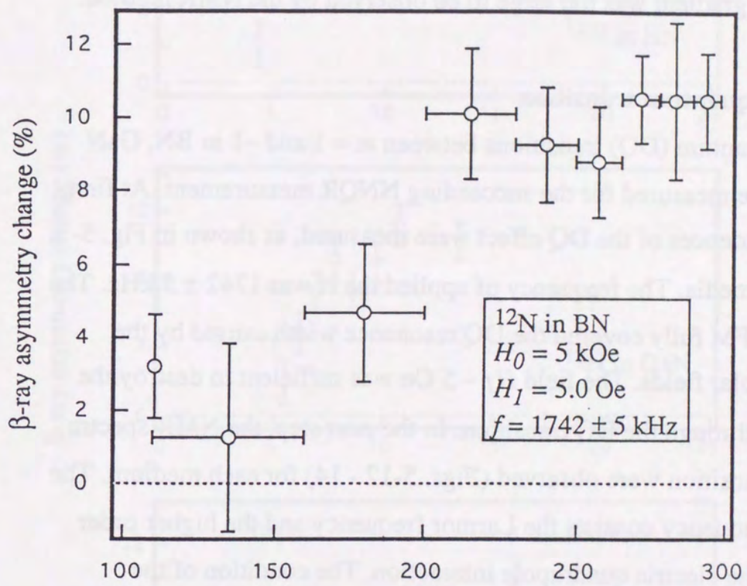

Figure 5-10 Temperature dependence of the NMR effect for ^{12}N in BN. The maintained polarization detected by NMR decreases at low temperatures. The horizontal bars show the temperature region.

(Fig. 5-8). It is not clear why the NMR effect partially vanished at lower temperatures. One of the reasons that there is an interstitial metastable site where at a lower temperature, majority sat without moving to the substitutional site. At that site, although the polarization was preserved, the electric field gradient was too large to be observed by the NMR method.

(iii) Double quantum transition

Double quantum (DQ) transitions between $m = 1$ and -1 in BN, GaN and AlN were measured for the succeeding NNQR measurement. At first, the H_1 dependences of the DQ effect were measured, as shown in Fig. 5-11, for each media. The frequency of applied the rf was 1742 ± 5 kHz. The width of the FM fully covered the DQ resonance width caused by the dynamic dipolar fields. The field $H_1 \sim 5$ Oe was sufficient to destroy the polarization through the DQ transition. In the next step, the NMR spectra of the DQ transition were observed (Figs. 5-12 - 14) for each medium. The resonance frequency consists the Larmor frequency and the higher order shift due to the electric quadrupole interaction. The condition of the applied rf was $H_1 = 9$ Oe for BN and 5 Oe for GaN and FM = ± 1 kHz. The spectra were analyzed by fitting them with a resonance function which was based on Lorentzian or Gaussian line shape function. The experimental results are listed in Table 5-3. The widths of these resonances are consistent with the one given by the dipolar broadening and the rf intensity.

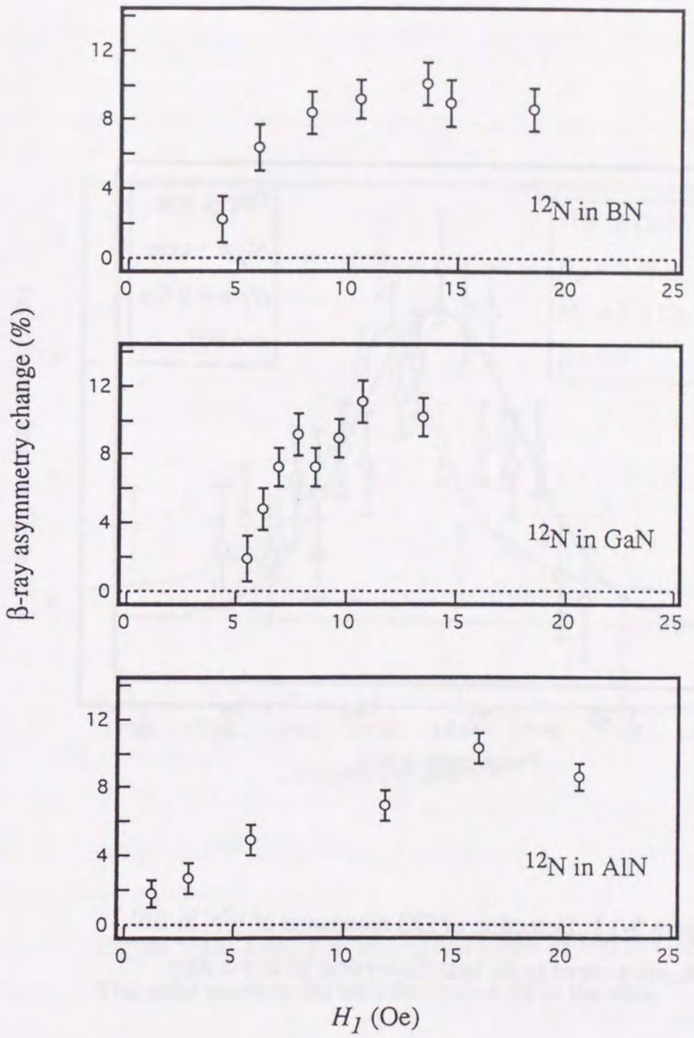

Figure 5-11 H_1 dependence of the double quantum (DQ) transition for ^{12}N in (a) BN, (b) GaN and (c) AlN.
$f = 1742 \pm 5$ kHz, $H_0 = 5$kOe. The crystal highly oriented axis is perpendicular to the external field for BN. The crystal c-axis is perpendicular to the external field for GaN. AlN sample was polycrystal.

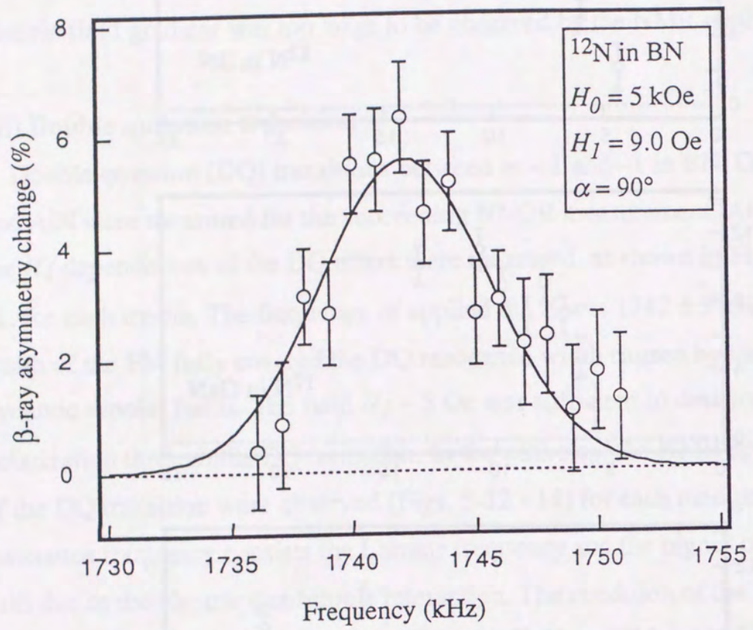

Figure 5-12 Detection of DQ resonance of ^{12}N in BN.
The solid curve is the best theoretical fit to the data.

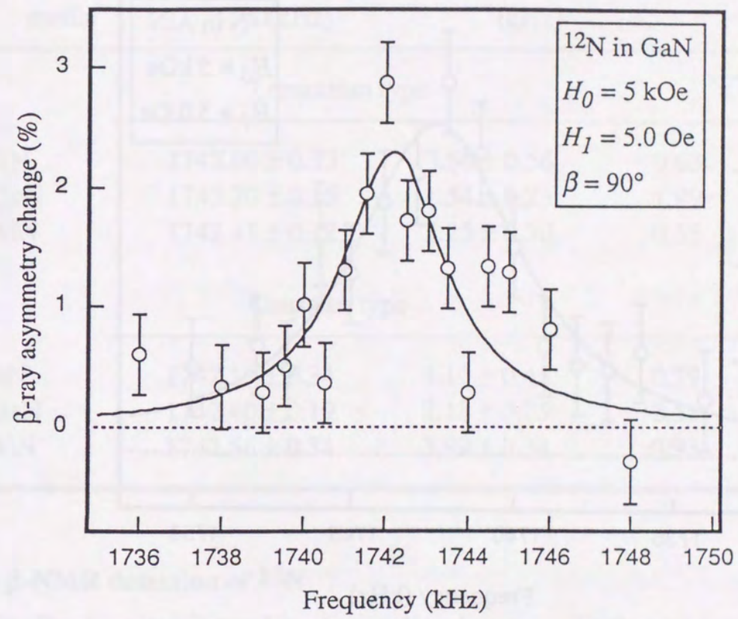

Figure 5-13 Detection of DQ resonance of ^{12}N in GaN.
The solid curve is the best theoretical fit to the data.

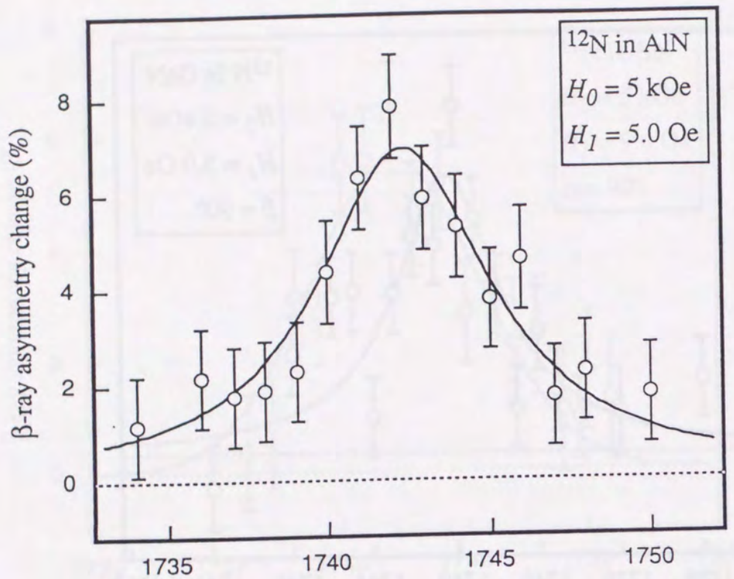

Figure 5-14 Detection of DQ resonance of ^{12}N in AlN. The AlN sample was the polycrystalline. The solid curve is the best theoretical fit to the data.

Table 5-3
Experimental results of the double quantum transition of ^{12}N in BN, GaN and AlN.

Implantation media	Center frequency (kHz)	Width (kHz)	χ^2
	Lorentzian type		
BN	1742.00 ± 0.33	3.56 ± 0.56	0.63
GaN	1742.20 ± 0.15	1.54 ± 0.23	1.99
AlN	1742.41 ± 0.32	3.25 ± 0.50	0.55
	Gaussian type		
BN	1742.19 ± 0.34	4.10 ± 0.45	0.79
GaN	1742.40 ± 0.19	2.18 ± 0.25	2.51
AlN	1742.56 ± 0.34	3.99 ± 0.34	0.93

(iv) β-NMR detection of ^{12}N

Finally, the electric quadrupole coupling frequency (ν_Q) was measured. Using the experimental DQ resonance frequency, two rf frequencies corresponding to a coupling frequency ν_Q were calculated. The rf intensity (H_1) and FM of the rf were properly tuned, since we needed to avoid any DQ resonance near to the Larmor frequency ($\nu_Q = 0$). The DQ transition can be suppressed if the rf power is small enough. However, H_1 can not be too small to observe the eqQ spectrum efficiently, since an rf with wide FM must be use because the NMR line is broadened by some reasons and H_1 must be properly increased. The use of frequency-modulated rf is to integrate the NMR effect spread in the rf range, and the NMR detection of the quadrupole effect easier. However an FM that is too wide causes the spectrum to be distorted, especially for the inner side of peaks, i.e., a

resonance peak is widened by the FM toward the inner side. Figs. 5-15~17 show the final results for the ν_Q measurements.

a. BN

Fig. 5-15 shows the NNQR spectrum for ^{12}N in BN. The experimental condition was that FM width was ±1 kHz, $H_1 \sim 2.8$ Oe at $H_0 = 5$kOe and $T = 300$K. Note that the width of FM (Δf) is twice as much when using ν_Q scale, i.e., $\Delta\nu_Q = 2\Delta f$. The horizontal bar in the figure shows the FM range of an applied rf. Fitting functions based on the Gaussian shape was used for a χ^2 analysis of the spectrum. The experimental results are listed in Table 5-4. According to the study of ^{12}B in BN, one another component that comes from ^{12}N located in substitutional boron site is suggested. Based on a peak search, however, in the region $\nu_Q \leq 2$ MHz, no apparent such peak from the possible component was found. It was therefore concluded that this component is located either far outside of the searched range that comes from a very large electric field gradient, or too close to that of the substitutional site. Furthermore, since the observed NMR effect is almost 80% of the maintained polarization, we concluded that the present peak is that resulting from ^{12}N in the nitrogen site.

b. GaN

Fig. 5-16 shows the spectrum for ^{12}N in GaN. It is expected that the site where ^{12}N is located with its polarization maintained is the only nitrogen substitutional site. Since the Ga atom is much heavier than N, it is unlikely for an implanted ^{12}N to settle in a Ga substitutional site.

The condition for the rf fields was FM = ±5 kHz and $H_1 = 0.8$ Oe at $H_0 = 5$kOe and $T = 300$K. The analysis was the same as for ^{12}N in BN. The experimental results are listed in Table 5-4. It was found that the field gradient was about one half that in BN.

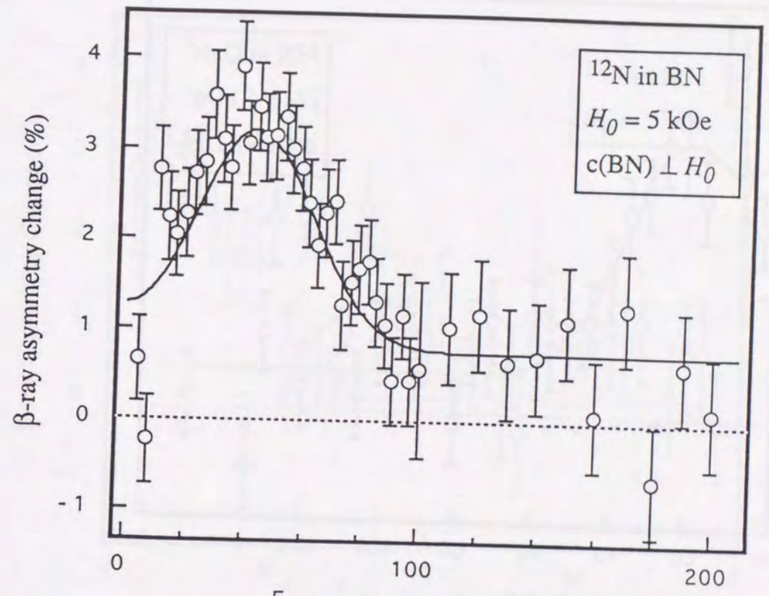

Figure 5-15 Typical NNQR spectrum of ^{12}N in BN.
The quadrupole coupling constant of ^{12}N in BN was detected by use of the NNQR method. The solid curve is the theoretical spectrum best fit to the data.

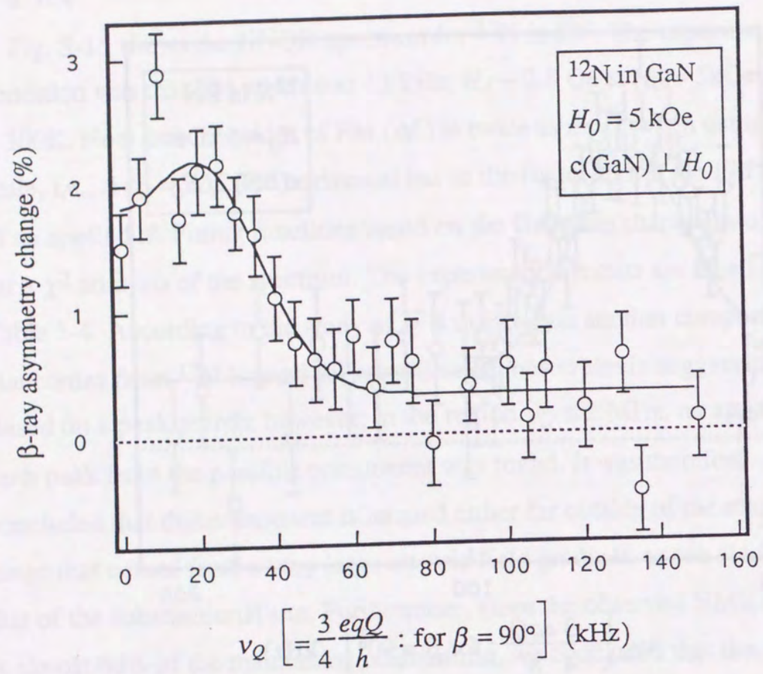

Figure 5-16 Typical NNQR spectrum of ^{12}N in GaN.
The solid curve is the theoretical spectrum best fit to the data.

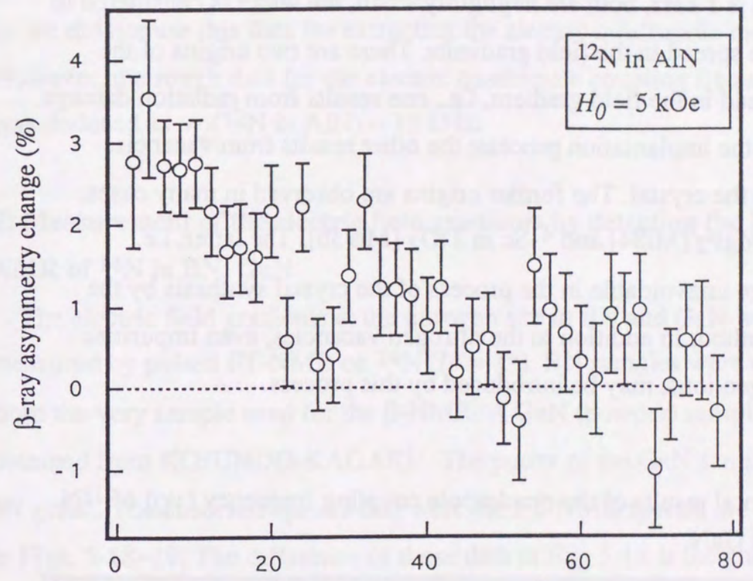

Figure 5-17 Typical NNQR spectrum of ^{12}N in AlN.
The quadrupole coupling constant of ^{12}N in AlN was detected by use of the NNQR method. A polycrystal pattern is expected. Resonance peaks at $\beta = 90°$ can not be seen clearly due to the broadening.

The width of the spectrum is accounted for by the FM width of the applied rf field and a reasonable spread of the field gradient. Since the rf intensity (H_1) is equal to about 1 kHz, and the dipolar broadening at the nitrogen site is 1 kHz, both are negligibly small, the width is considered to be due to the spread in the field gradients. There are two origins of the inherent spread in the field gradient, i.e., one results from radiation damage produced in the implantation process; the other results from vacancies which are in the crystal. The former origins are observed in many cases, e.g., ^{17}F in MgF_2 [Mi84] and ^{41}Sc in TiO_2 [Mi93b]. The latter, i.e., vacancies, are unavoidable in the process of the crystal synthesis by the MOCVD method. In addition to the nitrogen vacancies, even impurities such as oxygen ions, may be introduced by this process.

Table 5-4
Experimental results of the quadrupole coupling frequency (ν_Q) of ^{12}N in BN and GaN.

Implantation media	$\nu_Q = \frac{3}{4}\frac{eqQ}{h}$ (kHz)	Width (kHz) (HWHM)	χ^2
	Lorentzian		
BN	43.3 ± 2.4	20.7 ± 4.7	0.70
GaN	20.0 ± 1.7	16.1 ± 3.8	1.06
	Gaussian		
BN	42.6 ± 2.4	23.7 ± 3.7	0.68
GaN	20.6 ± 1.5	18.4 ± 2.1	1.15

c. AlN

Fig. 5-17 shows the NNQR detection of ^{12}N in AlN. The condition was $H_1 = 1.5$ Oe and FM = ±1 kHz. The spectrum did not show an explicit peak for eqQ. Since it was too difficult to precisely analyze this spectrum, so we did not use this data for extracting the electric quadrupole moment. However, the rough data for the electric quadrupole coupling frequency was deduced as $\nu_Q(^{12}N \text{ in AlN}) = 15$ kHz.

2) Measurement of the electric field gradients by detecting the FT-NMR of ^{14}N in BN, GaN

The electric field gradients at the nitrogen site in BN and GaN were measured by pulsed FT-NMR on ^{14}N ($I^{\pi} = 1^+$). BN samples were cut out from the very sample used for the β-NMR. A GaN (powder) sample was obtained from KOJUNDO-KAGAKU. The purity of the GaN sample was 4N grade. The observed spectra that were the FT-NMR spectra are shown in Figs. 5-18~19. The difference of these data in Fig. 5-18 is the choice of the initial sampling point for the Fourier transformation. Since the FID signals just after the stop of an rf pulse is often deformed by the rf pulse or that of the coil set up mismatching, so the derived Fourier-transformed spectrum is very much distorted. To avoid this distortion, initial point of the sampling is delayed after the pulse. However, note that the shape of the true component was also distorted as the sampling time is delayed. The effect of the choice of the initial point can be seen in the spectra. However the distances of frequencies of the relevant peaks are not moved appreciably.

From these spectra, one recognize a broad distortion near the Larmor frequency, i.e., between the two quadrupole peaks. This distortion is due to a mismatching of the rf conditions [He84], The distortion affects the frequencies of the satellite peaks. Here, it was considered in the analyses as

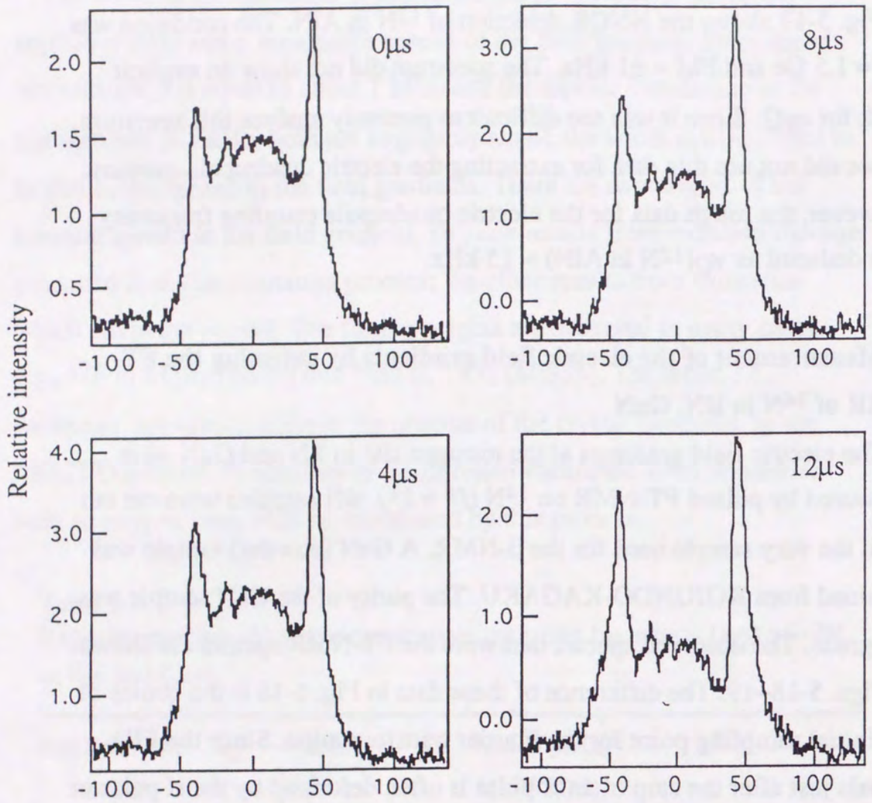

Figure 5-18 Typical FT-NMR spectra of ^{14}N in BN.
Sampling start point dependence of the FT-NMR spectra. The distortion near center was caused by the mismatching of the rf. It depends on the sampling start point for Fourier-transformation. The peak for the angle β=90° can be seen clearly. The highly oriented axis was perpendicular to the external field H_0. Applied external field was H_0.= 47 kOe.
Applied rf frequency was f = 14456.5kHz

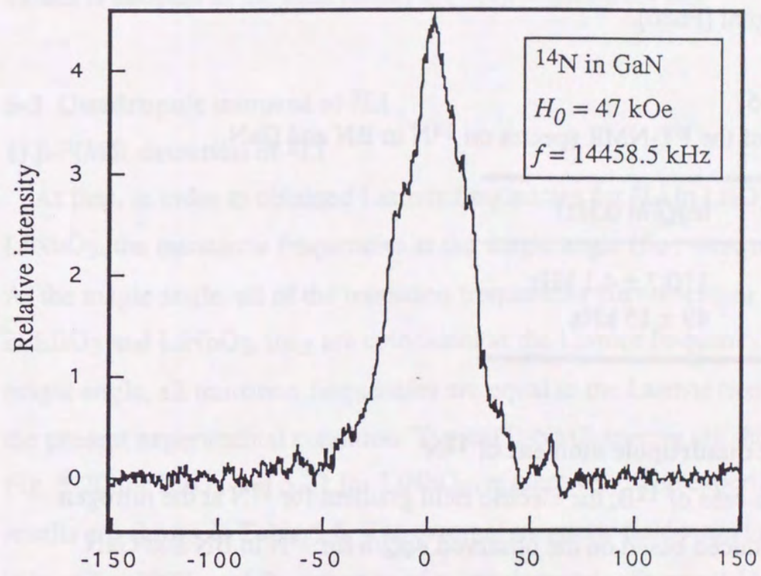

Figure 5-19 Typical FT-NMR spectrum of ^{14}N in GaN.
The distortion at center was caused by the mismatching of the rf.

being a simple Gaussian without any fine structures. Thus, these spectra were analyzed by fitting three Gaussian functions. The results are shown in Table 5-5. In the case of ^{14}N in GaN, we supposed that the width of spectrum was due to dipolar broadening as well as the exponential decay of the FID signal [Fu80].

Table 5-5
Results of the FT-NMR spectra on ^{14}N in BN and GaN.

Media	$\lvert eqQ/h \rvert$ (kHz)
BN	110.7 ± 4.1 kHz
GaN	49 ± 15 kHz

3) Electric quadrupole moment of ^{12}N

As in the case of ^{12}B, the electric field gradient for ^{12}N at the nitrogen site was deduced based on the observed eqQ/h for ^{14}N in BN and GaN combined with the known electric quadrupole moment of ^{14}N. The electric quadrupole moment of ^{14}N was recently reported by many authors. It had been difficult to accurately calculate the electric field gradient for a nitrogen molecule because of its possible complex molecular configurations. However, Schimacher et al. observed the hyperfine splitting of the excited nitrogen atom by using the IBSIGI (ion beam surface interaction grazing incidence) method and deduced the quadrupole moment of ^{14}N as $Q(^{14}N) = +20.0 \pm 0.2$ mb [Sc92]. Using this value, the electric field gradient at the nitrogen site in BN and GaN were deduced as $|q(\text{N in BN})| = (2.29 \pm 0.09) \times 10^{20}$ V/m^2 and $|q(\text{N in GaN})| = (1.0 \pm 0.3) \times 10^{20}$ V/m^2. Then, the quadrupole moment of ^{12}N was deduced as $|Q(^{12}N)| = 10.3 \pm 0.7$ mb from BN data and $|Q(^{12}N)| = 9.2 \pm 3.1$ mb from GaN. These values are in good agreement with each other within the

experimental concerning errors. This consistency also assures us of the validity of the speculation that the observed resonance peak for ^{12}N in BN came from ^{12}N in the nitrogen substitutional site. The average of these values is adopted as the final result, $|Q(^{12}N)| = 10.3 \pm 0.7$ mb.

5-3 Quadrupole moment of ^8Li

1) β-NMR detection of ^8Li

At first, in order to obtained Larmor frequencies for ^8Li in $LiIO_3$ and $LiNbO_3$, the resonance frequencies at the magic angle (β_M) were observed. At the magic angle, all of the transition frequencies are coincident. For ^8Li in $LiIO_3$ and $LiNbO_3$, they are coincident at the Larmor frequency. At the magic angle, all transition frequencies are equal to the Larmor frequency in the present experimental condition. Typical β-NMR spectra are shown in Fig. 5-20 for $LiIO_3$ and 5-21 for $LiNbO_3$, respectively. The experimental results are shown in Table 5-6. The external magnetic field was $H_0 = 4$ kOe at $T = 300$K, and the intensity of monochromatic rf's was 0.53 Oe.

Table 5-6
Experimental results of β-NMR at the magic angle for ^8Li in $LiIO_3$ and $LiNbO_3$. The external field was $H_0 = 4$ kOe.

Implantation media	Center frequency (kHz)	Width (kHz)	χ^2
Lorentzian type			
$LiIO_3$	2521.85 ± 0.06	0.64 ± 0.09	0.54
$LiNbO_3$	2521.69 ± 0.10	1.93 ± 0.16	1.00
Gaussian type			
$LiIO_3$	2521.85 ± 0.06	0.64 ± 0.09	0.54
$LiNbO_3$	2521.69 ± 0.10	1.93 ± 0.16	1.00

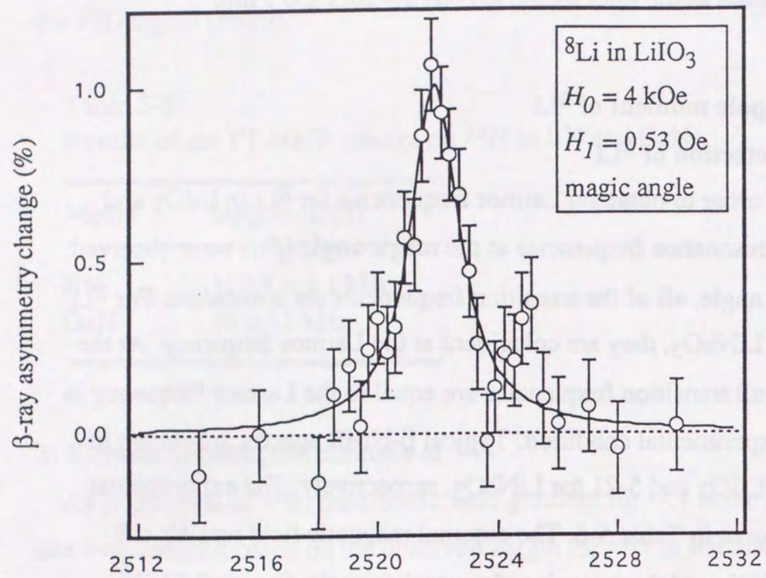

Figure 5-20 Typical β-NMR spectrum of ^{8}Li in $LiIO_3$.
The angle between the crystal *c*-axis and the external field was magic angle (54.7°).

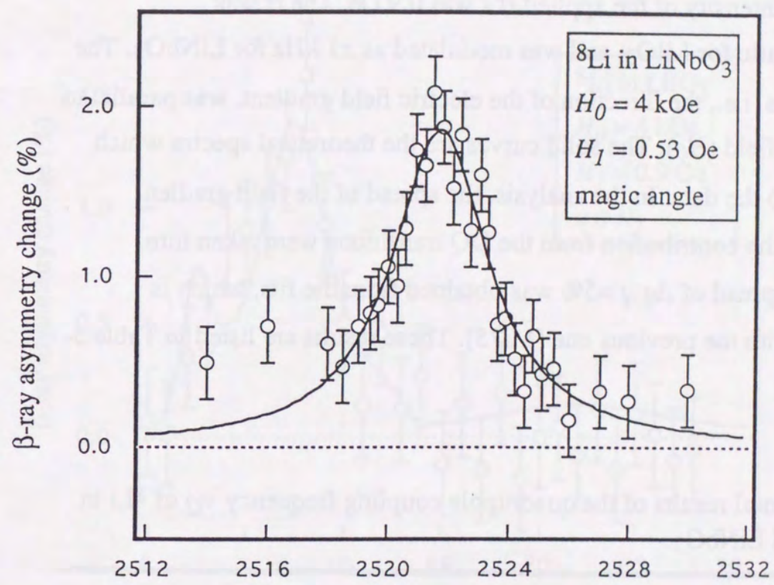

Figure 5-21 Typical β-NMR spectrum of ^{8}Li in $LiNbO_3$.
The angle between the crystal *c*-axis and the external field was magic angle (54.7°).

Finally, the electric quadrupole coupling frequency (ν_Q) was measured at room temperature. Typical NNQR spectra for ^{8}Li in $LiIO_3$ and $LiNbO_3$ are shown in Figs. 5-22 and 5-23, respectively. The external field was H_0 = 4 kOe. The intensity of the applied rf's was 0.9 Oe. The rf was monochromatic for $LiIO_3$, and was modulated as ±1 kHz for $LiNbO_3$. The crystal c-axis, i.e., the direction of the electric field gradient, was parallel to the external field (H_0). The solid curves are the theoretical spectra which are best fit to the data. In the analysis, the spread of the field gradient ($\Delta q/q$), and the contribution from the DQ transitions were taken into account. A spread of $\Delta q/q$ =5% was obtained from the fits, which is consistent with the previous one [Mi75]. These results are listed in Table 5-7.

Table 5-7
Experimental results of the quadrupole coupling frequency ν_Q of ^{8}Li in $LiIO_3$ and $LiNbO_3$.

Implantation media	$\nu_Q = \frac{1}{4}\frac{eqQ}{h}$ (kHz)	eqQ/h(kHz)	$\Delta q/q$ (kHz) (HWHM)	χ^2
$LiIO_3$	7.39 ± 0.27	29.6 ± 1.1	0.96 ± 0.16	0.75
$LiNbO_3$	11.18 ± 0.21	44.6 ± 0.88	2.14 ± 0.09	0.56

The coupling constants were determined to be $|eqQ/h$ (^{8}Li in $LiIO_3)| =$ 29.6 ± 1.1 kHz and $|eqQ/h$ (^{8}Li in $LiNbO_3)| = 44.68 \pm 0.88$ kHz. They are in good agreement with the previous values [Mi75, Ar88].

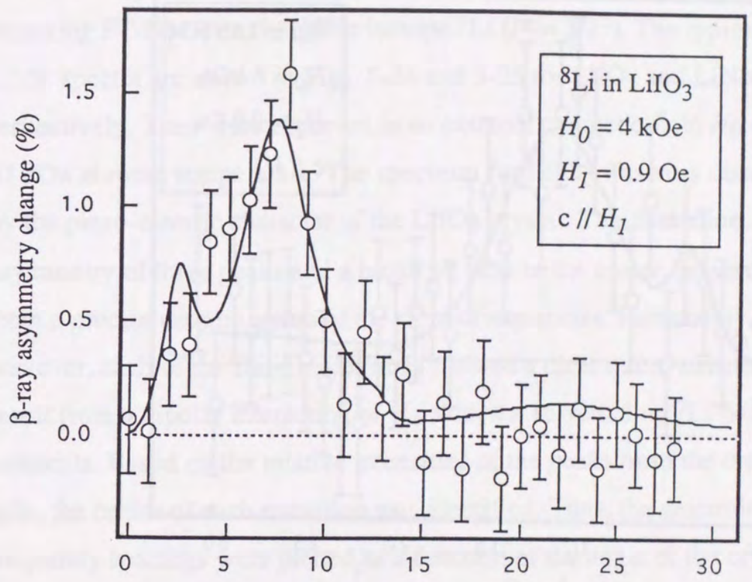

Figure 5-22 Typical NNQR spectrum of ^{8}Li in $LiIO_3$.
The quadrupole coupling constant of ^{8}Li in $LiIO_3$ was detected by use of the NNQR method. The solid curve is the theoretical spectrum best fit to the data.

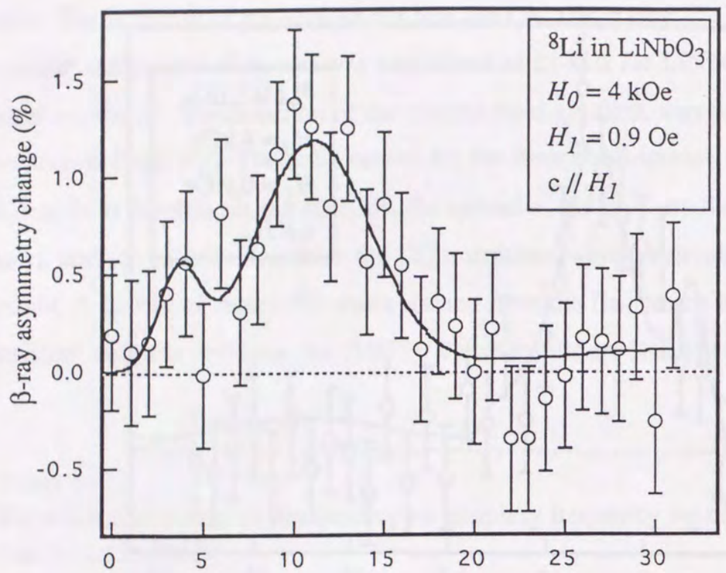

Figure 5-23 Typical NNQR spectrum of ^{8}Li in $LiNbO_3$.
The quadrupole coupling constant of ^{8}Li in $LiNbO_3$ was detected by use of the NNQR method. The solid curve is the theoretical spectrum best fit to the data.

2) Measurement of the electric field gradients by detecting the FT-NMR of ^{7}Li in $LiIO_3$ and $LiNbO_3$

The field gradients at the Li site in the crystal were measured by detecting FT-NMR on the stable isotope ^{7}Li ($I^\pi = 3/2^-$). The typical FT-NMR spectra are shown in Figs. 5-24 and 5-25 for $LiIO_3$ and $LiNbO_3$, respectively. They were observed in an external magnetic field H_0 = 47 kOe at room temperature. The spectrum for $LiIO_3$ was very disturbed by the piezo-electric character of the $LiIO_3$ crystal. This distortion, i.e., the asymmetry of three peaks and a broad pit near to the center, prevented us from a precise determination of the center frequencies. Fortunately, however, each of the three major lines showed a clear micro structure that result from a dipolar interaction of ^{8}Li with the surrounding ^{7}Li nuclear moments. Based on the relative intensities of the peaks from the dipolar split, the center of each transition was identified. Thus, the determined frequency spacings were plotted as a function of the angle of the crystal *c*-axis relative to the external magnetic field (Fig. 5-26). The solid and broken lines are the theoretical curves which best fit the data. The asymmetry factor (η) of the electric field gradient was assumed to be zero, because of the crystal symmetry. The quadrupole coupling constants were obtained as $|eqQ/h(^7\text{Li in } LiIO_3)| = 36.4 \pm 0.5$ kHz and $|eqQ/h(^7\text{Li in } LiNbO_3)| = 53.3 \pm 0.5$ kHz. It was found that the previously reported $|eqQ/h(^7\text{Li in } LiIO_3)| = 44 \pm 3$ kHz [Sa72] is in error because the piezo-electricity may not have been taken into account.

3) Electric quadrupole moment of ^{8}Li

The quadrupole moments of ^{7}Li has been reported by many authors recently [Vo91, Su85], and the results are all consistent. Here, we adopted the result based on Coulomb excitation by Völk, $Q(^7\text{Li}) = +40.0 \pm 0.6$ mb.

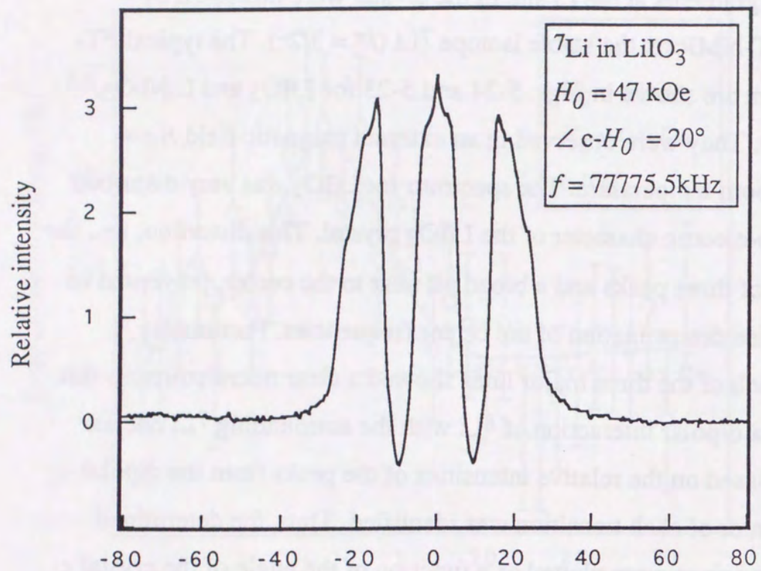

Figure 5-24 Typical FT-NMR spectrum of ^{7}Li in $LiIO_3$.
All transition peaks are shown. The distortion was occurred due to the piezo-electricity character of $LiIO_3$. The horizontal axis shows the deviation from the applied rf frequency.

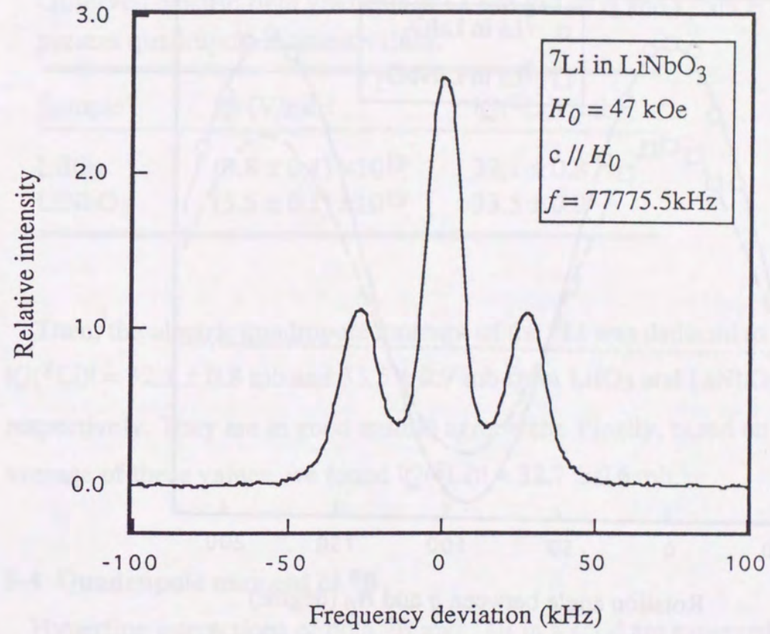

Figure 5-25 Typical FT-NMR spectrum of ^{7}Li in $LiNbO_3$.
All transition peaks are shown. The horizontal axis shows the deviation from the applied rf frequency.

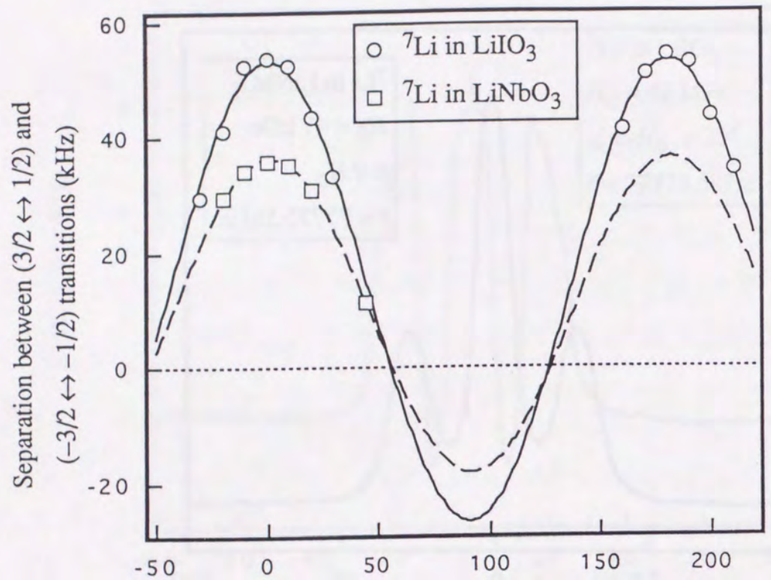

Figure 5-26 FT-NMR signal of ^{7}Li in $LiIO_3$ and $LiNbO_3$ as a function of the orientation of the crystal c-axis relative to H_0. The solid and broken curves are the best theoretical fit to the data.

Using this quadrupole moment, the electric field gradients at the Li site were obtained (Table 5-8).

Table 5-8
Observed electric field gradients at Li site in $LiIO_3$ and $LiNbO_3$ and the present quadrupole moment values.

Sample	$\|q\|$ (V/m^2)	$\|Q(^8\text{Li})\|$ (mb)
$LiIO_3$	$(3.8 \pm 0.1) \times 10^{19}$	32.1 ± 0.8
$LiNbO_3$	$(5.5 \pm 0.1) \times 10^{19}$	33.5 ± 0.9

Then, the electric quadrupole moment of the ^{8}Li was deduced to be $|Q(^8\text{Li})| = 32.1 \pm 0.8$ mb and 33.5 ± 0.9 mb from $LiIO_3$ and $LiNbO_3$, respectively. They are in good mutual agreement. Finally, based on the average of these values, we found $|Q(^8\text{Li})| = 32.7 \pm 0.6$ mb.

5-4 Quadrupole moment of ^{8}B

Hyperfine interactions of both ^{8}B and ^{12}B in a solid are expected to be similar because of the same atomic structure. The Knight shift and electric field gradient at the boron site in Mg were thus the same for both ^{8}B and ^{12}B. We determined these values for ^{8}B from a measurement of ^{12}B in Mg.

1) Measurement of the Larmor frequency and electric field gradient by detecting β-NMR of ^{12}B in Mg

As a first step, the Larmor frequency of ^{12}B in Mg was measured. Fig. 5-27 shows the NMR spectrum of the DQ transition at the temperature T ~ 100K. The external field was $H_0 = 7$ kOe. The condition of the applied monochromatic rf was $H_1 = 7.7$ Oe. The second component had been

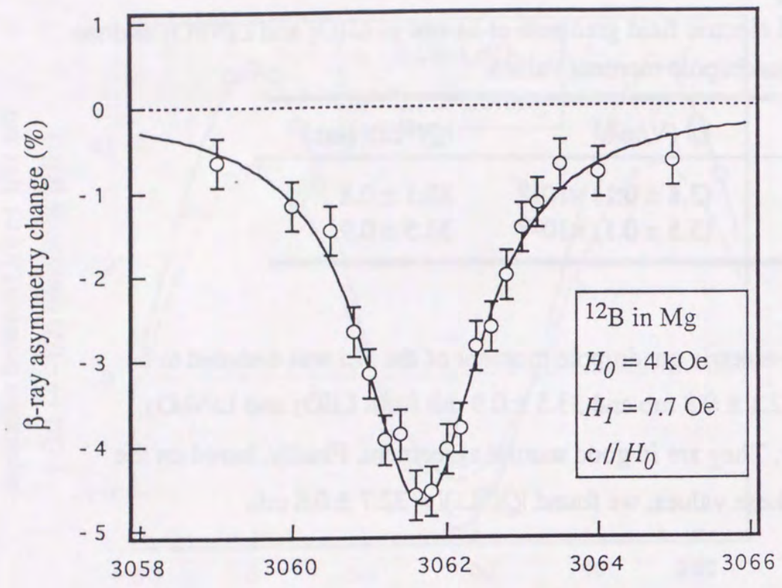

Figure 5-27 Detection of DQ transition of ^{12}B in Mg with a monochromatic rf.
The double quantum transition frequency was detected by β-NMR method. The solid curve is the theoretical best fit to the data.

observed at a higher frequency relative to the main peak. The existence of two components for ^{12}B in Mg was reported by Kitagawa [Ki90, Ki93c]. The spectrum was analyzed by fitting a Lorentzian or a Gaussian to the data. The fitting results are listed in Table 5-9. The widths of these results are consistent with the dipolar broadening as well as the contribution from the rf intensity. The maintained polarization was consistent with the observed value in Pt under the same condition of the recoil angle (13±8°). A typical NMR spectrum of ^{12}B in Pt is shown in Fig. 5-28.

Table 5-9
Fitting results of the double quantum transition of ^{12}B in Mg and the single quantum transition of ^{12}B in Pt at T ~ 100K and T ~ 300K. The external field was H_0 = 7 kOe and 4 kOe.

Function type	Center frequency (kHz)	Width (kHz)	χ^2
Mg			
H_0 = 7 kOe (T ~ 100K)			
Lorentzian	5358.60 ± 0.05	0.76 ± 0.11	0.74
Gaussian	5358.59 ± 0.05	0.74 ± 0.07	0.78
H_0 = 4 kOe (T ~ 300K)			
Lorentzian	3061.68 ± 0.03	0.95 ± 0.06	0.53
Gaussian	3061.69 ± 0.03	1.06 ± 0.05	1.27
Pt			
H_0 = 7 kOe (T ~ 100K)			
Lorentzian	5354.33 ± 0.03	0.54 ± 0.04	0.75
Gaussian	5354.32 ± 0.03	0.63 ± 0.04	0.59
H_0 = 4 kOe (T ~ 300K)			
Lorentzian	3059.10 ± 0.08	1.13 ± 0.12	0.71
Gaussian	3059.11 ± 0.08	1.33 ± 0.11	1.04

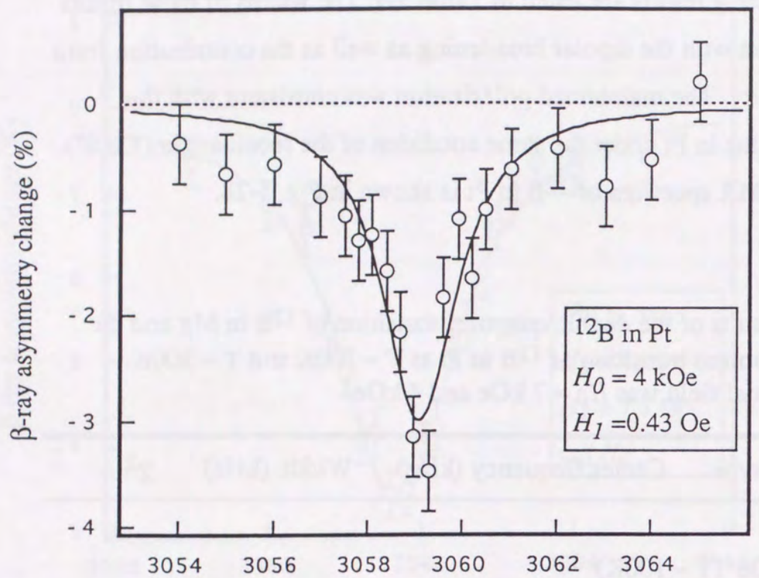

Figure 5-28 Typical β-NMR spectrum of ^{12}B in Pt with a monochromatic rf.
The solid curve is the theoretical best fit to the data.

It is very interesting that the Knight shift of ^{12}B in Mg relative to that in Pt is very large ($(\nu(\mathrm{Mg}) - \nu(\mathrm{Pt})) / \nu(\mathrm{Pt}) = 8.0 \times 10^{-4}$), which is comparable with other measurement in metals. Table 5-10 shows the Knight shifts of ^{12}B in several metals.

Table 5-10
Knight shifts of ^{12}B in metals.
The definition of the Knight shift is relative to the magnetic field in Pt, $K' = (\nu(\mathrm{M}) - \nu(\mathrm{Pt})) / \nu(\mathrm{Pt})$.

Metal	K' ($\times 10^{-4}$)	ref.
Mg	8.0(2.0)	present
Cu	6.5(1.9)	[Su67]
Au	6.5(1.6)	[Su67]
Au	7.3(8)	[We68]
Pd	–0.8(8)	[We68]

The spectrum for ^{12}B in Mg was observed by the NNQR method (Fig. 5-29). The external magnetic field was H_0 = 4 kOe, and the angle between the external field and the c-axis of the Mg crystal was $\beta = 0°$. The asymmetry factor (η) of the electric field gradient is expected to be zero due to the symmetry of the Mg crystal structure. The intensity of the applied monochromatic rf field was 0.4 Oe. The solid lines represent the theoretical case best fit to the data. In the spectrum of ^{12}B, the second component with a half coupling constant has been clearly seen. This component is discussed together with the case of ^{8}B in Mg in the Appendix. The coupling constant of ^{12}B was obtained from the main peaks as $|eqQ/h$ (^{12}B in Mg)| = 46.4 ±0.4 kHz. The present result is consistent

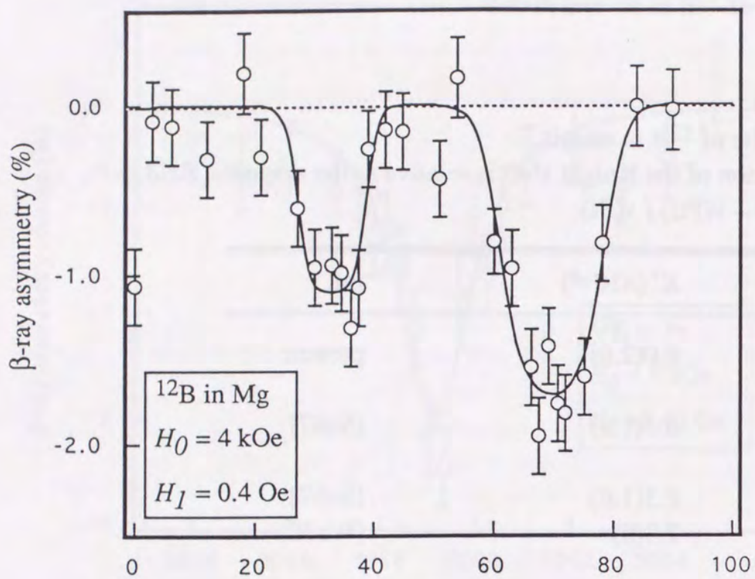

Figure 5-29 Typical NNQR spectrum of ^{12}B in Mg.
The solid curve is the theoretical spectrum best fit to the data. There are two component in the spectrum. The small component at the lower frequency is considered to be come from crystallographical disorders near the surface. See Appendix.

with the previous value $|eqQ/h|$ (^{12}B in Mg)| = 47.0 ± 0.1 kHz based on a detailed study of ^{12}B in Mg by Kitagawa [Ki93c]. Here, we adopt the previous value because of its high precision.

2) β-NMR detection of ^{8}B

From the study of Knight shift for ^{12}B in Mg, the Larmor frequency of ^{8}B in Mg was deduced. Using this value, the electric quadrupole coupling frequency (ν_Q) was measured by the NNQR method at room temperature. Fig. 5-30 shows the spectrum for ^{8}B in Mg. The external magnetic field was H_0 = 7 kOe. The angle between the external field and the c-axis of the Mg crystal was $\beta = 0°$. The intensity of the applied rf field was 9 Oe. The FM widths were ±5 kHz for inner rf's and ±15 kHz for outer rf's. The solid lines are for the theoretical case best fit to the data. The coupling constant was obtained as $|eqQ/h|$ (^{8}B in Mg)| = 243.6 ± 6.0 kHz. The small peak at lower frequency is due to partial depolarization, which means that a pair of outer rf's destroyed the inner resonance peaks (see Chapter 3-2-6 and Fig. 3-15a).

In contrast to the case of ^{12}B, no significant peak corresponding to the second component (more than 5% population) has been observed for the ^{8}B case. The main difference in these two cases is the implantation ranges of the nuclei in the crystal. The maximum depth of ^{8}B is about 3.4μm, while that of ^{12}B is just 1.5μm. Crystallographical disorders near to the surface might be the cause of the second population.

3) Electric quadrupole moment of ^{8}B

The quadrupole moment of ^{12}B is $|Q(^{12}\text{B})| = 13.20 \pm 0.25$ mb based on the present study. Using this quadrupole moment, the electric field gradient in Mg was determined to be $|q(\text{B in Mg})| = (1.48 \pm 0.03) \times 10^{20}$ V/m^2.

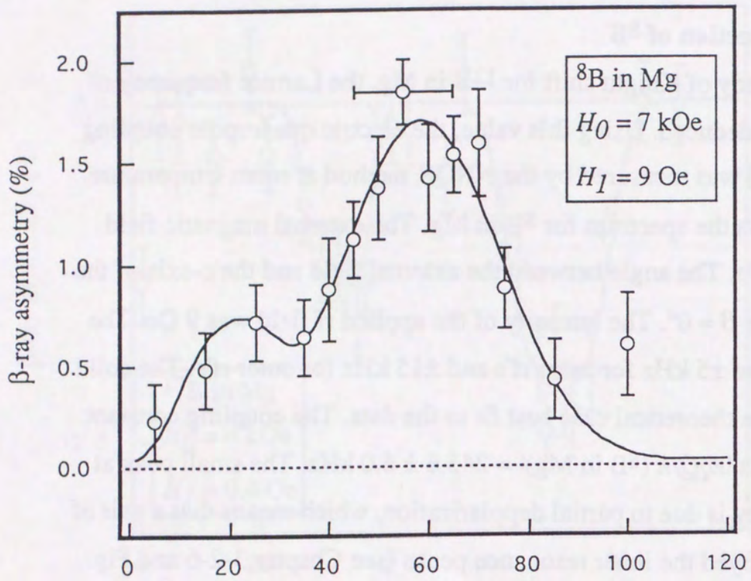

Figure 5-30 Typical NNQR spectrum of ^{8}B in Mg.

The quadrupole coupling constant of ^{8}B in Mg was detected by use of the NNQR method. The solid curve is the theoretical spectrum best fit to the data. The horizontal bar in the figure shows the FM width.

Thus, the electric quadrupole moment of ^{8}B was deduced to be $|Q(^8\text{B})| = 68.7 \pm 2.1$ mb.

Chapter 6

DISCUSSION

6-1 Hyperfine interactions of ^{8}Li in $LiIO_3$ and $LiNbO_3$ and quadrupole moment of ^{8}Li

A long-standing open question about the discrepancy in the experimental $Q(^8\text{Li}, 2^+)$ has been decisively ended by the present NNQR detection of ^{8}Li and the FT-NMR detection of ^{7}Li in $LiIO_3$ and $LiNbO_3$ crystals. The coupling constants of ^{8}Li in the substitutional sites of the single crystals of $LiIO_3$ and $LiNbO_3$ were determined as $|eqQ(^8\text{Li};LiIO_3)/h| = 29.6 \pm 1.1$ kHz and $|eqQ(^8\text{Li};LiNbO_3)/h| = 44.68 \pm 0.88$ kHz, respectively. These values are in quite good agreement with the known values [Ac74, Mi75]. The field gradients in the substitutional sites of both crystals were remeasured by the FT-NMR method at high fields as $|eqQ(^7\text{Li};LiIO_3)/h| = 36.4 \pm 0.5$ kHz and $|eqQ(^7\text{Li};LiNbO_3)/h| = 53.3 \pm 0.5$ kHz for each crystal. It is clear now that the cause of the above mentioned discrepancy was due to the incorrect $|eqQ(^7\text{Li};LiIO_3)/h|$ data [Sa72]. Using the recently determined value of $Q(^7\text{Li}) = -40.0 \pm 0.6$ mb [Vo91], $Q(^8\text{Li}, 2^+)$ were determined to be $|Q(^8\text{Li},2^+)| = 32.6 \pm 1.4$ mb, and 33.5 ± 0.9 mb from the runs using these two catchers (Table 6-1). From the average of these two values, $|Q(^8\text{Li},2^+)| = 32.7 \pm 0.6$ mb, was determined as the final result.

6-2 Quadrupole moment of ^{12}N and its hyperfine interactions

Another question about the $Q(^{12}\text{N}, 1^+)$ value was solved by the present NNQR detection of ^{12}N and the FT-NMR detection of ^{14}N in BN and GaN crystals, and $|Q(^{12}\text{N},1^+)| = 10.3 \pm 0.7$ mb was determined. This value is in quite good agreement with the expected value ($Q(^{12}\text{N}) \sim 10$

Table 6-1
Parameters used for the measurements of the quadrupole moments.

$A(I^\pi)$	Catcher	Temperature(K)	$\lvert eqQ/h\rvert$ (kHz)	Reference
^{8}Li(2$^+$)	$LiIO_3$	~300	29.6 ± 1.1	present
			29.2 ± 0.8	[Mi75]
	$LiNbO_3$	~300	44.68 ± 0.88	present
			43 ± 3	[Ak74]
^{7}Li(3/2$^-$)	$LiIO_3$	~300	36.4 ± 0.5	present
			44 ± 3	[Sa72]
	$LiNbO_3$	~300	53.3 ± 0.5	present
			54.5 ± 0.5	[Ak74]
$\lvert Q(^8\text{Li};LiIO_3)\rvert =$	32.6 ± 1.4 mb			
$\lvert Q(^8\text{Li};LiNbO_3)\rvert =$	33.5 ± 0.9 mb			
$\lvert Q(8\text{Li};2^+)\rvert =$	32.7 ± 0.6 mb			
^{11}B(3/2$^-$)	BN	~300	2902 ± 12	present
			2960 ± 100	[Si60]
	BN	4.2	2934 ± 4	[Co90]
^{12}B(1$^+$)	BN	~300	944 ± 17	present
	Mg	~100	47.0 ± 0.1	[Ki93]
^{8}B(2$^+$)	Mg	~100	243.6 ± 6.0	present
$\lvert Q(^{12}\text{B},1^+)\rvert =$	13.20 ± 0.25 mb			
$\lvert Q(^8\text{B},2^+)\rvert =$	68.3 ± 2.1 mb			
^{12}N(1$^+$)	BN	~300	56.8 ± 3.2	present
	GaN	~300	27.5 ± 2.0	present
^{14}N(1$^+$)	BN	~300	110.7 ± 4.1	present
	GaN	~300	49 ± 15	present
$\lvert Q(^{12}\text{N},1^+)\rvert =$	10.3 ± 0.7 mb			

mb) based on a study of the hyperfine interactions of ^{12}N in metals by Minamisono [Mi70].

Furthermore, Akai predicted the field gradient at ^{12}N site in Mg crystal. Therefore the quadrupole moment $Q(^{12}\mathrm{N})$ was extracted using the experimental $eqQ(^{12}\mathrm{N})$ value of ^{12}N in the Mg crystal [Oh93]. His calculation of the electric field gradient based on a KKR band structure calculation as summarized in the Appendix B. The field gradient was suggested as being $q = -1.92 \times 10^{20}$ V/m^2. The quadrupole moment was obtained as being $Q(^{12}\mathrm{N}) = 12.7$ mb using the observed quadrupole coupling constant $eqQ/h(^{12}\mathrm{N}$ in Mg$) = -59.3 \pm 1.0$ kHz [Ki90]. It is in good agreement with the present experimental result. This agreement shows that the theoretical method is powerful for studying the electronic structure of a dilute impurity at an interstitial site in metals.

On the other hand, the value deduced based on pion photoproduction $(Q(^{12}\mathrm{N}) = +49\mathrm{mb})$ is much larger than the present value [Ra80]. This discrepancy may be due to the cross-section data being inadequate used to deduce an quadrupole moment.

6-3 Proton halo in ^{8}B discovered by its quadrupole moment

The nuclear quadrupole moment of a state is separated into two matrix elements ($\hat{Q}(\mathrm{N_p})$ and $\hat{Q}(\mathrm{N_n})$) by the proton-neutron formalism [Ki93a] (Table 6-2):

$$Q(N_p, N_n) = \sqrt{\frac{16\pi}{5}}\left[\left\langle \sum e_n^{eff}\left(\tfrac{1}{2} + t_z\right) r_i^2 Y_{20}(\Omega_i)\right\rangle + \left\langle \sum e_p^{eff}\left(\tfrac{1}{2} - t_z\right) r_i^2 Y_{20}(\Omega_i)\right\rangle\right]$$
$$= e_n^{eff}\hat{Q}(N_n) + e_p^{eff}\hat{Q}(N_p)$$

where t_z is the z component of the isospin operator. The effective charges $e_p{}^{eff}$ and $e_n{}^{eff}$ of the proton and the neutron in light nuclei were obtained by Kitagawa and Sagawa as $e_p{}^{eff} = +1.25$ and $e_n{}^{eff} = +0.47$ [Ki93a], respectively.

Table 6-2
Theoretical and experimental quadrupole moments of the nucleus in A=8, 11, 12 systems.
The theoretical values were calculated using the empirical effective charge of the protons and neutrons ($e_p{}^{eff}$=1.25, $e_n{}^{eff}$=0.47) [Ki93a].The quadrupole moments are given in absolute values.

A	Nucleus	I^π	Quadrupole moment (mb) HO	WS	experiment	Reference
8	^{8}Li	2+	27.0	30.7	32.6 ± 0.7	present
	^{8}B	2+	48.8	75.0	68.7 ± 2.1	present
11	^{11}B	3/2−	58.9	39.0	+40.59 ± 0.10	[Su91]
	^{11}C	3/2−	38.7	29.4	+33.27 ± 0.24	[Su92]
12	^{12}B	1+	26.1	16.2	13.20 ± 0.25	present
	^{12}N	1+	11.2	5.2	10.3 ± 0.7	present

At first, we considered the $A = 8$ system. The density distributions of protons and neutrons in ^{8}B as a function of the radius were calculated using the Cohen-Kurath (CK) shell-model wavefunctions in the Woods-Saxon (WS) potential (Fig. 6-1). The parameters of the Woods-Saxon potential were taken from ref. [Bo69], except for the potential depth. The depth was adjusted so as to reproduce the experimental separation energy of a single nucleon in each shell-model configuration [Ki93a]. The proton distribution in ^{8}B (solid line) shows a substantial radial swelling, which overcomes the Coulomb and centrifugal barriers, compared with the neutron distribution (dashed line). Since the densities near to the surface are mainly due to the valence nucleons, as indicated by the dotted lines, the value of $\hat{Q}_{\rm th}$(N) reflects the distribution of the valence nucleons. The shell-model calculation is reliable for predicting the $\hat{Q}_{\rm th}$(N) for the deeply bound nucleons, and gives the same value of $\hat{Q}_{\rm th}(3) = 8.0$ mb for the three-neutron configuration in ^{8}B. We were therefore able to extract the value for five protons in the ^{8}B nucleus semiempirically as

$$\begin{aligned}\hat{Q}_{\rm emp}(5;\,^8{\rm B}) &= [Q_{exp}(^8{\rm B}) - e_n^{eff}\hat{Q}_{\rm th}(3)] \,/\, e_p^{eff} \\ &= [68.7 - 0.47 \times 8.0\,] \,/\, 1.25 \\ &= 49.8 \text{ mb} .\end{aligned}$$

If the five protons were deeply bound, since the conventional shell model with Harmonic oscillator potential predicts that $\hat{Q}_{\rm th}(5)$[HO] = 24.3 mb, the $\hat{Q}(5)$ obtained empirically is twice as large as the theoretical value. Taking into account the proton separation energy, and therefore the halo effect in ^{8}B, we obtained an improved theoretical of $\hat{Q}_{\rm th}(5)$[WS] = 58.1 mb which agrees perfectly with the present empirical value. Using the present wavefunction, the rms radii for protons and neutrons in ^{8}B were calculated with the halo effect. The rms radius $\langle r^2\rangle_{\rm p}^{1/2} = 3.03$ fm for protons is much larger than the $\langle r^2\rangle_{\rm n}^{1/2} = 2.16$ fm for a three-neutron core (Table 6-3). This is a clear evidence of a proton halo

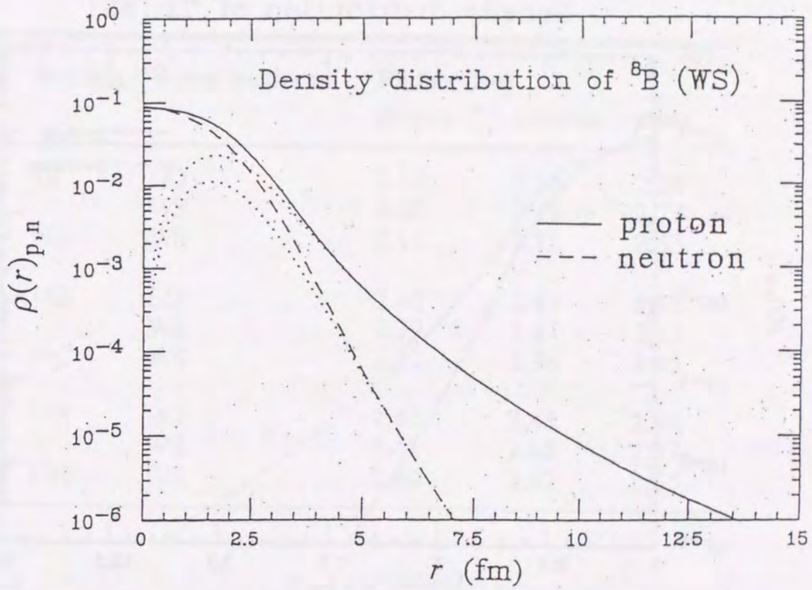

Figure 6-1 Density distribution of protons and neutrons in ^{8}B nuclei. The solid and broken curves correspond to proton and neutron distributions, respectively. The dotted curves are those for valence nucleons.

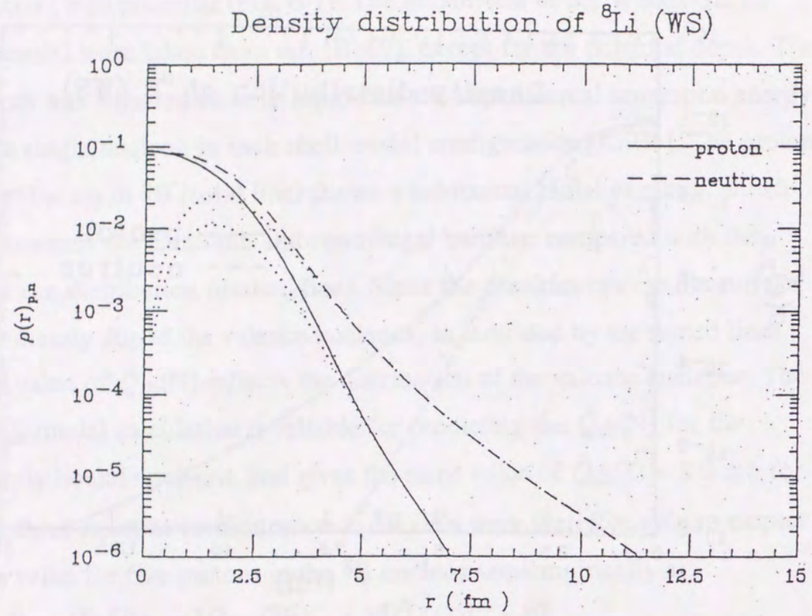

Figure 6-2 Density distribution of protons and neutrons in ^{8}Li nuclei. The solid and broken curves correspond to proton and neutron distributions, respectively. The dotted curves are those for valence nucleons.

Table 6-3
Root-mean-square (rms) radii of the proton and neutron distributions in nuclei of A=8, 11,12 systems.
The rms radii for the total mass are also given. [Ki93a]

A	Nucleus	Wavefunctions	Radius (fm) proton	neutron	mass
8	^{8}B	HO	2.32	2.16	2.26
		WS	3.03	2.16	2.74
	^{8}Li	WS	2.16	2.73	2.53
11	^{11}B	HO	2.40	2.43	2.42
		WS	2.39	2.47	2.43
	^{11}C	WS	2.51	2.38	2.45
12	^{12}B	HO	2.42	2.48	2.46
		WS	2.41	2.68	2.57
	^{12}N	WS	2.80	2.42	2.65

Table 6-4
Calculation of the rms radii of the proton and neutron distributions in the nuclei of A=8.

Nucleus	Q(mb)		Radius (fm) proton	neutron	mass	
^{8}B	65.8	cluster model	2.74	2.25	2.57	[Cs93]
	75.0	shell model	3.03	2.16	2.74	[Ki93]
^{8}Li	22.5	cluster model	2.20	2.59	2.45	[Cs93]
	30.7	shell model	2.16	2.73	2.53	[Ki93]

Nucleus	Radius (fm) last proton	^{7}Be core	mass	
^{8}B	3.75	2.33	2.51	[Ri93]

covering the ^{7}Be core in ^{8}B. The present rms radius for protons in ^{8}B is about 20% larger than the value of $\langle r^2\rangle_p^{1/2}$ = 2.45 fm determined based on the interaction cross sections using a radioactive beam of 800 *A*MeV ^{8}B [Ta88]. This discrepancy may be due to that the interaction cross section method in the high-energy region is not sensitive to such a low amplitude of the present halo distribution.

6-4 Neutron skins in ^{8}Li and ^{12}B detected by their quadrupole moments

As the next step, we considered ^{8}Li as having a normal bound last proton (E_{sp}(p) = 12.5 MeV) and a rather shallowly bound last neutron (E_{sp}(n) = 2.0 MeV). The density distributions of the protons and neutrons in ^{8}Li as function of the radius were calculated by using the Cohen-Kurath (CK) shell-model wavefunctions in the Woods-Saxon (WS) potential (Fig. 6-2).

The theoretical value for five neutrons $\hat{Q}_{th}(5)$ = 41.6 mb which completely accounts for the value which is deduced from the experimental value $|Q_{exp}(^{8}\text{Li},2^+)|$ = 32.7 ± 0.6 mb as following. As well as ^{8}B, the semiempirical value of $\hat{Q}(5)$ can be extracted as

$$\hat{Q}_{emp}(5;\,^{8}\text{Li}) = [Q_{exp}(^{8}\text{Li};2^+) - e_p^{eff}\hat{Q}_{th}(3)] \,/\, e_n^{eff}$$
$$= [32.7 - 1.25 \times 8.0] \,/\, 0.47$$
$$= 48.3 \text{ mb}\,.$$

The theoretical $\hat{Q}_{th}(5)$[HO] = 24.3 mb with a harmonic-oscillator potential is about half the empirical value, while the $\hat{Q}_{th}(5)$[WS] = 41.6 mb with Woods-Saxon potential is in good agreement with the empirical value. The rms radii, $\langle r^2\rangle_p^{1/2}$ = 2.16 fm and $\langle r^2\rangle_n^{1/2}$ = 2.72, were obtained theoretically while taking into account the halo effect, which shows a significant difference between the proton and neutron radial distribution (Table 6-3). This suggests a thin neutron skin covering the

^{7}Li core. Here, we use the word "skin" when the difference between $\langle r^2\rangle_p^{1/2}$ and $\langle r^2\rangle_n^{1/2}$ is rather smaller than the case of ^{8}B (0.9 fm).

The present rms radius for neutrons in ^{8}Li is also larger than the value of $\langle r^2\rangle_n^{1/2}$ = 2.44 fm determined from the interaction cross section [Ta88]. Similarly, from the nuclear interaction cross section measured at far low energies (25~65 *A*MeV) at GANIL [Li90], rms radii are determined as $\langle r^2\rangle_p^{1/2}$ = 2.17 and $\langle r^2\rangle_n^{1/2}$ = 2.80 fm. These radii are in quite good agreement with the present result; $\langle r^2\rangle_p^{1/2}$ = 2.16 fm and $\langle r^2\rangle_n^{1/2}$ = 2.72 fm. These agreements show the importance of studies on the energy dependence of the interaction cross section at low energies.

We next consider the A = 12 system (^{12}B and ^{12}N). Based on a shell-model calculation concerning this system, $\hat{Q}_{th}(5)$[WS] = 13 mb and $\hat{Q}_{th}(7)$[WS] = 0.11 mb were obtained using the Wood-Saxon potential for both the proton and neutron groups, respectively. The small value for the $\hat{Q}(7)$[WS] is because the valence nucleon is mainly in the $p_{1/2}$ state, and its finite value is due to configuration-mixing corrections.

These values give quadrupole moments of $Q(^{12}\text{B})$[WS] = 16.2 mb as shown in Table 6-2. This theoretical value is in good agreement with the present experimental value $|Q_{exp}(^{12}\text{B})|$ = 13.20 ± 0.25 mb. On the contrary, the shell model using harmonic-oscillator potential gives $Q(^{12}\text{B})$[HO] = 26.2 mb, which is in poor agreement with the experiment. This tendency is similar to the case of the A = 8 system.

The calculated rms radii of the protons and neutrons in ^{12}B with loosely bound neutrons, $\langle r^2\rangle_n^{1/2}$ = 2.68 fm and $\langle r^2\rangle_p^{1/2}$ = 2.41 fm (Table 6-3) show a thin neutron skin covering the ^{11}B core. The radii derived from the interaction cross section at ^{12}B energy of 800 *A*MeV $\langle r^2\rangle_n^{1/2}$ = 2.42 fm and $\langle r^2\rangle_p^{1/2}$ = 2.35 fm [Ta88] are both smaller than the present values. On the other hand, the radii determined using low

energies (25~65 *A*MeV) are rather large, $<r^2>_n^{1/2}$ = 2.93 fm and $<r^2>_p^{1/2}$ = 2.40 fm [Li90] which are in good agreement with the present results. This tendency is the same as in the case of ^{8}Li. The importance of the energy dependence of the interaction cross section has been also suggested by Fukuda et al. in the interpretation of interaction cross section of ^{11}Be [Fu91].

6-5 Quadrupole moment of ^{12}N

Finally, we consider the rms radius of ^{12}N (Table 6-2). Using the values of $\hat{Q}_{th}$(5)[WS] and $\hat{Q}_{th}$(7)[WS], the quadrupole moment of ^{12}N is given as $Q(^{12}N)$[WS] = 5.2 mb. This result is about 1/2 of the experimental value, and is not in agreement with the experiment one. On the contrary, the shell model using the harmonic-oscillator potential gives $Q(^{12}N)$[HO] = 11.2 mb, which is in good agreement with the experimental values. This tendency differs from the other cases (^{8}Li, ^{8}B and ^{12}B).

Here, we consider the case of the A = 11 system, where both nuclei (^{11}B and ^{11}C) have a deeply bound last proton and neutron. These calculation values are listed in Table 6-2. The results show that a calculation using the Cohen-Kurath potential is better than using the harmonic-oscillator potential in the case that there is no halo structure.

Even though the present theoretical calculation was successful for other nuclei (^{8}Li, ^{8}B, ^{11}B,^{11}C and ^{12}B), there is a discrepancy in the quadrupole moment between the theoretical calculation with a halo structure and the experimental result in the case of ^{12}N. This may be due to an inadequacy of the theoretical calculation for ^{12}N.

6-6 Other interpretations of the quadrupole moments and radii for ^{8}Li and ^{8}B

In this section we introduce other theoretical descriptions for nuclear quadrupole moments and radii.

Nakada et al. [Na93] discussed the E2 properties of A = 6-10 nuclei with a (0+2)$\hbar\omega$ large-scaled shell-model calculation that was developed by Wolter et al. [Wo90]. The effective interaction was determined by a fitting of the experimental energy levels of A = 6-16 nuclei. They calculated the quadrupole moments of ^{8}Li and ^{8}B using small effective charges (e_p^{eff} = 1.05 and e_n^{eff} = 0.05) as being $Q(^8Li)$ = 32.1 mb and $Q(^8B)$ = 62.7 mb without introducing any halo structures. These values are in good agreement with the experiments. They mentioned that the small effective charges may be due to the slower damping tail of the proton density, even though its amplitude is smaller than ones of ^{11}Li and ^{11}Be. However, nuclear radius calculated in this model is larger than one obtained based on the interaction cross section [Sa94]. Furthermore, it must be noted that in their view the core excitation (deformation) occurs considerably, even in the region which has been considered spherical region. This means that the wavefunctions that they used may not be sufficiently suitable. A reconsideration of their description might therefore be necessary.

Descouvemont et al. reported on a theoretical study of ^{8}Li and ^{8}B within the framework of the cluster model [De92]. They described ^{8}B and ^{8}Li as being three-cluster systems: ^{8}Li = α + t + n and ^{8}B = α + ^{3}He + p. They deduced the quadrupole moments as being $Q(^8Li)$ = 31 mb and $Q(^8B)$ = 73 mb. These values are in good agreement with experimental values. On the other hand, another report concerning a three-cluster calculation was carried out by Csótó [Cs93]. He deduced the quadrupole moments as being $Q(^8Li)$ = 22.5 mb and $Q(^8B)$ = 65.8 mb. Although

$Q(^8B)$ is in good agreement with the experimental value, $Q(^8Li)$ is rather inconsistent. This discrepancy is not discussed in his paper. These results show that the three-cluster model provides a good description for these nuclei, even though there is a slight discrepancy. Furthermore, Csótó calculated the rms radii for protons and neutrons in ^8Li and ^8B using the three-cluster model. These values are listed in Table 6-4. Although their results show the existence of neutron and proton skins, these amplitudes are rather smaller than our. It is very interesting that the neutron and proton skins have been deduced from different approaches: the shell model and the cluster model.

In astrophysics nuclear radius have an important role. The radius of ^8B has been discussed concerning the "solar neutrino problem" by Riisager et al. [Ri93]. It is the long-standing discrepancy between the experimentally and theoretically calculated neutrino flux from the Sun [Ba82]. If the contribution from ^8B neutrinos were half the presently assumed values, the theory and experiments would agree within a few standard deviations. They looked at the $^7Be(p, \gamma)^8B$ reaction through which ^8B is produced in the Sun. The tail of the proton distribution is important concerning the rate of the $^7Be(p, \gamma)^8B$ reaction at low energies and the high-energy solar neutrino flux. The proton capture reaction can be used as a probe for nuclear radii. They calculated the astrophysical S-factor of this reaction as well as the rms radii for ^8B. They used a two-body model for ^8B, which is considered to be approximated by a proton bound in the weak field from a ^7Be-like core [Ri92, Je92]. The potential is assumed to be a gaussian of range b = 1.90 fm and the strength is varied to adjust the proton separation energies E_{sp}(p). They pointed out the importance of the separation energy of the last proton in ^8B. The rms radius for ^8B for the experimental separation energy was 2.51 fm and the corresponding rms radius for the last proton was 3.75 fm (Table 6-4). Although the value

was quite a bit larger than the deduced rms radius of their ^7Be core (2.33 fm) their result phenomenologically shows an existence of a proton skin in ^8B.

Chapter 7

SUMMARY

We measured the quadrupole moments of ^{8}Li, ^{8}B, ^{12}B and ^{12}N using a modified β-NMR (NNQR) method. The results are $|Q(^{8}\mathrm{Li})| = 32.7 \pm 0.6$ mb, $|Q(^{8}\mathrm{B})| = 68.3 \pm 2.1$ mb, $|Q(^{12}\mathrm{B})| = 13.20 \pm 0.25$ mb and $|Q(^{12}\mathrm{N})| = 10.3 \pm 0.7$ mb. These values were mostly accounted for fairly well by the effect of spatial swelling in the distributions of shallowly bound valence nucleons. Above all, the neutron distributions of ^{8}Li and ^{12}B are in quite good agreement with that deduced based on the interaction cross sections measured at low energies. A prominent proton halo is suggested to cover the ^{7}Be core, in spite of the existence of Coulomb and centrifugal barriers in ^{8}B. The measurement of the nuclear interaction cross sections at low energies for proton-rich nuclei is planed in order to clarify the present picture. The implication of the quadrupole moment of ^{12}N, which is twice as large as the value obtained from the shell model calculation with a halo, has to be disclosed.

REFERENCES

Ab61 A. Abragam, The principles of Nuclear Magnetism, Oxford University Press, Oxford, (Original text 1961, paperback 1983)

Aj88 F. Ajzenberg-Selove, Nucl. Phys. **A490** (1988) 1

Aj90 F. Ajzenberg-Selove, Nucl. Phys. **A506** (1990) 1

Ar88 E. Arnold et al., Z. Phys. **A331** (1988) 295

Ba82 J.N. Bahcall et al., Rev. Mod. Phys. **54** (1982) 767

Be89 G.F. Bertsch, B.A. Brown and H. Sagawa, Phys. Rev. **C39** (1989) 1154

Bo69 A. Bohr and B.R. Mottelson, Nuclear Structure Volume 1, W.A. Benjamin, New York, (1969)

Br86 E. Browne et al., Table of Radioactive Isotopes, J. Wiley & Sons, New York, (1986)

Ca87 A. Catrllani et al., Phys. Rev. **B36** (1987) 6105

Co65 S. Cohen and D. Kurath, Nucl. Phys. **73** (1965) 1

Co90 C. Conor et al., Rev. Sci. Instrum. **61** (1990) 1059; C. Conor et al., J. Chem. Phys. **93** (1990) 7639

Cs93 A. Csótó, Phys. Lett. **B315** (1993) 24

De Denki Kagaku Kogyo, Research Center, 3-5-1 Ashahi-machi, Machida, Tokyo 194, Japan

De92 P. Descouvemont and D. Baye, Phys. Lett. **B292** (1992) 235; P. Descouvemont, Proc. of 2nd International Symposium on Nuclear Astrophysics, Karlsurhe, Germany, 1992, ed. F. Käppeler and K. Wisshak, IOP Publishing, London, p.369

de63 de-Shalit and A. Talmi, Nuclear Shell Theory, Academic, New York, (1963)

Fu81 E. Fukushima and S.B.W. Roeder, Experimental Pulse NMR -A Nuts and Bolts Approach-, Addison-Wesley, (1981)

Fu91 M. Fukuda et al., Phys. Lett. **B268** (1991) 339

Ga93 A. García and M.L. Cohen, Phys. Rev. **B47** (1993) 4215

Go91 I. Gorczyca and N.E. Christensen, Solid State Communications **80** (1991) 335

Ha70 T.K. Halstead, J. Chem, Phys. **53** (1970) 3427

Ha73 R.C. Haskell and L. Madansky, J. Phys. Soc. Japan **34** Suppl. (1973) 167

Ha88 O.-H. Han et al., J. Chem. Phys. **89** (1988) 6046

He84 P.M. Henrichs et al., J. Mag. Res. **60** (1984) 280

He90 K.L.G. Heyde, The Nuclear Shell Model, Springer-Verlag, (1990)

Hu85 N.-Z. Huang and W.Y. Ching, J. Phys. Chem. Solids **46** (1985) 977

It85 N. Itoh et al., J. Appl. Phys. **58** (1985) 1828

Je92 A.S. Jensen and K. Riisager, Nucl. Phys. **A537** (1992) 45

Ka Kawasaki Seitetsu, 2-2-3 Komachi, Chiyoda, Tokyo 100, Japan

Ki90 A. Kitagawa et al., Hyperfine Interactions **60** (1990) 869

Ki93a H. Kitagawa and H. Sagawa, Phys. Lett. **B299** (1993) 1

Ki93b H. Kitagawa and H. Sagawa, Nucl. Phys. **A551** (1993) 16

Ki93c A. Kitagawa, Ph. D. These, Osaka University (1993)

Ku73 D. Kurath and A. Arima, J. Phys. Soc. Japan **34** Suppl. (1973) 529

Li90 E. Liatard et al., Europhys. Lett. **13** (1990) 401

Ma Matsushita Electronics Corporation, Nagaokakyo, Kyoto 617, Japan

Mi70 T. Minamisono, Private communication ; Ph. D. Thesis, Osaka University (1970)

Mi71 T. Minamisono et al., J. Phys. Soc. Japan **30** (1971) 322

Mi73 T. Minamisono, J. Phys. Soc. Japan **34** Suppl. (1973) 324

Mi75 D.J. Millener and D. Kurath, Nucl. Phys. **A255** (1975) 315

Mi75 T. Minamisono et al., Phys. Rev. Lett. **34** (1975) 1465

Mi78 T. Minamisono et al., Hyperfine Interaction **4** (1978) 224

Mi74 T. Minamisono et al., Nucl. Phys. **A236** (1974) 416

Mi92 T. Minamisono et al., Phys. Rev. Lett. **69** (1992) 2058

Mi93 T. Minamisono et al., Hyperfine Interaction **80** (1993) 1315

Mi93b T. Minamisono et al., Nucl. Phys. **A559** (1993) 239

Mi93c T. Minamisono et al., Hyperfine Interaction **78** (1993) 159

Mi94 T. Minamisono, private communication

Mo73 M. Morita, Beta Decay and Muon Capture, W.A. Benjamin Inc., Reading, Massachusetts (1973)

Mu Murakami engineering co., 3-15-27, Kikuna, Kohoku-ku, Yokoyama, Kanagawa 222, Japan

Na93 H. Nakada and T. Otsuka, submitted to Phys. Rev. **C**

Na94 H. Nakada private communication

Ne70 R.K. Nesbet, Phys. Rev. **A2** (1970) 1208

Ng Electronics and Optoelectronics Research Laboratory, NGK co., 2-56 Suda, Mizuho, Nagoya 467, Japan

Oh93 T. Ohtsubo et al., Hyperfine Interactions **80** (1993) 1051

Or90 R. Orlando et al., J. Phys. Condensed Matter **2** (1990) 7769

Pe67 G.E. Peterson et al, J. Chem, Phys. **46** (1967) 4009

Pe76 G. Petzow, Metallographisehs Ätzen, Gebrüder Borntranger, Berlin-Stuttgart, (1976)

Pe92 P. Perlin et al., Phys. Rev. **B45** (1992) 13307

Ra73 G.M. Radutsky and V.A. Serdjutsky, Nucl. Phys. **B54** (1973) 302

Ra80 G.M. Radutskíi et al., Sov. J. Nucl. Phys. **31** (1980) 177

Ri92 K. Riisager et al., Nucl. Phys. **A548** (1992) 393

Ri93 K. Riisager and A.S. Jensen, Phys. Lett. **B301** (1993) 6

Sa72 V.M. Sarnatskii et al., Sov. Phys. Solid State **13** (1972) 2021

Sa84 H. Sagawa and B.A. Brown, Nucl. Phys. **A430** (1984) 84

Sa94 H. Sagawa, private communications

Sc92 A. Schirmacher and H. Winter, Phys. Rev. Lett. **69** (1992) 257

Si60 A.H. Silver and P.J. Bray, J. Chem. Phys. **32** (1960) 288

Si76 A. Shintani and S. Minagawa, J. Electrochem. Soc. **123** (76) 706

So90 Y. Someda et al., Annual Report of Osaka University, Laboratory of Nuclear Science, OULNS (1990) p.68,76

St50 R.M. Sternheimer, Phys. Rev. **80** (1950) 102

St85 R.M. Sternheimer, Z. Naturforsch **41a** (1985) 24

Su66 K. Sugimoto et al., J. Phys. Soc. Japan **21** (1966) 213

Su67 K. Sugimoto et al., J. Phys. Soc. Japan **25** (1967) 130

Su90 M. Suzuki and H. Tanji, Proceedings of 2nd International Conference on the New Diamond Science & Technology, (1990), Washington D.C.

Su91 D. Sundholm and J. Olsen, J. Chem. Phys. **94** (1991) 5051

Su92 D. Sundholm and J. Olsen, J. Chem. Phys. **96** (1992) 627

Ta76 M. Tanaka et al., Nucl. Phys. **A263** (1976) 1

Ta77 I. Tanihata et al., Phys. Lett. **67B** (1977) 392

Ta85 I. Tanihata et al., Phys. Rev. Lett. **55** (1985) 2676

Ta88 I. Tanihata et al, Phys. Lett. **B206** (1988) 592

Ta89 I. Tanihata, Proc. of 1st International Conference on Radioactive Nuclear Beams, Berkeley, 1989, World Scientific,(1990) p.429

Ta92 I. Tanihata et al., Phys. Lett. **B287** (1992) 307

Tr75 R.E. Tribble and T. Garey, Phys. Rev. **C12** (75) 967

To82 F. Touchard et al., Phys. Rev. **C25** (1982) 2756

Vo91 H.-G. Voelk and D. Fick, Nucl. Phys. **A530** (1991) 475

Wa86 M. Wakatsuki et al., Physica **139 & 140B** (1986) 256

We68 J. Wells et al., Phys. Lett. **27B** (1968) 448

Wo90 A.A. Wolters et al., Phys. Rev. **C42** (1990) 2053, 2062; comment in Phys. Rev. **C45** (1992) 477

Wy82 R.W.G. Wyckoff, Crystal Structure Volume 1, R.E. Kringer, (1982)

APPENDIX

A. Field gradients in Mg detected by ^{12}B and ^{12}N

From the detailed study of the electric quadrupole interactions for ^{12}B and ^{12}N using the β-NMR method [Ki90, Ki93c] there are two components in the NMR spectrum (Fig. 5-29). Amount of the main component is about 80% and one of the sub component is about 20%. The main electric field gradient is confirmed that it is parallel to the *c*-axis. In the condition of $\beta = 0°$, the sub component shows that the sign of the field gradient is inverse relation to the main component and its amplitude is about an half of one of main component. These results suggest that both component are same sites in the crystal but local directions of the small crystal block are different. The study of ^{8}B whose recoil energy is larger than ^{12}B (Table) showed that this phenomenon is occurred in surface of crystal (<1μm), since the implantation process is similar for both nuclei. It is considered to be due to the process of surface treatment. Further study of ^{12}B in Mg [Mi94], the field-gradient direction of the sub component is not distributed homogeneously but considered to be restricted. One interpretation is that in surface local crystal blocks are restricted and the direction of its *c*-axis is normal to the plane when main *c*-axis is contained in the plane. Now, further study is in progress in our laboratory.

B. Theoretical calculation of the field gradient at the trigonal site of Mg and the nuclear quadrupole moment of ^{12}N

While a number of theoretical studies have been made on substitutional impurities in metallic system in the past decade, little has been done for interstitial impurities such as ^{12}B and ^{12}N in Mg. The main reason is that,

whereas lattice relaxations are crucial for most interstitial impurity systems, the Korringa-Kohn-Rostoker (KKR) Green function method, a standard method of the electronic structure calculation of impurity system, cannot treat the effect of the lattice relaxations property. One of the way to avoid the difficulty is to use the super-cell method. Though obviously the super-cell method is not the best choice for the impurity in an unrelaxed lattice, the method is quite powerful in general because of its capability of handling arbitrary rearrangements of atoms around the impurity.

Akai et al. performed the KKR band structure calculation in the framework of the local-density approximation (LDA) on super-cells illustrated in Fig. A-1. To include the effects of the lattice relaxation around the impurity, they displace the nearest neighboring host atoms, keeping the local symmetry around the impurity unchanged, as is shown in Fig. A-1 by the arrows. In order to make direct comparisons of the total energies among various impurity locations and lattice relaxations possible, they fix the muffin-tin radii to values somewhat smaller than those for touching spheres so that they never intersect. The total energy of the system is calculated for various lattice relaxations, which gives the energy as a function of the relaxation. In Fig. A-2 the calculated total energies for various N locations are compared.

As is naturally expected, the location of N with the lowest energy is the octahedral-like (O-site) which has the biggest interstitial volume. The tetrahedral-like site (T-site) also has a rather big interstitial volume. The energy for this location, however, is the highest, 5.5 eV relative to the O-site case. Between two trigonal sites, the center of the basal triangle just below the O-site(Trig1-site) gives a lower energy, being 0.83 eV relative to the O-site. The energy gains due to the relaxation around N at the O-site and Trig1-site cases are 2.6 and 3.7 eV, respectively. The minimum

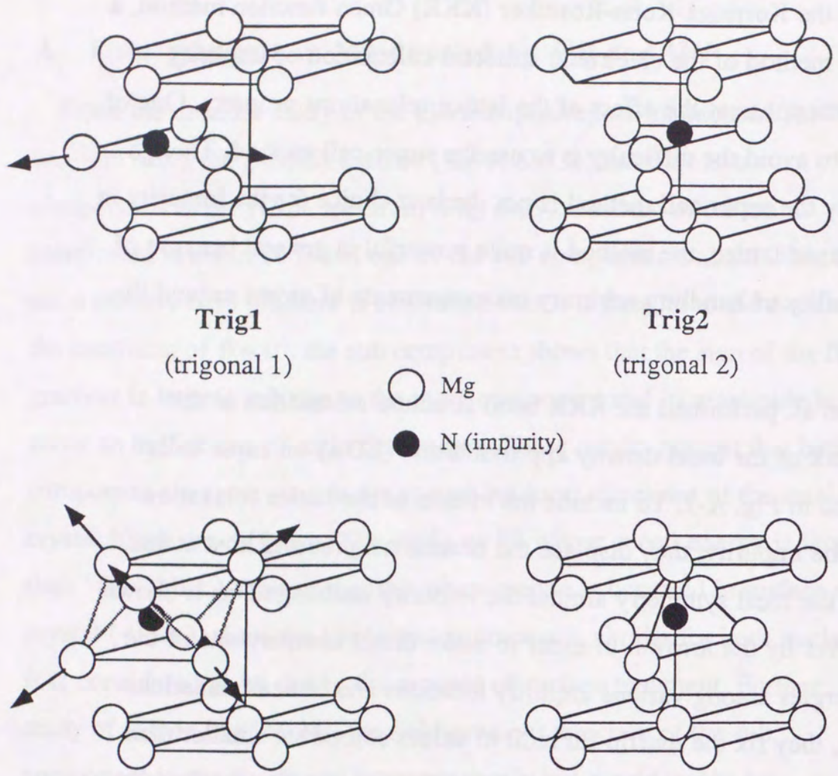

Fig. A-1 Four different types of the unit-cell used in the calculations. The big spheres represent the host atoms and the small filled one represents the impurity atom. The arrows show the direction of the local lattice relaxation for Trig1 and O cases.

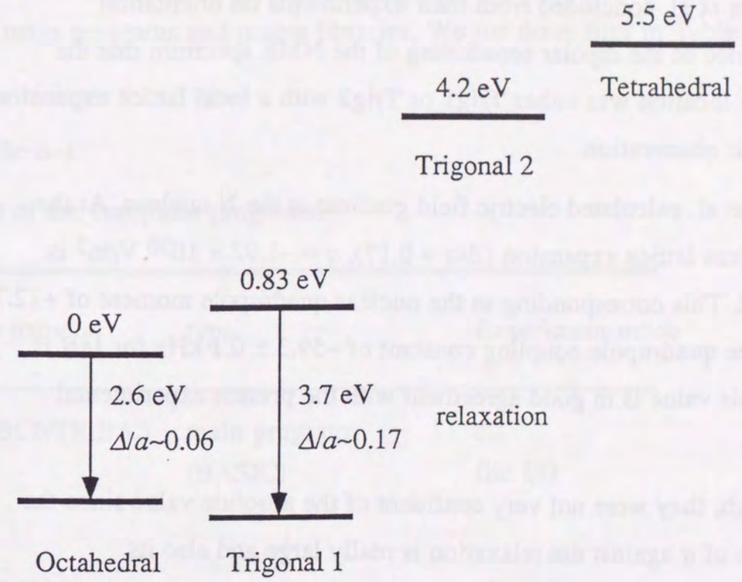

Fig. A-2 Energy scheme indicating the relative energies per unit cell (in eV) for various site occupations of N impurities in Mg. Also shown are the energies after the full lattice relaxations for the Octahedral and Trigonal 1 cases.

occurs at $\Delta/a \sim 0.06$ (O-site) and ~0.17 (Trig1-site), respectively, where Δ is the displacement of the neighboring Mg atoms and a is the lattice constant.

As for the location and the lattice relaxation of N impurities in Mg, Kitagawa et al. concluded from their experiments on orientation dependence of the dipolar broadening of the NMR spectrum that the impurity location was either Trig1 or Trig2 with a local lattice expansion than their observation.

Akai et al. calculated electric field gradient at the N nucleus. At the equilibrium lattice expansion ($\Delta/a = 0.17$), $q = -1.92 \times 10^{20}$ V/m^2 is obtained. This corresponding to the nuclear quadrupole moment of +12.7 mb, if the quadrupole coupling constant of -59.3 ± 0.1 kHz for ^{12}N is used. This value is in good agreement with the present experimental value.

Though, they were not very confident of the absolute value since the variation of q against the relaxation is really large and also its convergence with respect to the number of k-point sampling is slow (the results are for 216k-points in the irreducible zone); it seems rather hard to determined the q at the optimum configuration for their system.

C. A computer program list for NNQR: spin control and data-acquisition system

We list computer programs for β-NMR and NNQR method. These program are written by MASM (macro assembler). They contain two parts, main programs and macro libraries. We list these files in Table A-1

Table A-1

List of the computer programs.

File name	type	Experiment mode
LABCNTR.BAS	main program (BASIC)	all file I/O
LABCNTR1	macro libraries	all
LABCNTR2	macro libraries	all
IOCNTR	macro libraries	all
2APCNTR	main program	2AP mode
8APCNTR	main program	8AP mode
2RFCNTR	main program	2rf mode

LABCNTR.BAS

```
10000
'*****************************************************
10010 '
10020 '    experimental control program  (operating part)
10030 '
10040 '\cntr\LABCNTR.BAS"
10050 '
10060 '    by  A. Kitagawa  Ver 8.30  L.07  '89/03/10
10070 '1992.9.29 modify 21730 to use dif. mode for 2AP by
T.Ohtsubo L.08
10075 '1993.4.20 modify 23360 (adding L=0)by T.Yamaguchi
10080
'*****************************************************
10090 '
10100 CLEAR &H500,,&H4D4B,&H0
10110 PCFRG=1:FMFRG=0
10120 MSEG=SEGPTR(2)
10130 MSEG2=MSEG+&H400
10140 DIM FLMENU$(10),NMMENU$(10),MMENU(10),NSVDATA(10)
10150 DIM
RFGP$(127),RFDA%(1,127),NU#(127),UP#(15,127,2),DW#(15,127,
2)
10160 DIM
R(15,127,2),RER(15,127,2),UD(127,2),ER(127,2),ERC(127,2)
10170 DIM
RSEC(7,127,2),RERSEC(7,127,2),EFFECT(127,2),EFFERR(127,2)
10180 DIM X(255),Y(255),Z(255),ZC(255),DUMMY1(15)
10190 DIM
TWAIT%(31),RFDATA%(15,127),U%(1,15,127,3),D%(1,15,127,3),P
ARA(31)
10200 DIM SEM%(1,15)
10210 '
10220 ON ERROR GOTO *TRAP
10230 ON STOP GOSUB *STTRAP:STOP ON
10240 '
10250 '+++++ set experimental mode
10260 '
10270 LBLFRG=0:RFDTFRG=1:NCH=1:TRNSFRG=0:MNTFRG=0
10280 BSTIME=.1:BMCYC=4
10290 '
10300
DTDRIVES="B:":PRDRIVES="A:":SYDRIVES="A:\cntr\":DTDRIVE=1
10310 GOSUB *SELMENU
10320 IF TRNSFRG THEN OPEN "COM1:N81XN" AS #2
10330 GOSUB *PARAMAKE2
10340 HCFRG=1-(AP4FRG OR
AP8FRG):LPONEFRG%=0:LPMIN=4:MAXN3=0
10350 '
10360 '----- loding assembla program
10370 '
10380 MC=5:GOSUB *DSPWAITMES
10390 GOSUB *LDMPRG
10400 LAB%=0
10410 '
10420 '+++++ system initialize
10430 '
10440 *INIT
10450 MC=4:GOSUB *DSPWAITMES
10460 GOSUB *INITGP:GOSUB *GPLCL
10470 GOSUB *DSPINIT
10480 '
10490 '+++++ data input
10500 '
10510 *LDDATA
10520 GOSUB *RNMMAKE:GOSUB *DSPTITLE
10530 MC=5:PS="Ｒｕｎ　Ｎｏ．を入れて下さい":GOSUB *DSPM
10540 L1=23:C1=30:AS=RNM$:GOSUB *DSPSIN
10550
RNM$=LEFT$(AS,8):F=INSTR(RNM$,".")+INSTR(RNM$,"\")+INSTR(R
NM$,":")
10560 IF F THEN BEEP:GOSUB *CL3:GOTO *LDDATA
10570 GOSUB *DSPTITLE:GOSUB *CL3
10580 PS="新しいｒｕｎですか（0）、再開ですか（1）"
10590 NK=2:MC=5:GOSUB *DSPIN:ANSNR=ANSN+1
10600 ON ANSNR GOSUB *LDNEW,*LDOLD,*LDCNT
10610 '
10620 *LDDATA2
10630 IF NRF%=0 THEN *LDDATA
10640 GOSUB *DSPCLTG:GOSUB *DSPTITLE:GOSUB *DSPSET
10650 MC=7:PS="設定":GOSUB *DSPST
10660 PS="設定を確認して下さい。（Ｙ：0，Ｎ：1）"
10670 NK=1:MC=5:GOSUB *DSPIN
10680 IF ANSN THEN *LDDATA ELSE IF ANSNR=2 THEN GOSUB
*MDLP3
10690 GOSUB *CKRFMAKE:GOSUB *PARAMAKE1:GOSUB *RFDTMAKE
10700 *LDDATA3
10710 MC=5:PS="コメントを入れて下さい":GOSUB *DSPM
10720 L1=23:C1=24:AS=RNCMNT$:GOSUB *DSPSIN:RNCMNT$=AS
10730 A=INSTR(AS,CHR$(&H22)):IF A THEN RNCMNT$=LEFT$(AS,A-
1):GOTO *LDDATA3
10740 '
10750 '+++++main loop
10760 '
10770 *MAINLOOP
10780 GOSUB *DSPCLT:GOSUB *DSPTITLE
10790 MC=5:PS="待機中":GOSUB *DSPST
10800 TESTFRG=0
10810 PS="［0］キーで実行します。（設定変更［1］、停止［2］、
テスト［3］）"
10820 NK=3:MC=5:GOSUB *DSPIN
10830 ON ANSN GOTO *MLOOPSUB,*MIDEXIT,*TESTSTART
10840 GOTO *MAINSTART
10850 '
10860     *MLOOPSUB
10870     PS="０無変更、１時間間隔、２ｺﾒﾝﾄ、３ﾒﾓﾘｸﾘｱ、４表示、５ﾊﾝ
ﾄﾞｺﾋﾟｰ、６ﾛｰﾄﾞ、７計算"
10880     NK=7-LIFFRG:MC=5:GOSUB *DSPIN
10890     ON ANSN GOSUB
*MLP1,*MLP2,*MLP3,*MLP4,*MLP5,*MLP6,*MLP7
10900     GOTO *MAINLOOP
10910 '
10920 *TESTSTART
10930 PS="テスト実行ではデータエリアをクリアします宜しいですか
(y:0,n:1)"
10940 NK=1:MC=5:GOSUB *DSPIN
10950 IF ANSN THEN *MAINLOOP
10960 TESTFRG=1:LPMINB=LPMIN:LPMIN=60:MAXN3B=MAXN3:MAXN3=0
10970 '
10980 '+++++ 実行
10990 '
11000 *MAINSTART
11010 GOSUB *LPPRMAKE
11020 LPN3=0
11030 IF TTTURN#=0 THEN PS="start = " ELSE PS="restart="
11040 LOCATE 0,2:GOSUB *DSPTM
11050 '
11060 '  ----- operation loop
11070 '
11080     *MIDLOOP
11090     IF TESTFRG=0 THEN MC=4:PS="実行中" ELSE MC=6:PS="
テスト"
11100     GOSUB *DSPST
11110     LS=1:GOSUB *DSPREVS
11120     MC=5:PS="赤いボタンのＳＴＯＰスイッチで停止します
":GOSUB *DSPM
11130     TWAIT%(0)=&H0:LPN%=MAXN%:LPN2=0
11140         '
11150         ' +++++ assembla loop
11160         '
11170         *LTLOOP
11180         IF TRNSFRG THEN CLOSE #2
11190         STOP OFF
11200         DEF SEG=MSEG
11210         *LTLOOP1:CALL
LAB%(TWAIT%(0),SEM%(0,0),D%(0,0,0,1),U%(0,0,0,1),D%(0,0,0,
0),U%(0,0,0,0),RFDATA%(8*LBLFRG,1),NRF%,LPN%)
11220         IF TWAIT%(0)=0 AND MAXN2<>LPN2 THEN
LPN2=LPN2+1:GOTO *LTLOOP1
11230         '
11240         ' +++++
11250         '
11260     *LTEXIT
11270     STOP ON
11280     IF TRNSFRG THEN OPEN "com1:n81nn" AS #2
11290     GOSUB *DSPCLTG:GOSUB *DSPTITLE
11300     MC=1:PS="処理中":BEEP:GOSUB *DSPST
11310     EFRG%=TWAIT%(0) AND &HFF
11320     IF MAXN%<>LPN% AND EFRG% THEN
LP#=LPN2*32767#+MAXN%-LPN% ELSE LP#=LPTURN#
11330
LPN3=LPN3+1:TTTURN#=TTTURN#+LP#:DDATAS=DATE$:TDATAS=TIME$
11340     IF MDRF=0 AND LIFFRG=0 THEN GOSUB *CHECKFREQ
11350     '
11360     IF TESTFRG=1 THEN *LTERROR
11370     IF TRNSFRG THEN TRNSMODE%=1:GOSUB *TRNSDATA ELSE
GOSUB *RCONT
11380     '
11390     *LTERROR
11400     IF EFRG% AND &H1B THEN *MIDEXIT
11410     IF LPONEFRG%<>0 THEN *MIDEXIT
11420     IF INKEY$=CHR$(&H1B) THEN *MIDEXIT
11430 '
11440     GOTO *MIDLOOP
11450 '
11460 '+++++ stop operation
11470 '
11480 *MIDEXIT
11490 IF (EFRG% AND &H19)=0 THEN *MIDEXIT2
11500 *MIDERROR
11510 IF EFRG% AND &H8 THEN ERMS$="ＲＦコントロールエラー！"
11520 IF EFRG% AND &H1 THEN ERMS$="ＰＤＰコントロールエラー！
"
11530 IF EFRG% AND &H10 THEN ERMS$="ＲＦミスマッチ　エラー！"
11540 BEEP 1:MC=2:PS="エラー":GOSUB *DSPST:PRINT:PRINT
ERMS$;
11550 PS="状態を確認後、何かキーを押して下さい。停止画面に入ります"
11560 MC=2:GOSUB *DSPM
11570 *MIDE2:KS=INPUT$(1):IF KS="" THEN *MIDE2
11580 BEEP 0:COLOR 7
11590 '
11600 *MIDEXIT2
11610 GOSUB *DSPTITLE:MC=3:PS="停　止":GOSUB *DSPST
11620 IF TESTFRG THEN GOSUB *DSPCLT:GOSUB *DATNEW
11630 IF TESTFRG THEN LPMIN=LPMINB:MAXN3=MAXN3B
11640 PS="ランの終了（0）、継続（1）、"
11650 IF HCFRG=0 THEN AS="ノー" ELSE AS=""
11660 PS=PS+AS+"ハードコピー（2で切替）、その他の処理（3）"
11670 NK=3:MC=5:GOSUB *DSPIN
11680 ON ANSN GOTO *MAINLOOP,*MIDEXIT3,*MIDLOOPSUB
11690 IF TESTFRG<>1 THEN *MAINEXIT
11700 GOTO *MIDEXIT2
11710 *MIDEXIT3:HCFRG=(HCFRG+1) MOD 2:GOTO *MIDEXIT2
11720 '
11730     *MIDLOOPSUB
11740     PS="１ﾌﾟﾘﾝﾄ、２ｾｰﾌﾞ、３再表示、４表示ﾓｰﾄﾞ変更"
11750     NK=6:MC=5:GOSUB *DSPIN
11760     ON ANSN GOSUB
*PRNDATA,*SVRESULT,*MDLP3,*MLP4,*PRNPARA,*PRNSEM
11770     GOTO *MIDEXIT2
11780 '
11790 '----- run stop
11800 '
11810 *MAINEXIT
11820 IF TRNSFRG THEN TRNSMODE%=3:GOSUB *TRNSDATA:GOSUB
*CPEFFECT
11830 MC=7:PS="データのセーブ　中":GOSUB *DSPM
11840 GOSUB *SVRESULT
11850 IF TRNSFRG THEN *PSTOP
11860 MC=7:PS="データのプリント中":GOSUB *DSPM
11870 GOSUB *PRNDATA
11880 '
11890 '+++++ selection
11900 '
11910 *PSTOP
11920 GOSUB *DSPTITLE:MC=7:PS="終　了":GOSUB *DSPST
11930 PS="メニューへ（0）、新しいｒｕｎへ（1）、ハードコピー(2)、
停止へ戻る（3）"
11940 MC=7:GOSUB *DSPM
11950 *PSTOP2:ANSS=INKEY$:IF ANSS="" THEN LOCATE
70,0:PRINT TIME$;:GOTO *PSTOP2
11960 IF ANSS="3" THEN *MIDEXIT
11970 IF ANSS="2" THEN GOSUB *CL3:GOSUB *PRNHCOPY:GOTO
*PSTOP
11980 IF ANSS="1" THEN CONSOLE 0,25:GOSUB *CL0:GOTO *INIT
11990 IF ANSS=CHR$(&H1B) THEN FLNM1S="escdata":GOSUB
*SVCONT1:STOP ON:STOP
12000 IF ANSS<>"0" THEN BEEP:GOTO *PSTOP2
12010 '
12020 CONSOLE 0,24,1:COLOR 7
12030 VIEW (0,0)-(639,399):WINDOW (0,0)-(639,399):GOSUB
*CL0
12040 STOP OFF
12050 CLOSE
12060 *ERNEND:RUN "MENU.BAS"
12070 END
12080 '
12090 '##### subroutine series #####
12100 '
12110 '===== menu
12120 '
12130 '----- selection
12140 '
12150 *SELMENU
12160 PS="ＣＰＵ１台モード（0）／データ転送モード（1）"
12170 MC=5:NK=1:GOSUB *DSPIN
12180 TRNSFRG=ANSN
12190 GOSUB *DSPMENU
12200 MFLNMS=FLMENU$(ANSN):TITLES=NMMENU$(ANSN)
12210 RNMODE=MMENU(ANSN):NSVDATA=NSVDATA(ANSN)
12220 PS="通常モード（0）／微分データ同時表示モード（1）"
12230 MC=5:NK=1:GOSUB *DSPIN
12240 IF ANSN THEN RNMODE=RNMODE+1024:DSPMD%=2
12250 A%=RNMODE:GOSUB *FRGMAKE
12260 RETURN
12270 '
12280 '----- menu display
12290 '
12300 *DSPMENU
12310 GOSUB *DSPINIT
12320 RESTORE *MENUDATA
12330 READ NMENU
12340 FOR I=1 TO NMENU
12350     READ
CLMENU(I),CMNT$,FLMENU$(I),NMMENU$(I),MMENU(I),NSVDATA(I)
12360     COLOR CLMENU(I):LOCATE 0,I*2+1:PRINT I,CMNT$
12370 NEXT I
12380 PS="作業内容を選択して下さい":MC=5:NK=NMENU:GOSUB
*DSPIN
12390 IF ANSN=0 THEN *ERNEND
12400 IF CLMENU(ANSN)=1 THEN *DSPMENU
12410 RETURN
12420 '
12430 *MENUDATA
12440 DATA 9
12450 DATA 6,"ＬｉｆｅＴｉｍｅ測定",lifcntr,LifeTime,16,0
12460 DATA 3,"２ＡＰ実行",2apcntr,2AP mode,2,0
12470 DATA 3,"４ＡＰ実行",4apcntrt,4AP(8/8),6,15
12480 DATA 3,"８ＡＰ実行",8apcntr,8AP mode,8,3
12490 DATA 4,"４ＡＰ実行(rf on 8/rf
off8)",4apcntrd,4AP(8/8),2054,0
12500 DATA 3,"８ＡＰ(count 2,2 Back Ground
4)",8apcntrt,8AP(224),72,15
12510 DATA 7,"８ＡＰ(count 1,2-Back Ground
3)",8apcntrb,8AP(12-3),136,11
12520 DATA 3,"２ＡＰ(RFon+RFoff)",2apcntrb,RFon/off,66,15
12530 DATA 7,"２ＡＰ(RFon+RFoff-BG)",2apcntrb,doubleRF(-
BG),130,1
12540 '
12550 'RNMODE=ROBFRG+AP2FRG*2+AP4FRG*4+AP8FRG*8
12560
'RNMODE=RNMODE+LIFFRG*16+RF7FRG*32+PTSFRG*64+BGYFRG*128
12570
'RNMODE=RNMODE+DEXFRG*256+DAAFRG*512+cpdudfrg*1024+ps1frg*
2048
12580 '
12590 '----- parameters
12600 '
12610 *MLP1
12620 PS="何分間隔で途中経過を表示しますか（1－60）"
12630 MC=5:GOSUB *DSPM:INPUT ANS$
12640 ANSN=VAL(ANS$)
12650 IF ANSN>0 AND ANSN<60 THEN LPMIN=ANSN  ELSE
BEEP:GOTO *MLP1
12660 PS="表示何回毎に途中経過をプリントしますか（0：NO．n：
回数）"
12670 NK=9:MC=5:GOSUB *DSPIN
12680 MAXN3=ANSN
12690 RETURN
12700 '
12710 *MLP2
12720 MC=5:PS="コメントを入れて下さい":GOSUB *DSPM
12730 L1=23:C1=24:AS=RNCMNT$:GOSUB *DSPSIN:RNCMNT$=AS
12740 A=INSTR(AS,CHR$(&H22)):IF A THEN RNCMNT$=LEFT$(AS,A-
```

```
1):GOTO *MLP2
12750 RETURN
12760 '
12770 *MLP4
12780 PS="表示モードの選択（0：通常／1：上下／2：左右／3：二
画面）"
12790 NK=3:MC=5:GOSUB *DSPIN
12800 DSPMD%=ANSN
12810 IF ANSN<1 OR ANSN>2 THEN *MLP41
12820 PS="オートスケール　個別（0）／同一（1）"
12830 NK=1:MC=5:GOSUB *DSPIN
12840 DSPSCFRG=ANSN
12850 *MLP41
12860 IF ANSN>0 AND ANSN<3 THEN RETURN
12870 PS="表示チャンネルの選択（0：1、2CH／1：3、4CH）"
12880 NK=1:MC=5:GOSUB *DSPIN
12890 DSPCH%=ANSN
12900 RETURN
12910 '
12920 *MLP5
12930 PS="ハードコピーモードの選択（0：OFF／1：ON）"
12940 NK=1:MC=5:GOSUB *DSPIN
12950 HCFRG=ANSN
12960 RETURN
12970 '
12980 *MLP6
12990 PS="SINGLE LOOP モードの選択（0：OFF／1：ON）"
13000 NK=1:MC=5:GOSUB *DSPIN
13010 LPONEFRG%=ANSN
13020 RETURN
13030 '
13040 *MLP3
13050 PS="データエリアをクリアします宜しいですか（ｙｅｓ：0，ｎ
ｏ：1）"
13060 NK=1:MC=5:GOSUB *DSPIN
13070 IF ANSN=0 THEN GOSUB *DATNEW
13080 RETURN
13090 '
13100 *MLP7
13110 PS="ｏｎ　ｒｅｓｏｎａｎｃｅ点の指定（0：ｍａｘｉｍｕｍ）
"
13120 MC=5:GOSUB *DSPM:INPUT ANS$:ANSN=VAL(ANS$)
13130 IF ANSN>0 AND ANSN<NRF% THEN SP1=ANSN  ELSE
BEEP:GOTO *MLP7
13140 PS="ｏｆｆ　ｒｅｓｏｎａｎｃｅ点の指定（0：ｏｆｆ周波数の
点）"
13150 MC=5:GOSUB *DSPM:INPUT ANS$:ANSN=VAL(ANS$)
13160 IF ANSN>0 AND ANSN<NRF% THEN SP2=ANSN  ELSE
BEEP:GOTO *MLP7
13170 RETURN
13180 '
13190 '----- redisplay
13200 '
13210 *MDLP3
13220 GOSUB *CPEFFECT:GOSUB *DSPCLT:GOSUB *DSPCONT:GOSUB
*DSPEFFECT:RETURN
13230 '
13240 '----- display temprary data and save
13250 '
13260 *RCONT
13270 GOSUB *SVCONT:GOSUB *CPEFFECT:GOSUB *DSPCONT
13280 IF LPN3>=MAXN3 AND MAXN3<>0 THEN GOSUB
*PRNDATA:LPN3=0
13290 RETURN
13300 '
13310 '===== key input
13320 '
13330 *IKEY
13340 ANS$=INKEY$
13350 LOCATE 70,0:PRINT TIME$;
13360 IF ANS$="" THEN *IKEY
13370 IF ANS$=CHR$(&H1B) THEN BEEP 0:GOTO *PSTOP
13380 IF ANS$<"0" OR ANS$>CHR$(&H30+NK) THEN BEEP:GOTO
*IKEY
13390 ANSN=VAL(ANS$)
13400 LOCATE 70,0:PRINT SPACE$(9);
13410 RETURN
13420 '
13430 '===== initialize
13440 '
13450 '----- GPIB
13460 '
13470 *INITGP:RETURN
13480 '
13490 *GPTRG:RETURN
13500 '
13510 *GPLCL:RETURN
13520 '
13530 *CHECKFREQ
13540 GOSUB *INITGP:GOSUB *GPTRG:GOSUB
*GPLCL:GS=MID$(GS,10,CKL)
13550 IF CHECKRFS<>GS AND (EFRG% AND 6)=0 THEN
EFRG%=EFRG%+&H10
13560 RETURN
13570 '
13580 *INITGPE
13590 '
13600 '===== assembla load
13610 '
13620 *LDMPRG
13630 DEF SEG=MSEG
13640 IF LBLFRG THEN BS="lbl\" ELSE BS="vdg\"
13650 BLOAD SYDRIVES+BS+MFLNMS+".m"
13660 *LDMPRG2
13670 DEF SEG=MSEG2
13680 BLOAD SYDRIVES+"hcbasic.bin"
13690 RETURN
13700 '
13710 '===== data output
13720 '
13730 *TRNSDATA
13740 PS="モニタプログラムが未準備です。確認してください"
13750 MC=2:NK=1:BEEP 1:GOSUB *DSPM
13760 WRITE #2,"START"
13770 BEEP 0:GOSUB *CLJ:FOR I=0 TO 600:NEXT I
13780 IF LOC(2)>1 THEN *TRNSDATA1
13790 PS="モニタプログラムが未準備です。確認後" 0" を押してくだ
さい"
13800 MC=2:NK=1:BEEP 1:GOSUB *DSPIN
13810 IF LOC(2)>1 THEN AS=INPUT$(LOC(2),#2)
13820 BEEP 0:GOTO *TRNSDATA
13830 *TRNSDATA1
13840 INPUT #2,AS
13850 IF AS<>"OK" THEN *TRNSERROR
13860 WRITE #2,TRNSMODE%
13870 ON TRNSMODE% GOSUB *TRNS1,*TRNS2,*TRNS3
13880 WRITE #2,"ENT"
13890 INPUT #2,AS
13900 IF AS<>"END" THEN *TRNSERROR
13910 BEEP 0
13920 RETURN
13930 '
13940 *TRNSERROR
13950 RETURN
13960 '
13970 *TRNS1
13980 GOSUB *SEND1:GOSUB *SEND2
13990 RETURN
14000 '
14010 *TRNS2
14020 GOSUB *SEND2
14030 RETURN
14040 '
14050 *TRNS3
14060 RETURN
14070 '
14080 *SEND1
14090 WRITE #2,RNMODE,NRF%,NSVDATA,NCH,MAXN3
14100 FOR I=0 TO 15
14110    WRITE #2,TWAIT%(I),PARA(I)
14120 NEXT I
14130 FOR I=1 TO NRF%
14140    WRITE
#2,RFDATA%(0,I),RFDATA%(1,I),RFDATA%(2,I),RFDATA%(3,I),RFD
ATA%(4,I),RFDATA%(5,I),RFDATA%(6,I),RFDATA%(7,I)
14150 NEXT I
14160 WRITE #2,LPN3,DSPMD%,DSPCH%,HCFRG,SP1,SP2,DSPSCFRG
14170 WRITE #2,TITLES,RNMS
14180 WRITE #2,RNCMNT$
14190 RETURN
14200 '
14210 *SEND2
14220 WRITE #2,EFRG%,TTTURN#
14230 WRITE #2,TDATA$
14240 FOR I=0 TO 15
```



```
14250    WRITE #2,SEM%(0,I),SEM%(1,I)
14260 NEXT I
14270 FOR L=0 TO NCH-1
14280    FOR I=1 TO NRF%
14290       FOR J=0 TO NSVDATA
14300          WRITE
#2,U%(0,J,I,L),U%(1,J,I,L),D%(0,J,I,L),D%(1,J,I,L)
14310       NEXT J
14320    NEXT I
14330 NEXT L
14340 RETURN
14350 '
14360 '===== save
14370 '
14380 '----- faile check
14390 '
14400 *FILECHECK
14410 ANSN=0:OPEN FLNMS FOR INPUT AS #1
14420 PS="すでに同じランＮＯ．があります。続行しますか（Ｙ：0／
Ｎ：1）"
14430 CLOSE #1:BEEP 1:NK=1:MC=6:GOSUB *DSPIN:BEEP 0
14440 CS="変更する"
14450 *FILECHECK2:CLOSE #1
14460 RETURN
14470 '
14480 '----- check disk space
14490 '
14500 *DISKCHECK
14510 MC=2:GOSUB *DISKCHECK1
14520 RETURN
14530 *DISKCHECK1:IF DSKF(DTDRIVE$)<10000 THEN GOSUB
*TRAP32
14540 RETURN
14550 *DISKCHECK2:IF DSKF(DTDRIVE)<10 THEN GOSUB *TRAP32
14560 RETURN
14570 '
14580 '----- temporary results
14590 '
14600 *SVCONT
14610 EL=0:GOSUB *DISKCHECK
14620 T$=TIME$:GOSUB *PRDTMAKE1
14630
FLNM1$=RNMS+"."+CHR$(65+VAL(MID$(T$,1,2)))+MID$(T$,4,2)
14640 *SVCONT1
14650 FLNMS=DTDRIVES+"\TMP\"+FLNM1$
14660 *ERNSVC:OPEN FLNMS FOR OUTPUT AS #1
14670 FOR I=0 TO 15
14680    WRITE #1,I,TWAIT%(I),PARA(I)
14690 NEXT I
14700 FOR I=0 TO 15
14710    WRITE #1,I,SEM%(0,I),SEM%(1,I)
14720 NEXT I
14730 '
14740 FOR I=1 TO NRF%
14750    WRITE
#1,RFDATA%(0,I),RFDATA%(1,I),RFDATA%(2,I),RFDATA%(3,I),RFD
ATA%(4,I),RFDATA%(5,I),RFDATA%(6,I),RFDATA%(7,I)
14760    FOR J=0 TO NSVDATA
14770    WRITE
#1,U%(0,J,I,0),U%(1,J,I,0),D%(0,J,I,0),D%(1,J,I,0),U%(0,J,
I,1),U%(1,J,I,1),D%(0,J,I,1),D%(1,J,I,1)
14780    NEXT J
14790 NEXT I
14800 WRITE #1,RNCMNT$
14810 CLOSE #1
14820 RETURN
14830 '
14840 '----- final results
14850 '
14860 *SVRESULT
14870 EL=1:GOSUB *DISKCHECK
14880 AS=DTDRIVES+"\RESULT\":BS=".DAT":FLNMS=AS+RNMS+BS
14890 GOSUB *FILECHECK
14900 ON ANSN GOSUB *INPFILE
14910 *ERNSVR1:OPEN FLNMS FOR OUTPUT AS #1:WRITE #1,NRF%
14920 FOR K=0 TO NCH
14930    AS="ch"+STR$(K)+"  Freq(Hz)  U/D  (error)  Effect
(error)"
14940    FOR I=1 TO NRF%
14950    *ERNSVR11:WRITE #1,RNCMNT$:WRITE #1,A$
14960    WRITE
#1,NU#(I),UD(I,K),ER(I,K),EFFECT(I,K),EFFERR(I,K)
14970    IF AP8FRG THEN WRITE #1,"R1 R2 R3 R4":WRITE
#1,RSEC(0,I,K),RERSEC(0,I,K),RSEC(1,I,K),RERSEC(1,I,K),RSE
C(2,I,K),RERSEC(2,I,K),RSEC(3,I,K),RERSEC(3,I,K)
14980    NEXT I
14990 NEXT K
15000 *ERNSVR12:CLOSE #1
15010 FLNMS=DTDRIVES+"\asc\"+"A"+RIGHT$(RNMS,LEN(RNMS)-
1)+".DAT"
15020 *ERNSVR2:OPEN FLNMS FOR OUTPUT AS #1:WRITE
#1,NRF%,NSVDATA,NCH
15030 FOR K=0 TO NCH
15040    FOR I=1 TO NRF%
15050       FOR J=0 TO NSVDATA
15060          *ERNSVR21:WRITE
#1,NU#(I),UP#(J,I,K),DW#(J,I,K)
15070       NEXT J
15080    NEXT I
15090 NEXT K
15100 *ERNSVR22:WRITE #1,RNCMNT$:FOR I=0 TO 31:WRITE
#1,PARA(I):NEXT
15110 FOR I=0 TO 15:WRITE #1,SEM%(0,I),SEM%(1,I):NEXT
15120 CLOSE #1
15130 RETURN
15140 '
15150 '===== load
15160 '
15170 '----- continuous from temporary data
15180 '
15190 *LDOLD
15200 GOSUB *CLJ:AS=DTDRIVES+"\TMP\"+RNMS+".*":GOSUB
*DSPFILE
15210 AS=LEFT$(AS,LEN(AS)-1):BS="":CS="継続する実験データの
":GOSUB *INPFILE
15220 *ERNLDOLD:OPEN FLNMS FOR INPUT AS #1
15230 FOR I=0 TO 15
15240    INPUT #1,I,TWAIT%(I),PARA(I)
15250 NEXT I
15260 P=(RNMODE-PARA(15))+(NSVDATA-PARA(14))*4096:MC=2
15270 IF P THEN CLOSE:PS="Ｒｕｎモードが異なり継続できません！
":BEEP:GOSUB *DSPM:GOTO *LDDATA
15280 FOR I=0 TO 15
15290    INPUT #1,I,SEM%(0,I),SEM%(1,I)
15300 NEXT I
15310 '
15320 FOR I=1 TO PARA(0)
15330    INPUT
#1,RFDATA%(0,I),RFDATA%(1,I),RFDATA%(2,I),RFDATA%(3,I),RFD
ATA%(4,I),RFDATA%(5,I),RFDATA%(6,I),RFDATA%(7,I)
15340    FOR J=0 TO NSVDATA
15350    INPUT
#1,U%(0,J,I,0),U%(1,J,I,0),D%(0,J,I,0),D%(1,J,I,0),U%(0,J,
I,1),U%(1,J,I,1),D%(0,J,I,1),D%(1,J,I,1)
15360    NEXT J
15370 NEXT I
15380 INPUT #1,RNCMNT$
15390 CLOSE #1
15400 GOSUB *NUDTMAKE
15410 RNMS=LEFT$(RNMS,8):LOCATE 50,0:PRINT RNMS
15420 RETURN
15430 '
15440 '----- continuous of parameters
15450 '
15460 *LDCNT
15470 IF NRF%=0 THEN RETURN *LDDATA
15480 FLNMS=DTDRIVES+"\RESULT\"+RNMS+".dat"
15490 GOSUB *FILECHECK
15500 ON ANSN GOTO *LDDATA
15510 GOSUB *DATNEW
15520 RETURN
15530 '
15540 '----- read parameter file
15550 '
15560 *LDNEW
15570 FLNMS=DTDRIVES+"\RESULT\"+RNMS+".dat"
15580 GOSUB *FILECHECK
15590 ON ANSN GOTO *LDDATA
15600 '
15610 *LDNEW1
15620 TTTURN#=0
15630 IF LIFFRG<>0 THEN FS="\WTLF\" ELSE FS="\WAIT\"
15640 GOSUB *CLJ:AS=PRDRIVES+FS+"*.DAT":GOSUB *DSPFILE
15650 AS=LEFT$(AS,LEN(AS)-5):BS=".DAT"
15660 CS="タイムシークエンスデータの":GOSUB *INPFILE
15670 *ERNLDNEW1:OPEN FLNMS FOR INPUT AS #1
```

```
15680 INPUT #1,N
15690 FOR I=1 TO N
15700     INPUT #1,X,Y,Z
15710     TWAIT%(X)=Y
15720     IF X=0 THEN BMTIME=Z
15730     IF X=1 THEN RFTIME=Z
15740     IF X=2 THEN CTTIME=Z
15750     IF X=3 THEN BMCLTIME=Z
15760     IF X=4 THEN RFCUTTIME=Z
15770     IF X=5 THEN CTTIME2=Z
15780     IF X=6 THEN CTTIME3=Z
15790 NEXT I
15800 INPUT #1,TMCMNTS
15810 CLOSE #1
15820 '
15830 *LDNEW2
15840 IF LIFFRG<>0 THEN FS="LF" ELSE FS="RF"
15850 GOSUB *CLJ:AS=PRDRIVES+"\"+FS+"\*.DAT":GOSUB
*DSPFILE
15860 AS=LEFT$(AS,LEN(AS)-5):BS=".DAT"
15870 CS="マッピングする "+FS+" データの":GOSUB *INPFILE
15880 *ERNLDNEW2:OPEN FLNMS FOR INPUT AS #1
15890 INPUT #1,N
15900     NRF%=N
15910 FOR I=1 TO N
15920     INPUT #1,X,Y#,Z#
15930     IF X=0 THEN GOSUB *LDNEW4 ELSE GOSUB *LDNEW3
15940 NEXT I
15950 INPUT #1,RNCMNTS
15960 CLOSE #1
15970 '
15980 PS="しばらく御待ち下さい":MC=5:GOSUB *DSPM
15990 RNCMNTS=TMCMNTS+RNCMNTS
16000 IF LIFFRG<>0 THEN FOR I=1 TO
CTURN:NU#(I)=CTTIME*I:NEXT I:NRF%=CTURN
16010 GOSUB *RFDTMAKE
16020 GOSUB *DATNEW
16030 RETURN
16040 '
16050 *LDNEW3
16060 NU#(X)=Y#
16070 RFDA%(0,X)=INT(Z#/10000):RFDA%(1,X)=Z#-
RFDA%(0,X)*10000
16080 RETURN
16090 '
16100 *LDNEW4
16110 NRF%=NRF%-1
16120 IF Y#=0# THEN OFRF=Z#
16130 IF Y#=1# THEN MDRF=Z#
16140 IF Y#=2# THEN SFTRF=Z#
16150 IF Y#=3# THEN CTURN=Z#
16160 RETURN
16170 '
16180 '----- making of parameter data
16190 '
16200 '----- calculation of one cycle time
16210 '
16220 *PARAMAKE1
16230
A=BMTIME+BMCLTIME+(AP8FRG*2+AP4FRG+1)*(RFTIME+RFCUTTIME)
16240
B=(A+CTTIME+AP8FRG*CTTIME2+BGYFRG*CTTIME3)*(1+AP8FRG)
16250 IF PSLFRG THEN CYCTIME=B*2 ELSE CYCTIME=B*NRF%
16260 IF LIFFRG THEN CYCTIME=B+CTTIME*NRF%
16270 CYCTIME=CYCTIME/1000
16280 IF LIFFRG=0 AND LBLFRG<>0 THEN
CYCTIME=(AP8FRG+1)*BMCYC*NRF%
16290 IF LIFFRG<>0 AND LBLFRG<>0 THEN CYCTIME=BMCYC
16300 RETURN
16310 '
16320 '----- making of file name
16330 '
16340 *PARAMAKE2
16350 IF CPDUDFRG THEN TITLES=TITLES+"(dUD_mode)"
16360 IF TRNSFRG THEN TITLES=TITLES+"(trs_mode)"
16370 TITLES=LEFT$(TITLES,28)
16380 PRTITLES=TITLES
16390 RETURN
16400 '
16410 '----- calculation of loop number
16420 '
16430 *LPPRMAKE
16440 MAXN=(LPMIN*60-BSTIME)/CYCTIME
16450 L#=LPMIN*60:C#=CYCTIME:LPTURN#=L#/C#:IF LPTURN#<1
THEN LPTURN#=1
16460 IF LPTURN#>32767 THEN
MAXN2=INT(LPTURN#/32767):MAXN%=LPTURN#-MAXN2*32767 ELSE
MAXN2=0:MAXN%=INT(LPTURN#)
16470 LPTURN#=MAXN2*32767#+MAXN%
16480 RETURN
16490 '
16500 '----- making of flags on experimental mode
16510 '
16520 *FRGMAKE
16530 IF A% AND &H800 THEN PSLFRG=1 ELSE PSLFRG=0
16540 IF A% AND &H400 THEN CPDUDFRG=1 ELSE CPDUDFRG=0
16550 IF A% AND &H200 THEN DAAFRG=1 ELSE DAAFRG=0
16560 IF A% AND &H100 THEN DEXFRG=1 ELSE DEXFRG=0
16570 IF A% AND &H80  THEN BGYFRG=1 ELSE BGYFRG=0
16580 IF A% AND &H40  THEN PTSFRG=1 ELSE PTSFRG=0
16590 IF A% AND &H20  THEN RF7FRG=1 ELSE RF7FRG=0
16600 IF A% AND &H10  THEN LIFFRG=1 ELSE LIFFRG=0
16610 IF A% AND &H8   THEN AP8FRG=1 ELSE AP8FRG=0
16620 IF A% AND &H4   THEN AP4FRG=1 ELSE AP4FRG=0
16630 IF A% AND &H2   THEN AP2FRG=1 ELSE AP2FRG=0
16640 IF A% AND &H1   THEN ROBFRG=1 ELSE ROBFRG=0
16650 RETURN
16660 '
16670 '----- making of rf data and parameters
16680 '
16690 *RFDTMAKE
16700 FOR I=1 TO NRF%
16710     GOSUB *BTODATA:GOSUB *TRODATA
16720 NEXT I
16730 *PRDTMAKE
16740
PARA(0)=NRF%:PARA(1)=BMTIME:PARA(2)=RFTIME:PARA(3)=CTTIME:
PARA(4)=OFRF
16750
PARA(5)=MDRF:PARA(6)=SFTRF:PARA(7)=CYCTIME:PARA(8)=RFCUTTI
ME
16760 PARA(9)=CTTIME2:PARA(10)=CTTIME3:PARA(11)=BMCLTIME
16770 PARA(14)=NSVDATA:PARA(15)=RNMODE
16780 *PRDTMAKE1
16790 IF TTTURN#>32767 THEN PARA(13)=INT(TTTURN#/32767)
ELSE PARA(13)=0
16800 PARA(12)=TTTURN#-PARA(13)*32767#
16810 RETURN
16820 '
16830 *BTODATA
16840 RFDATA%(0,I)=I
16850 RFDATA%(1,I)=RFDA%(0,I)
16860 RFDATA%(2,I)=RFDA%(1,I)
16870 AS=MID$(AS,2,L)
16880
RFGP$(I)="?A"+CHR$(&H24)+"FR"+STR$(NU#(I)/1E+06)+"MH"+CHR$
(&HD)+CHR$(&HA)
16890 A%=VARPTR(RFGP$(I),0):B%=VARPTR(RFGP$(I),1):DEF
SEG=B%
16900
'RFDATA%(3,I)=VAL("&H"+HEX$(PEEK(A%+3))+HEX$(PEEK(A%+2)))
16910 A=VAL("&H"+HEX$(PEEK(A%+2))+HEX$(PEEK(A%+1)))
16920 IF A>32767 THEN RFDATA%(3,I)=A-65536! ELSE
RFDATA%(3,I)=A
16930 A=VAL("&H"+HEX$(PEEK(A%+4))+HEX$(PEEK(A%+3)))
16940 IF A>32767 THEN RFDATA%(4,I)=A-65536! ELSE
RFDATA%(4,I)=A
16950 RFDATA%(5,I)=PEEK(A%)
16960 'IF PEEK(A%+1)<>0 THEN RFDATA%(4,I)=SEGPTR(5) ELSE
RFDATA%(4,I)=B%
16970 RFDATA%(7,I)=INT(NU#(I)/32768!):RFDATA%(6,I)=NU#(I)-
RFDATA%(7,I)*32768!
16980 RETURN
16990 '
17000 *TRODATA
17010 AS=STR$(NU#(I))
17020 L=LEN(AS)-1
17030 AS=MID$(AS,2,L)
17040 L=9-LEN(AS)
17050 BS=STRING$(L,"0")+AS
17060 FOR J=0 TO 7
17070     RFDATA%(J+8,I)=VAL(MID$(BS,J+1,1))
17080 NEXT J
17090 RETURN
17100 '
17110 *NUDTMAKE
```



```
17120 TTTURN#=32767#*PARA(13)+PARA(12)
17130 *NUDTMAKE1
17140
NRF%=PARA(0):BMTIME=PARA(1):RFTIME=PARA(2):CTTIME=PARA(3):
OFRF=PARA(4)
17150
MDRF=PARA(5):SFTRF=PARA(6):CYCTIME=PARA(7):RFCUTTIME=PARA(
8)
17160 CTTIME2=PARA(9):CTTIME3=PARA(10):BMCLTIME=PARA(11)
17170 FOR I=1 TO NRF%
17180     GOSUB *BTDATA:GOSUB *TRODATA
17190 NEXT I
17200 RETURN
17210 '
17220 *BTDATA
17230 NU#(I)=RFDATA%(7,I)*32768!+RFDATA%(6,I)
17240 RETURN
17250 '
17260 *TRDATA
17270 NU#(I)=0
17280 FOR J=8 TO 15
17290 NU#(I)=NU#(I)+RFDATA%(J,I)*10#^(8-J)
17300 NEXT J
17310 RETURN
17320 '
17330 '----- making of rf check data
17340 '
17350 *CKRFMAKE
17360 CKL=LEN(STR$(NU#(NRF%)))-2
17370 A#=NU#(NRF%)*1E+16
17380 BS=STR$(A#)
17390 CHECKRFS=MID$(BS,2,CKL)
17400 RETURN
17410 '
17420 '----- initialize of rf data
17430 '
17440 *DATNEW
17450 FOR I=0 TO NCH+CPDUDFRG
17460   FOR J=0 TO NRF%
17470     FOR K=0 TO NSVDATA
17480       U%(0,K,J,I)=0:D%(0,K,J,I)=0
17490       U%(1,K,J,I)=0:D%(1,K,J,I)=0
17500     NEXT K
17510   NEXT J
17520 NEXT I
17530 TTTURN#=0:SEM#=0:FOR I=0 TO
15:SEM%(0,I)=0:SEM%(1,I)=0:NEXT I
17540 RETURN
17550 '
17560 '----- file name
17570 '
17580 *RNMMAKE
17590 DS=DATE$
17600 BS=STR$(VAL(MID$(DS,2,1))-
5)+HEX$(VAL(MID$(DS,4,2)))+MID$(DS,7,2)
17610 IF RNMS<>"" THEN CS=STR$(VAL(MID$(RNMS,6,3))+1) ELSE
CS="000"
17620 CS=RIGHT$("00"+RIGHT$(CS,LEN(C$)-1),3)
17630 RNMS="S"+MID$(BS,2,4)+CS
17640 RETURN
17650 '
17660 '----- input file name
17670 '
17680 *INPFILE
17690 PS=CS+"ファイル名を入力してください ("+BS+") "
17700 MC=5:GOSUB *DSPM:COLOR 4:INPUT ANS$
17710 IF ANS$="P" OR ANS$="p" THEN GOSUB *PRFILE:GOTO
*INPFILE
17720 FLNMS=AS+ANS$+BS
17730 RETURN
17740 '
17750 '----- display
17760 '
17770 '----- display effects
17780 '
17790 *DSPEFFECT
17800 IF LIFFRG<>0 THEN GOSUB *DSPEFFECTL ELSE GOSUB
*DSPEFFECTP
17810
TTTIME=TTTURN#*CYCTIME:TTMIN=INT(TTTIME/60):TTSEC=INT(TTTI
ME-TTMIN*60)
17820 LOCATE 0,2:COLOR 5:PRINT TDATA$+"
("+STR$(TTMIN)+"'"+STR$(TTSEC)+"'') ";
17830 A=SEM#:B=TTTURN#:PRINT "Loop="+STR$(B)+"
SEM="+STR$(A)+" ";
17840 PRINT CHR$(&H22)+LEFT$(RNCMNTS,40)+CHR$(&H22);
17850 RETURN
17860 '
17870 *DSPEFFECTP
17880 LOCATE 10,19+K:COLOR EFFCL(K)
17890 EFFMSGS=AKCNV$(STR$(EFFECTM(K)))+" ±
"+AKCNV$(STR$(EFFERRM(K)))+"% "
17900 PRINT "effect ("+STR$(P1)+"/"+STR$(P2)+")
="+EFFMSGS+SPACE$(10);
17910 RETURN
17920 '
17930 *DSPEFFECTL
17940 LOCATE 10,18+K:COLOR 4+K
17950 EFFMSGS=AKCNV$(STR$(TTUP#(K)))+" ／
"+AKCNV$(STR$(TTDW#(K)))+"count"
17960 PRINT "total UP/DOWN"+EFFMSGS+SPACE$(10);
17970 RETURN
17980 '
17990 '----- display parameters
18000 '
18010 *DSPSET
18020 GOSUB *DSPSET1:GOSUB *DSPSET2
18030 RETURN
18040 '
18050 *DSPSET1
18060 LOCATE 0,4:COLOR 4:PRINT"パラメータ設定";
18070 LOCATE 0,16:COLOR 4:PRINT"ビームタイム";:COLOR
6:PRINT BMTIME;:COLOR 4:PRINT"（ｍｓｅｃ）";
18080 LOCATE 0,17:COLOR 4:PRINT"ビームクール";:COLOR
6:PRINT BMCLTIME
18090     RT=RFTIME+BMTIME*ROBFRG
18100 IF LIFFRG=0 THEN LOCATE 0,17:COLOR 4:PRINT"ＲＦ　タイ
ム";:COLOR 6:PRINT RT;
18110     IF AP4FRG=1 THEN COLOR 4:PRINT"　×　2"
18120     IF AP8FRG=1 THEN COLOR 4:PRINT"　×　3"
18130 IF LIFFRG=0 THEN LOCATE 0,18:COLOR 4:PRINT"ＲＦCUTタ
イム";:COLOR 6:PRINT RFCUTTIME;
18140 LOCATE 0,20:COLOR 4:PRINT"カウント　　";:COLOR
6:PRINT CTTIME
18150 IF AP8FRG<>0 THEN LOCATE 10,19:COLOR 4:PRINT"前
";:COLOR 6:PRINT CTTIME2;
18160 IF BGYFRG<>0 THEN LOCATE 10,21:COLOR 4:PRINT"後
";:COLOR 6:PRINT CTTIME3;
18170 IF LIFFRG<>0 THEN PS="タイム　マップ（ｓｅｃ）" ELSE
PS="ＲＦ　　マップ（ｋＨｚ）　"
18180 LOCATE 0,7:COLOR 4:PRINT PS;
18190 LOCATE 40,7:COLOR 4:PRINT "点数　";:COLOR 6:PRINT
NRF%
18200 RETURN
18210 '
18220 *DSPSET2
18230 FOR I=1 TO NRF%
18240     X(I)=(NU#(I)+SFTRF)/10
18250     OFX=OFRF/10
18260     MDX=MDRF/10
18270 NEXT I
18280 N=NRF%
18290 IF OFX=0 THEN OFX=1E+08
18300 VIEW (0,160)-(639,240)
18310 GOSUB *CPWX
18320 WY1=30:WY2=215:MDY=150:DMDY=5:TY=90:BY=210
18330 WINDOW (WX1,-WY2)-(WX2,-WY1)
18340 LINE (TX,-MDY)-(O1X,-MDY),1:LINE (O2X,-MDY)-(BX,-
MDY),5
18350 DSPOFFRG=(AP2FRG OR ROBFRG OR AP4FRG OR AP8FRG)
18360 IF LIFFRG<>0 THEN XAXIS$="sec" ELSE XAXIS$="kHz"
18370 GOSUB *DSPXAXIS
18380 OFN=0:DMDY2=DMDY*5
18390 FOR I=1 TO NRF%
18400     IF X(I)>=OFX THEN GOSUB *DSPSET23 ELSE GOSUB
*DSPSET22
18410     DMDY2=DMDY2*-1
18420 NEXT I
18430 IF DSPOFFRG=1 THEN GOSUB *DSPSET24
18440 RETURN
18450 '
18460 *DSPSET22
18470 LINE (X(I)+MDX,-MDY+DMDY*5+DMDY2)-(X(I)-MDX,-MDY-
DMDY*5+DMDY2),2,B
```

```
18480 LINE (X(I),-MDY+DMDY*.6+DMDY2)-(X(I),-MDY-
DMDY*.6+DMDY2),6,B
18490 RETURN
18500 '
18510 *DSPSET23
18520 LINE (OX,-MDY+DMDY*5+DMDY2)-(OX,-MDY-
DMDY*5+DMDY2),6:OFN=OFN+1
18530 RETURN
18540 '
18550 *DSPSET24
18560 LOCATE 55,7:COLOR 4:PRINT " (内ｏｆｆ";
18570 COLOR 6:PRINT STR$(OFN);:COLOR 4:PRINT ") "
18580 RETURN
18590 '
18600 '----- display temporary data
18610 '
18620 *DSPCONT
18630 VIEW (0,32)-(639,367)
18640 N=NRF%
18650 IF DSPMD%=0 THEN T=0 ELSE T=1
18660 DSPSC2FRG=(DSPSCFRG AND T)
18670 C1=DSPCH%:IF CPDUDFRG THEN C2=2 ELSE C2=(DSPCH%+1)
MOD NCH
18680 IF DSPSC2FRG THEN GOSUB *DSPCONTSUB2
18690 FOR IK=0 TO T
18700    K=(IK+DSPCH%) MOD NCH
18710    IF IK AND DSPDUDFRG THEN K=NCH
18720    GOSUB *DSPCONTSUB:GOSUB *DSPEFFECT
18730 NEXT IK
18740 DSPSTMD%=DSPMD%
18750 RETURN
18760 '
18770 *DSPCONTSUB
18780 FOR I=1 TO N
18790    X(I)=(NU#(I)+SFTRF)/10
18800    OFX=OFRF/10
18810    MDX=MDRF/10
18820    Y(I)=UD(I,K)
18830    Z(I)=ER(I,K)
18840    ZC(I)=ERC(I,K)
18850    IF LIFFRG<>0 THEN IF ERC(I,K)=0 THEN ZC(I)=7-K
ELSE ZC(I)=3
18860 NEXT I
18870 P1=P1(K):P2=P2(K):DSP0FRG=AP8FRG
18880 DSPOFFRG=(AP2FRG OR ROBFRG OR AP4FRG)
18890 IF OFX=0 THEN OFX=1E+08
18900 IF LIFFRG<>0 THEN XAXIS$="sec" ELSE XAXIS$="kHz"
18910 IF AP8FRG<>0 THEN YAXIS$="(8AP)" ELSE YAXIS$="(U/D)"
18920 IF LIFFRG<>0 THEN YAXIS$="count"
18930 IF LIFFRG<>0 THEN DSPLOGFRG=1:SCAT2FRG=1 ELSE
DSPLOGFRG=0:SCAT2FRG=0
18940 GOSUB *DSPMODE:GOSUB *CL5
18950 GOSUB *CPWX
18960 IF DSPSC2FRG=0 THEN GOSUB *CPWY
18970 IF LIFFRG<>0 THEN IDY=1
18980 GOSUB *DSPPACK
18990 RETURN
19000 '
19010 *DSPCONTSUB2
19020 FOR I=1 TO N
19030    Y(I)=UD(I,C1)
19040    Z(I)=ER(I,C1)
19050 NEXT I
19060 FOR I=1 TO N
19070    Y(I+N)=UD(I,C2)
19080    Z(I+N)=ER(I,C2)
19090 NEXT I
19100 DSP0FRG=AP8FRG
19110 N=2*N:GOSUB *CPWY:N=N/2
19120 IF LIFFRG<>0 THEN IDY=1
19130 RETURN
19140 '
19150 '===== display messeges
19160 '
19170 '----- initialize of screen
19180 '
19190 *DSPINIT
19200 COLOR 7 :WIDTH 80,25
19210 SCREEN 3,0,0,1
19220 VIEW (0,32)-(639,367)
19230 CONSOLE 23,2,0,1
19240 GOSUB *CL5
19250 RETURN
19260 '
19270 '----- change scroll
19280 '
19290 *DSPCLT
19300 CONSOLE 2,21:CLS 1:CONSOLE 23,2
19310 RETURN
19320 '
19330 '-----
19340 '
19350 *DSPCLTG
19360 CONSOLE 2,21:GOSUB *CL0:CONSOLE 23,2
19370 RETURN
19380 '
19390 '----- display waiting
19400 '
19410 *DSPWAITMES
19420 GOSUB *DSPCLTG:COLOR MC:LOCATE 28,11:PRINT "しばらく
御待ち下さい";
19430 RETURN
19440 '
19450 '----- display file name
19460 '
19470 *DSPTITLE
19480 GOSUB *CL2:COLOR 5:LOCATE 0,0:PRINT TITLE$;
19490 LOCATE 40,0:PRINT "実験名=";:COLOR 6:LOCATE
50,0:PRINT RNM$;:COLOR 7
19500 RETURN
19510 '
19520 '----- display message
19530 '
19540 *DSPM
19550 GOSUB *CL3:LOCATE 0,23:COLOR MC:PRINT P$;
19560 RETURN
19570 '
19580 '----- display conditions
19590 '
19600 *DSPST
19610 LOCATE 0,1:COLOR MC:PRINT P$+STRING$(73,61);
19620 RETURN
19630 '
19640 '----- display questions
19650 '
19660 *DSPIN
19670 GOSUB *DSPM:GOSUB *IKEY:GOSUB *CL3:COLOR 7
19680 RETURN
19690 '
19700 '-----
19710 '
19720 *DSPSIN
19730 LOCATE C1,L1:COLOR 6:PRINT A$
19740 LOCATE C1-2,L1:COLOR 5:INPUT B$
19750 IF B$<>"" THEN A$=B$
19760 RETURN
19770 '
19780 '----- display time
19790 '
19800 *DSPTM
19810 LOCATE 0,2:COLOR 5:PRINT P$+TIME$+"
"+CHR$(&H22)+RNCMNT$+CHR$(&H22);
19820 RETURN
19830 '
19840 '===== graph package
19850 '
19860 '----- display file name
19870 '
19880 *DSPFILE
19890 GOSUB *DSPCLT:LOCATE 0,2:COLOR 4:FILES A$:COLOR 7
19900 RETURN
19910 '
19920 '----- erase texts and graphics
19930 '
19940 *CL0:GOSUB *CL4:GOSUB *CL5:RETURN
19950 '
19960 '----- erase upper text
19970 '
19980 *CL2:LSCROLL=2:LOCATE 0, 0:PRINT SPACE$(LSCROLL*80-
1);:RETURN
19990 '
20000 '----- erase lower text
20010 '
20020 *CL3:LSCROLL=2:LOCATE 0,23:PRINT SPACE$(LSCROLL*80-
1);:RETURN
20030 '
```



```
20040 '----- erase all text
20050 '
20060 *CL4:CLS 1:GOSUB *CL2:GOSUB *CL3:RETURN
20070 '
20080 '----- erase graphics
20090 '
20100 *CL5:CLS 2:RETURN
20110 '
20120 '----- character reverse
20130 '
20140 *DSPREVS
20150 IF DSPREV% THEN RETURN ELSE DEF SEG=&HA200:DSPREV%=1
20160 A=LS*160:FOR I=A TO A+156 STEP 2:B=PEEK(I)+2:POKE
I,B:NEXT I
20170 RETURN
20180 '
20190 '----- cancel reverse
20200 '
20210 *DSPNOMR
20220 IF DSPREV% THEN DEF SEG=&HA200:DSPREV%=0 ELSE
DSPREV%=0
20230 A=LS*160:FOR I=A TO A+156 STEP 2:B=PEEK(I)-2:POKE
I,B:NEXT I
20240 RETURN
20250 '
20260 '----- display characters
20270 '
20280 *GRACHR
20290 LL=LEN(SS$):SXX=MAP(XXX,0):SYY=MAP(YYY,1)
20300 FOR I=1 TO LL
20310    CC$=(MID$(SS$,I,1))
20320    PUT@ (SXX+8*(I-1),SYY),KANJI(ASC(CC$)),PSET,COL,0
20330 NEXT I
20340 RETURN
20350 '
20360 '----- set display mode
20370 '
20380 *DSPMODE
20390 ON DSPMD% GOTO
*DSPMODE1,*DSPMODE2,*DSPMODE3,*DSPMODE4
20400 *DSPMODE0
20410 VIEW (0,48)-(639,367)
20420 RETURN
20430 *DSPMODE1
20440 IF K THEN VIEW (0,200)-(639,367) ELSE VIEW (0,48)-
(639,199)
20450 RETURN
20460 *DSPMODE2
20470 IF K THEN VIEW (320,48)-(639,367) ELSE VIEW (0,48)-
(319,367)
20480 RETURN
20490 *DSPMODE3
20500 A=(K+DSPCH%) MOD 2
20510 IF A THEN SCREEN 3,0,1,17
20520 VIEW (0,48)-(639,367)
20530 RETURN
20540 *DSPMODE4
20550 VIEW (0,0)-(639,399)
20560 RETURN
20570 '
20580 '----- calculation of x-axis
20590 '
20600 *CPWX
20610 WINDOW(0,0)-(1,1):WDXSZ=MAP(1,0)
20620 MAXX=0:MINX=3E+08
20630 FOR I=1 TO N
20640    IF MAXX<X(I) AND X(I)<OFX THEN MAXX=X(I)
20650    IF MINX>X(I) THEN MINX=X(I)
20660 NEXT I
20670 MAXX=MAXX+MDX:MINX=MINX-MDX
20680 DX=MAXX-MINX
20690 IF DX=0 THEN DX=1:MINX=MINX-.5:MAXX=MAXX+.5
20700 TX=MINX-DX*.1:BX=MAXX+DX*.15:DMDX=DX*.02
20710 OX=BX-DX*.05:O1X=BX-DX*.13:O2X=BX-DX*.08
20720 WX2=BX+DX*.05:WX1=(WDXSZ*(TX-DMDX)-8*6*WX2)/(WDXSZ-
8*6)
20730 D=DX*1000:GOSUB
*CPDIV:DX=D/1000:IDX=ID/1000:IDX2=ID2/1000
20740 RETURN
20750 '
20760 '----- calculation of y-axis
20770 '
20780 *CPWY
20790 WINDOW(0,0)-(1,1):WDYSZ=MAP(1,1)
20800 MAXY=0:MINY=1E+08
20810 IF SCAT2FRG THEN GOSUB *CPWY2 ELSE GOSUB *CPWY1
20820 IF DSP0FRG AND MAXY<0 THEN MAXY=0
20830 IF DSP0FRG AND MINY>0 THEN MINY=0
20840 DY=MAXY-MINY
20850 IF DY=0 THEN DY=1:MINY=MINY-.5:MAXY=MAXY+.5
20860 TY=MINY-DY*.1:BY=MAXY+DY*.1:DMDY=DY*.05
20870 WY2=BY+DY*.05:WY1=(-WY2*16+(TY-DMDY)*WDYSZ)/(WDYSZ-
16)
20880 D=DY*100:GOSUB
*CPDIV:DY=D/100:IDY=ID/100:IDY2=ID2/100
20890 RETURN
20900 '
20910 *CPWY1
20920 FOR I=1 TO N
20930    IF MAXY<Y(I)+Z(I) THEN MAXY=Y(I)+Z(I)
20940    IF MINY>Y(I)-Z(I) THEN MINY=Y(I)-Z(I)
20950 NEXT I
20960 RETURN
20970 '
20980 *CPWY2
20990 FOR I=1 TO N
21000    IF MAXY<Y(I) THEN MAXY=Y(I)
21010    IF MINY>Y(I) THEN MINY=Y(I)
21020    IF MAXY<Z(I) THEN MAXY=Z(I)
21030    IF MINY>Z(I) THEN MINY=Z(I)
21040 NEXT I
21050 RETURN
21060 '
21070 '----- calculation of ticks
21080 '
21090 *CPDIV
21100 C=0
21110 FOR I=1 TO 10
21120    IF INT(D/10^(C+1))<>0 THEN C=C+1
21130 NEXT I
21140 A=INT(D/10^C)
21150 IF A>=2 AND A<4 THEN ID=5*10^(C-1):ID2=1*10^(C-1)
21160 IF A>=4 AND A<8 THEN ID=1*10^C:ID2=.2*10^C
21170 IF A>=8 THEN ID=2*10^C:ID2=.5*10^C
21180 IF A<2 THEN ID=2*10^(C-1):ID2=.5*10^(C-1)
21190 RETURN
21200 '
21210 '----- display graph
21220 '
21230 *DSPPACK
21240 WINDOW (0,0)-(1,1):WDXSZ=MAP(1,0):WDYSZ=MAP(1,1)
21250 WINDOW (WX1,-WY2)-(WX2,-WY1)
21260 XXX=WX1:YYY=-WY2:SS$=YAXIS$:COL=7:GOSUB *GRACHR
21270 XXX=MAP(WDXSZ-3*8,2):YYY=MAP(WDYSZ-
16*1,3):SS$=XAXIS$:COL=7:GOSUB *GRACHR
21280 LINE (TX,-TY)-(BX,-BY),4,B
21290 IF DSP0FRG THEN LINE (TX,-0)-(BX,-0),3
21300 GOSUB *DSPXAXIS
21310 GOSUB *DSPYAXIS
21320 GOSUB *DSPSCAT
21330 RETURN
21340 '
21350 '---- display x-axis
21360 '
21370 *DSPXAXIS
21380 T=INT(320/WDXSZ)
21390 ITX=INT(TX/IDX)*IDX+IDX:IBX=INT(01X/IDX)*IDX
21400 IF IBX=ITX THEN IBX=ITX+IDX
21410 T0=-TY:T1=-TY+DMDY:T2=-TY+DMDY*.5
21420 B0=-BY:B1=-BY-DMDY:B2=-BY-DMDY*.5
21430 ITX2=ITX-IDX
21440 IF ITX2<0 THEN ITX2=0
21450 GOSUB *DSPXSUBAXIS
21460 FOR IX=ITX TO IBX STEP IDX
21470    LINE (IX,T0)-(IX,T1),4:LINE (IX,B0)-(IX,B1),4
21480    IF T<>1 THEN ISMB=IX/100:GOSUB *DSPXSMBAXIS
21490    T=T*-1
21500    ITX2=IX
21510       GOSUB *DSPXSUBAXIS
21520 NEXT IX
21530 IF DSPOFFRG THEN GOSUB *DSPOFF
21540 RETURN
21550 '
21560 *DSPXSUBAXIS
21570 FOR IX2=ITX2 TO ITX2+IDX STEP IDX2
21580    IF IX2<TX OR IX2>01X THEN C=0 ELSE C=4
```

```
21590     LINE (IX2,T0)-(IX2,T2),C:LINE (IX2,B0)-(IX2,B2),C
21600 NEXT IX2
21610 RETURN
21620 '
21630 *DSPXSMBAXIS
21640 AS=STR$(ISMB):L=LEN(A$)-1
21650 IF L>6 THEN L=6
21660 XXX=IX-DX*.033:YYY=-
TY+DMDY:SS$=MID$(A$,2,L):COL=7:GOSUB *GRACHR
21670 RETURN
21680 '
21690 *DSPOFF
21700 LINE (O1X,T0)-(O2X,T0),0:LINE (O1X,B0)-(O2X,B0),0
21710 A$=STR$(OFX/100):L=LEN(A$)-1
21720 XXX=O1X-50:YYY=-TY+DMDY:SS$=MID$(A$,2,L):COL=5:GOSUB
*GRACHR
21730 LINE (OX,T0)-(OX,T1),4:LINE (OX,B0)-(OX,B1),4
21740 RETURN
21750 '
21760 '---- display y-axis
21770 '
21780 *DSPYAXIS
21790 T=INT(184/WDYSZ)
21800 ITY=INT(TY/IDY)*IDY+IDY:IBY=INT(BY/IDY)*IDY
21810 IF IBY=ITY THEN IBY=ITY+IDY
21820 T1=TX-DMDX:T2=TX-DMDX*.5:B1=BX+DMDX:B2=BX+DMDX*.5
21830 ITY2=ITY-1
21840 IF DSPLOGFRG THEN GOSUB *DSPYSUBAXISL ELSE GOSUB
*DSPYSUBAXIS
21850 FOR IY=ITY TO IBY STEP IDY
21860    LINE (T1,-IY)-(TX,-IY),4:LINE (B1,-IY)-(BX,-IY),4
21870    IF T<>1 THEN ISMB=IY:GOSUB *DSPYSMBAXIS
21880    T=T*-1
21890    ITY2=IY
21900       IF DSPLOGFRG THEN GOSUB *DSPYSUBAXISL ELSE
GOSUB *DSPYSUBAXIS
21910 NEXT IY
21920 RETURN
21930 '
21940 *DSPYSUBAXIS
21950 FOR IY2=ITY2 TO ITY2+IDY STEP IDY2
21960    IY3=IY2
21970    IF IY3<TY OR IY3>BY THEN *DSPYSUBAXIS2
21980    LINE (T2,-IY3)-(TX,-IY3),4:LINE (B2,-IY3)-(BX,-
IY3),4
21990 *DSPYSUBAXIS2:NEXT IY2
22000 RETURN
22010 '
22020 *DSPYSUBAXISL
22030 FOR IY2=10^ITY2 TO 10^(ITY2+IDY) STEP 10^ITY2
22040    IY3=LOG(IY2)/LOG(10)
22050    IF IY3<TY OR IY3>BY THEN *DSPYSUBAXISL2
22060    LINE (T2,-IY3)-(TX,-IY3),4:LINE (B2,-IY3)-(BX,-
IY3),4
22070 *DSPYSUBAXISL2:NEXT IY2
22080 RETURN
22090 '
22100 *DSPYSMBAXIS
22110 IF DSPLOGFRG THEN BS="10^":NL=3 ELSE BS="":NL=6
22120 A$=STR$(ISMB):L=LEN(A$)-1:XXX=WX1:YYY=-IY-DMDY*.5
22130 IF INSTR(A$,"E-") THEN A$=" 0.0":L=3
22140 IF L>NL THEN L=NL
22150 IF -YYY>WY1 AND -YYY<WY2 THEN
SS$=BS+MID$(A$,2,L):COL=7:GOSUB *GRACHR
22160 RETURN
22170 '
22180 '---- SCAT
22190 '
22200 *DSPSCAT
22210 DMX=DX*.004:DMY=DY*.01:DOFX=.2
22220 IF SCAT2FRG THEN GOSUB *DSPSCATON2 ELSE GOSUB
*DSPSCATON1
22230 IF LIFFRG=0 THEN GOSUB *DSPCALPOINT
22240 RETURN
22250 '
22260 *DSPCALPOINT
22270 IF P1 THEN LINE (X(P1)+DMX,-Y(P1)-DMY)-(X(P1)-DMX,-
Y(P1)+DMY),2,BF
22280 IF P2 THEN LINE (X(P2)+DMX,-Y(P2)-DMY)-(X(P2)-DMX,-
Y(P2)+DMY),5,B
22290 RETURN
22300 '
22310 *DSPSCATON1
22320 FOR I=1 TO N
22330    IF X(I)>=OFX THEN GOSUB *DSPSCATOFF:GOTO
*DSPSCATON11
22340    LINE (X(I)+MDX,-Y(I))-(X(I)-MDX,-Y(I)),ZC(I)
22350    LINE (X(I),-Y(I)-Z(I))-(X(I),-Y(I)+Z(I)),ZC(I)
22360    LINE (X(I)+DMX,-Y(I)-DMY)-(X(I)-DMX,-
Y(I)+DMY),ZC(I)
22370    LINE (X(I)+DMX,-Y(I)+DMY)-(X(I)-DMX,-Y(I)-
DMY),ZC(I)
22380 *DSPSCATON11
22390 NEXT I
22400 RETURN
22410 '
22420 *DSPSCATON2
22430 FOR I=1 TO N
22440    IF X(I)>=OFX THEN GOSUB *DSPSCATOFF:GOTO
*DSPSCATON21
22450    LINE (X(I)+DMX,-Z(I))-(X(I)-DMX,-Z(I)),ZC(I)-2
22460    LINE (X(I),-Z(I)-DMY)-(X(I),-Z(I)+DMY),ZC(I)-2
22470    LINE (X(I)+DMX,-Y(I)-DMY)-(X(I)-DMX,-
Y(I)+DMY),ZC(I)
22480    LINE (X(I)+DMX,-Y(I)+DMY)-(X(I)-DMX,-Y(I)-
DMY),ZC(I)
22490 *DSPSCATON21
22500 NEXT I
22510 RETURN
22520 '
22530 *DSPSCATOFF
22540 A3=O2X+IDX2*DOFX
22550 LINE (A3,-Y(I)-Z(I))-(A3,-Y(I)+Z(I)),4
22560 A1=A3-MDX:IF A1<O2X THEN A1=O2X-DMX
22570 A2=A3+MDX:IF A2>BX THEN A2=BX
22580 A4=A3+DMX:A5=A3-DMX
22590 LINE (A1,-Y(I))-(A2,-Y(I)),4
22600 IF P2=0 THEN C=5 ELSE C=7
22610 LINE (A4,-Y(I)+DMY)-(A5,-Y(I)-DMY),C
22620 LINE (A4,-Y(I)-DMY)-(A5,-Y(I)+DMY),C
22630 DOFX=DOFX+.4
22640 RETURN
22650 '
22660 '===== printer output
22670 '
22680 *PRNDATA
22690
TTTIME=TTTURN#*CYCTIME:TTMIN=INT(TTTIME/60):TTSEC=INT(TTTI
ME-TTMIN*60)
22700 IF HCFRG THEN GOSUB *PRNHCOPY
22710 IF NCH=2 THEN A=2 ELSE A=0
22720 IF CPDUDFRG THEN A=NCH
22730 A=LIFFRG*A
22740 FOR KC=0 TO A
22750    GOSUB *PRNLIST
22760 NEXT KC
22770 RETURN
22780 '
22790 *PRNHCOPY
22800 I=-1:GOSUB *PRNTITLE
22810 DEF SEG=MSEG2:IF HCFRG=2 THEN A=3 ELSE A=6
22820 CALL A
22830 'GOSUB *FF
22840 RETURN
22850 '
22860 *PRNLIST
22870 IF AP8FRG THEN N=2 ELSE N=40 \ (NSVDATA+1)
22880 PAGEE=(NRF%-1) \ N
22890 FOR I=0 TO PAGEE
22900    GOSUB *PRNTITLE
22910    IF LIFFRG THEN GOSUB *PRNTITLEL ELSE GOSUB
*PRNTITLEP
22920    IF I=PAGEE THEN MAXJ=NRF%-I*N ELSE MAXJ=N
22930    FOR J=1 TO MAXJ
22940       K=I*N+J
22950       NUR#=NU#(K)+SFTRF
22960       IF LIFFRG THEN GOSUB *PRNDATAL ELSE GOSUB
*PRNDATAP
22970       IF (J MOD 5)=0 THEN LPRINT
22980    NEXT J
22990 GOSUB *FF:NEXT I
23000 RETURN
23010 '
23020 *PRNTITLE
23030 LPRINT PRTITLE$,RNM$,DDATA$+" "+TDATA$+"
page"+STR$(PAGEE*KC+I+1):LPRINT
```



```
23040 LPRINT "set"+STR$(KC)+"
"+CHR$(&H22)+RNCMNT$+CHR$(&H22):LPRINT
23050 LPRINT USING "COUNT  ### 点  ";NRF%;
23060 LPRINT USING "total time = #### 分 ## 秒
";TTMIN,TTSEC;
23070 LPRINT "SEM = ",SEM#:LPRINT
23080 P2S="total count UP(ch##)=####### /
DOWN(ch##)=#######"
23090 LPRINT USING P2$;1,TTUP#(0),2,TTDW#(0)
23100 LPRINT USING P2$;3,TTUP#(1),4,TTDW#(1)
23110 RETURN
23120 '
23130 *PRNTITLEL
23140 P1S=" T(ms)     UP1      DOWN1      UP2      DOWN2
UP1-2   DOWN1-2"
23150 P2S="###### ######## ######## ######## ########
######## ########"
23160 LPRINT:LPRINT:LPRINT P1S:LPRINT
23170 RETURN
23180 '
23190 *PRNDATAL
23200 LPRINT USING
P2S;NUR#,UP#(0,K,0),DW#(0,K,0),UP#(0,K,1),DW#(0,K,1),UP#(0
,K,2),DW#(0,K,2)
23210 RETURN
23220 '
23230 *PRNTITLEP
23240 P2S="effect(on###/off###)=+###.####(###.####)%
mod.Freq. +- #########Hz"
23250 LPRINT USING
P2S;P1(KC),P2(KC),EFFECTM(KC),EFFERRM(KC),MDRF
23260 P1S="Freq.(Hz)    UP       DOWN       U/D      error
EFFECT    error"
23270 P2S="######## ######## ######## ######## +###.####(###.####)
+###.####(###.####)"
23280 LPRINT:LPRINT P1$:LPRINT
23290 RETURN
23300 '
23310 *PRNDATAP
23320 IF NSVDATA THEN GOSUB *PRNDATA1 ELSE GOSUB *PRNDATA0
23330 RETURN
23340 '
23350 *PRNDATA0
23360 L=0:LPRINT USING
P2S;NUR#,UP#(L,K,KC),DW#(L,K,KC),UD(K,KC),ER(K,KC),EFFECT(
K,KC),EFFERR(K,KC)
23370 RETURN
23380 '
23390 *PRNDATA1
23400 P2S="######## ######## ######## +###.####(###.####)"
23410 LPRINT USING
P2S;NUR#,UP#(0,K,KC),DW#(0,K,KC),R(0,K,KC),RER(0,K,KC)
23420 FOR L=1 TO NSVDATA
23430    LPRINT USING
P2S;L+1,UP#(L,K,KC),DW#(L,K,KC),R(L,K,KC),RER(L,K,KC)
23440 NEXT L
23450 P2S="                                    +###.####(###.####)
+###.####(###.####)"
23460 LPRINT USING
P2S;UD(K,KC),ER(K,KC),EFFECT(K,KC),EFFERR(K,KC)
23470 IF AP8FRG THEN *PRN8AP
23480 RETURN
23490 '
23500 *PRN8AP
23510 LPRINT "       ------------------------------------
-"
23520 P2S="    "                Rsec# =
###.####(###.####)"
23530 FOR M=0 TO 3
23540    LPRINT USING P2S;M+1,RSEC(M,K,KC),RERSEC(M,K,KC)
23550 NEXT M
23560 LPRINT
23570 P2S="    "       (Rsec#/Rsec#)-1 =
+###.####(###.####)%"
23580 M=0:N=1:GOSUB *PRN8AP2
23590 M=3:N=2:GOSUB *PRN8AP2
23600 M=0:N=2:GOSUB *PRN8AP2
23610 M=3:N=1:GOSUB *PRN8AP2
23620 P2S="    "                    8AP =
+###.####(###.####)%"
23630 LPRINT USING P2S;UD(K,KC),ER(K,KC)
23640 LPRINT "       ------------------------------------
-"
23650 RETURN
23660 '
23670 *PRN8AP2
23680 R=RSEC(M,K,KC)/RSEC(N,K,KC)
23690
E=R*SQR((RERSEC(M,K,KC)/RSEC(M,K,KC))^2+(RERSEC(N,K,KC)/RS
EC(N,K,KC))^2)
23700 LPRINT USING P2S;M+1,N+1,(R-1)*100,E*100
23710 RETURN
23720 '
23730 '----- beam current
23740 '
23750 *PRNSEM
23760 LPRINT PRTITLE$,RNM$,DATE$+" "+TIME$:LPRINT
23770 LPRINT CHR$(&H22)+RNCMNT$+CHR$(&H22):LPRINT
23780 LPRINT "--------- SEM CHECK ---------"
23790 LPRINT "     order     low      high"
23800 P2S="    10^##    ######   ######"
23810 FOR I=0 TO 15
23820    IF LBLFRG THEN A=I-2 ELSE A=I
23830    LPRINT USING P2S;A,SEM%(0,I),SEM%(1,I)
23840 NEXT I
23850 GOSUB *FF
23860 RETURN
23870 '
23880 '----- parameter values
23890 '
23900 *PRNPARA
23910 LPRINT PRTITLE$,RNM$,DATE$+" "+TIME$:LPRINT
23920 LPRINT CHR$(&H22)+RNCMNT$+CHR$(&H22):LPRINT
23930 LPRINT "--------- PARAMETER CHECK ---------"
23940 LPRINT "     No.     PARA      TWAIT%"
23950 P2S="    ##    ########   ######"
23960 FOR I=0 TO 31
23970    LPRINT USING P2S;I,PARA(I),TWAIT%(I)
23980 NEXT I
23990 GOSUB *FF
24000 RETURN
24010 '
24020 '----- form feed
24030 '
24040 *FF
24050 AS="LPT1:"
24060 OPEN AS FOR OUTPUT AS #1
24070 PRINT #1,CHR$(&HC);
24080 CLOSE #1
24090 RETURN
24100 '
24110 *PRNEND
24120 '
24130 '===== calculation of effects
24140 '
24150 *CPEFFECT
24160 IF TRNSFRG=0 THEN IF CPDUDFRG THEN GOSUB *CPDUDUD
ELSE IF NCH>1 THEN GOSUB *CPSUBUD
24170 FOR K=0 TO NCH-TRNSFRG
24180    TTUP#(K)=0:TTDW#(K)=0
24190    A=LIFFRG+AP2FRG*2+AP8FRG*3
24200    ON A GOSUB *CPEFFECTL,*CPEFFECT2AP,*CPEFFECT8AP
24210 NEXT K
24220 GOSUB *CPSEM
24230 RETURN
24240 '
24250 *CPEFFECTL
24260 FOR J=1 TO NRF%
24270    L=0
24280    ERC(J,K)=0
24290       GOSUB *CPUD
24300    IF A THEN UD(J,K)=LOG(UP#(0,J,K))/LOG(10) ELSE
UD(J,K)=0
24310    R(0,J,K)=UD(J,K)
24320    IF B THEN ER(J,K)=LOG(DW#(0,J,K))/LOG(10) ELSE
ER(J,K)=0
24330    RER(0,J,K)=ER(J,K)
24340 NEXT J
24350 RETURN
24360 '
24370 *CPEFFECT2AP
24380 UDOFF=0:EROFF=0:NUD=0:MAXEFF=0:UDOFF2=0:EROFF2=0
24390 CPMODE=PTSFRG+BGYFRG*2+1
24400 FOR J=NRF% TO 1 STEP -1
24410    FOR L=0 TO NSVDATA
24420       GOSUB *CPUD
```

```
24430     NEXT L
24440     RERSUM=0
24450        ON CPMODE GOSUB *CPRSEC0,*CPRSEC2,*CPRSEC4
24460        L=0:GOSUB *CPRSEC
24470     UD(J,K)=RSEC(0,J,K)
24480     ER(J,K)=UD(J,K)*SQR(RERSUM)
24490     IF (NU#(J)+SFTRF)>=OFRF THEN GOSUB *CPUDOFF
24500     IF NUD=0 THEN GOSUB *CPUDOFF2
24510 NEXT J
24520 IF NUD=0 THEN UDOFF=UDOFF2:EROFF=EROFF2
24530 UDOFF=UDOFF/EROFF:EROFF=1/SQR(EROFF)
24540 FOR J=1 TO NRF%
24550     IF (NU#(J)+SFTRF)>=OFRF THEN ERC(J,K)=7:GOTO
*CPEFFECT2APOFF
24560     GOSUB *CPEFFECT2
24570     IF ABS(EFFECT(J,K))>=MAXEFF THEN
MAXEFF=ABS(EFFECT(J,K)):MAXEFFNO=J
24580     *CPEFFECT2APOFF
24590 NEXT J
24600 GOSUB *CPEFFECTM
24610 RETURN
24620 '
24630 *CPEFFECT8AP
24640 UDOFF=0:EROFF=0:NUD=0:MAXEFF=0:UDOFF2=0:EROFF2=0
24650 CPMODE=PTSFRG+BGYFRG*2+1
24660 FOR J=1 TO NRF%
24670     FOR L=0 TO NSVDATA
24680        GOSUB *CPUD
24690     NEXT L
24700     RERSUM=0
24710     ON CPMODE GOSUB *CPRSEC1,*CPRSEC3,*CPRSEC5
24720
UD(J,K)=RSEC(0,J,K)*RSEC(3,J,K)/RSEC(1,J,K)/RSEC(2,J,K)-1
24730     ER(J,K)=(UD(J,K)+1)*SQR(RERSUM)
24740 NEXT J
24750 FOR J=1 TO NRF%
24760     IF (NU#(J)+SFTRF)>=OFRF THEN ERC(J,K)=7:GOTO
*CPEFFECT8APOFF
24770
EFFECT(J,K)=UD(J,K)*100:EFFERR(J,K)=ER(J,K)*100
24780     IF ABS(EFFECT(J,K))>=MAXEFF THEN
MAXEFF=ABS(EFFECT(J,K)):MAXEFFNO=J
24790     S=INT(ABS(EFFECT(J,K)/EFFERR(J,K)))
24800     IF S>2 THEN ERC(J,K)=2 ELSE ERC(J,K)=4+S
24810
*CPEFFECT8APOFF:UD(J,K)=UD(J,K)*100:ER(J,K)=ER(J,K)*100
24820 NEXT J
24830 IF SP1=0 THEN P1(K)=MAXEFFNO ELSE P1(K)=SP1
24840
EFFECTM(K)=UD(P1(K),K):EFFERRM(K)=ER(P1(K),K):EFFCL(K)=ERC
(P1(K),K)
24850 RETURN
24860 '
24870 '----- calculation of beam current in LBL
24880 '
24890 *CPSEM
24900 SEM#=0
24910 IF LBLFRG THEN A=2 ELSE A=0
24920 FOR I=0 TO 15
24930     SEM#=SEM#+(SEM%(1,I)*32768!+SEM%(0,I))*10#^(I-A)
24940 NEXT I
24950 RETURN
24960 '
24970 '----- calculation of counts and ratios
24980 '
24990 *CPUD
25000 UP#(L,J,K)=U%(1,L,J,K)*32768!+U%(0,L,J,K)
25010 DW#(L,J,K)=D%(1,L,J,K)*32768!+D%(0,L,J,K)
25020
TTUP#(K)=TTUP#(K)+UP#(L,J,K):TTDW#(K)=TTDW#(K)+DW#(L,J,K)
25030 IF UP#(L,J,K)<=0 THEN CH=1:UP#(L,J,K)=0:GOSUB
*ERCP:A=0 ELSE A=-1
25040 IF DW#(L,J,K)<=0 THEN CH=2:DW#(L,J,K)=0:GOSUB
*ERCP:B=0 ELSE B=-1
25050 IF A AND B THEN GOSUB *CPR
25060 RETURN
25070 '
25080 *CPR
25090 R(L,J,K)=UP#(L,J,K)/DW#(L,J,K)
25100 RER(L,J,K)=R(L,J,K)*SQR(1!/UP#(L,J,K)+1!/DW#(L,J,K))
25110 RETURN
25120 '
25130 '----- calculation of ratios in each section
25140 '
25150 *CPRSEC
25160 IF UPSEC#<1 OR DWSEC#<1 THEN
UPSEC#=1:DWSEC#=1:ERUPSEC#=1:ERDWSEC#=1
25170 RSEC(L,J,K)=UPSEC#/DWSEC#
25180
RERSEC(L,J,K)=RSEC(L,J,K)*SQR((ERUPSEC#/UPSEC#)^2+(ERDWSEC
#/DWSEC#)^2)
25190
RERSUM=RERSEC(L,J,K)/RSEC(L,J,K)*RERSEC(L,J,K)/RSEC(L,J,K)
+RERSUM
25200 RETURN
25210 '
25220 *CPRSEC0
25230 UPSEC#=UP#(0,J,K):DWSEC#=DW#(0,J,K)
25240 ERUPSEC#=SQR(UPSEC#):ERDWSEC#=SQR(DWSEC#)
25250 RETURN
25260 '
25270 *CPRSEC1
25280 FOR L=0 TO 3
25290     UPSEC#=UP#(L,J,K):DWSEC#=DW#(L,J,K)
25300     ERUPSEC#=SQR(UPSEC#):ERDWSEC#=SQR(DWSEC#)
25310     GOSUB *CPRSEC
25320 NEXT L
25330 RETURN
25340 '
25350 *CPRSEC2
25360 UPSEC#=0:DWSEC#=0
25370 FOR M=0 TO 3
25380
UPSEC#=UP#(L*4+M,J,K)+UPSEC#:DWSEC#=DW#(L*4+M,J,K)+DWSEC#
25390 NEXT M
25400 ERUPSEC#=SQR(UPSEC#):ERDWSEC#=SQR(DWSEC#)
25410 RETURN
25420 '
25430 *CPRSEC3
25440
L=0:UPSEC#=UP#(0,J,K)+UP#(1,J,K):DWSEC#=DW#(0,J,K)+DW#(1,J
,K)
25450 ERUPSEC#=SQR(UPSEC#):ERDWSEC#=SQR(DWSEC#):GOSUB
*CPRSEC
25460
L=1:UPSEC#=UP#(2,J,K)+UP#(3,J,K):DWSEC#=DW#(2,J,K)+DW#(3,J
,K)
25470 ERUPSEC#=SQR(UPSEC#):ERDWSEC#=SQR(DWSEC#):GOSUB
*CPRSEC
25480
L=2:UPSEC#=UP#(8,J,K)+UP#(9,J,K):DWSEC#=DW#(8,J,K)+DW#(9,J
,K)
25490 ERUPSEC#=SQR(UPSEC#):ERDWSEC#=SQR(DWSEC#):GOSUB
*CPRSEC
25500
L=3:UPSEC#=UP#(10,J,K)+UP#(11,J,K):DWSEC#=DW#(10,J,K)+DW#(
11,J,K)
25510 ERUPSEC#=SQR(UPSEC#):ERDWSEC#=SQR(DWSEC#):GOSUB
*CPRSEC
25520 RETURN
25530 '
25540 *CPRSEC4
25550 UPSEC#=UP#(0,J,K)-UP#(1,J,K)*CTTIME/CTTIME3
25560 ERUPSEC#=SQR(UP#(0,J,K)+UP#(1,J,K))
25570 DWSEC#=DW#(0,J,K)-DW#(1,J,K)*CTTIME/CTTIME3
25580 ERDWSEC#=SQR(DW#(0,J,K)+DW#(1,J,K))
25590 RETURN
25600 '
25610 *CPRSEC5
25620 A1=CTTIME2/CTTIME3:A2=CTTIME/CTTIME3
25630
UPB#=UP#(3,J,K)+UP#(4,J,K)+UP#(5,J,K):UPB1#=A1*UPB#:UPB2#=
A2*UPB#
25640
DWB#=DW#(3,J,K)+DW#(4,J,K)+DW#(5,J,K):DWB1#=A1*DWB#:DWB2#=
A2*DWB#
25650 L=0:UPSEC#=UP#(0,J,K)-UPB1#:DWSEC#=DW#(0,J,K)-DWB1#
25660
ERUPSEC#=SQR(UPSEC#+(A1+1)*UPB1#):ERDWSEC#=SQR(DWSEC#+(A1+
1)*DWB1#):GOSUB *CPRSEC
25670 L=1:UPSEC#=UP#(1,J,K)+UP#(2,J,K)-
UPB2#:DWSEC#=DW#(1,J,K)+DW#(2,J,K)-DWB2#
25680
ERUPSEC#=SQR(UPSEC#+(A2+1)*UPB2#):ERDWSEC#=SQR(DWSEC#+(A2+
1)*DWB2#):GOSUB *CPRSEC
25690
```



```
UPB#=UP#(9,J,K)+UP#(10,J,K)+UP#(11,J,K):UPB1#=A1*UPB#:UPB2
#=A2*UPB#
25700
DWB#=DW#(9,J,K)+DW#(10,J,K)+DW#(11,J,K):DWB1#=A1*DWB#:DWB2
#=A2*DWB#
25710 L=2:UPSEC#=UP#(6,J,K)-UPB1#:DWSEC#=DW#(6,J,K)-DWB1#
25720
ERUPSEC#=SQR(UPSEC#+(A1+1)*UPB1#):ERDWSEC#=SQR(DWSEC#+(A1+
1)*DWB1#):GOSUB *CPRSEC
25730 L=3:UPSEC#=UP#(7,J,K)+UP#(8,J,K)-
UPB2#:DWSEC#=DW#(7,J,K)+DW#(8,J,K)-DWB2#
25740
ERUPSEC#=SQR(UPSEC#+(A2+1)*UPB2#):ERDWSEC#=SQR(DWSEC#+(A2+
1)*DWB2#):GOSUB *CPRSEC
25750 RETURN
25760 '
25770 '----- calculaiton of time devided data
25780 '
25790 *CPDUDUD
25800 FOR J=1 TO NRF%
25810     FOR L=0 TO NSVDATA
25820        U%(0,L,J,NCH)=U%(0,L,J,0)-U%(0,L,J,NCH+1)
25830        D%(0,L,J,NCH)=D%(0,L,J,0)-D%(0,L,J,NCH+1)
25840        U%(0,L,J,NCH+1)=U%(0,L,J,0)
25850        D%(0,L,J,NCH+1)=D%(0,L,J,0)
25860        U%(1,L,J,NCH)=U%(1,L,J,0)-U%(1,L,J,NCH+1)
25870        D%(1,L,J,NCH)=D%(1,L,J,0)-D%(1,L,J,NCH+1)
25880        U%(1,L,J,NCH+1)=U%(1,L,J,0)
25890        D%(1,L,J,NCH+1)=D%(1,L,J,0)
25900     NEXT L
25910 NEXT J
25920 RETURN
25930 '
25940 *CPDUDCLR
25950 FOR J=1 TO NRF%
25960     FOR L=0 TO NSVDATA
25970        U%(0,L,J,NCH+1)=0:D%(0,L,J,NCH+1)=0
25980        U%(1,L,J,NCH+1)=0:D%(1,L,J,NCH+1)=0
25990     NEXT L
26000 NEXT J
26010 RETURN
26020 '
26030 '----- calculation of ch1 - ch2
26040 '
26050 *CPSUBUD
26060 FOR J=1 TO NRF%
26070     FOR L=0 TO NSVDATA
26080        U%(0,L,J,NCH)=U%(0,L,J,0)-U%(0,L,J,1)
26090        D%(0,L,J,NCH)=D%(0,L,J,0)-D%(0,L,J,1)
26100        U%(1,L,J,NCH)=U%(1,L,J,0)-U%(1,L,J,1)
26110        D%(1,L,J,NCH)=D%(1,L,J,0)-D%(1,L,J,1)
26120     NEXT L
26130 NEXT J
26140 RETURN
26150 '
26160 '----- calculation of off level
26170 '
26180 *CPUDOFF2
26190 UDOFF2=UDOFF2+UD(J,K)/ER(J,K)/ER(J,K)
26200 EROFF2=EROFF2+1/ER(J,K)/ER(J,K)
26210 RETURN
26220 '
26230 *CPUDOFF
26240 NUD=NUD+1
26250 IF NUD=1 OR NUD=2 THEN A=0 ELSE A=1
26260 UDOFF=UDOFF*A+UD(J,K)/ER(J,K)/ER(J,K)
26270 EROFF=EROFF*A+1/ER(J,K)/ER(J,K)
26280 RETURN
26290 '
26300 '----- calculation of effects
26310 '
26320 *CPEFFECT2
26330 EFFECT(J,K)=(UD(J,K)/UDOFF-1)*100
26340
EFFERR(J,K)=UD(J,K)/UDOFF*SQR((ER(J,K)/UD(J,K))^2+(EROFF/U
DOFF)^2)*100
26350 S=INT(ABS(EFFECT(J,K)/EFFERR(J,K)))
26360 IF S>2 THEN ERC(J,K)=2 ELSE ERC(J,K)=4+S
26370 RETURN
26380 '
26390 '----- maximum effect
26400 '
26410 *CPEFFECTM
26420 IF SP1=0 THEN P1=MAXEFFNO ELSE P1=SP1
26430 IF SP2 THEN UDOFF=UD(P2,K):EROFF=ER(P2,K)
26440 EFFECT=UD(P1,K)/UDOFF-1
26450
EFFERR=UD(P1,K)/UDOFF*SQR((ER(P1,K)/UD(P1,K))^2+(EROFF/UDO
FF)^2)
26460 S=INT(ABS(EFFECT/EFFERR))
26470 IF S>2 THEN EFFCL=2 ELSE EFFCL=4+S
26480
EFFECTM(K)=EFFECT*100:EFFERRM(K)=EFFERR*100:EFFCL(K)=EFFCL
26490 RETURN
26500 '
26510 '----- operation for no counting
26520 '
26530 *ERCP
26540 PS="ｃｈ"+STR$(CH+K*2)+":sec"+STR$(L)
26550 MC=6:PS=PS+"のカウントが行われていません！":GOSUB *DSPM
26560 RETURN
26570 '
26580 '##### error trap
################################################
26590 '
26600 '----- error
26610 '
26620 *DFNERR
26630
NERR(1)=56:NERR(2)=53:NERR(3)=68:NERR(4)=62:NERR(5)=0:NERR
(6)=0
26640 NERR(7)=61:NERR(8)=65:NERR(9)=55
26650 RETURN
26660 '
26670 *TRAP
26680 MC=2:GOSUB *DFNERR
26690 '
26700 *TRAP1
26710 IF ERR<>NERR(1) THEN *TRAP2
26720 PS="ファイル記述に誤りがあります！"
26730 IF ERL=15220 THEN GOSUB *ERWAIT:RESUME *LDDATA
26740 IF ERL=15670 THEN GOSUB *ERWAIT:RESUME *LDDATA
26750 IF ERL=15880 THEN GOSUB *ERWAIT:RESUME *LDDATA
26760 PS=PS+"ＴＭＰ．ＤＡＴに保存しますので中断して下さい"
26770 IF ERL=14660 THEN GOSUB
*ERWAITP:FLNMS=DTDRIVES+"\TMP.DAT":RESUME
26780 IF ERL=14910 THEN GOSUB
*ERWAITP:FLNMS=DTDRIVES+"\TMP.DAT":KILL FLNMS:RESUME
26790 IF ERL=15020 THEN GOSUB
*ERWAITP:FLNMS=DTDRIVES+"\TMP.DAT":KILL FLNMS:RESUME
26800 '
26810 *TRAP2
26820 IF ERR<>NERR(2) THEN *TRAP3
26830 PS="指定したファイルは存在しません！"
26840 IF ERL=15220 THEN GOSUB *ERWAIT:RESUME *LDOLD
26850 IF ERL=15670 THEN GOSUB *ERWAIT:RESUME *LDNEW1
26860 IF ERL=15880 THEN GOSUB *ERWAIT:RESUME *LDNEW1
26870 IF ERL=14410 THEN COLOR 7:RESUME *FILECHECK2
26880 '
26890 *TRAP3
26900 IF ERR<>NERR(3) THEN *TRAP4
26910 PS="ディスクに空き領域がありません。取り替えて下さい！"
26920 IF ERL=>14660 AND ERL=<14800 THEN GOSUB
*ERWAITP:CLOSE #1:RESUME *SVCONT
26930 IF ERL=>14810 THEN GOSUB *ERWAITP:CLOSE #1:RESUME
*SVRESULT
26940 GOTO *TRAP4
26950 *TRAP32
26960 PS="ディスクに空き領域がありません。取り替えて下さい！"
26970 IF EL=0 THEN GOSUB *ERWAITP:CLOSE #1:RETURN *SVCONT
26980 IF EL=1 THEN GOSUB *ERWAITP:CLOSE #1:RETURN
*SVRESULT
26990 '
27000 *TRAP4
27010 IF ERR<>NERR(4) THEN *TRAP5
27020 PS="ディスクが用意されていません！"
27030 IF ERL<>12060 THEN GOSUB *ERWAITP:RESUME
27040 PS="システムディスクが用意されていません！":GOSUB
*ERWAITP:RESUME
27050 '
27060 *TRAP5
27070 IF ERR<>NERR(5) THEN *TRAP6
27080 PS="プリンターが準備されていません！"
27090 IF ERL>=22680 AND ERL<=24110 THEN GOSUB
*ERWAITP:RESUME
```

```
27100 '
27110 *TRAP6
27120 IF ERR<>NERR(6) THEN *TRAP7
27130 PS="ＧＰＩＢが準備されていません！"
27140 IF ERL>=13470 AND ERL<=13580 THEN GOSUB
*ERWAITP:RESUME
27150 '
27160 *TRAP7
27170 IF ERR<>NERR(7) THEN *TRAP8
27180 PS="ディスクが保護されています。解除してください！"
27190 GOSUB *ERWAITP:RESUME
27200 '
27210 *TRAP8
27220 IF ERR<>NERR(8) THEN *TRAP9
27230 IF ERL=14660 THEN KILL FLNMS:COLOR 7:RESUME
27240 IF ERL=14910 OR ERL=15020 THEN GOSUB *CL3:LOCATE
0,23:PRINT"同名のファイルが存在します。削除していいですか？
";:GOSUB *ERINPT:RESUME
27250 '
27260 *TRAP9
27270 IF ERR<>NERR(9) THEN *TRAPEXIT
27280 IF ERL=14510 THEN CLOSE #2:RESUME *RSVEXIT
27290 '
27300 '-----
27310 '
27320 *TRAPEXIT
27330 CONSOLE 0,24,1:PRINT "ERROR ("+STR$(ERR)+") IN
"+STR$(ERL)
27340 BEEP:COLOR 7
27350 END
27360 '
27370 *ERWAITP
27380 GOSUB *DSPM:PRINT
27390 PRINT "用意が出来たら何かキーを押して下さい（ESC：プログラ
ムの中止）";
27400 BEEP 1:KS=INPUT$(1):BEEP 0
27410 IF KS="" THEN 27400 ELSE IF KS=CHR$(&H1B) THEN
*TRAPEXIT
27420 GOSUB *CL3:MC=7:RETURN
27430 '
27440 *ERWAIT
27450 GOSUB *DSPM:BEEP:FOR K=1 TO 5000:NEXT K:MC=7
27460 RETURN
27470 '
27480 *ERWAIT2
27490 MC=6:GOSUB *DSPM:BEEP:FOR K=1 TO 500:NEXT K:MC=7
27500 RETURN
27510 '
27520 *ERINPT
27530 PRINT "（Ｙｅｓ：０，ｎｏ：１）";
27540 BEEP 1:NK=1:GOSUB *IKEY
27550 BEEP 0:ON ANSN GOTO *ERINPT2
27560 KILL FLNMS:MC=7:RETURN
27570 *ERINPT2:PS="ファイル名を指定して下さい":GOSUB *DSPM
27580 INPUT FLNEWNMS:FLNEWNMS=LEFT$(FLNEWNMS,8)
27590 FLNMS=DTDRIVE$+"\result\"+FLNEWNMS+".dat":COLOR
7:RETURN
27600 '
27610 '----- STOP    KEY エラー処理
27620 '
27630 *STTRAP
27640 PS="
27650 BEEP 1:AS=INPUT$(1):BEEP 0
27660 IF AS=CHR$(&HB) THEN STOP OFF ELSE STOP ON
27670 RETURN
27680 '
27690 '----- TEST ROUTINE
27700 '
27710 *TESTSTORE
27720 TWAIT%(0)=&H2
27730 FOR K=0 TO NCH
27740    FOR I=1 TO NRF%
27750       FOR J=0 TO NSVDATA
27760          A#=10*I
27770          U%(1,J,I,K)=INT(A#*(K+J+1)/32768!)
27780          U%(0,J,I,K)=A#*(K+J+1)-U%(1,J,I,K)*32768#
27790          D%(1,J,I,K)=INT(A#*(K+J+5)/32768!)
27800          D%(0,J,I,K)=A#*(K+J+5)-D%(1,J,I,K)*32768#
27810       NEXT J
27820    NEXT I
27830 NEXT K
27840 RETURN
```


LAB1CNTR.ASM

```
;
;       Experimental control program, Initialize routine
;
;        for controller NEC PC9801VX   by  A.Kitagawa
;
;              1991/01/25
if1
        %out     LABCNTR   v.9.00 1.01
endif
if2
        %out path2
endif
;
;-------------------------------------------------------
;
;       Interface port address
;
inport  equ     01ad0h                  ;  I/O port
bmport  equ     01ad4h                  ;
rfport  equ     01ad2h                  ;
ctport  equ     01ad4h                  ;
ptlctr  equ     01ad6h                  ;
rfbitpl equ     01ad8h                  ;
rfbitph equ     01adah                  ;
secport equ     01adch                  ;
pt2ctr  equ     01adeh                  ;
dach1h  equ     01bd0h                  ;  D/A converter
dach1l  equ     01bd2h                  ;
dach2h  equ     01bd4h                  ;
dach2l  equ     01bd6h                  ;
ctch1   equ     01cd0h                  ;  counter board 1
ctch2   equ     01cd8h                  ;
ctch3   equ     01dd0h                  ;  counter board 2
ctch4   equ     01dd8h                  ;
ctch5   equ     01ed0h                  ;  counter board 3
ctch6   equ     01ed8h                  ;
;
;       addressing offset for data
;
adnrf   equ     900h                    ;  address of
number of rf
adrfdt  equ     904h                    ;  initial address
for rf data
adctu1  equ     908h                    ; initial address
for data  U1
adctd1  equ     90ch                    ;
D1
adctu2  equ     910h                    ;  initial address
for data U2
adctd2  equ     914h                    ;
D2
adctsem equ     918h                    ;  initial address
for beam current data
adwtlp  equ     91ch                    ; initial address
for waiting time data
adnlp   equ     920h                    ;  initial address
for number of roop
adwork  equ     924h                    ;  swap address
for data
aderror equ     91ch                    ;  error flag
;
;       parameter transfer
;
nparal  equ     12h                     ;  number of
parameter * 2
npara2  equ     10h                     ;  number of
parameter * 2-2
npara3  equ     24h                     ;  number of
parameter * 4
;
;       addressing offset for WAIT data
;
dummyt  equ     0002h                   ;  dummy time
bmtime1 equ     0004h                   ;  beam on time
(coarse)
bmtime2 equ     0006h                   ;  beam on time
(fine)
afptime equ     0008h                   ;  AFP for
excahnge population
bmcoolt equ     000ah                   ;  beam cooling
time
rftime1 equ     000ch                   ;  rf on time
(coarse)
rftime2 equ     000eh                   ;  rf off time
(fine)
rfkillt equ     0010h                   ;  rf effect kill
time
cttime1 equ     0012h                   ;  count time 1
(coarse)
cttime2 equ     0014h                   ;   count time 1
(fine)
cttime3 equ     0016h                   ;   count time 2
(coarse)
cttime4 equ     0018h                   ;  count time 2
(fine)
cttime5 equ     001ah                   ;   count time 3
(coarse)
cttime6 equ     001ch                   ;  count time 3
(fine)
;
;       addressing offset for rf data
;
bitdt1  equ     0h
        ; Bit data for RF selector
bitdth  equ     1h
dadt1l  equ     2h
        ; DA data
dadt1h  equ     3h
dadt21  equ     4h
dadt2h  equ     5h
;afpdt   equ     4h
        ; ?
;gpdt    equ     6h
dadt31  equ             6h
          ; DA data for 7RF mode's VCO
dadt3h  equ             7h
dadt41  equ             8h
dadt4h  equ             9h
dadt51  equ             0Ah
dadt5h  equ             0Bh
dadt61  equ             0Ch
dadt6h  equ             0Dh
dadt71  equ             0Eh
dadt7h  equ             0Fh
trdt    equ     10h
        ; Bit data for TR-3133B
;
;       number of roops
;
lpwait  equ     063Ch               ;63Ch or 383h  long
wait
lpulse  equ     02h                     ;  for control
pulse
;
;       control signal
;
bmstart equ     00010000b
bmstop  equ     00100000b
;
screset equ     00000001b
clock1  equ     00000010b
ctgate  equ     00000100b
clock2  equ     00001000b
ctgrst  equ     00000101b
ctgcl1  equ     00000110b
ctgcl2  equ     00001100b
workend equ     10000000b
;
rfstart equ     00000001b
rfstop  equ     00000010b
rfon    equ     00000100b
rfoff   equ     10000000b
afpbit  equ     10001000b
sbreset equ     01000000b
rfgate  equ     00000000b
off     equ     00000000b
;
;       counter control bit
;
holdall equ     00111111b
openall equ     11111111b
open1   equ     10111111b
open2   equ     01111111b
;
```

```
;       input bit
;
stopbit equ     00000010b
beamon  equ     00010000b
beamoff equ     00100000b
fton    equ     01000000b
ftoff   equ     00100000b
errfrg  equ     10001111b
;
;-------------------------------------------------
;
code    segment
        assume  cs:code,ds:code
;
;       including of macro part
;
        include lib\iocntr.asm
;
;       program start
;
begin:
;
;       swap of resister
;
        push    ds
        push    es
        push    ax
        push    bx
        push    cx
        push    dx
        push    di
        push    si
        push    bp
;
;      masking of interrupt
;
        mov     dx,02h
        mov     al,7fh
        out     dx,al
        mov     dx,0ah
        mov     al,0efh
        out     dx,al
        mov     dx,1fh
        mov     al,0fh
        out     dx,al
;
;       引数の受け渡し
;
        mov     bp,bx
        mov     di,adnlp
        mov     cx,nparal
loop0:
        mov     bx,ds:[bp]
        mov     ds:[di],bx
        add     di,0002h
        add     bp,0002h
        loop    loop0
;
        mov     bp,adnlp
        les     si,ds:dword ptr [bp]
        mov     cx,es:[si]
;
;      scalar initializing
;
        counter ctch1,holdall
        counter ctch3,holdall
        counter ctch5,holdall
        ctreset ctch1
        ctreset ctch2
        ctreset ctch3
        ctreset ctch4
        ctreset ctch5
        ctreset ctch6
;
;       GP-IB initializing
;
;        gpibini   <----- NOT USE
;        gpibifc
;        gpibren
;
;       large roop (1 sequence)
;
gloop:
;
        push    cx
        mov     bp,adwork
        mov     di,adnrf
        mov     cx,npara2
loop1:
        mov     bx,ds:[bp]
        mov     ds:[di],bx
        add     di,0002h
        add     bp,0002h
        loop    loop1
;
        mov     bp,adnrf
        les     si,ds:dword ptr [bp]
        mov     cx,es:[si]
;
        %out 3
;
;      main rootine
```


LAB2CNTR.ASM

```
;
;       end program
;
        pop     cx
        dec     cx
        ercheck aderror
        jcxz    retn
        jmp     gloop
;
;       flag set in erro or stop (from ercheck macro)
;
erretn:
        mov     bp,adnlp
        les     si,ds:[bp]
        mov     es:[si],cx
;
;       return to BASIC
;
retn:
;        gpibres   <----- NOT USE
;
        bpcntr bmport,bmstop,off,lpulse
;
;       reset of inetrupt masking
;
        mov     dx,02h
        mov     al,01h
        out     dx,al
        mov     dx,0ah
        mov     al,0e7h
        out     dx,al
        mov     dx,1fh
        mov     al,00h
        out     dx,al
;
;       return swaped resister
;
        pop     bp
        pop     si
        pop     di
        pop     dx
        pop     cx
        pop     bx
        pop     ax
        pop     es
        pop     ds
;
retbas  proc    far
        iret
retbas  endp
;
code    ends
;
if2
        %out end
endif
```

IOCNTR.ASM

```
;-------------------------------------------------
;       Macro routine libraries
;
;       for LABCNTR SYSTEM      by  A. Kitagawa
;
;               1991/01/25
;                add rfaddec3 for 4rf or 2rf mode (T.
Ohtsubo 93.6.22)
;
if1
        %out    IOCNTR    v.9.01 1.01
endif
        %out 1
;
;       LBL & VdG System
;
;-------------------------------------------------
;
;       bit control for I/O port
;
;         port    : port address
;         data    : 8bit data
;
bitcntr macro   port,data
        push    dx
        mov     dx,port
        mov     al,data
        out     dx,al
        pop     dx
        endm
;
;-------------------------------------------------
;
;      control pulse : send pulse from I/O port
;
;         adrs    : port address
;         before  : start bit
;         after   : stop bit
;         length  : pulse length (nuber of constant
routine)
;
bpcntr  macro   adrs,before,after,length
        even
        push    dx
        mov     dx,adrs
        mov     al,before
        out     dx,al
        wtloopc length
        mov     al,after
        out     dx,al
        pop     dx
        endm
;
;-------------------------------------------------
;
;       beam waiting: waiting until set up bit input
;
;         xx      :set up bit (0: mask, 1: set up)
;         inport  : input port
;
bmwait  macro   xx
        local   wait
        even
        push    dx
        mov     dx,inport
wait:
        in      al,dx
        and     al,xx
        mov     ah,00h
        cmp     ah,al
        jz      wait
        pop     dx
        endm
;
;-------------------------------------------------
;
;       error chedk
;
;         adrs    : address of error flag
;         erretn  : address for jumping in error
;
```

```
ercheck macro   adrs
        local   cont
        mov     bp,adrs
        les     si,ds:[bp]
        mov     ax,0000
        cmp     ax,es:[si]
        jz      cont
        jmp     erretn
cont:
        endm
;
;-------------------------------------------------------
;
;       trapping of error
;
;         port    : input port for error
;         frg     : masking of error flag
;         adrs    : address for error flag
;         ah      : error without input signal;
errin   macro   port,adrs,frg
        mov     dx,port
        in      al,dx
        and     ax,frg
        mov     bp,adrs
        les     si,ds:[bp]
        or      es:[si],ax
        endm
;
;-------------------------------------------------------
;
;      constant loop
;
;         wtime   : number of loops
;
wtloopc macro   wtime
        local   loop3
        even
        push    cx
        mov     cx,wtime
loop3:
        loop    loop3
        pop     cx
        endm
;
;-------------------------------------------------------
;
;       short loop
;
;         adwtlp  : initial address of number of loop
;         wtime   : off set
;
wtloop  macro   wtime
        local   loop3
        even
        nop
        push    cx
        push    es
        push    si
        push    bp
        mov     bp,adwtlp
        les     si,ds:[bp]
        add     si,wtime
        mov     cx,es:[si]
loop3:
        loop    loop3
        pop     bp
        pop     si
        pop     es
        pop     cx
        endm
;
;-------------------------------------------------------
;
;       long loop
;
;         adwtlp  :initial address of number of loop
;         wtime1  :off set (large loop)
;         wtime2  :off set (small loop)
;         lpwait  : number of large loops
;
wtloopl macro   wtime1,wtime2
        local   loop3
        local   loop4
        local   loope
        even
        push    cx
        push    es
        push    si
        push    bp
        mov     bp,adwtlp
        les     si,ds:[bp]
        add     si,wtime1
        mov     cx,es:[si]
        jcxz    loope
loop3:
        push    cx
        mov     cx,lpwait
loop4:
        loop    loop4
        pop     cx
        loop    loop3
loope:
        pop     bp
        pop     si
        pop     es
        pop     cx
        wtloop  wtime2
        endm
;
;-------------------------------------------------------
;
;       data taking from counter board
;
;         xx      : address of data stack
;         yy      : port address for counter board
;
in_data macro   xx,yy
        local   exit
        local   exit2
        local   lp
        push    dx
        push    bp
        push    si
        push    ds
        push    es
;;
        mov     dx,yy+4
        out     dx,al
        mov     dx,yy+1
        in      al,dx
        mov     ah,al
        mov     dx,yy
        in      al,dx
        mov     bp,xx
        les     si,ds:dword ptr [bp]
        add     ax,es:[si]
        jns     exit
        inc     es:word ptr [si+2]
        sub     ax,8000h
        jmp     exit2
exit:
        push    cx
        mov     cx,02h
lp:
        loop    lp
        pop     cx
        nop
exit2:
        mov     es:[si],ax
        pop     es
        pop     ds
        pop     si
        pop     bp
        pop     dx
        endm
;
;-------------------------------------------------------
;
;       rf data transfer
;
;-------------------------------------------------------
;
;       (I/O controll sub routine):  out put of set up
addres
;
;         ad      : port address
;         n       : off set of output data
;         si reg  :RF data address
;
dtout   macro   ad,n
        push    di
        mov     di,si
        add     di,n
        mov     al,es:[di]
        mov     dx,ad
        out     dx,al
        pop     di
        endm
;
;-------------------------------------------------------
;
;       (GP-IB Out mode)
;
gpibout macro
        push    es
        push    si
        push    di
        push    cx
        add     si,gpdt
        mov     ax,es:[si]
        inc     si
        inc     si
        mov     bx,es:[si]
        inc     si
        inc     si
        mov     cx,es:[si]
        mov     si,ax
        mov     es,bx
        mov     di,ax
        add     di,03h
        mov     ax,0401h
        mov     bx,03h
        int     0d1h
        pop     cx
        pop     di
        pop     si
        pop     es
        endm
;
;-------------------------------------------------------
;
;       (D/A Out mode)
;
;                 adrs      : data address
;                 ch1,chh   : DA port (#1 or #2)
;                 dt1,dth   : DA data (12bit)
;
daout    macro    adrs,ch1,chh,dt1,dth
        even
        push    dx
        push    bp
        push    si
        push    ds
        push    es
        mov     bp,adrs
; RF data address -> si reg.
        les     si,ds:dword ptr [bp]
        dtout   chh,dth
        wtloopc 9h
        dtout   ch1,dt1
        pop     es
        pop     ds
        pop     si
        pop     bp
        pop     dx
        endm
;
;-------------------------------------------------------
;
;       (Bit Out mode
;
bitout  macro
;        dtout   rfbitph,bitdth
        dtout   rfbitpl,bitdt1
        bitcntr rfbitpl,00h
        endm
;
;-------------------------------------------------------
;
```



```
;       rf control by bit out
;
brdtout macro   adrs
        bitcntr rfbitpl,00h
        mov     bp,adrs
; RF data address -> si reg.
        les     si,ds:dword ptr [bp]
;;
;;        gpibout      <----- Not use
;;        push    ax
        bitout
;;        dtout   rfbitpl,afpdt
;;        bitcntr rfbitpl,off
;;        pop     ax
        endm
;
;-------------------------------------------------------
;
;       TAKEDA TR3133B mode
;
trdtout macro   adrs
        local   loop2
        push    cx
;;
;;      reset signal
;;
        mov     dx,rfbitph
        mov     al,80h
        out     dx,al
        wtloopc 0010h
        mov     al,00h
        out     dx,al
        wtloopc 0004h
;;
;;      data in signal
;;
        mov     al,20h
        out     dx,al
        mov     bp,adrs
        les     si,ds:dword ptr [bp]
        add     si,trdt
        mov     cx,08h
;;
;;    data signal
loop2:
        mov     al,es:[si]
        add     al,20h
        out     dx,al
;;
;;      data shift signal
;;
        add     al,10h
        out     dx,al
        wtloopc 0008h
        sub     al,10h
        out     dx,al
;;
;;      increment of data singal
;;
        mov     al,20h
        out     dx,al
        wtloopc 0004h
        inc     si
        inc     si
        loop    loop2
;;
;;      stop data in singal
;;
        mov     al,00h
        out     dx,al
        wtloopc 0008h
;;
;;      entry signal
;;
        mov     al,40h
        out     dx,al
        wtloopc 0010h
        mov     al,00h
        out     dx,al
;;
;;       trapping error stop
;;
```

```
        errin   inport,aderror,errfrg
;;
        pop     cx
        endm
;
;-------------------------------------------------------
;
;       (main routine)
;
;         rfdata  : initial address of rf data
;         aderror : address of error flag
;         errfrg  : error flag
;
rfdtout macro   rfdata
        even
        push    dx
        push    bp
        push    si
        push    ds
        push    es
;;
        brdtout rfdata
        trdtout rfdata
;;
;;       trapping error stop
;;
        errin   inport,aderror,errfrg
;;
        pop     es
        pop     ds
        pop     si
        pop     bp
        pop     dx
        endm
;
;-------------------------------------------------------
;
;       rf selector mode
;
rfslct  macro
        push    dx
        push    bp
        push    si
        push    ds
        push    es
        mov     bp,adrfdt
        les     si,ds:dword ptr [bp]
        dtout   rfbitpl,bitdtl
        bitcntr rfbitpl,00h
        pop     es
        pop     ds
        pop     si
        pop     bp
        pop     dx
        endm
;
;-------------------------------------------------------
;
;       selection of counter open or hold
;
;         ctch    : counter address
;         hldsel  :selection flag 3F: all ch hold
;                  FF: all ch open
;                  BF: 1ch open
;                  7F: 2ch open
;
counter macro   ctch,hldsel
        push    dx
        mov     dx,ctch+6
        mov     al,hldsel
        out     dx,al
        pop     dx
        endm
;
;-------------------------------------------------------
;
;       counter reset
;
;         ctch    : counter address
;
ctreset macro   ctch
        push    dx
        mov     dx,ctch
        mov     al,00h
        out     dx,al
        mov     dx,ctch+1
        mov     al,00h
        out     dx,al
        mov     dx,ctch+2
        out     dx,al
        pop     dx
        endm
;
;-------------------------------------------------------
;
;       rf control selection
;
rfcntr  macro   before,after,t1,t2
        even
        rfslct
        bpcntr  rfport,rfstart,rfoff,1pulse
        bitcntr rfport,before
        in_data adctu1,ctch1
        in_data adctd1,ctch2
        in_data adctu2,ctch3
        in_data adctd2,ctch4
        ctreset ctch1
        ctreset ctch2
        ctreset ctch3
        ctreset ctch4
        wtloop1 t1,t2
        bitcntr rfport,after
        bpcntr  rfport,rfstop,after,1pulse
        endm
;
;-------------------------------------------------------
;
;       address increment
;
;         n       : increment
;
adrsinc macro   adress,n
        push    bp
        push    si
        push    ds
        mov     bp,adress
        mov     si,ds:[bp]
        add     si,n
        mov     [bp],si
        pop     ds
        pop     si
        pop     bp
        endm
;
;-------------------------------------------------------
;
;       address decrement
;
;         n       : decrement
;
adrsdec macro   adress,n
        push    bp
        push    si
        push    ds
        mov     bp,adress
        mov     si,ds:[bp]
        sub     si,n
        mov     [bp],si
        pop     ds
        pop     si
        pop     bp
        endm
;
;-------------------------------------------------------
;
;      counting selection
;
;       (sub routine)
;
countsb macro   t1,t2
        bpcntr  ctport,ctgrst,ctgate,1pulse
        bpcntr  ctport,ctgcl1,ctgate,1pulse
        wtloop1 t1,t2
        bpcntr  ctport,ctgcl2,ctgate,1pulse
        endm
;
```



```
;       (main routine)
;
;         section : outpurt selection number
;         n       : number of separation of counting gate
signal
;         ni      :incremant of data address
;         t1      :offset of parameter of time
;         t2      :
;
count   macro   section,n,ni,t1,t2
        local   lp
        local   exit
        even
        push    cx
        bitcntr secport,section
        counter ctch1,openall
        counter ctch3,openall
        bitcntr ctport,ctgate
        adrsinc adctu1,ni
        adrsinc adctd1,ni
        adrsinc adctu2,ni
        adrsinc adctd2,ni
        mov     cx,n
lp:
        countsb t1,t2
        dec     cx
        jcxz    exit
        jmp     lp
exit:
        bitcntr ctport,off
        counter ctch1,holdall
        counter ctch3,holdall
        bitcntr secport,off
        pop     cx
        endm
;
;-------------------------------------------------------
;
;       beam cooling selection
;
bmcool  macro
        even
        wtloop bmcoolt
        endm
;
;-------------------------------------------------------
;
;     output of controlbit for AFP with condition
;
;         port    : output port address
;         before  : output befor operation
;         adrs    : rf parameter address
;         n       : condition flag
;         t       : time parameter offset
;         afpbit  : control bit
;
afpcntr macro   port,before,adrs,n,t
        local   cont
        local   off
        even
        push    bp
        push    es
        push    si
        push    dx
        mov     al,0h
        mov     bp,adrs
        les     si,ds:dword ptr [bp]
        add     si,afpdt
        mov     bx,es:[si]
        and     bx,n
        jz      off
        mov     al,afpbit
        jmp     cont
off:
        mov     al,0h
        nop
cont:
        mov     dx,port
        add     al,before
        out     dx,al
        wtloop  t
        mov     al,before
        out     dx,al
        pop     dx
        pop     si
        pop     es
        pop     bp
        endm
;
;-------------------------------------------------------
;
;       rf kill selection
;
rfkill  macro
        even
        wtloop rfkillt
        endm
;
;-------------------------------------------------------
;
;       rf data address increment
;
rfadinc macro
        even
        adrsinc adrfdt,0020h
        endm
;
;-------------------------------------------------------
;
;       rf data address dectrement
;
rfaddec3 macro
        even
        adrsdec adrfdt,0060h
        endm
;
;-------------------------------------------------------
;
;       data address decrement
;
ctadinc macro   n
        even
        adrsinc adctu1,n
        adrsinc adctd1,n
        adrsinc adctu2,n
        adrsinc adctd2,n
        endm
;
;-------------------------------------------------------
;
;       read countin data
;
countin macro
        even
        in_data adctu1,ctch1
        in_data adctd1,ctch2
        in_data adctu2,ctch3
        in_data adctd2,ctch4
        ctreset ctch1
        ctreset ctch2
        ctreset ctch3
        ctreset ctch4
        endm
;
;-------------------------------------------------------
;
;       read beam current data
;
;         xx      : address for beam current data
;         yy      : counter address for reading beam
courrent data
;
in_sem  macro   xx,yy
        local   exit
        local   exit2
        local   lp
        even
        push    dx
        push    bp
        push    si
        push    ds
        push    es
        push    bx
;;
        mov     bp,xx
        les     si,ds:dword ptr [bp]
```

```
;;
        counter yy,holdall
        mov     bx,0000h
        mov     dx,yy+0Ch
        out     dx,al
        mov     dx,yy+8h
        in      al,dx
        mov     bl,al
        shl     bx,1h
        shl     bx,1h
        add     si,bx
;;
        mov     dx,yy+4h
        out     dx,al
        mov     dx,yy+1h
        in      al,dx
        mov     ah,al
        mov     dx,yy
        in      al,dx
;;
        add     ax,es:[si]
        jns     exit
        inc     es:word ptr [si+2]
        sub     ax,8000h
        jmp     exit2
exit:
        push    cx
        mov     cx,02h
lp:
        loop    lp
        pop     cx
        nop
exit2:
        mov     es:[si],ax
        ctreset yy
        ctreset yy+8h
        counter yy,openall
        pop     bx
        pop     es
        pop     ds
        pop     si
        pop     bp
        pop     dx
        endm
;
;-------------------------------------------------------------
;
;       GPIB control
;
;       (initialize)
;
gpibini macro
        push    es
        mov     ax,cs
        add     ax,098h
        mov     es,ax
        mov     ah,00h
        int     0d1h
        pop     es
        endm
;
;       (ifc set)
;
gpibifc macro
        push    bx
        mov     bh,01h
        mov     ah,01h
        int     0d1h
        pop     bx
        endm
;
;       (remote enable)
;
gpibren macro
        mov     ah,02h
        int     0d1h
        endm
;
;       (reset)
;
gpibres macro
        mov     ah,03h
        int     0d1h
        endm
;
;-------------------------------------------------------------
;
        %out 2
```


2APCNTR.ASM

```
;       NMR measurement program
;
;       2AP MODE
;
;       2APCNTR .M
;
        title 2APCNTR Main routine
if1
        %out Now 2APCNTR .ASM has been compiled
endif
;
;       initializing program including
;
        include lab\lablcntr.asm
;
main:
        in_sem  adctsem,ctch5
        bpcntr  bmport,bmstart,off,1pulse
        rfdtout adrfdt
        wtloopl bmtime1,bmtime2
        bpcntr  bmport,bmstop,off,1pulse
;
        bmcool
;
        rfcntr  rfon,rfoff,rftime1,rftime2
        rfkill
;
        count   00000001b,01h,40h,cttime1,cttime2
;
        rfadinc
        bpcntr  ctport,workend,off,1pulse
;
        dec     cx
        jcxz    extgl
        jmp     main
;
extgl:
        countin
        in_sem  adctsem,ctch5
;
;       end program including
;
        include lab\lab2cntr.asm
;
        end
```

8APCNTR.ASM

```
;       NMR mearuemetn control
;
;       8AP MODE
;
;       8APCNTR .M
;
        .sall
        title 8APCNTR Main routine
if1
        %out Now 8APCNTR .ASM has been compiled
endif
;
;       initializing part including
;
        include lab\lablcntr.asm
;
        ctadinc 0ch
;
main:
        in_sem  adctsem,ctch5
        bpcntr  bmport,bmstart,off,1pulse
        rfdtout adrfdt
        wtloopl bmtime1,bmtime2
        bpcntr  bmport,bmstop,off,1pulse
;
        bmcool
;
        rfcntr  off,rfoff,rftime1,rftime2
        rfkill
;
        count   00000001b,01h,34h,cttime3,cttime4
;
        rfcntr  rfon,rfoff,rftime1,rftime2
        rfkill
;
        count   00000010b,01h,04h,cttime1,cttime2
;
        rfcntr  rfon,rfoff,rftime1,rftime2
        rfkill
;
        in_sem  adctsem,ctch5
        bpcntr  bmport,bmstart,off,1pulse
        rfdtout adrfdt
        wtloopl bmtime1,bmtime2
        bpcntr  bmport,bmstop,off,1pulse
;
        bmcool
;
        rfcntr  rfon,rfoff,rftime1,rftime2
        rfkill
;
        count   00000100b,01h,04h,cttime3,cttime4
;
        rfcntr  rfon,rfoff,rftime1,rftime2
        rfkill
;
        count   00001000b,01h,04h,cttime1,cttime2
;
        rfcntr  off,rfoff,rftime1,rftime2
        rfkill
;
        rfadinc
        bpcntr  ctport,workend,off,1pulse
;
        dec     cx
        jcxz    extgl
        jmp     main
;
extgl:
        in_sem  adctsem,ctch5
;
;       end program including
;
        include lab\lab2cntr.asm
;
        end
```

2RFCNTR.ASM

```
;       NMR measurement program
;
;       2RF 2AP MODE (RF ON / OFF)
;                                               RF 1,2 * 5
(3,4 are dummy)
;                                               used by
Frequency synsesizer
;
;       2RF-2AP using frequency synsesizer
;
;               RF data for '4RF 2AP MODE' can be used.
;               Please set dummy data for No. 3 and 4
RF.
;
;       2RFCNTR.M
;
;
        by Moichi
;
;                               modified by A.K.
1991/11/08
;
                This is the my Last control program
;
                for LABCNTR system.
;
        modified by T.O.  1993.5.17
;                                       for control TR-3133 at
10MHz switching
;
        title 2RFCNTR Main routine
if1
        %out Now 2RFCNTR.ASM has been compiled
endif
;
;       initializing program including
;
        include lab\lab1cntr.asm
;
;       ctadinc 04h
;
main:
        in_sem  adctsem,ctch5
        rfdtout adrfdt
; for 10MHz switching
        bpcntr  bmport,bmstart,off,1pulse
        wtloop1 bmtime1,bmtime2
        bpcntr  bmport,bmstop,off,1pulse
;
        bmcool
;
        bpcntr  rfport,rfon,rfon,1pulse
        push      cx
           mov              cx,005h
; for 5 rf loop
rf1p1:  push      cx
        rfdtout adrfdt
           bpcntr rfport,045h,004h,1pulse    ; select RG1
0100 0101
        wtloop1   rftime1,rftime2
        rfadinc

        rfdtout adrfdt
           bpcntr rfport,025h,004h,1pulse    ; select RG2
0010 0101
        wtloop1 rftime1,rftime2

        rfadinc

        rfadinc

                pop             cx
                dec             cx
                jcxz     cont1
                rfaddec3
                jmp             rf1p1
cont1:   pop             cx
        bpcntr  rfport,rfoff,rfoff,1pulse
        rfkill
;
;       count   00000001b,01h,3ch,cttime1,cttime2
;       count   00000001b,01h,40h,cttime1,cttime2

        countin

        rfadinc

;
        dec     cx
        jcxz    extg1
        jmp     main
;
extg1:
        countin
        in_sem  adctsem,ctch5
;
;       end program including
;
        include lab\lab2cntr.asm
;
        end
```